Chapter 5: Information from Paleoclimate Archives

Coordinating Lead Authors: Valérie Masson-Delmotte (France), Michael Schulz (Germany)

Lead Authors: Ayako Abe-Ouchi (Japan), Juerg Beer (Switzerland), Andrey Ganopolski (Germany), Jesus Fidel González Rouco (Spain), Eystein Jansen (Norway), Kurt Lambeck (Australia), Juerg Luterbacher (Germany), Tim Naish (New Zealand), Timothy Osborn (UK), Bette Otto-Bliesner (USA), Terrence Quinn (USA), Rengaswamy Ramesh (India), Maisa Rojas (Chile), XueMei Shao (China), Axel Timmermann (USA)

Contributing Authors: Kevin Anchukaitis, Gerardo Benito, Peter Clark, Patrick De Deckker, Barbara Delmonte, Trond Dokken, Hubertus Fischer, Dominik Fleitmann, Claus Froehlich, Aline Govin, Alan Haywood, Chris Hollis, Ben Horton, Camille Li, Dan Lunt, Natalie Mahowald, Shayne McGregor, Stefan Mulitza, Frédéric Parrenin, Paul Pearson, Alan Robock, Joel Savarino, Jason Smerdon, Olga Solomina, Pavel Tarasov, Claire Waelbroeck, Dieter Wolf-Gladrow, Yusuke Yokoyama, James Zachos, Dan Zwartz

Review Editors: Anil K. Gupta (India), Fatemeh Rahimzadeh (Iran), Dominique Raynaud (France), Heinz Wanner (Switzerland)

Date of Draft: 16 December 2011

Notes: TSU Compiled Version

Table of Contents

Executive Summary

Radiative Forcings and Radiative Perturbations from Earth System Feedbacks

- Since AR4, several new estimates of past solar and volcanic radiative forcings have been produced, spanning at most the current interglacial period and the last 1500 years, respectively. Large uncertainties remain in the magnitude of these natural forcings, and contribute to the spread in climate model results.
- Past changes in atmospheric greenhouse gas concentrations (CO_2, CH_4, and N_2O) have been documented back to 800 ka (thousand years ago) from ice cores. The new data expand the AR4 statement that present-day concentrations very likely exceed by far the natural range of variability back to 800 ka.
- There is high confidence that atmospheric CO_2 concentration exceeded the pre-industrial level for extended periods (on a million-year timescale) during the past 65 Myr (million years) though the reconstructed values obtained from geological archives are very uncertain. Together with considerable uncertainties in reconstructed surface temperatures, this limits the use of past "high CO_2 worlds" for constraining climate sensitivity.

Earth System Responses and Feedbacks at Global and Hemispheric Scales

- During the Middle Pliocene (3.3 to 3.0 million years ago), atmospheric CO_2 concentrations between 330 ppm and 420 ppm were associated with global mean surface temperatures approximately 2–3°C warmer than for pre-industrial climate, and global mean sea level 10–30 m above that of present-day [medium confidence].
- For high (low) CO_2 worlds such as the Middle Pliocene (Last Glacial Maximum), surface air temperature reconstructions show a strong polar amplification, of 2–3 times global mean warming (cooling) [medium to high confidence]. Available simulations from coupled climate models seem to underestimate the strength of this amplification with respect to proxy-based reconstructions by 30–50%.
- New syntheses of Last Glacial Maximum land and ocean surface temperature reconstructions have allowed detailed comparisons with climate model simulations to constrain climate sensitivity. Complex models such as GCMs suggest that the response to to negative (e.g., glacial) versus positive (e.g., projections) radiative perturbations is not as linear as simpler models indicate, with cloud feedbacks responsible for an asymmetry in simulated climate sensitivity. It is, therefore, difficult to establish tight bounds on the climate sensitivity, although values in excess of 6°C for doubling of atmospheric CO_2 content are difficult to reconcile with our existing understanding.
- New records of glacial-interglacial variability since 800 ka (thousand years ago) have shown that interglacial periods prior to 400 ka were generally colder than the subsequent interglacials and were associated with lower than pre-industrial CO_2 and CH_4 concentrations in the atmosphere. These data show very likely positive climate-carbon cycle feedbacks. Since AR4, transient glacial-interglacial climate simulations have been performed with coupled climate-ice sheet models in response to orbital forcing. Models are only able to capture the full range of the glacial-to-interglacial global mean temperature difference when taking into account the positive CO_2 feedback.
- Annual mean land and ocean surface temperature estimated from new global syntheses indicate that the Last Interglacial period (130 to 116 ka) was approximately 2°C warmer than pre-industrial climate [medium confidence], with yet to be quantified uncertainties associated with seasonality of biological proxies and data scarcity over many continental and marine areas. Ocean-atmosphere coupled simulations capture the global patterns of surface temperature response to orbital forcing, but underestimate the magnitude of high latitude warming, possibly due to lack of vegetation feedbacks (Northern Hemisphere) and ice sheet feedbacks (Southern Hemisphere).
- There is evidence [high confidence] for centennial to millennial climate variability during the current and previous interglacials, which are superimposed on long-term trends caused by orbital forcing. New transient climate simulations explain the spatial and temporal complexity of the early-to-mid Holocene climate by the interplay of orbital forcing and the regional impacts of ice sheet decay.New multi-proxy statistical and modeling methods have been developed to estimate hemispheric temperature variations during the last centuries/millennia. Since AR4, larger amplitudes of temperature variations have been documented between the Medieval Climate Anomaly (about 950-1250 CE, MCA) and Little Ice Age (about 1450-1850 CE, LIA).
- Combining instrumental temperatures with proxy-based reconstructions and considering confidence intervals and sources of error, the 50-year mean Northern Hemisphere temperature for 1961–2010 CE was very likely warmer than any previous 50-year mean in the last 800 years. Comparison of the relative warmth of the Medieval and modern periods is still problematic but evidence for modern warming is

more extensive seasonally and geographically and provides medium confidence that 1961–2010 CE was the warmest 50-year period during the last 1300 years.

- At the multi-decadal scale, broad agreement exists between reconstructions of Northern Hemisphere temperature variability during the last millennium and simulations forced by natural and anthropogenic radiative forcings. Uncertainties in forcings and reconstructed temperatures limit the power of this comparison as a test of climate model performance. Internal variability as well as solar and volcanic forcing may have significantly influenced the onset of the Medieval Climate Anomaly and Little Ice Age. It may be partly responsible for differences between model simulations and reconstructions of the Medieval Climate Anomaly to the Little Ice Age transition. New climate model simulations highlight the importance of volcanic forcing, even for multi-decadal periods, and capture the magnitude of the estimated northern hemisphere temperature response to volcanic forcing.

Climate Responses at Regional Scales

- The Medieval Climate Anomaly was not characterized by uniformly warmer temperatures globally, but rather by a range of temperature, hydroclimate and marine changes with distinct regional and seasonal expressions.
- There is moderate confidence that the ongoing Arctic sea ice loss, increasing Arctic sea surface temperature and land surface air temperature are anomalous in the perspective of at least the last two millennia.
- In some areas of North America, European Alps and Scandinavia, current glacier length retreats appear exceptional in the context of the last 6 000 years [high confidence].
- Extended periods of megadroughts have been observed during interglacials in North America, South America, Africa and Europe. The length of past megadroughts partly exceeded those observed in the instrumental period and can be regarded as a natural part of interglacial climate variability. Extended intervals of drought associated with weak Indian Summer Monsoon in the last 2000 years may have been synchronous across a large region of southeastern Asia.
- Reconstructions of ENSO document with medium confidence that the large 20th century ENSO variability was unusual at least in the context of the last 350 years. It is likely that the probability of an El Niño event is increased in the two years following a major volcanic eruption.
- The strong positive phases of the North Atlantic Oscillation in the mid-1990s are not unusual in context of the past half millennium.

Past Changes in Sea Level and Related Processes

- There is high confidence that global mean sea level was above modern levels during warm intervals of the mid-Pliocene, implying reduced volume of polar ice sheets. Estimates range from +5 to +40 m with the range for the best estimate being +10 to +30 m. Direct geological evidence, together with ice sheet simulations, suggest that mid-Pliocene polar ice volume was characterized by a slightly reduced East Antarctic ice sheet compared to today and that most of the variation in ice volume occurred in the Greenland and West Antarctic ice sheets.
- There is robust evidence that changes in global mean sea level during interglacials since 800 ka were highly correlated with high latitude temperatures and radiative forcing.
- Global sea level was +4 to +6 m during the last interglacial relative to present [high confidence]. A sea level rise of up to +4 m during this time interval can be explained by Greenland ice sheet melting in combination with ocean thermal expansion. Direct geological evidence for a retreat of the West Antarctic ice sheet during the last interglacial remains equivocal.
- There is high confidence that on timescales of a century to a few millennia, rates of global mean sea level variations did not exceed 3 m per 1000 years (on average, 3 mm per year) within the last interglacial and the late Holocene. The magnitude and rate of current sea level change is unusual in the context of the past millennium [medium confidence].

Evidence and Processes of Abrupt Climate Change

- The modelled large-scale bipolar seesaw temperature pattern in response to a weakening of the Atlantic meridional overturning circulation (AMOC) closely resembles that reconstructed for glacial abrupt Dansgaard-Oeschger and Heinrich Events, thereby providing high confidence that both types of events are related to large-scale reorganizations of the AMOC.

- Both paleoclimate data and modelling provide robust evidence that reductions in the strength of the AMOC are very likely to have affected the position of the Atlantic Intertropical Convergence Zone, the strength of the West Africa, Asian, South American and Australian-Indonesian monsoons.
- The preferred occurrence of these events during glacial periods suggests with medium confidence that processes involving more massive glacial ice sheets and more extensive sea ice cover compared to interglacial periods, are required for generating this type of abrupt climate change.

Paleoclimate Perspective on Irreversibility

- New paleoclimate information and ice sheet models confirm that the West Antarctic and Greenland ice sheets are highly sensitive to small increases in polar warming and CO_2 concentrations compared to present-day levels [medium confidence], implying potential future irreversible melting on timescales of several millennia.
- High resolution marine sediment data and coupled ocean-atmosphere climate models consistently depict abrupt changes in ocean currents after a catastrophic freshwater inflow into the North Atlantic Ocean occurring about 8200 years ago (10^{14} m^3 possibly within <0.5 year) and complete recovery within about 200 years [high confidence].

5.1 Introduction

For the pre-instrumental period, documentary and proxy data from a range of paleoclimatic archives provide quantitative information on past regional to global climate changes as well as on variations in radiative forcing factors. Major progress since AR4 includes the acquisition of new and more precise information from paleoclimate archives, the synthesis of regional information, transient and more comprehensive modelling of past climate responses to forcings. This chapter assesses the understanding of past climate variations, using paleoclimate reconstructions as well as Earth-system and climate models of varying complexity, making use of standardized simulations such as those coordinated within the Paleoclimate Modelling Intercomparison Project (PMIP).

The quantification of uncertainties in paleoclimate information from regional to global scale is essential for for model evaluation. This chapter focuses on information since the middle Pliocene (since approximately 3 Ma), given the greater sparsity of proxy data with increasing geological age, but also refers to earlier warm periods. Paleoclimatic methods were covered in AR4 and only new proxies or methods are addressed here.

This chapter sets out by assessing new information and understanding of natural and anthropogenic radiative perturbations (Section 5.2) and the large scale (5.3) to regional (5.4) responses of the climate system to radiative perturbations and internally generated climate variability. The global-to-hemispheric scale approach addresses the relevance of Earth System feedbacks, and assesses the agreement between models and reconstructions on the magnitude and patterns of past climate anomalies. Section 5.3 includes an update of AR4 in the analysis of the methods and reconstructions of hemispheric temperature during the last millennia. Since AR4, further regional reconstructions of temperature, precipitation, droughts and modes of variability have emerged, expanding the framework for model-data comparisons (Section 5.4, Chapters 9 and 10).

New information on the magnitude, rates and causes of past sea level variations is assessed in Section 5.5, both for sea level high stands of past warm stages, and for major glacial-interglacial transitions. A detailed assessment of late Holocene regional sea level changes is presented. Cautionary notes regarding the information and uncertainties used to assess past changes in sea level are provided in the supplementary information to this chapter. The mechanisms underlying abrupt climate changes are addressed in Section 5.6 with the aim to evaluate the ability of climate models to resolve the magnitude and regional patterns of the climate anomalies. A paleoclimate perspective on irreversibility in the climate system (Section 5.7) addresses asymmetries in the response of ice sheets and the recovery processes of the Atlantic meridional overturning circulation to major perturbations.

5.2 Radiative Forcings and Radiative Perturbations from Earth System Feedbacks

5.2.1 External Forcings

5.2.1.1 Orbital Forcing

Orbital forcing is the only well-known (from precise astronomical calculations) forcing for both the past and future (see also FAQ 5.2). Changes in Earth's orbit – eccentricity, longitude of perihelion (precession), and axial tilt (obliquity) (Figure 5.2) (Berger and Loutre, 1991; Laskar et al., 2004) affect the annual, seasonal, and latitudinal distribution and magnitude of the solar energy received at the top of the atmosphere (Jansen et al., 2007) and the durations and intensities of local seasons (Huybers, 2006; Timm et al., 2008). Over the last million years, previous interglacial periods were characterized by different orbital configurations making it difficult to identify a best orbital analogue to our present interglacial (Tzedakis, 2010). Orbital forcing is the driver of glacial-interglacial changes (high confidence) on time scales of several thousand years. It also has significant impact on insolation distribution at the time scale of one thousand years (Schmidt et al., 2011) for explaining trends (Kaufman et al., 2009) and occurrence of abrupt events (Capron et al., 2010b).

5.2.1.2 Solar Forcing

Since AR4, models (e.g., Wenzler et al., 2005) have been improved to explain the instrumental records of total and spectral solar irradiance (TSI and SSI). Typical changes measured over an 11-year solar cycle are

0.1% for TSI and several percent for the ultra-violet (UV) part of SSI. Changes in TSI directly impact the Earth's surface, whereas changes in SSI primarily affect the stratosphere, but can influence the tropospheric circulation through dynamical coupling (Gray et al., 2010). Most models attribute all TSI and SSI changes exclusively to magnetic phenomena on the solar surface (sunspots, faculae, magnetic network), neglecting any potential internal phenomena such as changes in energy transport, and can successfully reproduce the measured TSI changes between 1978 and 2003 (Balmaceda et al., 2007; Crouch et al., 2008). The basic concept of these models is to divide the solar surface into different magnetic features each with a specific radiative flux. Sunspots are dark features that reduce irradiance; faculae and the magnetic network are bright features enhancing irradiance. TSI and SSI are calculated by adding the radiative fluxes of all features plus the contribution from the magnetically inactive surface. This approach requires detailed information of all the magnetic features and their temporal changes (Krivova and Solanki, 2008; Wenzler et al., 2006) (see also Section 8.2).

The extension of TSI and SSI into pre-instrumental times poses two main problems. Firstly, the instrumental period (since 1978 CE) used to calibrate the models does not show any significant multi-decadal trend. Secondly, detailed information about the various magnetic features is no longer available and must be deduced from proxies such as sunspots for the last 400 years and cosmogenic radionuclides (^{10}Be and ^{14}C) for the past millennia. Since all reconstructions rely ultimately on the same data (sunspots and cosmogenic radionuclides), but differ in the details of the applied models, the reconstructions agree rather well in their shape, but differ in their amplitude (Figure 5.1b) (Krivova et al., 2011; Lean et al., 2011; Schrijver et al., 2011; Wang et al., 2005b). ^{10}Be and ^{14}C records reflect not only the solar activity, but also the geomagnetic field intensity and effects of their respective geochemical cycles. Correcting for these non-solar components increases the uncertainty of the reconstructions (grey band in Figure 5.1c).

TSI reconstructions are characterized by distinct grand solar minima lasting 50–100 years that are superimposed upon long-term changes. Spectral analysis reveals the existence of cycles with periodicities of 87, 104, 130, 208, 350, 515, and 980 years (Stuiver and Braziunas, 1993) but varying amplitudes (Steinhilber et al., 2009; Vieira et al., 2011). Recent reconstructions show a considerably smaller difference (<0.1%) between the present and the Maunder minimum when the Sun was very quiet, than does the often used reconstruction of Lean et al. (1995) (0.24%). A new lower absolute value for TSI of 1360.8 ± 0.5 W m^{-2} (Kopp and Lean, 2011) was determined during the 2008 solar minimum, which is less than the value of 1365.5 W m^{-2} adopted for use in model runs and Figure 5.1. The effect of this difference on simulated changes is expected to be only minor (see also FAQ 5.2).

[INSERT FIGURE 5.1 HERE]

Figure 5.1: a) Two reconstructions of volcanic forcing for the past 1000 years derived from ice core sulfate and used for PMIP3-CMIP5 (Coupled Model Intercomparison Project) simulations (Schmidt et al., 2011). GRA: (Gao et al., 2008); CEA: (Crowley and Unterman, submitted; Crowley and Hyde, 2008; Timmreck et al., 2009). Volcanic sulfate peaks identified from their isotopic composition as originating from the stratosphere (Cole-Dai et al., 2009) are indicated by squares (green: Greenland; brown: Antarctica) (Baroni et al., 2008). **b)** TSI reconstructions back to 1000 CE. Proxies of solar activity (e.g., sunspots, ^{10}Be) are used to estimate the parameters of the models or directly TSI. All records except LBB (Lean et al., 1995) have been used for PMIP3-CMIP5 simulations (Schmidt et al., 2011). DB: (Delaygue and Bard, 2011); MEA: (Muscheler et al., 2007); SBF: (Steinhilber et al., 2009); WLS: (Wang et al., 2005b); VSK: (Vieira et al., 2011). Before 1600 CE, the 11-year cycle has been added artificially to the original data. **c)** TSI reconstruction (100-year low-pass filtered; grey shading: 1 standard deviation uncertainity range) for the past 9300 years (Steinhilber et al., 2009). The reconstruction is based on ^{10}Be and calibrated using the relationship between instrumental data of the open magnetic field, which modulates the production of ^{10}Be and TSI for the past 4 solar minima. **d)** Wavelet analysis (Torrence and Compo, 1998) of TSI showing the existence of several periodicities (87, 104, 130, 150, 208, 350, 515, 980, 2300 years) with varying amplitudes.

5.2.1.3 Volcanic Forcing

Since AR4, the patterns of sulphate injection caused by volcanic eruptions of the past 1500 years were estimated based on multiple Greenland and Antarctic ice core records and atmospheric modelling (Gao et al., 2008; Gao et al., 2006). Another reconstruction of volcanic aerosol optical depth was produced based on ice core records and the comparison between the Pinatubo deposition in Antarctica and satellite data (Crowley and Unterman, submitted; Crowley and Hyde, 2008; Schmidt et al., 2011; Timmreck et al., 2009). No quantitative estimate of associated uncertainty is available. These two reconstructions (Figure 5.1a) differ in

the source data, the identification of tropospheric versus stratospheric events and the methods to estimate optical depths; uncertainties on the seasonal timing of the eruptions arise from the resolution and dating uncertainties of ice core records. The radiative forcing of very large eruptions may be limited by specific scavenging processes (Timmreck et al., 2009) but this is not taken into account in the two available reconstructions. Stratospheric volcanic aerosols have a specific sulphur isotopic composition caused by mass-independent fractionation during photochemical reactions above the ozone layer (Baroni et al., 2007). The stratospheric character of several eruptions was assessed (Figure 5.1a) (Baroni et al., 2008; Cole-Dai et al., 2009).

5.2.1.4 Black Carbon Aerosol Forcing

Atmospheric black carbon was produced in pre-industrial times by fire occurrence and influenced by climatic and radiative forcing conditions as well as anthropogenic land cover changes (Justino et al., 2010; Pechony and Shindell, 2010; Power et al., 2008). New charcoal and pollen records show increased fire occurrence in the transition to the Holocene in North America (Marlon et al., 2009; Power et al., 2010). A long-term Holocene decline is indicated by the record of charcoal in Hudson Bay sediments, likely in response to a decrease in summer insolation (Hély et al., 2010). Widespread charcoal data also show less global biomass burning in the first centuries of the last millennium (Power et al., 2008), consistent with model simulations that suggest its variations are mostly driven by precipitation (Pechony and Shindell, 2010). A later increase in the 18th and 19th centuries is associated with anthropogenic activities, and followed by a decrease attributed to anthropogenic land cover changes and fire management. This is consistent with isotopic records of CH_4 and CO obtained from Antarctic firn and ice cores that show replacement of biomass burning by agricultural activities (Mischler et al., 2009; Wang et al., 2010). Two recent Antarctic ice cores indicate a large scale black carbon concentration decrease in the second half of the 20th century following grass fire and biofuels emission reductions (Bisiaux et al., in press) [see Chapters 7 and 8 for industrial contributions and radiative properties of black carbon].

5.2.2 Radiative Perturbations and Earth System Feedbacks

5.2.2.1 Atmospheric Concentrations of CO_2, CH_4, N_2O from Ice Cores

Air trapped in polar ice provides a direct, albeit low-pass filtered (Joos and Spahni, 2008; Köhler et al., 2011), record of past atmospheric GHG (greenhouse gas) concentrations complementing instrumental data (see AR5 Chapter 2). Since AR4, new and higher resolved records of CO_2, CH_4 and N_2O variations were obtained (Loulergue et al., 2008; Meure et al., 2006; Mischler et al., 2009; Siegenthaler et al., 2005). Centennial variations of up to 10 ppm CO_2, 40 ppb CH_4 and 10 ppb N_2O occur throughout the pre-industrial period. Existing long-term records have been extended from 650 ka to 800 ka (Loulergue et al., 2008; Lüthi et al., 2008; Schilt et al., 2010), showing lower than pre-industrial (280 ppm) GHG concentrations during so called “lukewarm interglacials” prior to 400 ka. The GHG concentrations stay within well-defined natural limits with maximum interglacial concentrations of about 300 ppm, 800 ppb, and 300 ppb for CO_2, CH_4 and N_2O, respectively, and minimum glacial concentrations of about 172 ppm, 350 ppb, and 200 ppb. Current atmospheric concentrations or rates of increase are not encountered in ice core records over the last 800 kyr for any of the three GHG (Joos and Spahni, 2008). The long CO_2 record reveals long-term (>200 kyr) trends in addition to glacial interglacial variations (Lüthi et al., 2008). By combining different ice cores, stacked high-resolution CO_2, CH_4, and N_2O records were compiled for the last glacial cycle (Schilt et al., 2010). Significant centennial variations in CH_4 and N_2O during the last glacial are linked to Northern Hemisphere (NH) rapid climate changes, while millennial CO_2 changes are connected to their Southern Hemisphere (SH) bipolar seesaw counterpart (Ahn and Brook, 2007; Ahn and Brook, 2008; Capron et al., 2010b; Grachev et al., 2009; Loulergue et al., 2008; Lüthi et al., 2008; Schilt et al., 2010) (see Section 5.6). New records of $\delta^{13}C$ of CO_2 provide important constraints on the sources and processes involved in past GHG changes (see also Chapter 6). Significant CO_2 $\delta^{13}C$ drops during the last two terminations was suggested to reflect upwelling of old, carbon enriched deep water contributing to the concurrent CO_2 increase (Lourantou et al., 2010a; Lourantou et al., 2010b). The small late Holocene CO_2 $\delta^{13}C$ decrease suggests that the multi-millennial CO_2 increase of 20 ppm can be explained by carbonate compensation and coral reef formation (Elsig et al., 2009). For CH_4, glacial-interglacial and millennial inter-hemispheric gradients and variations of carbon and hydrogen isotopes are consistent with changes in boreal and tropical wetlands [high confidence] (Bock et al., 2010; Fischer et al., 2008; Petrenko et al., 2009; Sowers, 2006; Sowers, 2010). GHG isotopes in ice cores

also confirm the anthropogenic origin of the current GHG increase (Ferretti et al., 2005; Mischler et al., 2009).

5.2.2.2 Atmospheric CO_2 Concentrations from Geological Proxy Data

Geological proxies provide indirect information on atmospheric CO_2 concentration on timescales beyond ice core records (see Section 5.2.2.1), that are comparable or much higher than those during the last decade. The geological proxy approach measures a response in a biological or geochemical system to changes in atmospheric or oceanic CO_2 concentrations, but with less precision and accuracy than the ice cores, and then calibrates the proxy method against modern systems (Figure 5.2; Table 5.1). Terrestrial proxies are based on the empirical relationship between stomatal pore density on tree leaves and CO_2 (Jordan, 2011; Royer et al., 2001), and on the carbon isotope composition of carbonate nodules in fossil soils (Cerling, 1991; Retallack, 2009). Marine proxies use the carbon isotope composition of long-chained alkenones preserved in marine sediments (Pagani, 2002), and the boron isotope composition of fossil foraminifera as an estimate for ocean pH together with estimates of alkalinity (Foster, 2008; Hemming and Hanson, 1992).

Since AR4, all four proxies have undergone further development (Beerling et al., 2009; Breecker et al., 2010; Foster, 2008; Henderiks and Pagani, 2007; Klochko et al., 2006) and have been applied more widely and at higher resolution to a range geological records, resulting in an increased number of atmospheric CO_2 estimates for the last 65 Ma (Beerling and Royer, 2011). While there is increased consensus between Cenozoic proxy CO_2 estimates, a significant degree of variation between the different techniques remains (Figure 5.2). This is particularly the case for the interval between 65 and 45 Ma, where the boron isotope proxy spans a range of 300 ppm to 3000 ppm, and estimates based on leaf stomatal density appear relatively insensitive to values above 1000ppm. An independent constraint on Early Eocene atmospheric CO_2 concentration is provided by the occurrence of the sodium carbonate mineral, nahcolite in about 50 Myr old lake sediments in the Green River Basin, USA (Lowenstein and Demicco, 2006). Nahcolite precipitates in association with halite at the sediment-water interface only at CO_2 levels >1125 ppm. There is closer agreement among the proxies in the middle and late Eocene (45–35 Ma) when CO_2 values were likely above 700 ppm, and then decreased in the earliest Oligocene (about 32 Ma) to a range of 400 ppm to 700 ppm (Pagani et al., in press; Pearson et al., 2009). Since the early Miocene (23 Ma) magnitudes were generally within in the range of pre-industrial values recorded in ice cores, with the exception of the Pliocene (about 5.3–2.6 Ma) - arguably one of the most relevant high-CO_2 geological analogues because continental and ocean configurations, ecosystems, and ice sheets were broadly similar to those of today. Accordingly, a number of recent CO_2 reconstructions based on marine proxies have been undertaken for this period (e.g., Pagani et al., 2010; Seki et al., 2010), converging towards consistent estimates comparable to present day levels. Proxy CO_2 reconstructions cluster in the range of 330 ppm to 420 ppm between 5 Ma and 3 Ma, the warmest part of the Pliocene (Figure 5.2), declining to pre-industrial values between 3 Ma and 2.6 Ma coincident with the intensification of Northern Hemisphere continental glaciations and the development of summer sea ice around Antarctica (McKay et al., submitted). A boron-based CO_2 reconstruction for the last 2 Myr from the eastern equatorial Pacific ocean overlaps the ice core record with sufficient resolution to directly compare geologically derived proxy data with ice core CO_2 measurements (Hönisch et al., 2009). Although errors (±25 ppm) are larger for the boron-based estimates, mean values are in close agreement with glacial-interglacial range of CO_2 for the last 800 kyr.

5.2.2.3 Past Changes in Mineral Dust Aerosol (MDA) Concentrations

Large spatial and temporal fluctuations in atmospheric MDA concentrations make it difficult to assess the global radiative forcing linked with past MDA changes. During glacials and stadials the dust concentrations in Greenlandic ice cores are higher by 1 to 2 orders of magnitude compared to interglacials and interstadials. This is mainly due to changes in the dust sources in Asia, the lifetime of atmospheric dust aerosols and transportation (Fischer et al., 2007). A strong coherence is observed with aeolian deposition in European loess formations (Antoine et al., 2009).

In central Antarctica glacial MDA concentrations are increased by a factor of 50–70 (Fischer et al., 2007; Lambert et al., 2008; Petit and Delmonte, 2009). This is due to reduced ice accumulation rates and an enhancement of dust production in southern South America and to a lesser extent in Australia (De Deckker et al., 2010; Vallelonga et al., 2010) and possibly to a change in the atmospheric lifetime (Delmonte et al.,

2008; Marino et al., 2009). Equatorial Pacific glacial-interglacial MDA fluxes co-vary with Antarctic records, but with a factor of 3–4 between interglacial and glacial periods (Winckler et al., 2008). They point to enhanced glacial emissions from Asian and northern South American dust sources (Maher et al., 2010). Global data synthesis is so far only available for the Last Glacial Maximum (LGM) showing 2–4 more dust deposition (Derbyshire, 2003; Maher et al., 2010). Because of uncertainties in radiative properties, estimates of glacial dust radiative forcing vary from –3 to +0.1 W m^{-2} with best estimate value around –1 W m^{-2} (Claquin et al., 2003; Mahowald et al., 2011; Mahowald et al., 2006; Patadia et al., 2009; Takemura et al., 2009; Yue et al., 2010).

5.3 Earth System Responses and Feedbacks at Global and Hemispheric Scales

5.3.1 High CO_2 Worlds and Temperature

Cenozoic (last 65 Myr) climate archives provide the opportunity to assess climate change (in particular temperature), in response to a range of atmospheric CO_2 concentrations similar to those projected for the 21st century (Chapter 12). Reconstructions of Cenozoic surface temperatures remain challenged by the limited number, and uneven geographical distribution, of proxy surface temperature data. Table 5.2 summarizes the methodology and utility of the five main sea surface temperature proxies, and also provides a qualitative confidence assessment of the assumptions required by each proxy method. There is little consistency in the way uncertainties are reported for proxy climate estimates in the literature. In most cases error bars represent the analytical and calibration error, with the calibration often assumed to be correct, and uncertainties associated with assumptions usually qualitatively assessed. In some cases compilations of global surface temperature data have reported qualitative confidence assessments, that take into account: (1) the quality of the age control, (2) number of samples, (3) fossil preservation and abundance, (4) performance of the proxy method utilized, and (5) agreement of multiple proxy estimates (e.g., Dowsett et al., submitted; MARGO Project Members, 2009).

Figure 5.3 illustrates global surface temperature proxy and general circulation model (GCM) data for three well studied periods of Earth history characterized by distinctly different atmospheric CO_2 concentrations - LGM (21–19 ka; about 185 ppm), mid Pliocene Warm Period (MPWP 3.3–3.0 Ma; 330–420 ppm), and Early Eocene Climatic Optimum (EECO, 54–48Ma, > 1000 ppm). There is a general correspondence between times of global warmth and high CO_2 but other factors (driven by tectonics) during the Cenozoic also played an important role in the carbon cycle (e.g., Zachos et al., 2008). The available sea and land surface reconstructions indicate with moderate confidence that mean surface temperatures were about +10°C above the pre-industrial mean for the EECO, the warmest part of the last 65 Myr, when atmospheric CO_2 was above 1000 ppm [moderate confidence] (Beerling and Royer, 2011; Lowenstein and Demicco, 2006; Pagani, 2005; Figure 5.2). New compilations of both terrestrial and marine temperature proxies and ensemble GCM simulations for MPWP show that global mean annual surface temperature was likely 2–3°C above the pre-industrial mean, and there is medium confidence that global mean sea level was about 10–30 m higher (Figure 5.2, Section 5.5.1).

Consistent features of GCMs and temperature proxy reconstructions are: that for warmer than pre-industrial (Eocene and Pliocene) climate states pole-equator temperature gradients are significantly reduced [medium confidence], and for both past warmer and colder (LGM) climates, polar amplification is two-three times the global mean [medium confidence]. Polar amplification (Box 5.1), is suppressed in meridional SST anomaly gradients compared with Surface Air Temprature (SAT) gradients due to the presence of high-latitude sea ice in the pre-industrial control period (Figure 5.3). The substantial extra-tropical amplification on both sea and land compared to the multi-model mean (see Box 5.2) may suggest that the high-latitudes are more sensitive to CO_2 forcing than the model simulations suggest (Lunt et al., 2010a). This could indicate a weakness in the climate models' ability to correctly simulate warmth at the higher latitudes, or it may result in part from a lack of coverage of high-latitude proxies, or uncertainties in the assumptions of the response of the proxy to temperature (Table 5.2).

The warm intervals of the Cenozoic, provide an opportunity to explore the long-term equilibrium sensitivity to current or near future concentrations of CO_2 (Dunkley Jones et al., 2010; Lunt et al., 2010a; Pagani et al., 2010; Zeebe et al., 2009). While the high end of climate model sensitivities is implied from the limited studies to date, these estimates are of low confidence, because current proxy methods cannot sufficiently

reduce the range of CO_2 and temperature uncertainties. This is also still the case for the abrupt transient warming of Palaeocene/Eocene Thermal Maximum (PETM) at about 55 Ma, associated with the release of a large mass carbon with low $\delta^{13}C$ composition. Two new syntheses of the PETM provide a useful update relevant to this assessment of this transient warming event (Dunkley Jones et al., 2010; McInerney and Wing, 2011). The abrupt (within 1kyr to 10 kyr) global warming estimated from surface temperature proxies remains in the range from +5°C to +9°C, and depending on carbon source (with $\delta^{13}C$ of clathrate of –60‰ or thermogenic of –5‰), mass balance modeling implies a magnitude of between 3000 and 8000 PgC, equivalent to 1000–2000 ppm pCO_2 for the perturbation (Panchuk et al., 2008; Zeebe et al., 2009). At present there is still too much uncertainty in the proxy and model reconstructions of global temperature (5–9°C) and pCO_2 (1000–2000 ppm on top of an uncertain background level) rise to derive a robust quantitative estimate of climate sensitivity from the PETM.

[INSERT FIGURE 5.2 HERE]

Figure 5.2: (Top) Radiative forcings and perturbations and orbital-scale Earth system responses 3.6 Ma to present. Changes in Earths orbital parameters, eccentricity, obliquity, and precession (Laskar et al., 2004). Sea level curve (purple) is the stacked benthic oxygen isotope proxy for ice volume and ocean temperature (Lisiecki and Raymo, 2005) calibrated to global average eustatic sea level (Miller et al., submitted; Naish and Wilson, 2009). Also shown are global eustatic sea level reconstructions for the last 500 kyr based on sea level calibration of the $\delta^{18}O$ curve using dated coral shorelines (grey line; Waelbroeck et al., 2002), and the Red Sea sediment cores (red line; Rohling et al., 2009; Siddall et al., 2003) and weighted mean estimates (2 standard deviation uncertainity) for far-field reconstructions of eustatic peaks during mid-Pliocene interglacials (red dots; Miller et al., submitted). The dashed horizontal line represents present day sea level. Tropical sea surface temperature based on a stack of 4 alkenone-based SST reconstructions (Herbert et al., 2010). Atmospheric CO_2 measured from EPICA Dome C ice core (blue line; Lüthi et al., 2008), and estimates of CO_2 from boron $\delta^{11}B$ isotopes in foraminifera in marine sediments (blue triangles; Hönisch et al., 2009; Seki et al., 2010), and phytoplankton alkenone-derived carbon isotope proxies (red diamonds; Pagani et al., 2010; Seki et al., 2010), plotted with 2 standard deviation uncertainity. Present and pre-industrial CO_2 concentrations are indicated with dashed grey line. **(Bottom)** Concentration of atmospheric CO_2 for the last 65 Ma is reconstructed from marine and terrestrial proxies complied by Beerling and Royer (2011) (see for details and data references;additional boron CO_2 proxy data from (Pearson and Palmer, 2000) are also included). Individual proxy methods are colour-coded. Errors represent reported uncertainties (plotted with 2 standard deviation uncertainity; see also Table 5.1 for assessment of confidence of proxies). Most of the data points for CO_2 proxies are based on duplicate and multiple analyses. The blue line is a median filter of all the data points with a time window of 5 Myr plotted from 46 to 30 Ma, and 1 Myr from 30 Ma to present. Shaded grey areas (from left to right) highlight past periods of global warmth during the Early Eocene (about +10°C global mean) and the early to mid Pliocene (about +3°C global mean) (see also Figure 5.3).

[INSERT FIGURE 5.3 HERE]

Figure 5.3: Comparison between paleoclimate proxy data and climate model output for **a)** SST, **b)** zonal mean meridional SST gradient, **d)** zonal mean meridional surface air temperature (SAT) gradient, and **e)** SAT anomalies for the Early Eocene Climatic Optimum (EECO, top row), the Mid-Pliocene Warm Period (MPWP, middle row) and the LGM (bottom row). Model temperature anomalies are calculated relative to the preindustrial value of each model in the ensemble* prior to calculating the multi model mean anomaly (a, e; colour shading). Zonal mean anomalies of the multi model mean (b, d) are plotted with a shaded band indicating 2 standard deviation uncertainity. Site specific temperature anomalies estimated from proxy data are calculated relative to present site temperatures and are plotted (a, e) using the same colour scale as the model data, and a circle size scaled to estimates of confidence. In the zonal plots (b, d) the proxy data anomalies are shown with error bars indicating 2 standard deviation uncertainity. Temperature proxy data compilations for the LGM are from MARGO Project Members (2009) and Bartlein et al. (2011), for the MPWP are from Dowsett et al. (submitted) and Salzmann et al. (2008), and for the EECO are from Hollis et al. (submitted). Polar amplification at each latitude **c)** is calculated as the zonal mean SST or SAT anomaly (b, d), normalised to the global mean temperature anomaly, and is plotted with shaded bands indicating 2 standard deviation uncertainity for each of the time periods. Global mean SST and SAT anomaly calculated from the model ensembles for each time period are shown as a number in **b)** and **d)**, respectively.
*Model ensembles include for: (i; LGM) PMIP3 ensemble; MIROC, CCSM4, AWI, MPI (ii; MPWP) PlioMIP ensemble; MIROC, NCAR, GISS, HadCM3 (Dowsett et al., submitted; Pope et al., 2011) (iii. EECO) EoMIP ensemble; HadCM3L, ECHAM5, CCSM3, GISS (Heinemann et al., 2009; Lunt et al., 2010b; Roberts et al., 2009; Winguth et al., 2010).

[INSERT TABLE 5.1 HERE]

Table 5.1: Summary of atmospheric CO_2 proxy methods and confidence assessment of their main assumptions.

[INSERT TABLE 5.2 HERE]

Table 5.2: Summary of SST proxy methods and confidence assessment of their main assumptions.

[START BOX 5.1 HERE]

Box 5.1: Polar Amplification

Polar amplification refers to the greater surface temperature change in polar regions compared with the global average in response to climate forcing. Instrumental temperature records show that the Arctic (Bekryaev et al., 2010) and the Antarctic Peninsula (Turner et al., 2005; Turner et al., 2009) are experiencing the strongest warming trends (0.5°C per decade over the past 50 years), almost twice larger than for the hemispheric or global mean temperature (Lemke et al., 2007). West Antarctic temperature also displays a warming trend of about 0.1°C per decade over the same time period (O'Donnell et al., 2010; Steig et al., 2009).

It is not entirely clear whether the polar amplification in the Arctic amplification is mainly caused by the sea ice/ocean system, in agreement with recent observations (Chylek et al., 2009; Polyakov et al., 2010; Screen and Simmonds, 2010; Semenov et al., 2010; Serreze et al., 2009; Spielhagen et al., 2011), or by atmospheric processes, such as increased downward long wave radiation (Graversen and Wang, 2009; Lu and Cai, 2009), water vapour and clouds (Graversen and Wang, 2009; Screen and Simmonds, 2010), or changes in atmospheric dynamics (Langen and Alexeev, 2007; Lu and Cai, 2009) as well as local radiative feedbacks linked with snow (Ghatak et al., 2010), and land surface vegetation changes (Bhatt et al., 2010). There are indeed several mechanisms that contribute to polar amplification, many of which were identified in early modelling studies (Manabe and Stouffer, 1980). The surface albedo feedback associated primarily with surface temperature driven albedo changes in sea ice and snow covered regions as well as the feedback related to the insulation effect of sea ice amplify surface temperature change near the poles (Soden et al., 2008). The longwave radiation feedback associated with surface temperature driven changes and the top of atmosphere longwave radiative loss to space opposes surface warming at all latitudes, but less so in the Arctic (Soden et al., 2008; Winton, 2006). Rising temperature globally is expected to increase the latent heat transport by the atmosphere into the Arctic (Kug et al., 2010), which warms primarily the lower troposphere. On average, CMIP3 models simulate enhanced latent heat transport (Held and Soden, 2006), but north of about 65°N, the sensible heat transport declines enough to more than offset the latent heat transport increase (Hwang et al., 2011). Ocean heat transport also plays a role in the simulated Arctic amplification, with both high late 20th century transport (Mahlstein and Knutti, 2011) and increases over the 21st century (Bitz et al., 2011) associated with higher amplification. Each of these mechanisms has specific fingerprints in the seasonality, latitudinal and vertical structure of temperature changes. Detection/attribution studies conducted for the Arctic and Antarctic (Gillett et al., 2008) concluded that human influence dominated the recent polar warming (see Chapter 10).

When forced by increasing concentrations of atmospheric GHG, climate models consistently simulate strong polar amplification (Bengtsson et al., 2004; Holland and Bitz, 2003; Masson-Delmotte et al., 2006; Meehl et al., 2007; Miller et al., 2010; Polyakov et al., 2002; Serreze and Francis, 2006) showed that, in climate model simulations covering the 20th and 21st centuries, polar amplification is primarily an Arctic phenomenon. The magnitude of polar amplification is of concern due to its impacts on polar ice sheet stability and sea level (see Chapter 13) and for the carbon cycle feedbacks for instance linked with permafrost melting (see Chapter 6).

Paleoclimate reconstructions allow model-data comparisons for latitudinal temperature changes and polar amplification under different climate states, such as high CO_2 worlds, glacial and interglacial climates. However, it should be noted that these past climate states correspond to different boundary conditions and forcings. The presence of glacial ice sheets induces a large radiative perturbation at high northern latitudes. During past interglacials, orbital forcing induces large changes in seasonal and latitudinal distribution of insolation, without significant changes in global mean radiative forcing and temperature. Figure 5.3 provides estimates of global and zonally-averaged latitudinal surface temperature anomalies and evaluates polar amplification for different time slices during the Cenozoic (LGM, MPWP and ECCO), representing a range of different atmospheric CO_2 concentrations. A difficulty in developing these temperature anomaly

comparisons is that for most intervals only a limited number of sites are available with quantitative proxy estimates of past temperatures, and the vast majority of these sites reflect most likely summer temperature estimates. Commonly hemispheric anomalies during warmer times are generated using climate models driven by known forcings, or by using data constrained model output approaches (Dowsett et al., 2005; Dowsett et al., submitted; Huber and Caballero, 2011; Masson-Delmotte et al., 2006; Otto-Bliesner et al., 2009). A consistent feature of GCMs and temperature proxy reconstructions are: that for warmer (Eocene and Pliocene) climate states pole-equator temperature gradients are significantly reduced, and for both past high and low CO_2 worlds, polar amplification is two to three times the global mean. Polar ampolification is unequivocal in SAT, but not resolved in SST due to the presence of high-latitude sea ice (Figure 5.3). Comparisons between proxy and GCM temperature reconstructions for these past times are addressed in more detail in Sections 5.3.1 (EECO, MPWP), 5.3.4 (LIG, Holocene), and 5.4.1 (LGM), respectively.

[END BOX 5.1 HERE]

5.3.2 Glacial Climate Sensitivity and Feedbacks

Glacial climates have been studied to better understand large magnitude changes in climate, validate climate model results, and estimate the climate sensitivity. The LGM is known to be relatively stable, the signal of the response is large enough compared to the internal variability and uncertainties in the proxy calibrations and dating, and both the response and the forcing (see Section 5.2) are clearly identified in reconstructions (Braconnot et al., 2007a; Braconnot et al., 2007b). Numerous new reconstructions have been completed since the AR4. Proxies used in glacial climate reconstructions include isotope-based temperature proxies in Antarctic ice cores (Masson-Delmotte et al., 2008) and ocean circulation, temperature, and salinity proxies (Butzin et al., 2005; Tagliabue et al., 2009). The MARGO SST reconstruction (MARGO Project Members, 2009), the most recent synthesis of the LGM SST, employed multiple proxy approaches to revise and refine previous synthesis efforts such as CLIMAP (CLIMAP Project Members, 1976, 1981) and GLAMAP (Sarnthein et al., 2003a; Sarnthein et al., 2003b). These LGM temperature reconstructions indicate a mean global temperature decrease of 5°C, with a tropical decrease in temperature of about 2°C (MARGO Project Members, 2009), a decrease in Antarctic temperatures of about 10°C (Stenni et al., 2010), and much larger decreases of Greenland temperature of 20–25°C (Köhler et al., 2010; Rohling et al., 2009; Siddall et al., 2010). The overall pattern of reconstructed tropical SST during the LGM generally is well simulated by atmosphere-ocean coupled GCMs except in regions of tropical upwelling, regions that also have biases in simulations for the present-day (Otto-Bliesner et al., 2009). In addition, questions remain regarding the temperature simulation of Antarctica, which may be the result of overestimation of ice sheet topography, an important boundary condition to the models (Masson-Delmotte et al., 2008). New ice sheet reconstructions based on several different methods (Lambeck et al., 2010a; Tarasov and Peltier, 2007) are introduced for PMIP3 climate model simulations, which are underway and the results of which may help clarify the relation between polar and global temperatures.

Climate sensitivity is estimated or constrained using paleoclimate data in three fundamental ways (Edwards et al., 2007), see also Chapters 9 and 10). First, climate sensitivity can be estimated using a pair of observed radiative forcing and the observed climate response to the radiative forcing (Edwards et al., 2007). In this method, there is an important assumption; i.e., the climate response to a certain amount of radiative forcing is the same even under different climate states (warm or cold climate), even though there is no guarantee that the climate sensitivity is independent on forcings and climate state. Second, multi-model simulations have been compared to proxy data (Otto-Bliesner et al., 2009; Schmittner et al., submitted), including models having structural differences, to show that the ratio of model climate sensitivity (LGM vs. 2 x CO_2) ranges from 0.6 to 2, which is mainly dependent on the cloud feedback through short wave radiation (Crucifix, 2006) (see Figure 5.4). Dust and vegetation are in many cases not included in these model runs because it is still difficult to take them into account in the models and there is still an uncertainty in their radiative forcing, although both processes contribute to increase the climate sensitivity through amplifying the temperature change (Lambert et al., 2008; Maher et al., 2010; Mahowald et al., 2006; McGee et al., 2010; Takemura et al., 2009; Winckler et al., 2008) (see Section 5.2.2.3). Climate sensitivity derived from the LGM experiments is therefore more likely overestimated than underestimated (Otto-Bliesner et al., 2009). Third, the physics perturbed ensemble method using a single climate model is used. Analyses which use EMIC and EBM based atmospheric model suggest a value for the climate sensitivity of around 2–3°C (Schmittner et al., submitted;

Schneider von Deimling et al., 2006). However, work using more complex models such as GCMs suggest that the response to large positive and negative radiative forcings may not be as linear as assumed in simple models (Crucifix, 2006; Hargreaves et al., 2007; Yoshimori et al., 2011). At least in some GCMs, positive forcing leads to a much larger temperature change than negative forcing of the same magnitude. It is, therefore, not possible to establish tight bounds on the climate sensitivity using only data from past climates colder than the present, although values in excess of 6°C for a doubling of atmospheric CO_2 content are difficult to reconcile with our existing understanding.

[INSERT FIGURE 5.4 HERE]

Figure 5.4: Strengths of feedbacks at LGM from data and multi-model ensembles. [PLACEHOLDER FOR SECOND ORDER DRAFT: PMIP3 models, others to be included.] Relation of feedback parameters between CO_2 doubling (2 x CO_2) and LGM climate simulations: **a)** scatter plot of climate feedback parameter (stratosphere-adjusted radiative forcing divided by the equilibrium temperature change); **b)** scatter plot of shortwave cloud feedback parameter (i.e., shortwave component of feedback parameter attributable to the change in clouds); **c)** zonal mean surface air temperature change for LGM, LGMGHG, and LGMICE experiments with respect to the preindustrial reference simulation. Here, LGMGHG refers to the experiment with CO_2 concentration being lowered to the LGM level while LGMICE refers to the experiment with prescribed LGM ice sheets and orbital parameters; and **d)** individual feedback parameters for 31-member physics parameter ensembles (PPE). In **a)** and **b)**, solid circles are for 4 Atmosphere-Ocean GCMs and blue (+) and (x) are for MIROC3.2 T42 and T21 Atmosphere GCM-slab ocean model PPE. Also plotted are the one-to-one lines. In **d)**, WV, LR, A, CSW, CLW denote water vapor, lapse-rate, surface albedo, shortwave cloud, and longwave cloud feedbacks, respectively. ALL denotes sum of all feedbacks. Data are obtained from Crucifix (2006), Yoshimori et al. (2009), and Yoshimori et al. (2011).

5.3.3 Earth System Response to Orbital Forcing During Glacial-Interglacial Cycles

Antarctic ice cores remain a significant source of information on orbital-scale climate variations over the past 800 kyr (Jouzel et al., 2007; Landais et al., 2010; Loulergue et al., 2008; Wolff et al., 2010). Since AR4, new datasets of atmospheric composition from Antarctic ice cores have helped to determine the magnitude and time-evolution of global radiative forcings, providing constraints on past climate sensitivity (Köhler et al., 2010) and carbon cycle-climate feedbacks (Lemoine, 2010). Antarctic ice-core data reveal a strengthening of the interglacial-glacial amplitude around to 400 ka, as well as a change in the relationship between Antarctic temperature and radiative forcing by GHG (Lang and Wolff, 2011; Masson-Delmotte et al., 2010a). Orbital-scale variability in GHG concentrations over the last several hundred thousand years covary (Figure 5.5) with proxy climate records including reconstructions of global ice-volume (Lisiecki and Raymo, 2005), climatic conditions in central Asia (Prokopenko et al., 2006), tropical (Herbert et al., 2010) and Southern Ocean SSTs (Lang and Wolff, 2011; Pahnke et al., 2003), deep ocean temperatures (Elderfield et al., 2010), biogeochemical conditions in the North Pacific (Jaccard et al., 2010), and deep ocean ventilation (Lisiecki et al., 2008). A detailed physical understanding of these covariations and their relationship to orbital forcing and GHG concentrations is still lacking.

During the last 800 kyr glacial-interglacial variability is characterized by dominant 100-kyr cyclicity and strong asymmetry between growth and decay of large continental ice sheets cycles (Lisiecki and Raymo, 2007). The nature of the 100-kyr cycles and the driver of glacial terminations remain debatable. It was suggested that late Pleistocene terminations are related to obliquity (Drysdale, 2009; Huybers and Wunsch, 2005). Alternatively, a new Antarctic ice core orbital age scale (Kawamura et al., 2007) and precise dating of the last four terminations in cave stalagmites from China (Cheng et al., 2009) were used to support that northern hemisphere deglaciations are driven by northern hemisphere summer insolation, i.e., primarily by precessional variations. In addition, analysis of ice volume variations show a tight phase relationship between the eccentricity variations and glacial cycles (Lisiecki, 2010).

Antarctic temperatures closely match atmospheric CO_2 concentration during last 800 kyr, which reflects the fact that CO_2 explains a large portion of annual mean glacial-interglacial temperature variations in Antarctica due to the greenhouse effect (Timmermann et al., 2009). At the same time it was found that during several most recent terminations, Antarctic temperature variations led changes in atmospheric CO_2 concentration by hundreds to several thousand years (Siegenthaler et al., 2005). This apparent lead of Antarctic warming compared to CO_2 rise can be explained by the bipolar seesaw response to a weakening of the AMOC during glacial terminations (Ganopolski and Roche, 2009) or as a result of early SH warming due to local insolation change (Timmermann et al., 2009) and therefore does not challenge the principal role of CO_2 variations in

driving Antarctic temperature. Antarctic temperature records also contain strong variation at the obliquity time scale (Jouzel et al., 2007) which likely results from the direct effect of obliquity on annual mean insolation (Mantsis et al., 2011). At the same time, the role of local orbital forcing in driving Antarctic temperature variability at the eprecessional time scale remains less certain. The coincidence between maxima in boreal summer insolation (Kawamura et al., 2007), length of the austral summer season (Huybers, 2009; Huybers and Denton, 2008) and austral spring insolation (Stott et al., 2007; Timmermann et al., 2009) has made it difficult to attribute the reconstructed Antarctic temperature variations to any one of these forcings.

Recent modeling work provides further support for the notion that variations in Earth's orbital parameters produce considerable effects on Earth's climate. In particular, in the high northern latitudes, summer temperatures can differ by up to 10°C between climate states corresponding to different orbital configurations. The largest changes in seasonal variations are caused by changes in precession (Braconnot et al., 2007b) while changes in obliquity cause synchronous variations in annual temperatures in high latitudes of several degrees (Mantsis et al., 2011). Experiments with general circulation models support the principal conjecture of Milankovitch theory that a reduction in summer insolation produces sufficient cooling to initiate ice sheet growth (Herrington and Poulsen, in press). Together with fast climate feedbacks amplifying the direct effect of the orbital forcing, carbon cycle (see Chapter 6), vegetation (Vavrus et al., 2008), oceanic (Born et al., 2010), and ice sheet feedbacks (see Box 5.3) might also play an important role for glacial inceptions. At the same time, it was proposed that the impact of aeolian dust deposition on snow and ice albedos may restrict ice sheet growth in areas with high rates of dust deposition (Krinner et al., 2006).

Experiments performed with climate-ice sheet models forced by orbital variations and reconstructed atmospheric CO_2 concentrations demonstrate that the models are able to simulate ice volume and other climate characteristics during the last and several previous cycles in agreement with paleoclimate data (Abe-Ouchi et al., 2007; Bonelli et al., 2009; Ganopolski et al., 2010) (see Figure 5.5). Moreover, in agreement with earlier simulations of glacial cycles (Pollard, 1982), it has been shown that 100 kyr cyclicity can be simulated with a constant CO_2 concentration, if the latter is below a typical interglacial value (Berger et al., 1999; Crowley and Hyde, 2008; Ganopolski and Calov, Submitted). However, the amplitude of 100 kyr ice volume cycles with constant CO_2 is smaller than suggested by reconstructions. Therefore, there is high confidence that CO_2 plays an important role in amplification of the glacial cycles, but how this positive feedback operates during different stages of glacial cycles is not yet well understood (see Chapter 6).

Paleoclimate records show that the dominant periodicity of the glacial cycles changed from 41 kyr to 100 kyr beween around 1.3 Ma and 0.7 Ma (the so-called Mid Pleistocene Transition, MPT) (Clark et al., 2006). The mechanisms of this transition is not well-understood and proposed explanation include gradual lowering of CO_2 concentration during Pleistocene (Berger et al., 1999; Crowley and Hyde, 2008; Saltzman and Verbitsky, 1993) or changes in subglacial conditions due to glacial erosion of a thick regolith layer (Clark and Pollard, 1998; Clark et al., 2006; Ganopolski and Calov, Submitted). The lack of significant precessional variability in benthic $\delta^{18}O$ records prior to the MPT poses an apparent problem for classical Milankovitch theory. Several alternative hypotheses explaining the absence of a precessional benthic $\delta^{18}O$ signal prior to MPT were proposed (Huybers, 2006; Raymo et al., 2006) but remain to be tested with comprehensive climate-ice sheet models.

[INSERT FIGURE 5.5 HERE]

Figure 5.5: Orbital forcing and proxy records over the past 800 kyr. **a)** Maximum summer insolation at 65°N (Berger and Loutre, 1991), **b)** the atmospheric concentration of CO_2 from Antarctic ice cores (Ahn and Brook, 2008; EPICA Community Members, 2004; Petit et al., 1999), **c)** Greenland temperature reconstructed from $\delta^{18}O$ in NGRIP ice core (North Greenland Ice Core Project members, 2004), **d)** the tropical SST stack (Herbert et al., 2010), **e)** the of Antarctic temperature stack based on up to seven different ice cores (Barbante et al., 2006; Blunier and Brook, 2001; Jouzel et al., 2007; Petit et al., 1999; Stenni et al., 2011; Watanabe et al., 2003), **f)** the stack of benthic $\delta^{18}O$, a proxy for global ice volume and deep ocean temperature (Lisiecki and Raymo, 2005), **g)** the reconstructed sea level (Waelbroeck et al., 2002). Solid lines represent orbital forcing and proxy records, dashed lines depict results of simulations with climate and climate-ice sheet models forced by variations of the orbital parameters and the atmospheric concentrations of the major GHG. Short dashed line - CLIMBER-2 (Ganopolski et al., 2010), long dashed line - IcIES (Abe-Ouchi et al., 2007), dotted line - Bern3D (Ritz et al., 2011) . Note the change of the time scale at 140 ka.

5.3.4 Past Interglacials

Past interglacials allow us to place current changes in the perspective of climate variability and understand past responses and natural feedbacks. Since AR4, new global quantitative data syntheses and multi-model comparisons have added to our assessment of the Last Interglacial (LIG), which extended from about 130 ka to 116 ka (Stirling et al., 1998a). No systematic simulations have been conducted for earlier interglacials and therefore assessments of model-data comparison are not yet useful.

Several recent compilations from marine, ice, and terrestrial archives, with updated age models, have provided an expanded view of the overall geographic patterns and strengths, though not temporal phasing because of the quality of the age controls, of earlier interglacials of the last 800 kyr (Jouzel et al., 2007; Lang and Wolff, 2011; Rohling et al., accepted). These reconstructions confirm implications from the EPICA Dome C Antarctic ice core record that the stronger interglacials of the last 425 kyr are a globally robust feature. Cooler, earlier interglacials (Jouzel et al., 2007) are consistent with higher ice volumes and reduced atmospheric concentration in GHG (Masson-Delmotte et al., 2010a; Tzedakis et al., 2009). The mechanisms for explaining differences in the mean intensity of past interglacials is not fully understood with a connection to the phase between precession and obliquity through time (Yin and Berger, 2010), long term changes in obliquity (Jouzel et al., 2007) and strength of the preceding glacial (Lang and Wolff, 2011) proposed.

The additive effects of large obliquity, which reached its maximum at 131 ka, large eccentricity, and the precessional parameter, which reached a minimum at 127 ka, (Figure 5.2) resulted in large positive insolation anomalies during boreal summer in the NH and austral spring in the SH. Global mean annual temperature (MAT) estimated from syntheses of terrestrial, marine and ice core data indicate with medium confidence a LIG about 2°C warmer than preindustrial (Clark and Huybers, 2009; Turney and Jones, 2010). Uncertainties include seasonality of biological proxies, which may be biased systematically towards summer conditions, and data scarcity over continental areas of North and South America, Africa, and Australia. Warming is widespread at middle to high latitudes of both hemispheres with little MAT change at low latitudes (Figure 5.6). MAT increases of more than 5°C are indicated over an extensive region of the northern continents. In Europe, annual warming coincides with strong warming in summer accompanied by smaller warming in winter (Brewer et al., 2008). The North GRIP ice core stable isotope record suggest a precipitation-weighted annual warming of at least 5°C, though some of the signal may be representing a reduced elevation of the central Greenland ice sheet (Masson-Delmotte et al., 2011) (Section 5.5.2). The Greenland warming is consistent with abundance of boreal forest pollen (de Vernal and Hillaire-Marcel, 2008) and isotope ratios of silt-fed sediment (Colville et al., 2011) in ocean cores off southern Greenland suggesting greater southern ice sheet retreat during the LIG than the early Holocene. East Antarctica ice cores suggest exceptionally warm early LIG temperatures, possibly more than 5°C warmer than present (Jouzel et al., 2007; Sime et al., 2009; Stenni et al., 2010).

The LIG is the strongest interglacial in marine records of the last 800 kyr (Lang and Wolff, 2011; Masson-Delmotte et al., 2010a). Global SST warming is estimated with medium confidence to be no more than 1°C, with thermosteric sea level rise above present unlikely to have exceeded 0.4 ± 0.3 m (McKay et al., 2011). SST were consistently much warmer during the LIG at latitudes north of 30°N, while south of 30°N the anomalies were regionally variable. Evidence, though fragmentary, indicates seasonally open water off northern Greenland and in the central Arctic at some time during the LIG (Adler et al., 2009; Nørgaard-Pedersen et al., 2007; Polyakov et al., 2010). The ocean warming may not have been globally synchronous, with regional features indicating early warmth (132–128 ka) in the Southern Ocean followed by a about 3 kyr to 5 kyr later establishment of peak warmth in the North Atlantic and Nordic Seas (Bauch et al., 2011; Govin et al., Submitted; Van Nieuwenhove et al., 2011).

New LIG climate model simulations have been completed since the AR4. The global MAT change predicted by these models is near zero, ranging from −0.4 to +0.3°C. Simulations for the mid-LIG (125 ka) capture the pattern of NH extratropical warming but not the magnitude (Figure 5.6). Simulations which predict vegetation indicate that feedbacks with natural land surface changes are important for reproducing the observed warmth (Schurgers et al., 2007). Model sensitivity studies also suggest that current models may not consistently fully capture changes in clouds, sea ice, large-scale circulation, and Greenland ice sheet elevation that could amplify the warming (Fischer and Jungclaus, 2010; Groll and Widmann, 2006; Kaspar et al., 2007; Kim et al., 2010). Of relevance for future projections, summer NH changes have been shown to have comparable magnitudes and climate feedbacks for 2 x CO_2 as for LIG (Masson-Delmotte et al., 2011). Models also underestimate the annual mean warming in central Antarctica in response to orbital forcing

only. There are two different mechanisms proposed to explain high LIG Antarctic temperatures but assessment with models is currently limited. The temperature overshoot at the beginning of the LIG and some previous interglacials is consistent with a bipolar seesaw response to the termination of the previous glacial (Ganopolski and Roche, 2009; Masson-Delmotte et al., 2010a; Masson-Delmotte et al., 2010b). The disintegration of the Western Antarctic Ice Sheet (WAIS), as a result of warming of the Southern Ocean provided by a bipolar seesaw response and/or insolation-warmed North Atlantic Deep Water conveying heat to the Circumpolar Deep Water around Antarctica (Duplessy et al., 2007), has been invoked to explain the high Antarctic temperatures during the rest of the LIG (Holden et al., 2010).

The current interglacial, the Holocene extending from 11.7 ka to the present, lacks a strong global or latitudinal temperature change. New transient climate model simulations indicate a spatial and temporal complexity associated with weaker orbital forcing than the LIG and impacts of regional remnants of the LGM ice sheets (Section, 5.4.1.2, Figure 5.10). Many of the glacier changes in the NH and SH are consistent with the orbital forcing but with exceptions associated with dynamic responses to the solar insolation changes (Box 5.2).

[INSERT FIGURE 5.6 HERE]

Figure 5.6: Model-data comparison of annual mean surface temperature anomalies for the Last Interglacial. Top panel are proxy data estimates of Turney and Jones (2010) and McKay et al. (2011). McKay et al.(2011) calculated an annual anomaly for each record as the average SST of the 5 kyr period centered on the warmest temperature between 135 ka and 118 ka and then subtracting the average SST of the late Holocene (5 ka to 0 ka). Turney and Jones (2010) calculated the annual temperature anomalies relative to 1961–1990 CE by averaging the LIG temperature estimates across the isotopic plateau in the marine and ice records and the period of maximum warmth in the terrestrial records. In both reconstructions the anomalies are not necessarily synchronous in time geographically. Middle and bottom panels are respectively annual and June-July-August multi-model averages, left, and standard deviations, right, of model simulations for 125ka. Two models are assessed: CCSM3 and HadCM3. [Note: more model simulations and estimate of spread are expected for the SOD].

5.3.5 Global and Hemispheric Temperature Variations During the Last 2000 Years

Research focused on hemispheric and global temperatures is important for a better understanding of the climate response to external forcings, since changes at regional scales (Section 5.4) and in atmospheric circulation, that link regional to larger-scale changes (Section 5.4.3), may be more strongly influenced by internal variability. Expanded proxy data networks and better understanding of existing and newly developed reconstruction methods have supported a more complete characterization of the uncertainties (Section 5.3.5.1) associated with hemispheric and global surface temperature changes during the last 2000 years as well as more extensive comparisons with GCM simulations (Section 5.3.5.2).

5.3.5.1 Limitations and Uncertainties

Reconstructing NH, SH or global-mean temperature variations over the last 2000 years remains a challenge due to limitations of the individual proxy records and in the statistical methods used to calibrate and integrate multi-proxy information (Frank et al., 2010; Jones et al., 2009). Since AR4, there has been development of statistical methods that use simple compositing and scaling of local or regional temperature sensitive proxy records into global or hemispheric averages using uniform or proxy-dependent weighting (Christiansen, 2011; Hegerl et al., 2007; Juckes et al., 2007; Ljungqvist, 2010; Mann et al., 2008) or by using climate field reconstruction methods (Ljungqvist et al., Submitted). The latter apply temporal and spatial relationships between instrumental and proxy records to the pre-instrumental period. New developments for both of the above approaches include Bayesian hierarchical methods (Li et al., 2010a; McShane and Wyner, 2011; Tingley and Huybers, 2010) that a priori specify simple parametric forms for the proxy-temperature relationships and allow for the estimation of a probability distribution of temperature evolutions that are compatible with the available proxy and instrumental data.

An improved understanding of potential reconstruction method uncertainties and biases has been achieved, particularly through using millennial GCM simulations as a surrogate reality in which pseudo-proxy records are created and reconstruction methods are replicated and tested (Bürger et al., 2006; González-Rouco et al., 2009; Mann, 2007; Smerdon et al., 2010). A key finding is that some published reconstructions are likely to underestimate the overall amplitude of past temperature change (Christiansen et al., 2009; Lee et al., 2008;

Riedwyl et al., 2009; Smerdon and Kaplan, 2007; Smerdon et al., 2011). The magnitude of this amplitude attenuation in real-world reconstructions is uncertain but will be larger for: a) cases with weaker correlation between instrumental temperatures and proxies (a lower signal-to-noise ratio; Christiansen et al., 2009; Lee et al., 2008; Smerdon et al., 2011); b) if errors in the proxy data are assigned (perhaps implicitly) to the temperature data (Ammann et al., 2010); or c) if the data are detrended in the calibration phase (Lee et al., 2008; Mann, 2007). The 20th century trends in proxies may contain relevant temperature information (Ammann and Wahl, 2007), but contamination of the proxy trend by non-climatic influences cannot be excluded (von Storch et al., 2006). Recent developments to mitigate the loss of low-frequency variance in global and hemispheric reconstructions have been made (though regional errors in areas such as the equatorial Pacific with few proxies may remain in field reconstructions (Smerdon et al., 2011). These developments include applying local inverse calibrations and then averaging (Christiansen, 2011), increasing the correlations between proxies and temperature through temporal smoothing (Lee et al., 2008), or assigning part or all of the temperature-proxy error to the proxy data (Hegerl et al., 2007; Juckes et al., 2007; Mann et al., 2008).

New developments in data assimilation experiments (Crespin et al., 2009; Goosse et al., 2010; Luterbacher et al., 2010; Widmann et al., 2010) in which millennium simulations are nudged or selected to follow local and regional proxy-based reconstructions, as well as Bayesian methods, can facilitate a process-based understanding of past climate variations at regional scales (Section 5.4). The resulting simulations are dependent on the assimilated proxy data and specified external forcing and have limited value for independent data-model comparisons, but they provide useful insight into the relative roles of internal variability and external forcing.

Two fundamental limitations for deriving past temperature variability at global/hemispheric scales are the relatively short instrumental period and the number, geographical distribution, reliability and climate signal of proxy records (Jones et al., 2009; McShane and Wyner, 2011). The database of high-resolution proxies has been expanded since AR4 (Mann et al., 2008; Wahl et al., 2010) (see new developments in Section 5.4), but data are still sparse in the tropics, SH and over the oceans. The short instrumental period and the paucity of proxy data in specific regions may preclude obtaining accurate estimates of the covariance of temperature and proxy records (Juckes et al., 2007). In climate field reconstructions the sparsity of proxy data may lead to regional errors in areas such as the equatorial Pacific with low proxy availability (Smerdon et al., 2011).

Additional sources of uncertainty that are currently not fully considered include the influence of structural uncertainties by using a range of statistical reconstruction methods and their parameter space (Frank et al., 2010) and considering non-stationarity in proxy-climate relationships(e.g., Sturm et al., 2010). An example of the latter is the divergence between some tree ring chronologies and instrumental temperatures during the latter decades of the 20th century (Briffa et al., 1998). This phenomenon does not affect all tree ring records (Esper and Frank, 2009; Wilson et al., 2007b), and a number of factors may contribute to those records that do show divergence, including drought stress, non-linear responses to warming, delayed snowmelt, and changes in seasonality and reductions in solar radiation (D'Arrigo et al., 2008; Porter and Pisaric, 2011).

5.3.5.2 Reconstruction and Simulation of Global and Hemispheric Temperatures

Large-scale temperature reconstructions published since AR4 (Figure 5.7; Table 5.3) suggest greater overall amplitude of NH temperature and stronger evidence that the MCA (illustrated here as 950–1250 CE) and the 20th century were warmer than the average over the last 1000 or even 2000 years, while the LIA (illustrated here as 1450–1750 CE) was significantly cooler. Comparison of the relative warmth of the MCA and modern periods is still problematic due to considerable uncertainties (Table 5.3). Combining instrumental temperatures with the proxy-based reconstructions (including their published confidence intervals and considering the existence of unquantified sources of error), the 50-year mean NH temperature for 1961–2010 was very likely warmer than any previous 50-year mean in the last 800 years. Evidence for modern warming (Chapter 2) is more extensive seasonally and geographically than the evidence for Medieval warmth and provides medium confidence that 1961–2010 was the warmest 50-year period in the last 1300 years.

The number of GCM simulations of the last millennium has increased since AR4 (Hofer et al., 2011; Jansen et al., 2007; Jungclaus et al., 2010; Servonnat et al., 2010; Swingedouw et al., 2011), complemented by the PMIP3/CMIP5 standardized experiments (Schmidt et al., 2011). The simulations have used different

estimations of natural and anthropogenic forcings; in particular the PMIP3/CMIP5 simulations are driven by weaker solar irradiance variations than many of the earliear experiments (Section 5.2; Figure 5.1). Simulated NH temperatures lie mostly within the uncertainties of the available reconstructions during the last millennium (Figure 5.7a). While this is illustrative of the agreement between GCMs and reconstructions, it is not very discriminating since models with different climate sensitivities might appear to be consistent with depicted uncertainty ranges because of internal variability and uncertainties in the forcings and reconstructions.

Figure 5.7b-d provide additional tests of model-data agreement by compositing the temperature response to a number of distinct forcing events, as well as giving insight into the response to different forcings. The models simulate a significant cooling for the NH in response to individual volcanic events (Figure 5.7b-c; peaks between 0.07°C and 0.39°C depending on model) that lasts 3 to 5 years; reconstructions with annual resolution also show cooling on average (0.03°C to 0.31°C). Since many reconstructions do not have annual resolution, similar composites (Figure 5.7c) are formed to show the response to changes in multi-decadal volcanic forcings (representing clusters of eruptions). Both the simulated and reconstructed response are significant and comparable in magnitude, although simulations show a faster recovery after peak negative forcing (<5 years). Even at multi-decadal timescales, the solar forcing estimated over the last millennium shows weaker variations than volcanic forcing (Figure 5.7d, Section 5.2). Compositing the response to these weaker multi-decadal fluctuations in solar irradiance shows cooling in both simulations and reconstructions of NH temperature of between 0.0°C and 0.2°C or between 0.0°C and 0.1°C, respectively. In both cases cooling shows a double peak (aligned with the forcing change and lagged by 20 years), probably arising from concurrent variations in volcanic forcing (red line in Figure 5.7d).

Another measure of the amplitude of NH temperature variations during the last millennium is illustrated by the temperature differences between the MCA and the LIA (spatial pattern Figure 5.8; NH mean Figure 5.7e) and between the LIA and the 20th century (Figure 5.7f). The close correspondence between the multi-model and multi-reconstruction means hides a very wide range of individual results (NH mean temperature differences from less than 0.1°C to more than 0.8°C; see Figure 5.7e,f and 5.8b,e; see Chapters 9 and 10 for a comparsion of reconstructed and simulated variability across various frequency ranges). The simulated MCA-LIA spatial patterns show warmer MCA conditions almost globally, though the amplitude is heterogeneous and the pattern varies considerably between models (especially outside the tropics where the signal-to-noise ratio is smaller; Figure 5.8e, f). The simulated changes are much reduced with weaker solar variability, and the inter-model differences suggest that internal variability may have significantly influenced the MCA-to-LIA transition (Jungclaus et al., 2010). The simulated anomalies also differ from the reconstruction of Mann et al.(2009), particularly in the tropical Pacific.

[INSERT FIGURE 5.7 HERE]

Figure 5.7: Comparisons of simulated and reconstructed NH temperature change. **a)** Simulations shown by coloured lines (thick lines: multi-model-mean; thin lines: multi-model 90% range; red/blue lines: models forced by stronger/weaker solar variability, though other forcings and model sensitivities also differ between the red and blue groups); overlap of reconstructed temperatures shown by green shading; all data are expressed as anomalies from their 1500–1850 CE mean and smoothed. Note that some reconstructions represent a smaller spatial domain than the full NH or a specific season, while annual temperatures for the full NH mean are shown for the simulations. Superposed composites (time segments from selected periods positioned so that the years with peak negative forcing are aligned) of the forcing and temperature response to **b)** individual volcanic forcing events; **d)** multi-decadal changes in volcanic activity; **f)** multi-decadal changes in solar irradiance. Upper panels show the volcanic or solar forcing for the individual selected periods together with the composite mean (thick); in **d)**, the composite mean of the volcanic forcing (red) during the solar composite is also shown. Lower panels show the NH temperature composite means and 90% range of spread between simulations (dark red line, pink shading) or reconstructions (green line and shading), with overlap shaded in orange. Mean NH temperature difference between **e)** MCA (950–1250 CE) and LIA (1450–1750 CE) and **f)** 20th century (1900–2000) and LIA, from reconstructions (light green), multi-reconstruction mean and range (dark green), multi-model mean and range (brown), and simulations (red). Models forced by stronger/weaker solar variability are shown by circles/triangles; where an ensemble of simulations is available from one model, the ensemble mean is show in red and the individual ensemble members by brown circles. Results are sorted into ascending order and labelled. Further details are given in the supplementary material.

[INSERT FIGURE 5.8 HERE]

Figure 5.8: Average (AVG; a, d), standard deviation of the average (SD; b, e) and signal to noise ratio (SNR=|AVG|/SD); c, f) for the MCA-LIA annual temperature change in the ensemble of forced simulations of the last

millennium produced with different Atmosphere-Ocean GCMs, both for strong (a, b, c) and for weak (d, e, f) solar forcing variability levels. For the simulations starting in 1000 CE, the period 1000 CE to 1250 CE was selected to define the MCA. 10 (11) simulations provided by 6 (2) different GCMs have been used for the strong (weak) solar forcing ensemble. The contributing models have been CCSM3, CSIRO, CSM1.4, CNRM, ECHO-G, IPSL and the MPI-ESM. A list of the model simulations involved and main characteristics is provided in the supplementary material. All simulated fields were interpolated to the smallest resolution in the ensemble (i.e., R21 for the CSIRO simulations).

Table 5.3: Comparison of modern Northern Hemisphere temperature estimates (reconstructions or instrumental data) with earlier reconstructed values, using published uncertainty ranges to assess likelihood. Actual likelihood that modern temperatures are warmer than earlier temperatures will be significantly reduced by additional sources of error that are not included in the quantified uncertainties. Further descriptions of the reconstructions are provided in supplementary material. All years refer to CE.

Study	Likelihood assessment[1]	Warmest 20th century 50-year reconstructed mean compared with previous 50-year reconstructed means[2]	1961–2010 CE instrumental mean compared with 50-year reconstructed means
Leclercq and Oerlemans (2011)	Likely warmer than: Very likely warmer than:	All (back to 1600–1649) All (back to 1600–1649)	All (back to 1600–1649) All (back to 1600–1649)
Christiansen and Ljungqvist (Submitted)	Likely warmer than: Very likely warmer than:	All (back to 1000–1049) All (back to 1000–1049)	All (back to 1000–1049) All (back to 1000–1049)
Ljungqvist (2010)	Likely warmer than: Very likely warmer than:	1026–1075 onwards 1068–1117 onwards	All (back to 1–50) All (back to 1–50)
Mann et al. (2009)	Likely warmer than: Very likely warmer than:	N/A N/A	839–888 onwards 1054–1103 onwards
Mann et al. (2008)	Likely warmer than: Very likely warmer than:	(CPS) 559–608 onwards (EIV) N/A (EIV Land&Marine) N/A (CPS) 565–614 onwards (EIV) N/A (EIV Land&Marine) N/A	(CPS) All (back to 200–249) (EIV) 1058–1107 onwards (EIV) All (back to 300–349) (CPS) All (back to 200–249) (EIV) 1067–1116 onwards (EIV) 974–1023 onwards
Loehle and McCulloch (2008)	Likely warmer than: Very likely warmer than:	1404–1453 onwards 1415–1464 onwards	992–1041 onwards 1248–1297 onwards
Frank et al. 2007	Likely warmer than: Very likely warmer than:	All (back to 831–880) 1056–1105 onwards	All (back to 831–880) 977–1026 onwards
Hegerl et al. (2007)	Likely warmer than: Very likely warmer than:	All (back to 558–607) 1391–1440 onwards	All (back to 558–607) All (back to 558–607)
Juckes et al. (2007)	Likely warmer than: Very likely warmer than:	All (back to 1000–1049) 1073–1122 onwards	All (back to 1000–1049) All (back to 1000–1049)
Ammann and Wahl (2007)	Likely warmer than: Very likely warmer than:	1396–1445 onwards 1572–1621 onwards	All (back to 1000–1049) All (back to 1000–1049)
D'Arrigo et al. (2006)	Likely warmer than: Very likely warmer than:	All (back to 713–762) 721–770 onwards	All (back to 713–762) 721–770 onwards
Moberg et al. (2005)	Likely warmer than: Very likely warmer than:	1104–1153 onwards 1114–1163 onwards	All (back to 1–50) All (back to 1–50)
Pollack and Smerdon (2004)	Likely warmer than: Very likely warmer than:	All (back to 1500) All (back to 1500)	All (back to 1500) All (back to 1500)
Briffa et al. (2001)	Likely warmer than: Very likely warmer than:	All (back to 1402–1451) 1553–1602 onwards	All (back to 1402–1451) All (back to 1402–1451)

Notes:
[1]Modern temperatures (50-year means of the proxy reconstruction values or instrumental data) are considered likely (very likely) warmer than pre-1850 reconstructed values if they lie above a 50-year mean of the reconstructed values plus 0.42 SE (1.29 SE), where SE is the standard error of the reconstruction estimated from the published uncertainty range.
[2]If the 20th century reconstructed values were replaced by instrumental data, N/A is recorded.

5.4 Regional Changes and Phenomena

This section assesses past regional climate changes with a focus on selected time slices since the LGM and the most recent millennia, beginning with longer-term temperature changes, followed by changes in sea ice distribution, atmospheric circulation, including monsoonal systems, precipitation related changes and changes in prominent modes of variability.

5.4.1 Regional Temperature Changes

5.4.1.1 Last Glacial Maximum

A recent synthesis of marine proxy data for the LGM (MARGO Project Members, 2009), Figure 5.3 lower left panel, updates earlier estimates of marine temperatures (CLIMAP Project Members, 1976, 1981). Mean annual cooling is largest (up to −10 ºC relative to today) in the mid-latitude North Atlantic with the western Mediterranean also cooling significantly (−6 ºC). Seasonally ice free conditions were documented, however, in the northeastern North Atlantic and in the eastern Nordic Seas, in contrast to the widely used CLIMAP reconstruction which suggested perennial sea ice for these areas. Proxy-based reconstruction of the polar front in the Southern Ocean indicates a northward shift in position to 45ºS, associated with a −2ºC to −6ºC cooling during glacial austral summer relative to today. The tropical band (30ºS–30ºN) is characterized by the good convergence amongst the marine temperature proxies. Reconstruction of mean annual SST in the inner tropics (15ºS–15ºN) indicate cooling relative to today of −2.9 ± 1.3ºC in the Atlantic, −1.4 ± 0.7ºC in the Indian, and −1.2 ± 1.1ºC in the Pacific. Of particular significance is a cooling of 1ºC to 3ºC reconstructed for the western Pacific warm pool. MARGO reconstructs large longitudinal SST gradients for all of the ocean basins, in contrast to simulations of the LGM climate (Braconnot et al., 2007b; Kageyama et al., 2006). A recent pollen based synthesis of terrestrial climates during the LGM (Bartlein et al., 2011) generally show year-round cooling in most regions, with a few, so far unexplained, deviations in Alaska and in Africa. The compilation also document reduced hydrological cycle in Eurasia, North America and Africa during the LGM.

5.4.1.2 Early to Mid Holocene (about 10 ka to 2 ka)

Several high-latitude regions show higher reconstructed seasonal temperatures during the early to mid Holocene than in the late 20th century. Newer studies confirm the basic SAT distribution summarised in AR4. Since Holocene climate change largely results from orbitally driven changes in the seasonal distribution of solar insolation, the periods of higher temperatures than now were very likely caused by the associated orbital configuration and enhanced NH summer insolation (Jansen et al., 2007). Terrestrial early to mid Holocene summer season temperatures warmer than today are ubiquous in the mid to high latitude in both northern Eurasia and Northern North America, reflecting both warmer summers and winters (e.g., Bartlein et al., 2011; Wanner et al., 2008) (Figure 5.10). A new synthesis of Greenland ice core data reconstructs homogeneously 2°C to 3°C higher MAT over Greenland than preindustrial, as well as significant changes in ice sheet topography (Vinther et al., 2009). Marine records often indicate a muted Holocene SST warming (Lang and Wolff, 2011; Leduc et al., 2010). Discrepancies among different proxies suggest significant imprints of seasonality and regional oceangraphic dynamics on proxies (Leduc et al., 2010). The highest early to mid Holocene North Atlantic and sub-Arctic SSTs were restricted to the stratified uppermost surface ocean layer, below which no Holocene thermal maximum is detected (Andersson et al., 2010; Hald et al., 2007). In the high latitude Southern Ocean, SST trends follow the decrease in austral summer duration (Shevenell et al., 2011). Near surface temperatures in both hemispheres are characterized by high-amplitude, millennial to centennial scale variations, particularly after 5 ka to 4 ka (Euler and Ninnemann, 2010; Moros et al., in press; Risebrobakken et al., 2003; Shevenell et al., 2011). In monsoon regions, cooler MAT in winters follow reduced orbital insolation and in summers enhanced cloudiness (Bartlein et al., 2011).

Summer insolation anomalies in the NH peaked during the early Holocene with more than 8% greater insolation than today. In response to orbital forcing, PMIP2 coupled ocean-atmosphere models are able to produce the signs of temperature change observed for Europe but not the exact patterns and amplitudes (Brewer et al., 2007). At latitudes north of 40°N, atmosphere-ocean-sea ice feedbacks alter the direct effect of seasonal insolation changes such that maximum warming occurs in autumn and remains important for

moderating the winter responses (Otto et al., 2009b; Zhang et al., 2010). Northward shift of boreal and temperate forests are correctly reproduced in BIOME4 forced with PMIP2 simulations (Wohlfahrt et al., 2008) though the magnitude of the temperature-vegetation feedback may be less than previously thought (Otto et al., 2009a; Otto et al., 2009b).

The last 2 kyr has the densest coverage of proxy climate records with decadal or higher temporal resolution, particularly after 1500 CE. Here we focus on those reconstructions (Figure 5.11) that are most relevant to understanding the effects of dynamical and radiative influences on regional temperatures (Figure 5.8h; 5.9). No single mechanism accounts for the observed regional temperature anomalies associated with the MCA and LIA. Some model simulations (Jansen et al., 2007; Figure 5.8, 5.9) support a significant contribution to global and hemispheric temperature variations from solar irradiance changes (Section 5.3.5), though internal variability could also be important especially if solar variability is assumed to be weak (Jungclaus et al., 2010; Schmidt et al., 2011). Changes in the persistence or frequency of climate modes could explain some of the regional temperature anomalies (Diaz et al., in press; Graham et al., 2011; Graham et al., 2007; Mann et al., 2009; Seager et al., 2007; Seager et al., 2008; Trouet et al., 2009): more frequent La Niña-like conditions during the MCA have been proposed together with a dynamic link between Northern Hemisphere temperatures and Indo-Pacific Warm Pool hydrology (Oppo et al., 2009; Tierney et al., 2010b); changes in Atlantic SSTs may have led to warm conditions in northwestern Europe through SST-forced changes to large-scale circulation patterns such as the North Atlantic Oscillation (NAO). These ocean-atmosphere interactions could arise from combinations of internal variability and dynamical responses to solar irradiance and explosive tropical volcanism (e.g., Mann et al., 2005; Meehl et al., 2009). There is high confidence that the MCA was not characterized by concurrently warmer global temperatures, but rather by a range of temperature, hydroclimate and oceanic changes with distinct regional and seasonal expressions (Jansen et al., 2007).

5.4.1.3 Northern Hemisphere Mid to High Latitudes

Marine proxy records indicate warm SST north of Iceland from 1100 CE to 1400 CE, followed by a generally colder period that may have ended during the 20th century (Sicre et al., 2008), while further north in the Fram Strait, modern SST of the advected Atlantic Water appear warmer than those reconstructed for the last 2000 years (Spielhagen et al., 2011). Portions of the Arctic and sub-Arctic experienced warm periods during medieval times comparable to any subsequent period, except for the most recent decades (Kobashi et al., 2010; Spielhagen et al., 2011; Vinther et al., 2010).

Temperature reconstructions from tree ring records provide evidence for various regions (Western Himalayas, Tibetan Plateau, Tianshan Mountains and western High Asia) that partly fits the concepts of the MCA and LIA: warm conditions from the 11th to the 15th century, lower temperature afterwards and warming within the 20th century in the Western Himalaya (Esper et al., 2007a; Yadav et al., 2011; Zhang et al., 2009; Zhu et al., 2008). Late 20th century warmth in parts of China is likely unprecedented compared with the last 500 years; prior to this, 1000 year to 2000 year long cold and warm season temperature reconstructions (based on documentary evidence and natural proxies) consistently show warm conditions during the MCA but the large uncertainty precludes a quantitative comparison with modern temperatures (Ge et al., 2006; Ge et al., 2010b; Holmes et al., 2009; Wang et al., 2007; Yang et al., 2009; Zhang et al., 2009). Comparison of temperature reconstructions with climate model simulations (Liu et al., 2005; Peng et al., 2009; Zhang et al., 2011) indicates that centennial variations of China temperatures were closely related to solar irradiance and volcanic activity, with GHG playing a larger role in the last 150 years. The simulated internal variability appears weaker compared to some of the reconstructions (Ge et al., 2003; Yang et al., 2002) but not all (Wang et al., 2007).

In North America, multiple studies based on tree-rings or lake sediments provide evidence for warmer summer conditions during the MCA followed by colder conditions in northwest Canada, Canadian Rockies, Alaska and Colorado (Hu et al., 2001; Loso, 2009; Luckman and Wilson, 2005; MacDonald et al., 2009; Salzer and Kipfmueller, 2005; Thomas and Briner, 2009), although not in the Gulf of Alaska (Wilson et al., 2007a). These studies indicate that temperatures during the 20th century were likely warmer then those prevailing during the MCA. This is supported by lake, ice core and tree-ring data in the extended Arctic region north of 60ºN (Kaufman et al., 2009) that showed summer warming since 1900 CE superimposed on a 2000-year cooling trend consistent with orbital forcing.

Scandinavian summer temperatures reconstructed from tree rings (Briffa et al., 1992; Gouirand et al., 2008; Grudd, 2008; Grudd et al., 2002; Gunnarson et al., 2011; Helama et al., 2009; Kirchhefer, 2001; Linderholm et al., 2009; Lindholm et al., 2011) indicate warm conditions around 760 CE and from 980 CE to 1100 CE that were comparable or higher than 20th century (Büntgen and Schweingruber, 2010). Tree ring evidence from the Alps (Büntgen et al., 2006; Büntgen et al., 2005; Corona et al., 2010; Nicolussi et al., 2009) also points to warm conditions around 1000 CE, followed by generally lower temperatures, however the late 20th century warmth here appears to be unprecedented over the past 1500 years. (Guiot et al., 2010) combined tree rings with other proxies to reconstruct April to September temperatures across the whole of Europe, identifying a warm medieval period, followed by cooler conditions during the period from 1350 CE to 1650 CE. The last decades of the 20th century were likely warmer than any other period within the past 1400 years though not outside the uncertainty range of the MCA reconstructed values. Documentary evidence suggests that from 2001 to 2010 CE mean European summer temperature stands substantially above any other 10-year period since 1500 CE, and the hot summer of 2010 CE in eastern Europe and western Russia was likely the warmest in this period (Barriopedro et al., 2011). Information on pre-16th century winter temperature conditions in Europe is scarce (e.g., Brázdil et al., 2010; Dobrovolný et al., 2010; Glaser, 2008; Glaser and Riemann, 2009). Taking into consideration reconstructed uncertainties from historical documents, Glaser and Riemann (2009) show that current winter conditions in central Europe are the warmest in the context of the past millennium.

5.4.1.4 Southern Hemisphere Mid to High Latitudes

Progress has been made in the SH since AR4, where new tree ring records from the Andes, northern and southern Patagonia, Tierra del Fuego, New Zealand and Tasmania (Boninsegna et al., 2009; Cook et al., 2006; Villalba et al., 2009), ice cores, lake sediments and documentary evidence from southern South America (Neukom et al., 2011; Prieto and García Herrera, 2009; Tierney et al., 2010a; Vimeux et al., 2009; von Gunten et al., 2009) and terrestrial and shallow marine geological records from eastern Antarctica (Verleyen et al., 2011) allow a better understanding of past temperature variations (Neukom et al., 2011). A multi-proxy reconstruction for southern South American (Neukom et al., 2011) finds austral summer temperatures between 900 CE and 1350 CE that are mostly warmer than the 20th century climatology (though associated with large uncertainties), with a sharp transition after 1350 CE to colder conditions that last until approximately 1700 CE. Similar changes have been simulated with two climate models (ECHO-G and CCSM;Luterbacher et al., 2011), although there are differences in the timing of the MCA-LIA transition and in the amplitude of simulated warming during the last two centuries.

In contrast to the Arctic (Kaufman et al., 2009), proxy records from coastal East Antarctica do not show clear evidence of an MCA-like warm phase and only weak or indirect evidence for cool intervals during the LIA period (Verleyen et al., 2011). New paleo records from Australasia provide evidence of MCA warming around 1250–1330 CE, somewhat later than maximum medieval warmth described from many Northern Hemisphere regions (Gergis et al., submitted). Following peak medieval warmth in the early 1300s, a cooling trend reaching a temperature anomaly of approximately 0.5 ± 0.18°C below the 1961–1990 CE climatology during the peak of the LIA, 1830–1859 CE (Gergis et al., submitted).

[INSERT FIGURE 5.9 HERE]

Figure 5.9: Regional temperature reconstructions, comparison with model simulations over the past millennium (1001–1999 CE). Temperature anomalies with respect to a reference period as indicated in each panel (black bold line), and uncertainty estimated provided by each individual reconstruction (gray envelope). Individual temperature anomalies from Last Millennium simulations (colors). All lines are smoothed by applying a 50 year moving average. The models used are: Pre-PMIP3: ECHO-G (González-Rouco et al., 2006), CCSM (Ammann et al., 2007), CCSM-Bern (Hofer et al, 2011), MPI-ESM, MPI-ESM E1 (Jungclaus et al., 2010), CNRM (Swingedouw et al., 2011). PMIP3: CCSM4-NCAR (Landrum et al., submitted), GISS (Schmidt et al., 2006), HadCM3-Edin (Tett et al., 2006), MIROC-ESM (Watanabe et al., 2011). Reconstructions by region: Arctic (Kaufman et al., 2009), Europe (Büntgen et al., 2011), China (Ge et al., 2010a), South America (Neukom et al., 2011), Antarctica (Schneider et al., 2006), Australasia (Gergis et al., submitted).

[INSERT FIGURE 5.10 HERE]

Figure 5.10: Model-data comparison of surface temperature anomalies for the mid-Holocene (about 6 ka). Top panel are proxy data estimates from pollen-based reconstruction of Bartlein et al. (2010) and the GHOST global database for alkenone-derived SST records (Leduc et al., 2010). Large symbols are used to indicate grid points with significant

anomalies (i.e., those that exceed twice the pooled standard error of the reconstructions) while small symbols indicate anomalies that are not significant by this measure. Middle and bottom panels are respectively annual and June-July-August multi-model averages, left, and standard deviations, right, of model simulations. Eight models are assessed: AWI-COSMOS, BCC-CSM-1, CCSM4, CNRM-CM5, KNMI-ECEarth, MPI-ESM, MRI-CGCM3, and UBRIS_HadCM3_MOSES2.1.

5.4.1.5 Holocene Sea Ice Reconstructions

Since AR4, new estimates of past sea ice variations have been produced. Proxies of sea ice extent have been further developed from biomarkers in deep sea sediments (e.g., IP25, Belt et al., 2007) and from sea ice biota preserved in sediments (e.g., de Vernal and Rochon, 2011; Justwan and Koç, 2008). Indirect information based on drift wood and beach erosion has also been compiled (Funder et al., 2011).There are still remaining uncertainties and differences between the methods, making it difficult to provide quantitative estimates of past sea ice extent. Since AR4 several new Holocene sea ice reconstructions for the Arctic and sub-Arctic have been published, resolving multi-decadal to century scale variability. In general, these sea ice reconstructions parallell surface temperature reconstructions from the same regions, yet they display spatial heterogeneity and no pan-Arctic synchroneity of such events have been firmly documented.

Summer sea ice cover apparently was reduced compared to late 20th century levels both in the Arctic Ocean and along East Greenland between 8 ka and 6.5 ka (e.g., Funder et al., 2011; Moros et al., 2006; Polyak et al., 2010). The response and memory of this sea ice cover to summer insolation warming was shown to be central for explaining the reconstructed warmer winter temperatures over the adjacent land (Otto et al., 2009b; Zhang et al., 2010). During the last 6 kyr a long-term trend of a more extensive Arctic sea ice cover was characterised by both by a long-term trend driven by the orbital forcing, but also punctuated by strong century- to millennial scale variability. Several sea ice proxies indicate relatively reduced sea ice cover 800 CE to 1200 CE in line with temperature proxies with an increased sea ice cover in the LIA (see overview in Polyak et al. 2010). Proxy reconstructions also document the 20th century ice loss trend, as also observed in historical sea ice data sets (Divine and Dick, 2006), with a decline since the late 19th century. There is moderate confidence that the modern ice loss and increasing SSTs in the Arctic are anomalous in the perspective of at least the last two millennia (England et al., 2008; Kaufman et al., 2009; Kinnard et al., 2008; Macias Fauria et al., 2010; Polyakov et al., 2010; Spielhagen et al., 2011).

In the Southern Ocean fewer high resolution records exist. Data from the Indian Ocean sector of the Southern Ocean document an increasing sea ice trend during the Holocene, following the orbital forcing as in the Arctic, with a rather abrupt increase between 5 ka and 4 ka (Denis et al., 2010).

[START BOX 5.2 HERE]

Box 5.2: Glacier Variations During the Holocene

Glacier variations provide information on past climate independent of other climate proxies. Despite uncertainties on the response of glacier length to temperature (role of precipitation in mass balance change, lag between mass balance and glacier front reactions), new global and hemispheric temperature variations were estimated over the past centuries from syntheses of glacier lenght variations (Leclercq and Oerlemans, 2011). Glacier variations allow to place recent changes in the perspective of the current interglacial period (the Holocene).

New data on the Holocene glaciers have improved the accuracy of many glacial chronologies as well as our ability to assess the causes of glacier variability. The cosmogenic isotope (^{10}Be, ^{26}Al, ^{36}Cl) dating technique has extensively been deployed to date glacial moraines, especially in the areas formerly underrepresented in the global data sets, such as the tropics and the SH (Glasser et al., 2009; Jomelli et al., 2011; Licciardi et al., 2009; Schaefer et al., 2009). The ^{14}C and dendrochronological dates (Joerin et al., 2008; Menounos et al., 2009) as well as sediments from glacier-fed lakes that allow continuous glacier reconstructions (Bowerman and Clark, 2011; Larsen et al., 2011; Matthews and Dresser, 2008) have also provided widespread information on the former glacier variability and decreased the uncertainties in many paleoglaciological reconstructions.

The new data generally confirm the opposite multi-millennial trends in glacier changes in the SH and NH, consistent with the opposite orbital trends of summer insolation in both hemispheres. However, there are some exceptions, such as the southern Himalayas glaciers (Seong et al., 2009), which advanced in the early Holocene. The modeling (Rupper et al., 2009) shows that in the Asian monsoon area might be a result of decrease in summer temperatures as a dynamic response to the changes in solar insolation. The evidence for intra- and inter-hemispheric synchronism of submillennial glacier fluctuations is still inconclusive (Wanner et al., 2011; Wanner et al., 2008). The broad similarities of glacier variations in the outer tropics and those in Europe during the early Holocene and in the LIA were reported (Jomelli et al., 2009; Licciardi et al., 2009), but the explanation of this phenomena is still controversial implying either the migrations of the Atlantic Intertropical Convergence Zone (Licciardi et al., 2009) or forcings from the tropical Pacific (Francou et al., 2003). The coherency of high frequency variations in New Zealand with NH glaciers also remains controversial (Schaefer et al., 2009; Winkler and Matthews, 2010). Glacial chronologies for the last 2 kyr, which are much better constrained due to the precise tree-ring dating, reveal a broad coincidence between major glacier advances in the Alps, Alaska and Southern Tibet centered around 200 CE, 400 CE, 600 CE, 800 CE to 900 CE, 1100 CE, 1300 CE and in the 17th through the 19th centuries (Solomina et al., 2008). This multi-centennial variability was suggested to be linked with variations in solar activity (Holzhauser et al., 2005; Luckman and Wilson, 2005; Wiles et al., 2008), changes in North Atlantic circulation (Nesje, 2009), or dynamic link between the NH temperature and Indo-Pacific Warm pool (see "Regional temperature changes") but further evidences and modeling are required to explain large scale glacier-climate interractions.

Modern glacier retreat in the retrospective of Holocene variations

Consistently with global warming, glaciers are currently globally retreating (see Chapter 4) releasing organic remains from previous warm periods. These are confident evidences of reduced sizes of glaciers in the past, but the precise glacier extent in the previous warm periods is difficult to assess. In some regions, such as British Columbia (Koch et al., 2004) the glaciers already appear to be less extensive at present than they have been throughout the Holocene or at least in the last 6 ka (Scandivavia, tropical Andes) (Nesje, 2009; Thompson et al., 2006), but in others they are still larger and did not reach the equilibrium with the modern climate which is changing with very high speed. Joerin et al. (2008) found that the equilibrium-line altitude in the Alps was at least 220 m higher in the early and mid Holocene than in the end of the 20th century. Since mean annual temperatures remained almost unchanged during the mid-Holocene (von Grafenstein et al., 1999), it is suggested that these changes were related to enhanced seasonality with higher summer temperatures at that time. During the MCA, some glaciers were smaller than in the early 21st century (western Antarctic Peninsula, southern Swiss Alps) (Hall et al., 2010; Scapozza et al., 2010), however, prominent advanced occurred during the MCA (1050 CE to 1150 CE) in the Alps (Holzhauser et al., 2005), Patagonia (Luckman and Villalba, 2001), New Zealand (Schaefer et al., 2009), SE Tibet (Yang et al., 2008). In the western North American glaciers were similar however some prominent advances occurred during the MCA between 1050 CE and 1150 CE in the Alps, Alaska, Patagonia, New Zealand, SE Tibet. In western North America it was similar to those at the peak of the LIA and was forced by increased winter precipitation due to prolonged La Niña-like conditions(Koch and Clague, 2011). The change in length involves complex dynamics of ice flow and, hence, is delayed sometimes by decades from the climatic signal. Therefore while comparing the Holocene glacier length variations with their current status one has to take into account that the modern glaciers are still adjusting to the current warming and very likely will continue to retreat in response to the rising temperature (see Chapter 4).

[INSERT BOX 5.2, FIGURE 1 HERE]

Box 5.2, Figure1: Time-distance diagrams for glaciers front and (or) of equilibrium-line altitude (ELA) variations. The selected series are well chronologically constrained and reptersent different climatic regions in the Northern and Southern Hemispheres. **a)** The Holocene – Northern Scandinavia. Depression of equilibrium-line altitude (dELA) from Northern Folgefonna based on lacustrine sediments (Bakke et al., 2005a; Bakke et al., 2005b; Bakke et al., 2010; Nesje, 2009). The Alps. Summary of glacier variations (Ivy-Ochs et al., 2009). Himalaya, Central Nepal. dELA defined from the position of moraines dated by exposure rates with dating uncertainties (Gayer et al., 2006). Bolivian Andes. ELA of the Telata glacier from ^{10}Be dates (Jomelli et al., 2011). **b)** Last 2000 years – ELA variations in Northern Norway based on the bulk density sediment record (Bakke et al., 2005b). The Alps. Fluctuations of the Great Aletsch glacier. Bars - life-time of the fossil trees (Holzhauser et al., 2005). Southern Tibetan Plateau. Summary of glacier variations (after Yang et al., 2003; Yang et al., 2008). Glacial advances in the tropical Andes (Peru and Bolivia) with dating uncertainties (after Jomelli et al., 2008; Jomelli et al., 2009).

[END BOX 5.2 HERE]

5.4.2 Regional Changes in Atmospheric Circulation

5.4.2.1 Monsoon Systems and Convergence Zones

Among the dominant tropical rainfall features are the Monsoon systems and the major atmospheric convergence zones such as the Intertropical Convergence Zones (ITCZ). Given their societal relevance, it is of considerable importance to document historical changes in the Monsoon systems and to isolate the roles of various natural and anthropogenic factors in the observed changes in Monsoon behaviour. Since AR4 reconstructions of Monsoon changes have been expanded using a variety of proxy archives such as speleothems (Dykoski et al., 2005; Fleitmann et al., 2003; Hu et al., 2008; Wang et al., 2005a), lake sediments (Wolff et al., 2011), marine sediments (Tjallingii et al., 2008; Weldeab et al., 2006; Weldeab et al., 2007) and tree ring chronologies (Buckley et al., 2010; Cook et al., 2010).

Most of the current Monsoon systems have been found to respond strongly to orbital forcing and in particular to precession (Figure 5.11). Speleothem data from southeastern China document rainfall changes that are dominated by precessional cycles (Clemens et al., 2010; Wang et al., 2008), whereas Monsoon proxies from regions closer to the major Northern Hemispheric ice sheets, such Northern Africa, the Arabian Peninsula and Arabian Sea also exhibit high variance on eccentricity timescales and feature glacial inceptions and terminations (Bar-Matthews et al., 2003; Schulz et al., 1998; Weldeab et al., 2007) (Figure 5.12). The 100 kyr variability seen in some Monsoon records is indicative of remote influences from the ice sheets via the atmosphere, as confirmed in climate model experiments (Timm et al., 2010) and the effect of CO_2 radiative forcing. The impact of millennial-scale variations of North Atlantic SST associated with Dansgaard–Oeschger and Heinrich events on Monsoon systems (Stager et al., 2011) (Figure 5.11) are further assessed using proxy data and climate model experiments in Section 5.6.1.

Increasing (decreasing) boreal (austral) summer insolation during the early to mid-Holocene, led to an overall drying in Southern Hemispheric summer Monsoon systems and increased rainfall in the Northern Hemisphere (Wang et al., 2008). These out-of-phase interhemispheric trends reversed after the mid Holocene Optimum around 8 ka to 9 ka (Burns, 2011; Cruz et al., 2009) (Figure 5.11). Qualitatively similar responses to insolation forcing have also been documented in coupled GCM simulations (Braconnot et al., 2007a; Kutzbach et al., 2008) and transient model simulations (Figure 5.11), thereby providing high confidence in the orbital control mechanism of interhemispheric rainfall variability. Regionally, the phase relation between orbital insolation changes and precipitation-related proxies shows complex spatial variations (Cai et al., 2010; Kutzbach et al., 2008). Alternating east-west differences in Monsoonal rainfall have been observed for South America (Cruz et al., 2009) Asia (Hong et al., 2005) and South Africa (Chase et al., 2010; Kristen et al., 2010).

Monsoon systems and ITCZs can exhibit variability on a range of timescales. Interannual SST changes associated with the El Niño-Southern Oscillation (ENSO) phenomenon and the Indian Ocean Dipole are known to affect Indian, East Asian, West African, and Australian Monsoons as well as the South Pacific Convergence Zone the Central American Monsoons (see Chapter 14). On multidecadal timescales influences of North Atlantic multidecadal SST variations have been demonstrated for the West African Monsoon and the Indian Monsoon systems, both using paleo-climate reconstructions (Shanahan et al., 2009) and climate model experiments (Zhang and Delworth, 2006). Climate model simulations of the last millennium (Liu et al., 2009a) suggest that solar variability and volcanic forcing exert a discernable influence on the global Monsoon systems, with decreased global Monsoon rainfall accompanying periods of reduced shortwave radiative forcing. An assessment of the response of Monsoon Systems to volcanic forcing using paleo proxy data has revealed wetter conditions occurred over mainland Southeast Asia in the year of a major volcanic eruption, with drier conditions in central Asia (Anchukaitis et al., 2010), suggesting considerable discrepancies between model simulations and proxy data.

A large amount of multidecadal Monsoon variability on regional scales cannot be explained by external forcings or as a result of North Atlantic SST variability. Extended intervals of Monsoon failures and dry spells have been reconstructed for the last few millennia for West Africa (Wolff et al., 2011), India and

southeastern Asia (Berkelhammer et al., 2010; Buckley et al., 2010; Cook et al., 2010; Davis et al., 2005; Fleitmann et al., 2004; Sinha et al., 2007; Staubwasser and Weiss, 2006; Zhang et al., 2008, Buckley et al., 2010) and Australia (Mohtadi et al., 2011).

[INSERT FIGURE 5.11 HERE]

Figure 5.11: Millennial and orbital scale variability of global Monsoon systems: upper left: Boreal summer insolation changes at 20°N; middle left: East Asian Monsoon record compiled from the Hulu cave $\delta^{18}O$ anomaly record (Wang et al., 2001) and the Sanbao $\delta^{18}O$ anomaly cave records (Wang et al., 2008) in China (red) (the Hulu data were reduced by 1 ‰ to account for a regional offset with the Sanbao cave record), West African Monsoon proxy from salinity reconstructions in the Gulf of Guinea (Weldeab et al., 2007); lower left: simulated annual mean rainfall anomalies in east Asia (covering the grid boxes of Hulu and Sanbao cave) from two climate model simulations covering the last 120 kyr, conducted with the orbitally-accelerated LOVECLIM model (red)(Timm et al., 2008) and a series of climate snapshot experiments with the HADCM3 model (gray)(Singarayer and Valdes, 2010); upper right: February insolation at 20°S; middle right: $\delta^{18}O$ anomalies from Botuvera speleothem data (Brazil) (Cruz et al., 2009), characterizing South American Monsoon changes; lower right: same as lower left, but for simulated rainfall anomalies in Brazil (covering the grid boxes of the Botuvera cave). Note, that $\delta^{18}O$ anomalies in speleothems represent a mixture of local rainfall changes and changes in the source region of the moisture (LeGrande and Schmidt, 2009; Pausata et al., 2011).

5.4.2.2 Megadroughts and Floods

Paleo drought reconstructions provide estimations of the frequency, duration and severity of past dry periods. Megadroughts are comparable in intensity to present drought events but with durations longer than several years to a decade (e.g., Seager et al., 2009).

Figure 5.12 shows regional PDSI (Palmer Drought Severity Index) values reconstructed using tree rings in North America and Monsoon Asia (Cook et al., 2004; Cook et al., 2010), duration of droughts, their severity, and their frequency. Proxy information indicates that intervals lasting from decades to centuries of more frequent severe drought in western Africa are characteristic of the monsoon and appear to be linked to variations in Atlantic temperatures (Shanahan et al., 2009; see also Section 5.6). Proxy reconstructions and model experiments suggest that strengthening of the zonal SST gradient in the tropical Pacific or more severe La Niña conditions, and possibly warming of the Indian Ocean, during periods of the MCA may have contributed to arid conditions in North America (Graham et al., 2011; Graham et al., 2007; Seager et al., 2008), contrasting with wetter conditions in Asia (Buckley et al., 2010; Graham et al., 2011; Graham et al., 2007), although direct evidence of SST variability and ENSO state is more equivocal (Emile-Geay et al., in press). During the MCA, positive NAO conditions (see Section 5.4.3.2) and AMO phases may have favored wetter winter conditions in NW Europe and arid in NW Africa (Esper et al., 2007b; Graham et al., 2007) although Touchan et al (2011) do not find evidence of overall changes in mean drought conditions in northwestern Africa. The transition from the MCA to the LIA appears to coincide with monsoon weakening and megadrought occurrence in Asia (Buckley et al., 2010; Cook et al., 2010), while in North America an apparent shift toward overall wetter conditions occurs in the middle of the 14th century (Cook et al., 2004).

Recent evidence from southern South America indicates that the period from1000 CE to 1250 CE was characterized by wetter than normal conditions in most regions followed by much drier conditions until 1400 CE and wetter conditions similar to present afterwards (Boucher et al., 2011). Chinese historical records indicate that some previous droughts were more severe than those observed during the 20th century, with the most severe drought event in eastern China during the last 1500 years occurring between 1634 CE and 1644 CE, and more frequent droughts in the 12th to 14th centuries (Zheng et al., 2006).

[INSERT FIGURE 5.12 HERE]

Figure 5.12: Severity, duration, and frequency of droughts in the Monsoon Asia (Cook et al., 2010) and North American (Cook et al., 2004) Drought Atlases. The box in **a)** and **d)** indicates the region over which the tree ring reconstructed Palmer Drought Severity Index (PDSI) values have been averaged to form the regional mean time series in **c)** and **f)**, respectively. The covariance of drought (PDSI < 0) duration and cumulative severity is shown in panels **b)** and **e)**, along with the respective frequency histograms for each quantity. Not shown in **b)** is an outlier with an apparent duration of 24 years, corresponding to the 'Strange Parallels' drought identified in Cook et al. (2010). Return intervals for droughts of given durations are estimated as the mean interval between their occurrence, with minimum and maximum intervals indicated, and are plotted in the same panels. No error bars are present if there is only a single observation of a drought of that duration. The period of analysis is restricted to the period 1300 CE to 1950 CE for

Monsoon Asia, following Cook et al. (2010), and from 800 CE to 2006 CE for North America, following Cook et al. (2004).

Sedimentary, botanical and historical records (Baker, 2008; Brázdil et al., 2006; Brázdil et al., 2012) reveal strong variability and perhaps non-stationarity in flood frequency and preferential clustering of paleofloods in the past (Benito et al., 2008; Ely et al., 1993; Glaser et al., 2010; Knox, 2000; Stewart et al., in press; Støren et al., in press).In some instances increased floor frequency may have coincided with relatively cool and wet climate conditions (Benito et al., 2008; Luterbacher et al., in press; Macklin et al., 2006) (Figure 5.13).In the Rhine in Basel (Switzerland) severe summer floods were particularly frequent between 1651 CE and 1750 CE, overlapping the Maunder Minimum, which has been related to enhanced precipitation; whilst severe winter floods have not occurred since the late 19th century, despite a significant increase in winter precipitation (Wetter et al., 2011).

Overall, multiple studies suggest that current flood magnitudes are not unusual within the context of the last 1000 years (e.g., Benito et al., 2011; Brázdil et al., 2012; Enzel et al., 1993; Greenbaum et al., 2000; Herget and Meurs, 2010; Mudelsee et al., 2003). The highest peak flows in the modern instrumental record were exceeded by reconstructed flows during the historical period in the rivers Rhine (Herget and Meurs, 2010; Wetter et al., 2011), Vltava (Brázdil et al., 2005), Tiber (Calenda et al., 2005), Llobregat (Thorndycraft and Benito, 2006), and Gardon (Sheffer et al., 2008). Recent extreme floodings in the UK are not exceptional within the last centuries (Macdonald, 2007). The severity of 20th century floods in eastern China was matched by earlier events in the historical record, and the mid-17th century in particular was subject to more flooding (Zheng et al., 2006). In the western Mediterranean region, the frequency of large floods (>50-yr floods) has decreased since the late 19th century, whereas the extraordinary and ordinary floods increased over the 20th century (Figure 5.13.A-C). This decrease in frequency of large floods since the 19th century has occurred in other rivers of central and north-western Europe (Figure 5.13 F-I). However, recent flooding are difficult to evaluate in the context of climate change due to extensive river regulation (dams, dikes) and land-use changes. In mid-to-high latitude regions, comparison of flood magnitudes along centennial records should consider the role of snow melt and ice jams during (see also Chapter 4 on cryosphere changes) cold periods of the Little Ice Age (1550 CE to 1850 CE). Global warming has changed the spatial (latitudinal) and temporal (seasonal) distribution of these ice and snowmelt related flooding (Beltaos and Prowse, 2009). In southern Norway, high flood frequency at about 2300, 1200 and 200 years ago occurred in relation with the amount of solid winter precipitation and related spring/summer snowmelt (Støren et al., 2010). In the winter rainfall zone of southern Africa, decreasing frequency of large floods occurred during warmer conditions (e.g., from 1425 CE to 1600 CE and after 1925 CE) and increased during wetter, colder conditions (Benito et al., 2011). In contrast, in India modern floods are the largest for the last 3000 years, interpreted as a strengthening of the monsoon conditions (Kale, 2008).

[INSERT FIGURE 5.13 HERE]

Figure 5.13: Flood frequency from paleofloods, historical and instrumental records in selected European rivers. Number of floods that exceeded a particular discharge threshold or flood level within a centred window of 31-years. Flood categories include large-catastrophic floods (CAT) that produced high discharge or severe damages, and extraordinary floods (EXT) causing inundation of the floodplain with moderate to minor damages. Legend at each panel indicates for each category the period of record, number of floods, and the average occurrence interval (in years). **a)** Tagus River combined paleoflood, historical and instrumental flood records from Aranjuez with thresholds of 300–700 m^3s^{-1} (EXT) and >700 m^3s^{-1} (CAT) (Benito et al., 2003a; Benito et al., 2003b). **b)** Segura River Basin (SE Spain) documentary and instrumental records at Murcia (Barriendos and Rodrigo, 2006; Barriendos and Martin-Vide, 1998; Machado et al., in press). **c)** Gardon River combined discharges from paleofloods at La Baume (Sheffer et al., 2008), documented floods (since the 15th century and historical and daily water stage readings at Anduze (1741 CE to 2005 CE; Neppel et al., 2010). Discharge thresholds referred to Anduze are 1000–3000 m^3s^{-1} (EXT) and >3000 m^3s^{-1} (CAT). At least five floods larger than the 2002 CE-flood (the largest in the gauged record) occurred in the period 1400 CE to 1800 CE (Sheffer et al., 2008). **d)** Tiber River floods in Rome from observed historical stages (since 1100 CE; Calenda et al., 2005; Camuffo and Enzi, 1996; Camuffo et al., 2003) and continuous stage readings (1870 CE to present) at the Ripetta landing (Calenda et al., 2005). Discharge thresholds set at 2300–2900 m^3s^{-1} (EXT) and >2900 m^3s^{-1} (CAT; >17 m stage at Ripetta). Recent flooding is difficult to evaluate in context due to river regulation structures. **e)** Nahal Zin (Israel) 2000-year paleoflood record, combined with historical data (1935 CE to 1946 CE) and instrumental records (from 1951 CE to present) after Greenbaum et al. (2000). Discharge threshold for large floods was set at 400 m^3s^{-1} (CAT). Large floods occurred at 1.38 ± 0.88 ka and the last 60 years, the former is related with regional humid conditions as recorded in high Dead Sea levels (Greenbaum et al., 2006). **f)** Vltava River combined documentary and instrumental flood record at Prague (Brázdil et al., 2005) discharge thresholds: CAT, flood index 2 and 3 or discharge

>2900 m^3s^{-1}; EXT flood index 1 or discharge 2000–2900 m^3s^{-1}. **g)** Elbe River combined documentary and instrumental flood record (Mudelsee et al., 2003). Classes refer to Mudelsee et al. (2003) strong (EXT) and exceptionally strong (CAT) flooding. **h)** Oder River combined documentary and instrumental flood record (Mudelsee et al., 2003). **i)** River Ouse at York combined documentary and instrumental flood record (Macdonald and Black, 2010). Discharge thresholds for large floods was set at 500 m^3s^{-1} (CAT) and for ordinary floods at 350–500 m^3s^{-1} (EXT). The map shows the location of rivers used in the flood frequency plots.

5.4.3 Modes of Climate Variability

Since AR4 new proxies and model simulations have provided new insights into the forced and unforced past variability of the ENSO, the Indian Ocean Dipole (IOD), the NAO and longer term variability associated with the Atlantic Multidecadal Oscillation (AMO).

5.4.3.1 Tropical Modes

Changes in the statistics of interannual variability associated with ENSO have been studied in response to external forcing, using GCMs and climate reconstructions from historical and proxy data (corals, tree rings, ice cores and sediment cores). Climate models run under LGM boundary conditions simulate wide ranges of ENSO behaviour and very little consistency (Liu et al., 2007; Zheng et al., 2008). Reliable annually-resolved ENSO proxies are sparse (Koutavas and Joanidis, 2009; Wolff et al., 2011) and do currently not allow ruling out any of the simulated ENSO responses to LGM boundary conditions. In recent GCM experiments a weakening of the Atlantic Meridional Overturning Circulation, such as during Heinrich stadial 1 (about 18.5 ka to 14.8 ka) or the Younger Dryas (about 12.8 ka to 11.5 ka) consistently triggers intensification of ENSO amplitude and in some cases a reduction of the annual cycle in the Eastern Equatorial Pacific (Merkel et al., 2010; Timmermann et al., 2007). For the mid-Holocene period (9 ka to 4 ka), a number of proxy data indicate with medium to high confidence a reduction of ENSO variability (Carre et al., 2005; Donders et al., 2008; Koutavas et al., 2006; Tudhope et al., 2001; Woodroffe et al., 2003), in qualitative accordance with PMIP3 and other GCM modeling experiments (Brown et al., 2008a; Brown et al., 2008b; Bush, 2007; Zheng et al., 2008). Interactions with an intensified western Pacific monsoon circulation (Liu et al., 2000), an enhanced zonal equatorial SST gradient associated with an intensified Walker Circulation (Zheng et al., 2008) and reduced level of tropical atmospheric noise (Chiang et al., 2009) have been suggested to explain the reduction of ENSO variance during the mid-Holocene. Reconstructions of ENSO for the last millennium document a highly variable ENSO system (Figure 5.14) (McGregor et al., 2010; Wilson et al., 2010). Efforts to extract the variance changes in different ENSO proxies using statistical techniques document with medium to high confidence an active ENSO phase during the 20th century and a weaker ENSO phase during the period from 1660 CE to 1880 CE (McGregor et al., 2010). ENSO variance reconstructions prior to this are still quite uncertain. Furthermore, significant inter-proxy uncertainties exist (McGregor et al., 2010; Wilson et al., 2010) as documented for instance by a large divergence among the running variances of the individual reconstructions around the period from 1650 CE to1670 CE. Climate model simulations (Meehl et al., 2009) and some proxy data from the eastern tropical Pacific suggest a possible effect of solar irradiance change on the mean state of the tropical Pacific (Marchitto et al., 2010). However, there is no evidence that the reconstructed multidecadal variance changes of ENSO (Figure 5.14) are directly related to solar irradiance changes (McGregor et al., 2010). According to some reconstructions of volcanic events and some ENSO proxies a slightly increased probability exists in the occurrence of El Niño events in the 2 years following major volcanic eruptions (Adams et al., 2003; McGregor et al., 2010; Wilson et al., 2010). Simplified intermediate ENSO models are able to reproduce this behaviour (Emile-Geay et al., 2008; Mann et al., 2005), whereas some GCM experiments show an initial cooling and a subsequent warming due to the recharge of heat into the equatorial thermocline (McGregor and Timmermann, 2010).

Another mode of interannual tropical climate variability with far reaching teleconnections and hydroclimate impacts (Chang et al., 2006; Kabanda and Jury, 1999) is the Indian Ocean Dipole mode (IOD) (Saji et al., 1999). Whereas it can occur independently from ENSO, it is in general heavily affected by eastern equatorial Pacific sea surface conditions. The IOD has been reconstructed using coral records (Abram et al., 2008; Abram et al., 2007; Charles et al., 2003; Nakamura et al., 2009; Pfeiffer and Dullo, 2006) as well as annually varved lake sediments (Wolff et al., 2011). For LGM conditions, model simulations (Liu et al., 2007) suggest that a weaker Asian monsoon would lead to a shoaling of the equatorial Indian Ocean thermocline, which can amplify the amplitude of IOD events. As the Asian summer monsoon amplifies towards the mid-Holocene, IOD variability weakens in one modelling study (Brown et al., 2009). A more extensive

comparison of simulated IOD behaviour and paleo-proxy reconstructions (Abram et al., 2007) for the Holocene still remains an outstanding task. Reconstructions of the IOD index since 1846 CE exhibit a gradual increase in the frequency and strength of IOD events during the twentieth century (Abram et al., 2008), that may be related to an intensification of seasonal upwelling off the coast of Sumatra.

5.4.3.2 Extratropical Modes

Orbital-scale variability of the NAO and AO was investigated in a series of modeling studies. Robust evidence from climate model simulations under LGM conditions indicates a weakening of the AO and its variability, owing to stronger planetary wave activity (Lü et al., 2010). A significant model-dependent distortion of the simulated LGM NAO pattern may result from the strong topographic ice sheet forcing (Handorf et al., 2009; Justino and Peltier, 2005; Pausata et al., 2009). The simulated NAO during the mid-Holocene (Gladstone et al., 2005) resembles the pre-industrial NAO. Only 30% of the models run under mid-Holocene conditions exhibit a mean intensification of the NAO. A six-member ensemble of orbitally accelerated transient GCM experiments covering the period from 7 ka to 0 ka reveals a weakening of the NAO during the Holocene. Robust proxy evidence for these model-based results has not yet been established. In order to better understand the interannual to multidecadal-scale behaviour of the NAO and AO several centuries-long proxy indices have been reconstructed based on long instrumental pressure and ship logbook information, single proxy archives or multi-proxy paleoenvironmental data from Eurasia and North America and Greenland (Appenzeller et al., 1998; Cook et al., 2002; Cullen et al., 2001; D'Arrigo et al., 1993; Glueck and Stockton, 2001; Küttel et al., 2010; Luterbacher et al., 2002; Mann, 2002; Rodrigo et al., 2001; Slonosky et al., 2001; Timm et al., 2004; Trouet et al., 2009). Whereas, the reconstructions differ in several aspects (Cook et al., 2002; Luterbacher et al., 2002; Schmutz et al., 2000; Timm et al., 2004; Trouet et al., 2009) they demonstrate with high confidence (taking into consideration associated reconstruction uncertainties) that the strong positive NAO phases within the early 20th century and the mid 1990s are not unusual in the context of the past half millennium. Effects of the solar insolation anomalies on the NAO have been found in GCM experiments (Shindell et al., 2001; Swingedouw et al., 2011), but a direct statistically robust evidence for such an effect from long term NAO reconstructions is still lacking.

Large-scale SST variations are observed in the North Atlantic Ocean on multidecadal timescales, most prominent is the basin-wide variation of the Atlantic multidecadal oscillation (AMO), marked by alternation of warm and cold SST anomalies in the North Atlantic with a timescale of about 60–80 years (Delworth and Mann, 2000). It has been suggested, on the basis of climate model simulations and an 8,000-year long climate proxy record from the North Atlantic region (including five ice-core records from Greenland and the Canadian Arctic, one lacustrine record from the Yucatan peninsula and a marine record from the Cariaco Basin) (Knudsen et al., 2011), that AMO variations are internally driven and related to multidecadal fluctuations in the Atlantic meridional overturning circulation. However, recent model experiments with GCMs forced by solar and volcanic forcing for the past millennium indicate that external solar and volcanic forcing may play a considerable role in driving or at least pacemaking AMO variations (Otterå et al., 2010). It is also suggested that the large hemispheric temperature-anomalies associated with the AMO may impose multidecadal changes to the NAO (Goodkin et al., 2008). Due to the wide range of impacts outside the North Atlantic region, both marine (Black et al., 2007; Kilbourne et al., 2008; Saenger et al., 2009; Sicre et al., 2008) and terrestrial proxy archives (Gray et al., 2004) from different locations have been used to reconstruct the AMO. Whereas most of these records show a good correspondence with the instrumental data during the industrial period, they exhibit only very little joint variability prior to the industrial period (Winter et al., 2011). The reasons for this divergence are hirtherto unknown.

[INSERT FIGURE 5.14 HERE]

Figure 5.14: Compilation of the different ENSO reconstructions. Left panel: Grey dots indicate the data points from 11 individual ENSO reconstructions (McGregor et al., 2010), (Li et al., 2011) normalised through the 1900 CE to 1978 CE period, with the reconstruction ensemble mean displayed in blue. The underlying red line is Niño 3 region SSTA obtained from the HadISST data set (Rayner et al., 2003); Right panel: Grey dots indicate the 30-year running variance of each of the 11 different ENSO reconstructions with the ensemble mean running variance displayed in blue, while the overlying dashed red line is the 30-year running variance of the normalised HadISST Niño 3 region SSTA. The dashed cyan lines indicate the 10 and 90 percentiles obtained from a χ^2 distribution using the number of available ENSO proxies shown by the purple line.

5.5 Past Changes in Sea Level and Related Processes

Information on the reconstruction of past sea level, on processes causing sea level to change and on approaches to incorporate these processes in numerical models is summarized in a supplement to this section (see Appendix 5.A). This supplementary information provides important background information on uncertainties that has been used in the assessment of past sea level changes and it is intended to guide readers in their own evaluation of the existing literature.

5.5.1 The Mid-Pliocene

Estimates of middle Pliocene global mean sea level (GMSL) highstands range from +40 m (Brigham-Grette and Carter, 1992) to +5 m (Miller et al., 2005), indicating that there was significantly less ice at that time than present. Miller et al. (submitted) obtained a peak global mean sea level (eustatic) estimate of 20 ± 10 m higher than present for interglacial high stands within the Pliocene interval 2.7–3.2 Ma by averaging 34 globally distributed estimates. According to this study, the likely (66%) eustatic sea level highstand was 12–33 m relative to present sea level. The reported uncertainties take into account non-thermal subsidence and regional tectonics. The influence of mantle dynamic processes (Müller et al., 2008), although potentially significant at any single site used for Pliocene sea level reconstructions, is presently unquantifiable, and the estimated regional variability due to glacial isostatic adjustment (e.g., Raymo et al., 2011) is of the order of the regional tectonic variability.

Direct geological evidence from the Northern Hemisphere (Maslin et al., 2000) and Antarctica (Naish et al., 2008), together with climate-driven ice sheet models (Dolan et al., 2011; Pollard and DeConto, 2009), suggest that most of the variation in mid-Pliocene ice volume was associated with the Greenland and West Antarctic ice sheets, with smaller changes in the East Antarctic Ice Sheet (EAIS). Sedimentary record indicates that the West Antarctic Ice Sheet retreated from the Ross embayment between 4.6 and 3.3 Ma (Naish et al., 2009c). An ice sheet/ice shelf model that includes ice shelf buttressing and migrating marine-based grounding lines shows complete deglaciation of the marine-based portions of the WAIS and thinning and recession on the margins of the EAIS, contributing up to +7m of sea level rise during orbital-scale Pliocene interglaciations (Pollard and DeConto, 2009). Some ice sheet models (Dolan et al., 2011; Hill et al., 2010) impose a boundary condition in their climate models of a sea level highstand of 15–20 m and these cannot be used to infer sea level sensitivity to climate forcings.

5.5.2 The Last Interglacial

Emerged paleo-shorelines provide high confidence that GMSL during the LIG was at least 6 m higher than today (Dutton and Lambeck, submitted; Kopp et al., 2009) (Figure 5.15). Kopp et al. (2009) used a probabilistic assessment of LIG sea level that included a physical model to account for differences between local sea level and GMSL due to glacial isostatic adjustment (Lambeck and Nakada, 1992) and was based on the age model for a global stack of benthic $\delta^{18}O$ records (Lisiecki and Raymo, 2005). Because this $\delta^{18}O$ stack reflects temperature as well as ice volume, the timing of the sea level signal is likely modulated by changes in deep-ocean temperature, particularly during the penultimate deglaciation into the LIG (Skinner and Shackleton, 2006). Additional uncertainty comes from the constraints used to establish the start of the LIG in the $\delta^{18}O$ stack at ~126 ka (Lisiecki and Raymo, 2005), whereby other studies place the start at 129–130 ka (Muhs et al., 2011; Stirling et al., 1998b). These uncertainties apply to the timing, but not the amplitude, of sea level changes reported by Kopp et al. (2009). They concluded that the LIG GMSL was significantly higher than most previous estimates, with a 95% probability that it exceeded 6.6 m, a 67% probability that it exceeded 8.0 m, and a 33% probability that it exceeded 9.4 m. Some of the data included in this analysis, however, are from localities where one or several conditions for their use in reconstructing sea level are not met: at Cape Cuvier, western Australia, O'Leary et al. (2008) identified a late LIG highstand at +8.5 m to +10 m but this area appears to have been subject to recent tectonic uplift (Denman and van de Graaff, 1977); for sites from Bermuda and the Bahamas, glacio-isostatic contributions are likely to be important (Figure 5.15); coral data from some sites (e.g., Seychelles) do not meet screening criteria to provide an accurate date (Israelson and Wohlfarth, 1999); geomorphological evidence from some sites is not supported by adequate chronological control (e.g., erosion notches on Bermuda) (Hearty et al., 2007). As a result, the Kopp et al. (2009) global compilation that includes such data needs to be interpreted with caution if used to estimate LIG ice volumes. Nevertheless, a compilation of LIG fossil corals dated by closed-system U/Th, corrected

for isostatic effects and that does meet the above conditions, provides independent confirmation of the Kopp et al. (2009) result that LIG global mean sea level was between +6 m (high confidence) and 10 m (low confidence) (Dutton and Lambeck, submitted).

There is medium confidence that thermal expansion of the LIG water column was small (0.3 ± 0.4 m in the model results by McKay et al., 2011), leaving high confidence that the primary sources of the +6 m LIG sea level highstand were from glaciers and the Greenland and West Antarctic ice sheets. There is little evidence for how much mountain glaciers retreated during the LIG, and thus what their contribution to sea level may have been, but the modern glacier budget provides an upper limit of about 0.6 m sea level equivalent (Radic and Hock, 2011). Both the NGRIP and GISP Greenland ice cores indicate that the Greenland summit region remained ice covered during the LIG (Andersen et al., 2004; Landais et al., 2006; Raynaud and Lorius, 2004; Suwa et al., 2006) (Figure 5.16) [PLACEHOLDER FOR SECOND ORDER DRAFT: NEEM PROJECT RESULTS]. Ice core constraints for the presence of LIG ice on southern Greenland remain equivocal (e.g., Andersen et al., 2004; Koerner and Fisher, 2002; Lhomme et al., 2005), whereas geological data indicate that sufficient ice melted from southern Greenland to contribute 1.6 m to 2.2 m of sea level rise (Colville et al., 2011). Models of Greenland and other Arctic ice masses forced by climatologies inferred from data or simulated by climate models find a contribution of about 2 m to 4 m of early LIG sea level rise over several millennia (Robinson et al., 2011; Stone et al., submitted) (Figure 5.15). However, in most of these simulations the effect of insolation on Greenland ice sheet mass balance was not explicitly accounted for and may lead to some underestimation of simulated Greenland ice sheet mass loss during Eemian (van de Berg et al., 2011). Geological constraints for retreat of the West Antarctic Ice sheet (WAIS) during the LIG are equivocal due to chronological uncertainties (Naish et al., 2009b). A coupled ice sheet/ice shelf model reconstructed only a minimal contribution to the LIG sea level highstand due to WAIS loss from the Pine Island, Weddell and Siple Coast sectors (Pollard and DeConto, 2009).

In summary, there is high confidence that GMSL during the LIG was at least 6 m higher than today which requires glacier melting, thermosteric rise, and contributions from the Greenland ice sheet and WAIS. The more poorly documented sea levels of up to 10 m would also require a contribution from the East Antarctic Ice Sheet. Any of these high LIG sea levels has significant implications for the equilibrium response of both polar ice sheets to only moderate levels of warming.

There is moderate confidence that local LIG sea levels experienced a meter-scale fluctuation sometime between 126 ka and 120 ka, suggesting substantial sea level variability during warm climates (Hearty et al., 2007; Kopp et al., 2009; Rohling et al., 2008a; Thompson and Goldstein, 2005). Regional sea level variability and uncertainties in sea level proxies and their ages, however, cause considerable differences in the timing and amplitude of the reported fluctuation.

Based on their GMSL reconstruction, Kopp et al. (2009) estimated a median projection for rates of sea level fall of –3.0 m kyr^{-1} (67% range of –4.7 to –1.2 m kyr^{-1}) into this fluctuation, providing insight into possible ice sheet accumulation rates in a warm climate. Sea level subsequently rose at a comparable rate (3.5 m kyr^{-1}, 67% range of –4.4 to 7.4 m kyr^{-1}). However, these rates are based on a LIG duration derived from the global $\delta^{18}O$ stack (Lisiecki and Raymo, 2005), which is 3–4 kyr shorter than the duration based on closed-system U/Th ages on fossil corals (Dutton and Lambeck, submitted), suggesting rates may have been about 70% lower. Stratigraphic relationships particularly in coral reef sequences suggest the possibility of an episode of abrupt 2–3 m rise in sea level (Blanchon et al., 2009; Hearty et al., 2007), but these have yet to be adequately dated or replicated to establish an exact age and rate for such an event, and may instead largely reflect ongoing isostatic adjustments from the penultimate deglaciation (Dutton and Lambeck, submitted).

Dutton and Lambeck (submitted) found that all well-dated fossil-corals from western Australia showed evidence of an oscillation at about 125–126 ka based on closed-system U/Th ages. Individual records from other stable regions that were similarly screened, including San Salvador and Great Inagua island (Chen et al., 1991) in the Bahamas and from Yucatan (Blanchon et al., 2009), also point to a 1–2 m change in sea level at this time, while chronologically constrained data from Bermuda (Muhs et al., 2002) exclude rapid sea level changes (greater than a few m in 1 kyr or 2 kyr). They also found that application of an open-system model to the U-Th data at all sites produces stratigraphic age-inversions in several places where the vertical stratigraphy is well defined, and that the spatial and temporal coherency of the sea level oscillation seen in the closed-system ages is not reproduced. The ages and stratigraphic context of corals used in their

analysis suggest that sea level fell by 1–2 m and that the entire sea level oscillation was completed in about 2 kyr with a minimum elevation at about 126–125 ka (Figure 5.15). The error on these absolute ages is on the order of ~1–2 kyr but the error of the relative ages is closer to 1 kyr. These observations thus provide medium confidence in a mid-LIG (warm-climate) sea level oscillation of about1–2 m kyr^{-1}.

Rohling et al. (2008a) argued that variability in the $\delta^{18}O$ record from two Red Sea cores identifies several short-term (about 1000 year duration) oscillations of as much as 10 m throughout the LIG. Based on their age model for the duration of the LIG, Rohling et al. (2008a) estimated rates of sea level rise ranging from 1.0 m to 2.5 m per century. There are several issues that question the validity of these results. First, factors other than ocean volume contribute to the $\delta^{18}O$ signal. Second, the sea level oscillations do not replicate between the two cores. Third, the core with highest amplitude LIG changes has similar-scale $\delta^{18}O$ variability during the middle-to-late Holocene as well (Siddall et al., 2003) when direct measures of sea level indicate that oscillations are unlikely to have exceeded ±0.5 m (Section 5.5.3). Fourth, the rates derived by Rohling et al. (2008a) are based on a duration of the LIG from 123.5 ka to 119 ka, which is about three times shorter than the 130ka to 116 ka interval based on closed-system U/Th ages on fossil corals. We thus assign very low confidence to this particular reconstruction of sea level change from the Red Sea.

5.5.3 The Holocene

The first decrease in ice volume of 5–10 m occurred at about 19.6 ka (Clark et al., 2004; De Deckker and Yokoyama, 2009; Hanebuth et al., 2009; Yokoyama et al., 2000) with retreat of ice most likely occurring in the NH (Clark et al., 2009), but with a small but unquantified contribution from Antarctica. Most of the melting occurred within the first 9000 years and sea level rose at an average rate of about 6 mm yr^{-1} from about 19 ka to 14.5 ka (Clark et al., 2009; Lambeck et al., 2002). Near the end of the Pleistocene, at the Bølling-Allerød boundary about 14.6 ka, a major global rise in sea level occurred (Meltwater Pulse 1A, MWP-1A) of about 20 m within less than 500 years (Bard et al., 1990; Hanebuth et al., 2000) but because of the response to the rapid changes in ice volume required to produce these meltwater pulses, the amplitude of this rise will be spatially variable (Clark et al., 2002). The source of MWP-1A remains widely debated with most attention being on scenarios in which the Antarctic Ice Sheet contributed significantly (Bassett et al., 2005; Clark et al., 2002; Clark et al., 2009) or very little (Bentley et al., 2010; Mackintosh et al., 2011). During the early part of the Holocene the rise was about 60 m globally over approximately 5000 years (Lambeck et al., 2002), with a possible meltwater pulse (MWP-1B) immediately after the end of the Younger Dryas (Bard et al., 2010; Edwards et al., 1993; Fairbanks, 1989). The end of the Younger Dryas also defines the end of Termination I and coincides with start of the present interglaciation when post-LGM global surface temperatures were first comparable to today (Denton et al., 2010).

Coral-based sea level records suggest that rates of ice volume change during the early Holocene were relatively constant (Bard et al., 1996; Edwards et al., 1993; Fairbanks, 1989; Lambeck et al., 2002), whereas higher resolution sea level records suggest two periods of more rapid ice mass loss between about 9 ka and 8.5 ka (Cronin et al., 2007; Hijma and Cohen, 2010) and from 7.5 ka to 6.5 ka (Bird et al., 2007; Bird et al., 2010; Yu et al., 2007). Rates of GMSL rise decreased significantly at about 7 ka to 6 ka (Lambeck and Chappell, 2001) resulting in the occurrence of sea level highstands with amplitudes ranging from a few decimeters to several meters in equatorial ocean basins (Azmy et al., 2010; Horton and Edwards, 2006; Kench et al., 2009; Switzer et al., 2010) as a consequence of GIA.

For the past about 5 kyr GMSL has been close to present sea level but not constant. Ocean volumes did continue to increase during this interval with a GMSL rise of 2–3 m between about 6 ka and 3 ka (Lambeck et al., 2004; Lambeck et al., 2010b). Peltier (2002) also suggested that cessation of land-ice volume change did not occur until about 4 ka. About 50% of this ocean volume increase can be attributed to a Late Holocene ice reduction over Marie Byrd Land, Antarctica (Stone et al., 2003).

Spatial variability in sea level change during the Late Holocene has remained significant because of the residual isostatic response to the last deglaciation and for which comprehensive and predictive models exist (Milne and Mitrovica, 2008). Local sea level records spanning this interval and based on consistent sea level indicators (Goodwin and Harvey, 2008; Lambeck et al., 2002; Moriwaki et al., 2006; Woodroffe et al., submitted) (Figure 5.17) indicate that fluctuations in global sea level during this interval have not exceeded ~ ±25 cm on time scales of a few hundred years.

The observational record for the past 2 kyr up to pre-industrial times is of the highest precision, with three types of proxies capable of resolving decimeter-scale sea level fluctuations on sub-centennial timescales. These are: salt-marsh plants and microfauna that form distinctive elevation zones reflecting variations in tolerances to the frequency and duration of tidal inundation (Donnelly et al., 2004; Gehrels et al., 2008; Horton and Edwards, 2006; Kemp et al., 2009; Long et al., in press); coral microatolls found in intertidal environments close to lowest spring tides (Goodwin and Harvey, 2008; Smithers and Woodroffe, 2001; Woodroffe and McLean, 1990); and coastal archaeological features constructed with direct (e.g., fish ponds and certain harbour structures) or indirect (e.g., water wells) relationships to sea level (Anzidei et al., 2011; Auriemma and Solinas, 2009; Lambeck et al., 2004; Sivan et al., 2004).

Reconstructions from salt marsh records have been validated against regional twentieth century tide-gauge records and justify their application to time periods prior to tide-gauge observations. Regionally, as along the US Atlantic coast and Gulf of Mexico coast, these records reveal some consistencies in sea level oscillations over multi-decadal and millennial timescales (González and Törnqvist, 2009; Kemp et al., in press; van de Plassche et al., 1998) (Figure 5.17) but they have not yet been identified as truly global phenomena. There are also considerable differences between records based on different types of data sets that may be due to different local responses to global processes driving sea level change or to uncertainties in the methods and assumptions used to reconstruct sea level at levels of accuracy of 20–25 cm or better.

The most robust signal captured in the salt-marsh proxy sea level records from both northern and southern hemispheres, is an acceleration late in the nineteenth century (Figure 5.17) that is widely interpreted to mark the transition from relatively low rates of change during the late Holocene (order tenths of mm yr^{-1}) to modern rates (order mm yr^{-1}). Variability in both the magnitude and the timing (1840 CE to 1920 CE) of this acceleration occurs (Gehrels et al., 2008; Gehrels et al., 2011; Gehrels et al., 2006; Kemp et al., in press; Kemp et al., 2009), this is to be expected given the processes responsible (see Chapter 13) and the accuracy and precision (in height and time) of the LSL reconstructions.

A summary of estimates of sea level change and, where possible, estimates of rates of change is given in Table 5.4.

Table 5.4: Estimates of sea level change and, where possible, estimates of rates of change. Small sample sizes and unevaluated model uncertainties preclude a meaningful estimation of probabilistic uncertainties. Best estimates of magnitudes and rates of past sea level change are based on an expert judgment, considering the available information and associated uncertainties.

Geological Period	Note	Magnitudes of sea level change		Rates of sea level change		Unresolved issues
		Best estimate	Maximum	Best estimate	Maximum	
Pliocene	(i)	+20 ± 10 m				Corrections for non-eustatic contributions
Termination II	(ii)	+120–135 m		20–60 m/<3000 yr		Phasing with climate forcing and insufficient direct observational data
Last Interglacial	(iii) (iv)	+4–5 m +4–6 m	+8 m	1–2 m/1000 yr	1.6 m/100 yr	Chronology & relation of corals to msl Conversion of $\delta^{18}O$ to msl
Termination I	(v) (vi)	+120–135 m		~60 m/6000 yr	~20 m/<500 yr	Phasing Source for meltwater pulses
0 to ~ 1900 CE	(vii)	0 ± 0.25 m		0.25 m/100 yr		Spatial variability of non-GIA origin
1900–2000 CE	(viii)	+150 mm		1.0–3.0 mm/yr		

Notes :

(i) Raymo et al., 2011; Miller et al., 2011 (Section 5.5.1)
(ii) Section 5.5.2
(iii) Coral evidence. Figure 5.15 (D) (Dutton and Lambeck) and (A) (Kopp et al., 2009) (Section 5.2)
(iv) Rohling et al., 2009 (Section 5.2)
(v) From LGM to ~6000 yrs BP (Section 5.5.3)
(vi) MWP-1A (Section 5.5.3)
(vii) Section 5.5.3
(viii) See Chapter 13. The rates increase from early in the century to late in the century.

[INSERT FIGURE 5.15 HERE]

Figure 5.15: Sea level during the Last Interglacial. **a)** The estimate of global mean sea level by Kopp et al. (2009) (red line). The orange lines correspond to the 16th and 84th percentiles. **b)** Predicted sea levels for selected sites in the Caribbean and North Atlantic on the assumption that ice volumes during the interval from 129 ka to 116 ka are equal to those of today and isostatic effects (Lambeck et al., in press), displaying the spatial variability that can be expected across the region. These predictions are strongly dependent on the ice loads over North America both before and after the interglacial period as well as on mantle rheology and observations from these sites provide more information on ice histories than on the global sea level function. **c)** Same as b) but for different sites along the Western Australia coast. The dependence on details of the ice sheet and on earth-model parameters is less important at these sites than for those in b). Thus data from these locations, assuming tectonic stability, is more appropriate for estimating LIG ice volumes. **d)** Local LIG relative sea level reconstructions from Western Australia based on coral elevations and closed-system U-Th ages that pass diagenetic screening. All results are for in-situ samples and *Porites* species. Age error bars correspond to 2 standard deviation uncertainties. Ages are based on the assumption of closed system behaviour and the decay constants of Cheng et al. (2000), $\delta^{234}U$ values within 5‰ of modern sea water, ^{232}Th concentrations less than 2 ppb, and calcite < 2%. All elevations have been normalised to the upper growth limit of corals corresponding to mean low water spring or mean low sea level. The Western Australian reef locations contributing to the result in a) are distributed along almost 1300 km of coastline and experience different responses of the land and sea surfaces to changes in glaciation before and after the Last Interglacial period because of different coastal geometries and different distances from the former ice sheets (c). The blue line indicates the simplest interpretation of local sea level consistent with reef stratigraphy and should be considered as lower limits by an amount indicated by the blue upper limit error bars. The sea level oscillation at about 126 ka to 125 ka (vertical gray band) is consistent with observed stratigraphy and geochronology at sites (e.g., Yukutan, Bahamas) when data is reduced using the same criteria (from Dutton and Lambeck , submitted). The differences from a) in the timing of the start and end of the interglacial interval, as well as in the timing of the lowstand in the middle of the interval may be a consequence of different assumptions used in deriving the model ages. The higher amplitudes in a) are a consequence of including geomorphological information that is poorly constrained in age and data from areas that may be subject to tectonics. **e)** The Western Australian evidence (thick blue line) from d) compared the model-predicted result (red line) from c) for a reference site midway between the northern and southern most localities, the reference ice volume model for the LIG interval (the blue shading) and earth rheology and ice sheet parameters based on rebound analyses from different regions spanning the interval from Marine Isotope Stage 6 to the present (c.f. Lambeck et al., 2006). The difference between the observed and predicted functions provides an estimate of the global mean sea level (green line). Uncertainties in this estimate include the observational uncertainties from d) and estimates of the model uncertainties. **f)** Ice sheet model estimates for global mean sea level during the Last Interglacial for Greenland and Antarctica based on (red curve) the Potsdam CLIMBER intermediate complexity model (Robinson et al., 2011) plus the Antarctic model of Pollard and DeConto (2009), and (blue curve) the Hadley Centre GCM (Stone et al., submitted) with the same Antarctic model. **g)** Same as f) but for Greenland only. **h)** Same as f) but for the Antarctica only. Both east and west Antarctica are included in this model but nearly all of the melt is from West Antarctica.

[INSERT FIGURE 5.16 HERE]

Figure 5.16: [PLACEHOLDER FOR SECOND ORDER DRAFT: more results for climate-ice sheet model results will be included] Modelled Greenland ice sheet distribution at the Last interglacial when the ice sheet volume is the minimum for each model. **a)** For the case of Robinson et al (2011) as their "best guess" and **b)** for the case of Stone et al (submitted) as their "best guess" with contour interval of 500 meters to show the altitude. Red points in the figures show the locations of ice core drilling sites: Dye3, GRIP/GISP (summit), NGRIP, NEEM, Camp Century from the south to the north.

[INSERT FIGURE 5.17 HERE]

Figure 5.17: Sea level change during recent and late Holocene time. **a-d)** High resolution relative sea level results from saltmarsh data at representative sites, without corrections for glacial isostatic movement of land and sea surfaces. Locations are given on the map. The North Carolina (a) result is representative of other North American Atlantic coast locations (Kemp et al., in press). The rate of change occurring late in the 19th century are seen in all high resolution saltmarsh records – e.g., (c) Gehrels et al. (2008); (d) Garcia-Artola et al. (2009); Leorri et al. (2008) that extend into

modern time and is consistent with Roman archaeological evidence (Lambeck et al., 2004). The oscillation in sea level at about 1000 CE seen in the North Carolina record occurs in some (González and Törnqvist, 2009; van de Plassche et al., 1998) but not all records (c.f., Gehrels et al., 2011; Kemp et al., in press). **e)** Estimates of global sea level change from the instrumental record (Jevrejeva et al., 2010). **f-i)** Observed lower resolution records, without isostatic corrections except for Blekinge (i) where the isostatic signal dominates the observed sea level change (Yu et al., 2007), back to 7 ka. The Kiritibati result (f) is for three different locations on the island with each group referred to a locxal height datum [PLACEHOLDER FOR THE SECOND ORDER DRAFT: the final panel will have the separate records from the three microatoll fields reduced to a common datum]. The vertical axis for North Queensland (g) and Mediterranean France (h) correspond to relative sea level with the latter being for three nearby locations for which differential isostatic effects are less than the observational errors (Lambeck and Bard, 2000). Accuracy estimates are discussed in the original papers and include height uncertainties arising from the measurements themselves, from relating the measurement to mean sea level, and, in the case of (i) from the isostatic correction. **j)** Estimates of global mean sea level for the last 6 kyr (j) with the contributing records corrected for the isostatic effects at each location (Lambeck et al., 2010b).

5.6 Evidence and Processes of Abrupt Climate Change

Paleoclimate archives are a rich source of information to study climate changes that happened at a rate faster than the rate of background climate variability. A variety of mechanisms have been suggested to explain the emergence of abrupt climate changes. Most of them invoke the existence of nonlinearities, or, more specifically, thresholds in the underlying dynamics of one or more Earth system components. Both internal dynamics as well as external forcing can trigger abrupt changes in the climate state.

5.6.1 Dansgaard-Oeschger and Heinrich Events, Impacts and Mechanisms

Greenland ice core records spanning the last glacial cycle depict 25 abrupt Dansgaard-Oeschger (DO) events (North Greenland Ice Core Project members, 2004), marked by an abrupt transition (on a timescale of a few decades) from a cold phase (stadial) into a warm phase (interstadial). Subsequently, a more gradual cooling precedes a sudden jump to cold stadial conditions that last for a millennium or longer. Thermal gas-fractionation methods (Huber et al., 2006; Landais et al., 2004) suggest that the rate of regional warming in Greenland associated with these events and millennial-scale variability during the last glacial termination (Brinkhuis et al., 2006; Capron et al., 2010b) ranged from 3°C to 16°C (±2.5°C) within several decades and was accompanied by an abrupt shift in dust and deuterium excess, representing major reorganizations in atmospheric circulation (Steffensen et al., 2008; Thomas et al., 2009). The effects of seasonally varying climate responses (Flückiger et al., 2008), changes in sea ice cover and atmospheric circulation as well as changes in ice sheet topography may have contributed to the magnitude and abruptness of DO events in Greenland (Li et al., 2010b). Corresponding variations in high-resolution SST reconstructions from the eastern subtropical North Atlantic attain values up to 5°C and exhibit smoother stadial-interstadial transitions (on timescales of centuries) compared to the Greenland record (Martrat et al., 2007). Precise synchronization between Greenland and high-resolution Antarctic records (Barbante et al., 2006; Capron et al., 2010a; Capron et al., 2010b; Stenni et al., 2011) has further revealed a one-to-one correspondence between DO events and millennial-scale Antarctic climate change: Northern Hemispheric abrupt stadial-interstadial transitions typically terminate gradual warming trends in Antarctica that accompany stadial phases in the Northern Hemisphere.

As witnessed by the presence of layers of ice-rafted detritus in marine sediments and other sedimentary indicators, some DO stadials correspond to periods of Northern Hemispheric ice sheet instabilities, known as Heinrich events and associated cold phases as Heeinrich stadials. There is strong evidence to suggest that these Heinrich events were accompanied by global sea level rise (Gonzalez and Dupont, 2009; Siddall et al., 2008), rising Antarctic temperatures and weakened North Atlantic Deep Water formation (e.g., Gutjahr et al., 2010; Zahn et al., 1997). The total amount of freshwater release has been estimated to range from essentially zero to several tens of meters in global sea level equivalent (Rohling et al., 2008b; Siddall et al., 2006; Siddall et al., 2008; Yokoyama et al., 2003). Mechanisms to explain the origin of millennial-scale meltwater pulses include ice sheet instabilities, as illustrated by ice sheet climate modelling experiments (Calov et al., 2002; Calov et al., 2010; Marshall and Koutnik, 2006) and ice shelf melting in response to subsurface ocean warming prior weakening of the AMOC (Alvarez-Solas et al., 2010; Marcott et al., 2011; Shaffer et al., 2004) (see Box 5.3).

Evidence for climate variability related to DO events and Heinrich stadials has been reported from the northern North Pacific (Harada et al., 2008; Kiefer et al., 2001; Okazaki et al., 2010; Ono et al., 2005) and the tropical and subtropical North Pacific (Hendy and Kennett, 2000; Stott et al., 2002), with amplitudes reaching several degrees Celsius. In particular, abrupt events such as the Bølling and Allerød Warmings and the Younger Dryas cooling during the last glacial termination left a detectable and widespread imprint on North Pacific SSTs (Harada et al., 2008; Kiefer and Kienast, 2005; Kienast et al., 2006). Atmospheric changes in response to North Atlantic cooling (Okumura et al., 2009; Xie et al., 2008), as well as ocean circulation changes in response to a weakening of the AMOC (Harada et al., 2009; Saenko et al., 2004; Schmittner et al., 2007), have been suggested to explain the presence of millennial-scale variability in the Pacific. Atmospheric circulation changes in response to North Atlantic cooling also exert a strong influence on tropical hydroclimate. North Atlantic cooling (Krebs and Timmermann, 2007; Otto-Bliesner and Brady, 2010) and sea ice variations (Chiang and Bitz, 2005), associated with DO and Heinrich stadials, are very likely to have affected tropical hydroclimate: the position of the North Atlantic ITCZ (Peterson and Haug, 2006), along with a possible contraction of the ITCZ (Collins et al., 2011) and the characteristics of the monsoons in Asia (Wang et al., 2008), Australia-Indonesia (Mohtadi et al., 2011), west African and Arabia (Higginson et al., 2004; Itambi et al., 2009; Ivanochko et al., 2005; Mulitza et al., 2008; Tjallingii et al., 2008; Weldeab et al., 2007). Furthermore, DO stadials were associated with Antarctic warming events, as recorded in polar ice core records (Capron et al., 2010b; Stenni et al., 2011). Recent compilations of global vegetation data (Harrison and Goñi, 2010), $\delta^{18}O$ data of O_2 and CH_4 concentrations in air bubbles in ice cores (Loulergue et al., 2008; Severinghaus et al., 2009) and climate-vegetation models subjected to North Atlantic freshwater forcing (Bozbiyik et al., 2011b; Köhler et al., 2005; Menviel et al., 2008; Obata, 2007) illustrate further that North Atlantic cooling associated with DO and Heinrich stadials influenced vegetation patterns worldwide.

Climate model simulations forced by North Atlantic freshwater anomalies show that the reconstructed large-scale teleconnection patterns of DO and Heinrich stadials are qualitatively similar to those simulated in response to a weakening of the AMOC (Menviel et al., 2011; Otto-Bliesner and Brady, 2010). Since AR4, new proxy data have increased the confidence to a high level that a relation exists between DO events and North Atlantic Ocean circulation changes (e.g., Barker et al., 2010; McManus et al., 2004; Piotrowski et al., 2008; Thornalley et al., 2011). New compilations of benthic radiocarbon age data in the deep North Pacific reveal with medium confidence the presence of well-ventilated deep water during Heinrich stadial 1, which has been interpreted as the temporary emergence of a deep Pacific Meridional Overturning Circulation (Okazaki et al., 2010). Heinrich stadials during the last glacial period and associated Antarctic warmings were accompanied by rises of atmospheric CO_2 concentrations reaching several tens of ppm (Ahn and Brook, 2008). Whether these millennial-scale glacial CO_2 variations have a terrestrial source (Bozbiyik et al., 2011a; Köhler et al., 2005; Menviel et al., 2008; Obata, 2007), or an oceanic origin (Schmittner and Galbraith, 2008) is still controversial.

Newly available marine records (Grützner and Higgins, 2010; Kleiven et al., 2011; Martrat et al., 2007) and Antarctic trace gas records (Loulergue et al., 2008; Schilt et al., 2010) have increased the confidence to a high level that abrupt climate change events, similar to the DO and Heinrich stadials of the last glacial cycle, occurred during the past 800 kyr and, with less confidence, extended back to 1100 ka. The preferred occurrence of these events during glacial periods suggests with medium confidence that processes involving larger ice sheets, more extensive sea ice cover compared to the recent interglacial periods, may be required for generating this type of variability.

5.6.2 Climate Response to Abrupt Deglacial Meltwater Pulses

By forcing climate models transiently with orbitally-induced insolation variations, changes in GHG concentrations, estimates of ice sheet extent and albedo and different histories representing freshwater fluxes from the disintegrating ice sheets (Liu et al., 2009b; Menviel et al., 2011), the time history of some well-dated paleo proxy data can be reproduced in a qualitative sense (Figure 5.18). These results indicate that the reconstructed patterns can be explained through a combination of changes in the strength of the AMOC, a modulation of the interhemispheric SST gradient superimposed on orbitally and CO_2-induced climate changes. However, confidence in the magnitude, duration and location of deglacial meltwater pulses remains low. Accordingly, the information is insufficient to fully assess the actual role of Northern Hemisphere freshwater releases in shaping the last deglaciation. One issue that has emerged from these simulations is

that, at least regionally, in places such as Greenland rapid transitions such as Bølling Allerød warming occurred on timescales of about 10 years (Capron et al., 2010b), whereas the simulated changes in Greenland are happening on timescales in the order of 100 years (Liu et al., 2009b) (Figure 5.18). The reasons for this discrepancy are hitherto unresolved.

Since AR4 there has been renewed interest in the triggering mechanisms of the Younger Dryas meltwater pulse and the Younger Dryas Cold event. Rapid drainage of meltwater into the Arctic Ocean via a Mackenzie River flood has recently been put forward (Murton et al., 2010) as a cause for the Younger Dryas, contrasting the evidence presented for a sustained freshwater routing through St. Lawrence River (Carlson et al., 2007). Current climate models require a century to multi-century-scale freshwater forcing to generate a 1,300-year long Younger Dryas event (see Figure 5.18), thereby challenging the hypothesis that an extreme flood caused this event. Firestone et al. (2007) proposed an extraterrestrial impact as the cause for the Younger Dryas. Their hypothesis has been falsified with high confidence (Paquay et al., 2009; Pinter et al., 2011). While spatial pattern of the Younger Dryas climate anomalies can in principle be understood with high confidence as a response to reduced AMOC strength following a freshwater perturbation, a more detailed history of freshwater forcing is needed to reconcile model solutions and climate proxy data (see Figure 5.18). The postglacial 8.2 ka North Atlantic cooling event is discussed in Section 5.7.2.

In summary, the understanding of what generates global climate anomalies associated with Dansgaard-Oeschger events and Heinrich stadials has improved considerably since AR4. Despite this progress, the assessment of model sensitivities to the freshwater history associated with different stages of ice sheet melt is still limited by the considerable uncertainty of the deglacial freshwater history. Another uncertainty in simulating deglacial abrupt climate change is associated with the range of climate model responses to even the same freshwater perturbations.

[INSERT FIGURE 5.18 HERE]

Figure 5.18: Comparison of paleo proxy data for the last glacial termination (left panels) and 3 transient paleo climate model simulations (right panels) for the period from 18 ka to 11 ka (Liu et al., 2009b; Menviel et al., 2011). **a)** Pa/Th isotope ratio (solid), a proxy for ocean ventilation, from an Atlantic sediment core with uncertainty range (dashed) (McManus et al., 2004); **b)** Composite of Alkenone based SST reconstructions from the Portugese margin in the East Atlantic using cores MD01-2443 (Martrat et al., 2007) and SU8118 (Bard et al., 2000), linearly interpolated onto an equidistant 100 year time grid; **c)** Reflectance of Cariaco sediment core, a proxy for rainfall (Peterson et al., 2000); **d)** Reconstructed Antarctic temperature anomaly stack, relative to 18 ka and based ice core data EPICA Dome C (Jouzel et al., 2007), Dome Fuji (Watanabe et al., 2003), Vostok (Petit et al., 1999), Talos (Stenni et al., 2011), EPICA Dronning Maud Land (Barbante et al., 2006), Byrd (Blunier and Brook, 2001), Law Dome (Morgan et al., 2002); **e)** North Atlantic freshwater forcing applied to the transiently forced CCSM3 (red) (Liu et al., 2009b), and LOVECLIM (black) (Menviel et al., 2011) climate models to mimic millennial-scale variability during the last glacial termination. Both model simulations apply time-varying GHG, orbital and ice sheet forcing; **f)** Simulated maximum of the meridional streamfunction in the North Atlantic [1Sv = 10^6 m^3s^{-1}]; **g)** Simulated Northeastern Atlantic SST anomalies relative to 18 ka averaged over the ocean grid points in the region 15°W–10°W, 36°N–42°N; **h)** Simulated changes in precipitation in percentage, relative to 18 ka in the Cariaco area (8°N–13°N, 67°W–63°W); **i)** Simulated Antarctic continent temperature anomalies relative to 18 ka.

5.7 Paleoclimate Perspective on Irreversibility in the Climate System

The notion of irreversibility implies that after a perturbation the climate system will never return to its initial state even when the perturbation is removed. This requires the existence of multiple equilibrium states in the system. In practice, considering the timescales of perturbations and climate components, irreversibility of climate change can be defined such that the recovery timescale to reach the initial state (through natural processes) is significantly longer than the duration of causal perturbation.

5.7.1 Cryosphere

Modeling studies suggest the existence of multiple equilibrium states for different ice sheets with respect to temperature, CO_2 concentration and orbital forcing phase spaces (Calov and Ganopolski, 2005; DeConto and Pollard, 2003; Ridley et al., 2010). This implies a possibility of irreversible changes in the climate-cryosphere system in the past and future. An abrupt increase in global ice volume (mostly in the Antarctic ice sheet) at the Eocene/Oligocene boundary 33 Ma, likely caused by gradual atmospheric CO_2 concentration decline on geological time scale (Pagani et al., 2005; Pearson et al., 2009), is consistent with the existence of

threshold behaviour in the East Antarctic Ice sheet simulated by the ice sheet models under CO_2 concentrations of 600–800 ppm (DeConto and Pollard, 2003; Langebroek et al., 2009). Proxy records suggest that WAIS collapse might happen during some previous interglacials (Naish et al., 2009a). Together with results of model simulations (Pollard and DeConto, 2009) they suggest that WAIS is very sensitive to the ambient ocean temperature and it is likely that WAIS will melt completely for atmospheric CO_2 concentration above 400 ppm.

Observational evidence suggest that the Greenland ice sheet was much smaller than today during the late Pliocene when atmospheric CO_2 concentration and global temperature were only moderately higher than present (Alley et al., 2010) which is supported by the results of simulations with ice sheet models (Dolan et al., 2011; Koenig et al., 2011). The Greenland ice sheet was also likely considerably reduced during interglacials exceptionnaly long (Marine Isotope Stage 11) and exceptionally warm in the Arctic (Marine Isotope Stage 5.5) (Colville et al., 2011; de Vernal and Hillaire-Marcel, 2008). This would support modelling results which indicate that temperature or CO_2 thresholds for melting and re-growth of the Greenland ice sheet may lay in close proximity to the present climate state (Gregory and Huybrechts, 2006; Lunt et al., 2008) and that the Greenland ice sheet may have multiple equilibrium states under present day climate state (Ridley et al., 2010). This would imply that anthropogenic global warming can lead to irreversible melting of the Greenland ice sheet (Charbit et al., 2008) which may not re-grow till the onset of a new ice age some 50 kyr from now (Berger and Loutre, 2002).

5.7.2 Ocean Circulation

Numerous modeling studies demonstrate high sensitivity of the AMOC to increased freshwater flux into the North Atlantic (Stouffer et al., 2006). Some intermediate complexity model results also suggest that under present climate conditions AMOC may have multiple equilibrium states (Rahmstorf et al., 2005) although this was not yet confirmed with the comprehensive climate models. Experiments with coupled climate models provide evidence that the sensitivity of the AMOC to freshwater perturbation is larger for glacial boundary conditions than for interglacial conditions (Swingedouw et al., 2009) and that the recovery timescale of the AMOC is longer for LGM conditions than for the Holocene (Bitz et al., 2007).

The abrupt climate change event at 8.2 ka is an example with which to study the recovery time of the AMOC to freshwater perturbation under near-modern boundary conditions. Since AR4 substantial new observational and model evidence are published. The pattern of reconstructed and modelled surface ocean and atmospheric climate anomalies is consistent with a reduction in the strength of the AMOC, see Figure 5.19. Although only indirect evidence for changes in AMOC strength can be inferred from proxy records (Figure 5.19), available proxy records from the North Atlantic support the hypothesis that freshwater input into the North Atlantic reduced the amount of deep and central water-mass formation as seen in Figure 5.19 as reduced Nordic Seas overflows, reduced intermediate water temperatures and reduced ventilation state of North Atlantic Deep Water (Bamberg et al., 2010; Ellison et al., 2006; Kleiven et al., 2008; McManus et al., 2004). A concomittant cooling of SST and atmospheric temperatures in the North Atlantic and in Greenland has been observed (Figure 5.19) with the climate anomaly associated with the event lasting 100–150 years. The additional freshwater that entered the North Atlantic during the 8.2 ka event is estimated to range between 1.6 and $8 \cdot 10^{14}$ m^3 (Barber et al., 1999; Clarke et al., 2004; von Grafenstein et al., 1998). The duration of the meltwater pulse may have been as short as 0.5 years (Clarke et al., 2004). Based on the paleoceanographic reconstructions, the freshwater perturbation of this size was insufficient to trigger a complete collapse of the AMOC (Figure 5.19). The reconstructions consistently show that the shallow and deep overturning circulation of the North Atlantic recovered completely after the cessation of the meltwater perturbation. The recovery timescale was on the order of 200 years (Bamberg et al., 2010; Ellison et al., 2006) (Figure 5.19 c, d). One record points to a partial recovery on a decadal timescale (Kleiven et al., 2008). It is possible that this record is affected by a threshold effect due to the vertical displacement of deep water masses. Both recovery timescale and sensitivity of the AMOC to the freshwater perturbation are consistent with model experiments for the 8.2 ka event using coarse resolution models, GCMs and eddy permitting models (LeGrande and Schmidt, 2008; Li et al., 2009; Spence et al., 2008). The recovery of temperatures out of the cold anomaly appears overprinted with natural variability in the proxy data, and is more gradual in data than in the GCM experiments (Figure 5.19 e, f).

Associated with the North Atlantic climate and AMOC induced anomalies is a characteristic teleconnection pattern with widespread Northern Hemisphere cooling and drying and a southward displacement of the ITCZ (See Figure 5.19 e, f). These patterns are highly consistent between paleoclimate observations and the ensemble response to a freshwater perturbation in the North Atlantic of 0.1 Sv. Model experiments indicate that a hemispheric see-saw pattern existed during the event, and there is some support from observations that this likely was the case.

[INSERT FIGURE 5.19 HERE]

Figure 5.19: Compilation of selected paleoenvironmental and climate model data for the 8.2 ka event documenting temperature and ocean circulation changes around the event and the spatial extent of climate anomalies following the event. Published age constraints for the period of release of freshwater from glacier lakes Agassiz and Ojibway are bracketed in a). Vertical grey bar denotes the main cold event as found in Greenland Ice core records (Thomas et al., 2007). **a)** Black curve: NorthGrip $\delta^{18}O$ (temperature proxy) from Greenland Summit. Red curve: Simulated Greenland temperature in an 8.2 ka event simulation with the ECBilt-CLIO-VECODE model (Wiersma et al., 2011). Blue curve: Simulated Greenland temperature in an 8.2 event simulation with the CCSM3 model (Morrill et al., in press). **b)** North Atlantic/Nordic Seas SST-reconstructions, age models are aligned on the peak of the cold-event (less than 100-year adjustment). Blue curve: Nordic Seas (Risebrobakken et al., 2011). Black curve: Gardar Drift south of Iceland (Ellison et al. 2006). **c)** Deep- and intermediate water records. Black curve: Sortable silt record (overflow strength proxy) from Gardar Drift south of Iceland (Ellison et al., 2006), Atlantic intermediate water temperature reconstruction (Bamberg et al., 2010). **d)** Black curve: $\delta^{13}C$ (deep water ventilation proxy) at 3.4 km water depth south of Greenland (Kleiven et al., 2008). Age model is aligned on the minimum overflow strength in c) (less than 100-year adjustment). Modelled change in the strength of the AMOC: Green curve: An 8.2 ka event simulation with the GISS model (LeGrande et al., 2006). Red curve: An 8.2 ka event simulation with the ECBilt-CLIO-VECODE (v. 3) model (Wiersma et al., 2011). Blue curve: An 8.2 ka event simulation with the CCSM3 model (Morrill et al., in press). **e)** Spatial distribution of the ensemble mean annual mean surface temperature anomaly (°C) from a multi-model water housing experiment with 0.1 Sv freshwater forcing in the NW Atlantic (Stouffer et al., 2006). Paleoclimate data from records resolving the 8.2 ka event are plotted with symbols: C=cold anomaly, W=warm anomaly, X=No significant anomaly. Main data sources: (Wiersma et al., 2011), Morrill et al. 2011 with supplements (complete literature list in supplementary information). **f)** Spatial distribution of the ensemble mean annual mean precipitation anomaly (mm day^{-1}) from a multi-model water housing experiment with 0.1 Sv freshwater forcing in the NW Atlantic (Stouffer et al., 2006). Paleoclimate data from records resolving the 8.2 ka event are plotted with symbols: D=dry anomaly, W=wet anomaly, X=No significant anomaly. Main data sources: (Wiersma et al., 2011), Morrill et al. in press with supplements (complete literature list in supplementary information).

[START BOX 5.3 HERE]

Box 5.3: Earth-System Feedbacks and their Role in Climate Change

The response of the Earth system to perturbation is determined by the adjustment time (inertia) of individual components of the Earth system and by feedbacks within and between these components (some of which are represented in Box 5.3, Figure 1). An initial response is amplified if positive feedbacks dominate, but damped if negative feedbacks are stronger. The time-evolution of the response to a temporary perturbation, such as a radiative forcing anomaly, is governed by the magnitude and timescale of these processes. The Earth system may then return to its initial state on a timescale controlled by its inertia and by the relative strength of negative and positive feedbacks. Alternatively, the changes may be irreversible (Section 5.7) if the temporary perturbation drives the Earth system to a new equilibrium state in which it remains for a very long time after the removal of the initial perturbation. The existence of multiple equilibria is closely linked to the existence of nonlinear feedbacks. A third type of response is the excitation of oscillatory behaviour, involving a combination of positive and delayed negative feedbacks. On timescales of 10^4–10^5 years the Earth system is continuously forced by orbitally-induced variations in the distribution of solar radiation. As a result, the slow components of the Earth system, that have similar response timescales (10^3–10^5 years), such as ice sheets and the marine and terrestrial carbon cycle, may in fact never be in equilibrium with the continuously varying external forcings. The implications of this potential non-equilibrium behaviour are far reaching and concern in particular estimates of climate sensitivity. Two types of equilibrium climate sensitivity have been introduced (see Chapter 1):

- The *Charney climate sensitivity* characterizes the equilibrium response of the climate system to radiative forcings, allowing for fast feedbacks between atmosphere, ocean, sea ice and land, but

assuming the stationarity of Earth system components, such as the carbon cycle, ice sheets and vegetation. This concept has been adopted in TAR and AR4. Most recent AR5 updates on the probability distribution of the Charney climate sensitivity can be found in Chapter 12.

- In contrast, the *Earth-system sensitivity* (Hansen et al., 2008; Lunt et al., 2010a) accounts also for other Earth system feedbacks and slow processes such as the equilibration of ice sheets, vegetation and the carbon cycle on timescales of hundreds to thousands of years and beyond.

While climate and Earth-system sensitivities can be readily calculated from radiative perturbation experiments conducted with climate and Earth-system models, the applicability of these equilibrium concepts to paleo proxy data is less straightforward. Possible non-equilibrium effects need to be considered. When considering climate change over the next few centuries and beyond, the relative importance of slow Earth-system feedbacks will increase. Since AR4, slow components such as ice sheets, vegetation or the carbon cycle have been incorporated into climate models. By analysing the role of slow feedbacks using such Earth-system models in combination with climate proxy data, estimates of the Earth-system sensitivity have been derived and range from 30% to 50% (Lunt et al., 2010a) to about 100% above the Charney climate sensitivity (Hansen et al., 2008). Despite this large uncertainty there is medium confidence that Earth-system feedbacks will enhance any warming above the level associated with the short-term Charney climate sensitivity.

Ice sheets have played an essential role in Earth's climate history. They interact with the atmosphere, the ocean, the lithosphere and the surrounding vegetation (see Box 5.3, Figure 1). Ice sheets form when snow accumulation exceeds summer melting. Expansion of an ice sheet replaces previously vegetated areas, with relatively low albedo, by higher-albedo ice, leading to major changes in surface albedo and heat balance, and changing the mass balance of the ice sheet. As ice sheets grow in height and area, surface temperatures drops as a result of the lapse rate effect, but also snow accumulation decreases because colder air holds less moisture (inset in Box 5.3, Figure 1, shows typical vertical profiles of temperature and humidity). This so-called elevation-desert effect (Oerlemans, 1980) is an important negative feedback for ice-sheets and limits their growth under cold conditions. Ice sheets also affect the atmospheric stationary wave structure and associated regional patterns of temperature and snowfall (e.g., Roe and Lindzen, 2001). The enormous weight of mature ice sheets causes a depression of the underlying bedrock, a drop in ice sheet height and hence a warming of its surface as a result of the lapse rate effect. The lithospheric adjustment has been shown to play an important role in delaying the ice sheet response to orbital forcing. Higher ice sheets are associated with enhanced calving at their margins, because the ice flow will be accelerated directly by increased pressure and indirectly by lubrication from pressure-induced melting at the base of the ice sheet. This negative feedback on the ice sheet has been suggested as a mechanism to generate ice sheet instabilities that operate on millennial timescales. Calving, basal lubrication and other forms of thermo-mechanical coupling may have played important roles in accelerating glacial terminations, and hence in contributing to the temporal saw-tooth structure (Figure 5.5) of glacial cycles. Other processes that need to be considered are ice-sheet/ice shelf ocean instabilities.

Major uncertainties remain in our understanding of the details of Earth-system feedbacks (for example, those associated with the interactions between oceans, ice shelves and ice sheets). Quantifying the magnitudes of these feedbacks relative to each other and for different past climate periods requires concerted modelling efforts, using a range of Earth-system models in combination with the analysis of quantitative reconstructions of past climate variations.

[**INSERT BOX 5.3, FIGURE 1 HERE**]

Box 5.3, Figure 1: Schematic illustration of multiple interactions between ice sheets, solid Earth, and climate system which can drive internal variability and affect the coupled ice sheet – climate response to external forcings on timescales of hours to millions of years.

[END BOX 5.3 HERE]

[START FAQ 5.1 HERE]

FAQ 5.1: How Unusual is the Current Sea Level Rate of Change?

The current rate of mean global sea level change, estimated at 1.7 ± 0.2 mm per year for the entire 20th century and 3.2 ± 0.5 mm per year since 1993 (the satellite altimetry era) (Chapter 13) is unusual in the context of the last two millennia. However, this rate is not unusual relative to past periods of rapid ice sheet decay, such as during transitions between glacial and interglacial periods. Exceptional tectonic effects can also drive very rapid local sea level changes, with rates exceeding the current rates of change. The basis for this answer is presented next.

Sea level at any location is a measure of the position of the sea surface relative to the land, both of which may be moving relative to the center of the Earth, reflecting a combination of climate (e.g., ocean temperature changes and thermal expansion/contraction, changes in terrestrial glacier ice mass, current velocities) and geophysical factors (e.g., land subsidence or uplift, glacial isostatic adjustments, changes in Earth rotation). Local and regional changes in these factors results in significant deviations from the global estimate of the mean rate of sea level change. For example, sea level is falling at rates approaching 10 mm per year along the Swedish coast of the Gulf of Bothnia, due to ongoing uplift caused by the loss of continental ice since the last glacial period. In contrast, sea level rose at rate of about 12 mm per year from 1940 to 2005 in Bangkok, mainly in response to ground subsidence.

The average rate of global sea level change over the 20th century (1.7 ± 0.2 mm per year) may seem small relative to observations of wave and tidal oscillations around the globe, which can be orders of magnitude larger. However, when this rate is integrated over time, the magnitude of sea level becomes quite significant, especially in the heavily populated, low-lying coastal regions of the Earth.

In the pre-instrumental period, estimates of the global rate of sea level change are derived from indirect measures of sea level change recorded in sedimentary, biological and archaeological archives. These proxy records are spatially limited, and reflect both local and global conditions. Reconstruction of a global signal is strengthened when individual records from widely different environmental settings converge on a common signal.

Sea level reconstructions for the last two millennia offer an opportunity to use proxy records to overlap with, but extend beyond the instrumental period. A recent example of such a reconstruction used sedimentary evidence from salt-marsh deposits on the Atlantic Coast of the United States, combined with sea level reconstructions based on tide gauge data and model predictions, to document an average rate of local sea level change since the late 19th century of 2.1 mm per year. This century-long rate of sea level rise exceeded any other century-scale sea level change rate in the entire 2000-year record.

On longer timescales, much larger rates and amplitudes of sea level changes were encountered. During the late Quaternary, glacial-interglacial climate cycles resulted in global sea level changes of up to about 120 m to140 m. Much of this change occurred in the transition from a full glacial period to an interglacial period; such transitions occurred over a duration of 10,000-15,000 years, at average rates of 10-15 mm per year. These high rates are only sustainable when the planet is emerging from periods of extreme glaciation when there are large high-latitude ice sheets in contact with the oceans. During some intervals of the transition from the last glacial maximum (about 21,000 years ago) to the present interglacial (Holocene), global sea level rose abruptly by 15-20 m within 100-300 years, which translates to rates of 50-200 mm per year of sea level rise over these short intervals of time. Many of these estimates of rapid changes in sea level are based on the analysis of fossil coral reef deposits.

On even longer geologic timescales, major geological processes such as formation of a submerged ocean basaltic plateau can displace sufficient water to raise sea level by 5–10 m but the duration of plateau formation is millions to tens-of-millions of years and the maximum rate of the associated change in sea level is less than 0.01 mm per year.

It is important to note that these examples from the geological record, which indicate rates of sea level change greater than observed today, all occur in special circumstances in either time or location: at times of transition from full glacial to interglacial condition; at locations where the long-term after effects of these transitions are still occurring; at locations of major tectonic upheavals or at locations in major deltas where

subsidence due to a sediment compaction, sometimes amplified by human factors such as ground-fluid extraction.

In summary, the current rate of mean global sea level change is unusual relative to that observed and/or estimated over the last two millennia.

[INSERT FAQ 5.1, FIGURE 1 HERE]

FAQ 5.1, Figure 1: Estimates of the average rate of sea level change (mm per year) for 4 select time intervals: last glacial/interglacial transition; last 2 millennia; 20th century; satellite altimetry era (1993-2010). See text for discussion.

[END FAQ 5.1 HERE]

[START FAQ 5.2 HERE]

FAQ 5.2: Is the Sun a Major Driver of Climate Changes?

The Sun is the main driver of the climate system. Is it therefore also a major driver of climate changes? The answer depends strongly on the time scales we consider. The sun is a major driver of climate change on timescales such as seasonal and orbital, but it is not a major driver of the observed climate changes over the past 40 years. The basis for these answers is presented next.

In equatorial regions the electromagnetic solar power arriving at the top of the Earth's atmosphere reaches a maximum of ~1360 watts per square meter (W m^{-2}) at noon. This power per square meter is called **Total Solar Irradiance (TSI)**. The total power received by the whole Earth amounts to $1.7 \cdot 10^{17}$ W which corresponds to a global average incoming power of ~340 W m^{-2} (a quarter of 1360 W m^{-2}). This power is subject to changes on time scales ranging from minutes to billion of years depending on its generation and emission by the Sun and the Sun-Earth distance. Its distribution on Earth varies with latitude and season. About 30% is reflected back into space by clouds, snow, ice etc.

Solar energy is generated in the Sun's core by fusion processes turning hydrogen into helium. Every second the Sun loses more than 4 million tons of mass by the electromagnetic radiation emitted into space. The standard solar model predicts that on time scales of billion of years this emission steadily increases leading to a large change in the average insolation (Figure 1a). However, the rate of change is extremely small, about 0.1 W m^{-2} per million years.

The Earth's orbit around the Sun is elliptical which results in annual insolation fluctuations of about 3% (between the smallest and the largest distance). Eccentricity, the deviation of the Earth's elliptical orbit from a circle, is disturbed by the gravitational pull of the other planets with cycles of about 100,000 and about 400,000 years (Figure 1b). The mean annual change in the total solar radiation received between a glacial and an interglacial period is only about 0.2–0.3 W m^{-2}. Orbital forcing is the only forcing which can be calculated accurately for several million years from the past into the future (Sections 5.2.1.1 and 5.3.3).

The total amount of radiation emitted by the Sun is related to its magnetic activity. Satellite-based TSI records begin in 1978, and show changes in phase with the 11-year activity cycle. The average change of TSI over an 11-year cycle is about 0.1% corresponding to about 1.4 W m^{-2}. TSI reconstructions spanning past centuries to millennia (Figure 1c) are based on sunspots (back to 1600 CE) and cosmogenic radionuclides for older times (i.e., ^{10}Be in ice cores and ^{14}C in tree rings), which represent proxies of the solar magnetic activity. Solar activity over the recent past is characterized by a high value during the most recent period (1950–2010 CE), distinct periods of 50 to 100 years of very low activity called grand solar minima (e.g., Maunder minimum; 1645–1715 CE), and cycles with several well-defined periodicities up to 2200 years. Most estimates of the average TSI change between the Maunder minimum and the instrumental period (since 1978) ranges from 0.1 to 0.2% (see Figure 5.1).

Satellite measurements since 1991 show that much larger changes (100% or more) in solar irradiance have occurred for particular wavelengths of radiation (especially ultra-violet, UV). Changes in UV radiation affect

upper atmosphere (including the ozone layer), which can in turn influence tropospheric circulation and surface climate.

In contrast to GHG, solar insolation is unevenly distributed on the globe. The response of the climate system is complex and does not only depend on the forcing strength in W m^{-2} but also on its duration and its specific properties. The present increase in global radiative forcing as a result of the man-made GHG is estimated to be 2 W m^{-2}.

Considering the background information provided above, we return to the question "Is the sun a major driver of climate change?"

- Yes, in terms of the long-term evolution of the energy production in the Sun since the formation of the solar system 4.55 billion years ago.
- Yes, in terms of driving glacial-interglacial cycles on Earth in response to changes in Earth's orbital parameters. On these time scales, the change in the mean global insolation is small (about 0.2 W m^{-2}), but the change in the latitudinal distribution of the insolation is large (up to several tens of W m^{-2}).
- Inconclusive, in terms of driving multi-decadal to millennial scale climate changes because estimates of the amplitude of the solar irradiance changes on these time scales are very uncertain partly because recent decades have been characterized by relatively high solar activity. The irradiance characteristics of a low-activity Sun are not well known, though the last minimum between cycles 23 and 24 (2008–2010 CE) provided a short glimpse of a low-activity sun. Statistical analysis of the past 10,000 years of solar activity suggests that the recent period of high activity may end within the next 1–2 cycles (11–22 years). When a period with low activity does occur, better estimates of long-term changes in solar irradiance will become available.
- No, in terms of being a major driver of the climate changes over the past 40 years because instrumental TSI and SSI records contain no significant trend; whereas records of global mean temperature and GHG concentrations contain significant trends of increasing values. This lack of agreement in trends demonstrates that the Sun did not play a role during this period.

[INSERT FAQ 5.2, FIGURE 1 HERE]

FAQ 5.2, Figure 1: Long-term variation of the mean global insolation at 1 AU (mean Sun-Earth distance). **a)** after the formation of the solar system 4.55 billion years ago the insolation was around 25% lower than today. It will steadily increase for the next about 5 billion years until the Sun will become a red giant and destroys life on Earth. **b)** Changes of the mean global insolation for the past and the future one million years as a result of the planetary effects on the eccentricity (deviation from a circle) of the Earth's orbit around the Sun. **c)** Mean global insolation derived from the reconstructed total solar irradiance (TSI) covering approximately the past 10,000 years. These variations are caused by partly cyclic changes of the solar magnetic activity (see Section 5.2.1.2).

[END FAQ 5.2 HERE]

References

Abe-Ouchi, A., T. Segawa, and F. Saito, 2007: Climatic Conditions for modelling the Northern Hemisphere ice sheets throughout the ice age cycle. *Climate of the Past*, **3,** 423-438.

Abram, N. J., M. K. Gagan, J. E. Cole, W. S. Hantoro, and M. Mudelsee, 2008: Recent intensification of tropical climate variability in the Indian Ocean. *Nature Geoscience*, **1,** 849-853.

Abram, N. J., M. K. Gagan, Z. Y. Liu, W. S. Hantoro, M. T. McCulloch, and B. W. Suwargadi, 2007: Seasonal characteristics of the Indian Ocean Dipole during the Holocene epoch. *Nature*, **445,** 299-302.

Adams, J. B., M. E. Mann, and C. M. Ammann, 2003: Proxy evidence for an El Niño-like response to volcanic forcing. *Nature*, **426,** 274-278.

Adler, R. E., et al., 2009: Sediment record from the western Arctic Ocean with an improved Late Quaternary age resolution: HOTRAX core HLY0503-8JPC, Mendeleev Ridge. *Global and Planetary Change*, **68,** 18-29.

Ahn, J., and E. Brook, 2007: Atmospheric CO_2 and climate from 65 to 30 ka BP. *Geophysical Research Letters*, **34,** L10703.

Ahn, J., and E. J. Brook, 2008: Atmospheric CO_2 and climate on millennial time scales during the last glacial period. *Science*, **322,** 83-85.

Alley, R. B., P. U. Clark, P. Huybrechts, and I. Joughin, 2005: Ice sheet and sea level changes. *Science*, **310,** 456-460.

Alley, R. B., et al., 2010: History of the Greenland Ice Sheet: paleoclimatic insights. *Quaternary Science Reviews*, **29,** 1728-1756.

Alvarez-Solas, J., S. Charbit, C. Ritz, D. Paillard, G. Ramstein, and C. Dumas, 2010: Links between ocean temperature and iceberg discharge during Heinrich events. *Nature Geoscience*, **3,** 122-126.

Ammann, C., and E. Wahl, 2007: The importance of the geophysical context in statistical evaluations of climate reconstruction procedures. *Climatic Change*, **85,** 71-88.

Ammann, C., M. Genton, and B. Li, 2010: Technical Note: Correcting for signal attenuation from noisy proxy data in climate reconstructions. *Climate of the Past*, **6,** 273-279.

Ammann, C., F. Joos, D. Schimel, B. Otto-Bliesner, and R. Tomas, 2007: Solar influence on climate during the past millennium: Results from transient simulations with the NCAR Climate System Model. *Proceedings of the National Academy of Sciences of the United States of America*, **104,** 3713-3718.

Anchukaitis, K. J., B. M. Buckley, E. R. Cook, B. I. Cook, R. D. D'Arrigo, and C. M. Ammann, 2010: Influence of volcanic eruptions on the climate of the Asian monsoon region. *Geophysical Research Letters*, **37,** L22703.

Andersen, K., et al., 2004: High-resolution record of Northern Hemisphere climate extending into the last interglacial period. *Nature*, DOI 10.1038/nature02805**,** 147-151.

Anderson, J. B., S. S. Shipp, A. L. Lowe, J. S. Wellner, and A. B. Mosola, 2002: The Antarctic Ice Sheet during the Last Glacial Maximum and its subsequent retreat history: a review. *Quaternary Science Reviews*, **21,** 49-70.

Andersson, C., F. S. R. Pausata, E. Jansen, B. Risebrobakken, and R. J. Telford, 2010: Holocene trends in the foraminifer record from the Norwegian Sea and the North Atlantic Ocean. *Climate of the Past*, **6,** 179-193.

Antoine, P., et al., 2009: Rapid and cyclic aeolian deposition during the Last Glacial in European loess: a high-resolution record from Nussloch, Germany. *Quaternary Science Reviews*, **28,** 2955-2973.

Anzidei, M., F. Antonioli, A. Benini, K. Lambeck, D. Sivan, E. Serpelloni, and P. Stocchi, 2011: Sea level change and vertical land movements since the last two millennia along the coasts of southwestern Turkey and Israel. *Quaternary International*, **232,** 13-20.

Appenzeller, C., T. F. Stocker, and M. Anklin, 1998: North Atlantic oscillation dynamics recorded in Greenland ice cores. *Science*, **282,** 446-449.

Auriemma, R., and E. Solinas, 2009: Archaeological remains as sea level change markers: A review. *Quaternary International*, **206,** 134-146.

Azmy, K., E. Edinger, J. Lundberg, and W. Diegor, 2010: Sea level and paleotemperature records from a mid-Holocene reef on the North coast of Java, Indonesia. *International Journal of Earth Sciences*, **99,** 231-244.

Baker, V. R., 2008: Paleoflood hydrology: Origin, progress, prospects. *Geomorphology*, **101,** 1-13.

Bakke, J., S. O. Dahl, and A. Nesje, 2005a: Lateglacial and early Holocene palaeoclimatic reconstruction based on glacier fluctuations and equilibrium-line altitudes at northern Folgefonna, Hardanger, western Norway. *Journal of Quaternary Science*, **20,** 179-198.

Bakke, J., S. O. Dahl, Ø. Paasche, R. Løvlie, and A. Nesje, 2005b: Glacier fluctuations, equilibrium-line altitudes and palaeoclimate in Lyngen, northern Norway, during the Lateglacial and Holocene. *The Holocene*, **15,** 518-540.

Bakke, J., S. O. Dahl, Ø. Paasche, J. Riis Simonsen, B. Kvisvik, K. Bakke, and A. Nesje, 2010: A complete record of Holocene glacier variability at Austre Okstindbreen, northern Norway: an integrated approach. *Quaternary Science Reviews*, **29,** 1246-1262.

Balmaceda, L., N. Krivova, and S. Solanki, 2007: Reconstruction of solar irradiance using the group sunspot number. *Advances in Space Research*, **40,** 986-989.

Bamberg, A., Y. Rosenthal, A. Paul, D. Heslop, S. Mulitza, C. Rühlemann, and M. Schulz, 2010: Reduced North Atlantic Central Water formation in response to early Holocene ice sheet melting. *Geophysical Research Letters*, **37,** L17705.

Bar-Matthews, M., A. Ayalon, M. Gilmour, A. Matthews, and C. J. Hawkesworth, 2003: Sea–land oxygen isotopic relationships from planktonic foraminifera and speleothems in the Eastern Mediterranean region and their implication for paleorainfall during interglacial intervals. *Geochimica et Cosmochimica Acta*, **67,** 3181-3199.
Barbante, C., et al., 2006: One-to-one coupling of glacial climate variability in Greenland and Antarctica. *Nature*, **444,** 195-198.
Barber, D., et al., 1999: Forcing of the cold event of 8,200 years ago by catastrophic drainage of Laurentide lakes. *Nature*, **400,** 344-348.
Bard, E., B. Hamelin, and R. G. Fairbanks, 1990: U-Th ages obtained by mass spectrometry in corals from Barbados: sea level during the past 130,000 years. *Nature*, **346,** 456-458.
Bard, E., B. Hamelin, and D. Delanghe-Sabatier, 2010: Deglacial Meltwater Pulse 1B and Younger Dryas Sea Levels Revisited with Boreholes at Tahiti. *Science*, **327,** 1235-1237.
Bard, E., F. Rostek, J. L. Turon, and S. Gendreau, 2000: Hydrological impact of Heinrich events in the subtropical northeast Atlantic. *Science*, **289,** 1321-1324.
Bard, E., B. Hamelin, M. Arnold, L. Montaggioni, G. Cabioch, G. Faure, and F. Rougerie, 1996: Deglacial sea level record from Tahiti corals and the timing of global meltwater discharge. *Nature*, **382,** 241-244.
Barker, S., G. Knorr, M. J. Vautravers, P. Diz, and L. C. Skinner, 2010: Extreme deepening of the Atlantic overturning circulation during deglaciation. *Nature Geoscience*, **3,** 567-571.
Baroni, M., M. H. Thiemens, R. J. Delmas, and J. Savarino, 2007: Mass-Independent Sulfur Isotopic Compositions in Stratospheric Volcanic Eruptions. *Science*, **315,** 84-87.
Baroni, M., J. Savarino, J. Cole-Dai, V. Rai, and M. Thiemens, 2008: Anomalous sulfur isotope compositions of volcanic sulfate over the last millennium in Antarctic ice cores. *Journal of Geophysical Research-Atmospheres*, **113,** D20112.
Barriendos, M., and F. S. Rodrigo, 2006: Study of historical flood events on Spanish rivers using documentary data. *Hydrological Sciences Journal*, **51,** 765-783.
Barriendos, V. M., and J. Martin-Vide, 1998: Secular Climatic Oscillations as Indicated by Catastrophic Floods in the Spanish Mediterranean Coastal Area (14th–19th Centuries). *Climatic Change*, **38,** 473-491.
Barriopedro, D., E. M. Fischer, J. Luterbacher, R. M. Trigo, and R. García-Herrera, 2011: The Hot Summer of 2010: Redrawing the Temperature Record Map of Europe. *Science*, **332,** 220-224.
Bartlein, P., et al., 2011: Pollen-based continental climate reconstructions at 6 and 21 ka: a global synthesis. *Climate Dynamics*, **37,** 775-802.
Bassett, S., G. Milne, J. Mitrovica, and P. Clark, 2005: Ice sheet and solid earth influences on far-field sea level histories. *Science*, **309,** 925-928.
Bauch, H. A., E. S. Kandiano, J. Helmke, N. Andersen, A. Rosell-Mele, and H. Erlenkeuser, 2011: Climatic bisection of the last interglacial warm period in the Polar North Atlantic. *Quaternary Science Reviews*, **30,** 1813-1818.
Beerling, D., and D. Royer, 2011: Convergent Cenozoic CO_2 history. *Nature Geoscience*, **4,** 418-420.
Beerling, D. J., A. Fox, and C. W. Anderson, 2009: Quantitative uncertainty analyses of ancient atmospheric CO_2 estimates from fossil leaves. *American Journal of Science*, **309,** 775-787.
Bekryaev, R. V., I. V. Polyakov, and V. A. Alexeev, 2010: Role of Polar Amplification in Long-Term Surface Air Temperature Variations and Modern Arctic Warming. *Journal of Climate*, **23,** 3888-3906.
Belt, S. T., G. Massé, S. J. Rowland, M. Poulin, C. Michel, and B. LeBlanc, 2007: A novel chemical fossil of palaeo sea ice: IP25. *Organic Geochemistry*, **38,** 16-27.
Beltaos, S., and T. Prowse, 2009: River-ice hydrology in a shrinking cryosphere. *Hydrological Processes*, **23,** 122-144.
Bengtsson, L., V. A. Semenov, and O. M. Johannessen, 2004: The Early Twentieth-Century Warming in the Arctic—A Possible Mechanism. *Journal of Climate*, **17,** 4045-4057.
Benito, G., A. Díez-Herrero, and M. Fernández de Villalta, 2003a: Magnitude and Frequency of Flooding in the Tagus Basin (Central Spain) over the Last Millennium. *Climatic Change*, **58,** 171-192.
Benito, G., A. Sopeña, Y. Sánchez-Moya, M. a. J. Machado, and A. Pérez-González, 2003b: Palaeoflood record of the Tagus River (Central Spain) during the Late Pleistocene and Holocene. *Quaternary Science Reviews*, **22,** 1737-1756.
Benito, G., V. R. Thorndycraft, M. Rico, Y. Sanchez-Moya, and A. Sopena, 2008: Palaeoflood and floodplain records from Spain: Evidence for long-term climate variability and environmental changes. *Geomorphology*, **101,** 68-77.
Benito, G., et al., 2011: Hydrological response of a dryland ephemeral river to southern African climatic variability during the last millennium. *Quaternary Research*, **75,** 471-482.
Bentley, M. J., C. J. Fogwill, A. M. Le Brocq, A. L. Hubbard, D. E. Sugden, T. J. Dunai, and S. P. H. T. Freeman, 2010: Deglacial history of the West Antarctic Ice Sheet in the Weddell Sea embayment: Constraints on past ice volume change. *Geology*, **38,** 411-414.
Berger, A., and M. F. Loutre, 1991: Insolation values for the climate of the last 10 million years. *Quaternary Sciences Reviews*, **10,** 297-317.
Berger, A., and M. F. Loutre, 2002: An Exceptionally Long Interglacial Ahead? *Science*, **297,** 1287-1288.
Berger, A., X. Li, and M. Loutre, 1999: Modelling northern hemisphere ice volume over the last 3 Ma. *Quaternary Science Reviews*, **18,** 1-11.
Bhatt, U. S., et al., 2010: Circumpolar Arctic Tundra Vegetation Change Is Linked to Sea Ice Decline. *Earth Interactions*, **14,** 1-20.

Bird, M. I., L. K. Fifield, T. S. Teh, C. H. Chang, N. Shirlaw, and K. Lambeck, 2007: An inflection in the rate of early mid-Holocene eustatic sea level rise: A new sea level curve from Singapore. *Estuarine, Coastal and Shelf Science*, **71,** 523-536.

Bird, M. I., W. E. N. Austin, C. M. Wurster, L. K. Fifield, M. Mojtahid, and C. Sargeant, 2010: Punctuated eustatic sea level rise in the early mid-Holocene. *Geology*, **38,** 803-806.

Bisiaux, M. M., et al., in press: Large scale changes in 20th century black carbon deposition to Antarctica. *Atmospheric Chemistry and Physics*, **11,** 27815-27831.

Bitz, C. M., J. C. H. Chiang, W. Cheng, and J. J. Barsugli, 2007: Rates of thermohaline recovery from freshwater pluses in modern, Last Glacial Maximum, and greenhouse warming climates. *Geophysical Research Letters*, **34,** L07708.

Bitz, C. M., J. K. Ridley, M. M. Holland, and H. Cattle, 2011: 20th and 21st century Arctic climate in global climate models. *Arctic Climate Change – The ACSYS Decade and Beyond*, P. Lemke, Ed.

Black, D. E., M. A. Abahazi, R. C. Thunell, A. Kaplan, E. J. Tappa, and L. C. Peterson, 2007: An 8-century tropical Atlantic SST record from the Cariaco Basin: Baseline variability, twentieth-century warming, and Atlantic hurricane frequency. *Paleoceanography*, **22,** PA4204.

Blanchon, P., A. Eisenhauer, J. Fietzke, and V. Liebetrau, 2009: Rapid sea level rise and reef back-stepping at the close of the last interglacial highstand. *Nature*, **458,** 881-884.

Blunier, T., and E. Brook, 2001: Timing of millennial-scale climate change in Antarctica and Greenland during the last glacial period. *Science*, **291,** 109-112.

Bock, M., J. Schmitt, L. Moller, R. Spahni, T. Blunier, and H. Fischer, 2010: Hydrogen Isotopes Preclude Marine Hydrate CH_4 Emissions at the Onset of Dansgaard-Oeschger Events. *Science*, **328,** 1686-1689.

Bonelli, S., S. Charbit, M. Kageyama, M. N. Woillez, G. Ramstein, C. Dumas, and A. Quiquet, 2009: Investigating the evolution of major Northern Hemisphere ice sheets during the last glacial-interglacial cycle. *Climate of the Past*, **5,** 329-345.

Boninsegna, J. A., et al., 2009: Dendroclimatological reconstructions in South America: A review. *Palaeogeography, Palaeoclimatology, Palaeoecology*, **281,** 210-228.

Born, A., K. Nisancioglu, and P. Braconnot, 2010: Sea ice induced changes in ocean circulation during the Eemian. *Climate Dynamics*, **35,** 1361-1371.

Boucher, É., J. Guiot, and E. Chapron, 2011: A millennial multi-proxy reconstruction of summer PDSI for Southern South America. *Climate of the Past*, **7,** 957-974.

Bowerman, N. D., and D. H. Clark, 2011: Holocene glaciation of the central Sierra Nevada, California. *Quaternary Science Reviews*, **30,** 1067-1085.

Bozbiyik, A., M. Steinacher, F. Joos, T. F. Stocker, and L. Menviel, 2011a: Fingerprints of changes in the terrestrial carbon cycle in response to large reorganizations in ocean circulation. *Clim. Past*, **7,** 319-338.

——, 2011b: Fingerprints of changes in the terrestrial carbon cycle in response to large reorganizations in ocean circulation. *Climate of the Past*, **7,** 319-338.

Braconnot, P., et al., 2007a: Results of PMIP2 coupled simulations of the Mid-Holocene and Last Glacial Maximum - Part 2: feedbacks with emphasis on the location of the ITCZ and mid- and high latitudes heat budget. *Climate of the Past*, **3,** 279-296.

Braconnot, P., et al., 2007b: Results of PMIP2 coupled simulations of the Mid-Holocene and Last Glacial Maximum-Part 1: experiments and large-scale features. *Climate of the Past*, **3,** 261-277.

Brázdil, R., Z. W. Kundzewicz, and G. Benito, 2006: Historical hydrology for studying flood risk in Europe. *Hydrological Sciences Journal*, **51,** 739-764.

Brázdil, R., C. Pfister, H. Wanner, H. von Storch, and J. Luterbacher, 2005: Historical climatology in Europe - The state of the art. *Climatic Change*, **70,** 363-430.

Brázdil, R., Z. W. Kundzewicz, G. Benito, G. Demaree, N. MacDonald, and L. A. Roald, 2012: Historical floods in Europe in the past millennium. *Changes of Flood Risk in Europe*, Z. W. Kundzewicz, Ed.

Brázdil, R., P. Dobrovolný, J. Luterbacher, A. Moberg, C. Pfister, D. Wheeler, and E. Zorita, 2010: European climate of the past 500 years: new challenges for historical climatology. *Climatic Change*, **101,** 7-40.

Breecker, D. O., Z. D. Sharp, and L. D. McFadden, 2010: Atmospheric CO_2 concentrations during ancient greenhouse climates were similar to those predicted for AD 2100. *Proceedings of the National Academy of Sciences of the United States of America*, **107,** 576-580.

Brewer, S., J. Guiot, and F. Torre, 2007: Mid-Holocene climate change in Europe: a data-model comparison. *Climate of the Past*, **3,** 499-512.

Brewer, S., J. Guiot, M. F. Sanchez-Goñi, and S. Klotz, 2008: The climate in Europe during the Eemian: a multi-method approach using pollen data. *Quaternary Science Reviews*, **27,** 2303-2315.

Briffa, K., T. Osborn, F. Schweingruber, I. Harris, P. Jones, S. Shiyatov, and E. Vaganov, 2001: Low-frequency temperature variations from a northern tree ring density network. *Journal of Geophysical Research-Atmospheres*, **106,** 2929-2941.

Briffa, K., et al., 1992: Fennoscandian summers from AD-500-temperature changes on short and long timescales. *Climate Dynamics*, **7,** 111-119.

Briffa, K. R., F. H. Schweingruber, P. D. Jones, T. J. Osborn, S. G. Shiyatov, and E. A. Vaganov, 1998: Reduced sensitivity of recent tree-growth to temperature at high northern latitudes. *Nature*, **391,** 678-682.

Brigham-Grette, J., and L. Carter, 1992: Pliocene marine transgressions of northern Alaska: circumarctic correlations and paleoclimatic interpretations. *Arctic*, **45,** 74-89.
Brinkhuis, H., et al., 2006: Episodic fresh surface waters in the Eocene Arctic Ocean. *Nature*, **441,** 606-609.
Brown, J., A. H. Lynch, and A. G. Marshall, 2009: Variability of the Indian Ocean Dipole in coupled model paleoclimate simulations. *Journal of Geophysical Research-Atmospheres*, **114,** D11105.
Brown, J., A. W. Tudhope, M. Collins, and H. V. McGregor, 2008a: Mid-Holocene ENSO: Issues in quantitative model-proxy data comparisons. *Paleoceanography*, **23,** PA3202.
Brown, J., M. Collins, A. W. Tudhope, and T. Toniazzo, 2008b: Modelling mid-Holocene tropical climate and ENSO variability: towards constraining predictions of future change with palaeo-data. *Climate Dynamics*, **30,** 19-36.
Buckley, B. M., et al., 2010: Climate as a contributing factor in the demise of Angkor, Cambodia. *Proceedings of the National Academy of Sciences of the United States of America*, **107,** 6748-6752.
Büntgen, U., and F. Schweingruber, 2010: Environmental change without climate change? *New Phytologist*, **188,** 646-651.
Büntgen, U., D. C. Frank, D. Nievergelt, and J. Esper, 2006: Summer temperature variations in the European Alps, AD 755-2004. *Journal of Climate*, **19,** 5606-5623.
Büntgen, U., J. Esper, D. Frank, K. Nicolussi, and M. Schmidhalter, 2005: A 1052-year tree-ring proxy for Alpine summer temperatures. *Climate Dynamics*, **25,** 141-153.
Büntgen, U., et al., 2011: 2500 Years of European Climate Variability and Human Susceptibility. *Science*, **331,** 578-582.
Bürger, G., I. Fast, and U. Cubasch, 2006: Climate reconstruction by regression – 32 variations on a theme. *Tellus A*, **58,** 227-235.
Burns, S. J., 2011: Speleothem records of changes in tropical hydrology over the Holocene and possible implications for atmospheric methane. *The Holocene*, **21,** 735-741.
Bush, A. B. G., 2007: Extratropical influences on the El Niño-Southern Oscillation through the late Quaternary. *Journal of Climate*, **20,** 788-800.
Butzin, M., M. Prange, and G. Lohmann, 2005: Radiocarbon simulations for the glacial ocean: The effects of wind stress, Southern Ocean sea ice and Heinrich events. *Earth and Planetary Science Letters*, **235,** 45-61.
Cai, Y. J., et al., 2010: The variation of summer monsoon precipitation in central China since the last deglaciation. *Earth and Planetary Science Letters*, **291,** 21-31.
Calenda, G., C. P. Mancini, and E. Volpi, 2005: Distribution of the extreme peak floods of the Tiber River from the XV century. *Advances in Water Resources*, **28,** 615-625.
Calov, R., and A. Ganopolski, 2005: Multistability and hysteresis in the climate-cryosphere system under orbital forcing. *Geophysical Research Letters*, **32,** L21717.
Calov, R., A. Ganopolski, V. Petoukhov, M. Claussen, and R. Greve, 2002: Large-scale instabilities of the Laurentide ice sheet simulated in a fully coupled climate-system model. *Geophysical Research Letters*, **29,** 2216.
Calov, R., et al., 2010: Results from the Ice sheet Model Intercomparison Project-Heinrich Event INtercOmparison (ISMIP HEINO). *Journal of Glaciology*, **56,** 371-383.
Camuffo, D., and S. Enzi, 1996: The analysis of two bi-millenary series: Tiber and Po river floods. *Climatic Variations and Forcing Mechanisms of the Last 2000 Years*, P. D. Jones, R. S. Bradley, and J. Jouzel, Eds., Springer, 433–450.
Camuffo, D., G. Sturaro, and G. Benito, 2003: An opposite flood pattern teleconnection between the Tagus (Iberian Peninsula) and Tiber (Italy) rivers during the last 1000 years. *Palaeofloods, Historical Data & Climatic Variability: Applications in Flood Risk Assessment*, G. B. V. R. Thorndycraft, C. Llasat & M. Barriendos, Ed., Centro de Ciencias Medioambientales, 295–300.
Capron, E., et al., 2010a: Synchronising EDML and NorthGRIP ice cores using $\delta^{18}O$ of atmospheric oxygen ($\delta^{18}O$ atm) and CH_4 measurements over MIS5 (80-123 kyr). *Quaternary Science Reviews*, **29,** 222-234.
Capron, E., et al., 2010b: Millennial and sub-millennial scale climatic variations recorded in polar ice cores over the last glacial period. *Climate of the Past*, **6,** 345-365.
Carlson, A. E., P. U. Clark, B. A. Haley, G. P. Klinkhammer, K. Simmons, E. J. Brook, and K. J. Meissner, 2007: Geochemical proxies of North American freshwater routing during the Younger Dryas cold event. *Proceedings of the National Academy of Sciences of the United States of America*, **104,** 6556-6561.
Carre, M., I. Bentaleb, M. Fontugne, and D. Lavallee, 2005: Strong El Niño events during the early Holocene: stable isotope evidence from Peruvian sea shells. *Holocene*, **15,** 42-47.
Cerling, T., 1991: Carbon-Dioxide in the atmosphere - Evidence from Cenozoic and Mesozoic paleosols. *American Journal of Science*, **291,** 377-400.
Chang, P., et al., 2006: Climate fluctuations of tropical coupled systems - The role of ocean dynamics. *Journal of Climate*, **19,** 5122-5174.
Chappell, J., A. Omura, T. Esat, M. McCulloch, J. Pandolfi, Y. Ota, and B. Pillans, 1996: Reconciliaion of late Quaternary sea levels derived from coral terraces at Huon Peninsula with deep sea oxygen isotope records. *Earth and Planetary Science Letters*, **141,** 227-236.
Charbit, S., D. Paillard, and G. Ramstein, 2008: Amount of CO_2 emissions irreversibly leading to the total melting of Greenland. *Geophysical Research Letters*, **35,** L12503.

Charles, C. D., K. Cobb, M. D. Moore, and R. G. Fairbanks, 2003: Monsoon-tropical ocean interaction in a network of coral records spanning the 20th century. *Marine Geology*, **201,** 207-222.
Chase, B. M., M. E. Meadows, A. S. Carr, and P. J. Reimer, 2010: Evidence for progressive Holocene aridification in southern Africa recorded in Namibian hyrax middens: Implications for African Monsoon dynamics and the "African Humid Period". *Quaternary Research*, **74,** 36-45.
Chen, J. H., H. A. Curran, B. White, and G. J. Wasserburg, 1991: Precise chronology of the last interglacial period: 234U-230Th data from fossil coral reefs in the Bahamas. *Geological Society of America Bulletin*, **103,** 82-97.
Cheng, H., R. L. Edwards, J. Hoff, C. D. Gallup, D. A. Richards, and Y. Asmerom, 2000: The half-lives of uranium-234 and thorium-230. *Chemical Geology*, **169,** 17-33.
Cheng, H., et al., 2009: Ice Age Terminations. *Science*, **326,** 248-252.
Chiang, J. C. H., and C. M. Bitz, 2005: Influence of high latitude ice cover on the marine Intertropical Convergence Zone. *Climate Dynamics*, **25,** 477-496.
Chiang, J. C. H., Y. Fang, and P. Chang, 2009: Pacific Climate Change and ENSO Activity in the Mid-Holocene. *Journal of Climate*, **22,** 923-939.
Christiansen, B., 2011: Reconstructing the NH mean temperature: Can underestimation of trends and variability be avoided? *Journal of Climate*, **24,** 674-692.
Christiansen, B., and F. C. Ljungqvist, Submitted: Reconstruction of the extra-tropical NH mean temperature over the last millennium with a method that preserves low-frequency variability. *Journal of Climate*, **submitted**.
Christiansen, B., T. Schmith, and P. Thejll, 2009: A Surrogate Ensemble Study of Climate Reconstruction Methods: Stochasticity and Robustness. *Journal of Climate*, **22,** 951-976.
Chylek, P., C. K. Folland, G. Lesins, M. K. Dubey, and M. Y. Wang, 2009: Arctic air temperature change amplification and the Atlantic Multidecadal Oscillation. *Geophysical Research Letters*, **36,** L14801.
Claquin, T., et al., 2003: Radiative forcing of climate by ice-age atmospheric dust. *Climate Dynamics*, **20,** 193-202.
Clark, P., and D. Pollard, 1998: Origin of the middle Pleistocene transition by ice sheet erosion of regolith. *Paleoceanography*, **13,** 1-9.
Clark, P., et al., 2006: The middle Pleistocene transition: characteristics. mechanisms, and implications for long-term changes in atmospheric pCO_2. *Quaternary Science Reviews*, **25,** 3150-3184.
Clark, P. U., and P. Huybers, 2009: GLOBAL CHANGE Interglacial and future sea level. *Nature*, **462,** 856-857.
Clark, P. U., J. X. Mitrovica, G. A. Milne, and M. E. Tamisiea, 2002: Sea level Fingerprinting as a Direct Test for the Source of Global Meltwater Pulse IA. *Science*, **295,** 2438-2441.
Clark, P. U., A. M. McCabe, A. C. Mix, and A. J. Weaver, 2004: Rapid Rise of Sea Level 19,000 Years Ago and Its Global Implications. *Science*, **304,** 1141-1144.
Clark, P. U., et al., 2009: The Last Glacial Maximum. *Science*, **325,** 710-714.
Clarke, G., D. Leverington, J. Teller, and A. Dyke, 2004: Paleohydraulics of the last outburst flood from glacial Lake Agassiz and the 8200 BP cold event. *Quaternary Science Reviews*, **23,** 389-407.
Clemens, S. C., W. L. Prell, and Y. Sun, 2010: Orbital-scale timing and mechanisms driving Late Pleistocene Indo-Asian summer monsoons: Reinterpreting cave speleothem $\delta^{18}O$. *Paleoceanography*, **25,** PA4207.
CLIMAP Project Members, 1976: The surface of the ice-age earth. *Science*, **191,** 1131-1137.
——, 1981: *Seasonal reconstructions of the Earth's surface at the last glacial maximum*. Geological Society of America.
Cole-Dai, J., D. Ferris, A. Lanciki, J. Savarino, M. Baroni, and M. Thiemens, 2009: Cold decade (AD 1810-1819) caused by Tambora (1815) and another (1809) stratospheric volcanic eruption. *Geophysical Research Letters*, **36,** L22703.
Collins, J. A., et al., 2011: Interhemispheric symmetry of the tropical African rainbelt over the past 23,000 years. *Nature Geoscience*, **4,** 42-45.
Colville, E. J., A. E. Carlson, B. L. Beard, R. G. Hatfield, J. S. Stoner, A. V. Reyes, and D. J. Ullman, 2011: Sr-Nd-Pb Isotope Evidence for Ice sheet Presence on Southern Greenland During the Last Interglacial. *Science*, **333,** 620-623.
Cook, E., B. Buckley, J. G. Palmer, P. Fenwick, M. Peterson, G. Boswijk, and A. Fowler, 2006: Millennia-long tree-ring records from Tasmania and New Zealand: a basis for modelling climate variability and forcing, past, present and future. *Journal of Quaternary Science*, **21,** 689-699.
Cook, E. R., R. D. D'Arrigo, and M. E. Mann, 2002: A well-verified, multiproxy reconstruction of the winter North Atlantic Oscillation index since AD 1400. *Journal of Climate*, **15,** 1754-1764.
Cook, E. R., C. A. Woodhouse, C. M. Eakin, D. M. Meko, and D. W. Stahle, 2004: Long-Term Aridity Changes in the Western United States. *Science*, **306,** 1015-1018.
Cook, E. R., K. J. Anchukaitis, B. M. Buckley, R. D. D'Arrigo, G. C. Jacoby, and W. E. Wright, 2010: Asian Monsoon Failure and Megadrought During the Last Millennium. *Science*, **328,** 486-489.
Corona, C., J. Guiot, J. Edouard, F. Chalie, U. Büntgen, P. Nola, and C. Urbinati, 2010: Millennium-long summer temperature variations in the European Alps as reconstructed from tree rings. *Climate of the Past*, **6,** 379-400.
Crespin, E., H. Goosse, T. Fichefet, and M. E. Mann, 2009: The 15th century Arctic warming in coupled model simulations with data assimilation. *Climate of the Past*, **5,** 389-401.
Cronin, T. M., P. R. Vogt, D. A. Willard, R. Thunell, J. Halka, M. Berke, and J. Pohlman, 2007: Rapid sea level rise and ice sheet response to 8,200-year climate event. *Geophysical Research Letters*, **34,** L20603.

Crouch, A., P. Charbonneau, G. Beaubien, and D. Paquin-Ricard, 2008: A model for the total solar irradiance based on active region decay. *Astrophysical Journal*, **677,** 723-741.
Crowley, T., and M. Unterman, submitted: Technical Details Concerning Development of a 1200-Year Proxy Index for Global Volcanism. *Climate of the Past*.
Crowley, T. J., and W. T. Hyde, 2008: Transient nature of late Pleistocene climate variability. *Nature*, **456,** 226-230.
Crucifix, M., 2006: Does the Last Glacial Maximum constrain climate sensitivity? *Geophysical Research Letters*, **33,** L18701.
Cruz, F. W., et al., 2009: Orbitally driven east-west antiphasing of South American precipitation. *Nature Geoscience*, **2,** 210-214.
Cullen, H. M., R. D. D'Arrigo, E. R. Cook, and M. E. Mann, 2001: Multiproxy reconstructions of the North Atlantic Oscillation. *Paleoceanography*, **16,** 27-39.
Cutler, K. B., et al., 2003: Rapid sea level fall and deep-ocean temperature change since the last interglacial period. *Earth and Planetary Science Letters*, **206,** 253-271.
D'Arrigo, R., R. Wilson, and G. Jacoby, 2006: On the long-term context for late twentieth century warming. *Journal of Geophysical Research*, **111,** D03103.
D'Arrigo, R., R. Wilson, B. Liepert, and P. Cherubini, 2008: On the 'Divergence Problem' in Northern Forests: A review of the tree-ring evidence and possible causes. *Global and Planetary Change*, **60,** 289-305.
D'Arrigo, R. D., E. R. Cook, G. C. Jacoby, and K. R. Briffa, 1993: NAO and sea surface temperature signatures in tree-ring records from the North-Atlantic sector. *Quaternary Science Reviews*, **12,** 431-440.
De Deckker, P., and Y. Yokoyama, 2009: Micropalaeontological evidence for Late Quaternary sea level changes in Bonaparte Gulf, Australia. *Global and Planetary Change*, **66,** 85-92.
De Deckker, P., M. Norman, I. D. Goodwin, A. Wain, and F. X. Gingele, 2010: Lead isotopic evidence for an Australian source of aeolian dust to Antarctica at times over the last 170,000 years. *Palaeogeography Palaeoclimatology Palaeoecology*, **285,** 205-223.
de Vernal, A., and C. Hillaire-Marcel, 2008: Natural variability of Greenland climate, vegetation, and ice volume during the past million years. *Science*, **320,** 1622-1625.
de Vernal, A., and A. Rochon, 2011: Dinocysts as tracers of sea surface conditions and sea ice cover in polar and subpolar environments. *IOP Conference Series: Earth and Environmental Science*, **14,** 012007.
DeConto, R. M., and D. Pollard, 2003: Rapid Cenozoic glaciation of Antarctica induced by declining atmospheric CO_2. *Nature*, **421,** 245-249.
Delaygue, G., and E. Bard, 2011: An Antarctic view of Beryllium-10 and solar activity for the past millennium. *Climate Dynamics*, **36,** 2201-2218.
Delmonte, B., P. S. Andersson, M. Hansson, H. Schoberg, J. R. Petit, I. Basile-Doelsch, and V. Maggi, 2008: Aeolian dust in East Antarctica (EPICA-Dome C and Vostok): Provenance during glacial ages over the last 800 kyr. *Geophysical Research Letters*, **35,** L07703.
Delworth, T., and M. Mann, 2000: Observed and simulated multidecadal variability in the Northern Hemisphere. *Climate Dynamics*, **16,** 661-676.
Denis, D., X. Crosta, L. Barbara, G. Massé, H. Renssen, O. Ther, and J. Giraudeau, 2010: Sea ice and wind variability during the Holocene in East Antarctica: insight on middle–high latitude coupling. *Quaternary Science Reviews*, **29,** 3709-3719.
Denman, P. D., and W. J. E. van de Graaff, 1977: Emergent Quaternary marine deposits in the Lake MacLeod area, Western Australia, 32-36 pp.
Denton, G. H., and T. J. Hughes, 2002: Reconstructing the Antarctic Ice Sheet at the Last Glacial Maximum. *Quaternary Science Reviews*, **21,** 193-202.
Denton, G. H., R. F. Anderson, J. R. Toggweiler, R. L. Edwards, J. M. Schaefer, and A. E. Putnam, 2010: The Last Glacial Termination. *Science*, **328,** 1652-1656.
Derbyshire, E., 2003: Loess, and the Dust Indicators and Records of Terrestrial and Marine Palaeoenvironments (DIRTMAP) database. *Quaternary Science Reviews*, **22,** 1813-1819.
Diaz, H. F., R. M. Trigo, M. K. Hughes, M. E. Mann, E. Xoplaki, and D. Barriopedro, in press: Spatial and temporal characteristics of Climate in medieval times revisited. *Bulletin of the American Meteorological Society*, 10.1175/BAMS-D-10-05003.1.
Divine, D. V., and C. Dick, 2006: Historical variability of sea ice edge position in the Nordic Seas. *Journal of Geophysical Research*, **111,** C01001.
Dobrovolný, P., et al., 2010: Monthly, seasonal and annual temperature reconstructions for Central Europe derived from documentary evidence and instrumental records since AD 1500. *Climatic Change*, **101,** 69-107.
Dolan, A. M., A. M. Haywood, D. J. Hill, H. J. Dowsett, S. J. Hunter, D. J. Lunt, and S. J. Pickering, 2011: Sensitivity of Pliocene ice sheets to orbital forcing. *Palaeogeography, Palaeoclimatology, Palaeoecology*, **309,** 98-110.
Donders, T. H., F. Wagner-Cremer, and H. Visscher, 2008: Integration of proxy data and model scenarios for the mid-Holocene onset of modern ENSO variability. *Quaternary Science Reviews*, **27,** 571-579.
Donnelly, J. P., P. Cleary, P. Newby, and R. Ettinger, 2004: Coupling instrumental and geological records of sea level change: Evidence from southern New England of an increase in the rate of sea level rise in the late 19th century. *Geophysical Research Letters*, **31,** L05203.

Dorale, J. A., B. P. Onac, J. J. Fornós, J. Ginés, A. Ginés, P. Tuccimei, and D. W. Peate, 2010: Sea level Highstand 81,000 Years Ago in Mallorca. *Science*, **327,** 860-863.
Dowsett, H. J., M. A. Chandler, T. M. Cronin, and G. S. Dwyer, 2005: Middle Pliocene sea surface temperature variability. *Paleoceanography*, **20,** PA2014.
Dowsett, H. J., et al., submitted: A confidence-assessed Pliocene global sea surface temperature dataset. *Nature Geoscience*.
Drysdale, R., 2009: Evidence for obliquity forcing of glacial Termination II. *Science*, **325,** 1527-1531.
Dunkley Jones, T., A. Ridgwell, D. Lunt, M. Maslin, D. Schmidt, and P. Valdes, 2010: A Palaeogene perspective on climate sensitivity and methane hydrate instability. *Philosophical Transactions of the Royal Society a-Mathematical Physical and Engineering Sciences*, **368,** 2395-2415.
Duplessy, J. C., D. M. Roche, and M. Kageyama, 2007: The deep ocean during the last interglacial period. *Science*, **316,** 89-91.
Dutton, A., and K. Lambeck, submitted: Ice volume and sea level during the Last Interglacial. *Science*.
Dykoski, C., et al., 2005: A high-resolution, absolute-dated Holocene and deglacial Asian monsoon record from Dongge Cave, China. *Earth and Planetary Science Letters*, **233,** 71-86.
Edwards, R. L., et al., 1993: A Large Drop in Atmospheric $^{14}C/^{12}C$ and Reduced Melting in the Younger Dryas, Documented with ^{230}Th Ages of Corals. *Science*, **260,** 962-968.
Edwards, T., M. Crucifix, and S. Harrison, 2007: Using the past to constrain the future: how the palaeorecord can improve estimates of global warming. *Progress in Physical Geography*, **31,** 481-500.
Elderfield, H., et al., 2010: A record of bottom water temperature and seawater $\delta^{18}O$ for the Southern Ocean over the past 440-kyr based on Mg/Ca of benthic foraminiferal *Uvigerina* spp. *Quaternary Science Reviews*, **29,** 160-169.
Ellison, C. R. W., M. R. Chapman, and I. R. Hall, 2006: Surface and deep ocean interactions during the cold climate event 8200 years ago. *Science*, **312,** 1929-1932.
Elsig, J., et al., 2009: Stable isotope constraints on Holocene carbon cycle changes from an Antarctic ice core. *Nature*, **461,** 507-510.
Ely, L. L., Y. Enzel, V. R. Baker, and D. R. Cayan, 1993: A 5000-Year Record of Extreme Floods and Climate Change in the Southwestern United States. *Science*, **262,** 410-412.
Emile-Geay, J., K. Cobb, M. Mann, and A. Wittenberg, in press: Estimating Tropical Pacific SST variability over the Past Millennium; Part 2: Reconstructions and Uncertainties. *Jounral of Climate*.
Emile-Geay, J., R. Seager, M. A. Cane, E. R. Cook, and G. H. Haug, 2008: Volcanoes and ENSO over the past millennium. *Journal of Climate*, **21,** 3134-3148.
England, J. H., T. R. Lakeman, D. S. Lemmen, J. M. Bednarski, T. G. Stewart, and D. J. A. Evans, 2008: A millennial-scale record of Arctic Ocean sea ice variability and the demise of the Ellesmere Island ice shelves. *Geophysical Research Letters*, **35,** L19502.
Enzel, Y., L. L. Ely, P. K. House, V. R. Baker, and R. H. Webb, 1993: Paleoflood evidence for a natural upper bound to flood magnitudes in the Colorado River Basin. *Water Resources Research*, **29,** 2287-2297.
EPICA Community Members, 2004: Eight glacial cycles from an Antarctic ice core. *Nature*, **429,** 623-628.
Esper, J., and D. Frank, 2009: Divergence pitfalls in tree-ring research. *Climatic Change*, **94,** 261-266.
Esper, J., D. Frank, R. Wilson, U. Büntgen, and K. Treydte, 2007a: Uniform growth trends among central Asian low- and high-elevation juniper tree sites. *Trees-Structure and Function*, **21,** 141-150.
Esper, J., D. Frank, U. Büntgen, A. Verstege, J. Luterbacher, and E. Xoplaki, 2007b: Long-term drought severity variations in Morocco. *Geophysical Research Letters*, **34,** L17702.
Euler, C., and U. Ninnemann, 2010: Climate and Antarctic Intermediate Water coupling during the late Holocene. *Geology*, **38,** 647-650.
Fairbanks, R. G., 1989: A 17,000 year glacio-eustatic sea level record : influence of glacial melting rates on the Younger Dryas event and deep ocean circulation. *Nature*, **342,** 637-642.
Ferretti, D., et al., 2005: Unexpected changes to the global methane budget over the past 2000 years. *Science*, **309,** 1714-1717.
Firestone, R. B., et al., 2007: Evidence for an extraterrestrial impact 12,900 years ago that contributed to the megafaunal extinctions and the Younger Dryas cooling. *Proceedings of the National Academy of Sciences of the United States of America*, **104,** 16016-16021.
Fischer, H., et al., 2008: Changing boreal methane sources and constant biomass burning during the last termination. *Nature*, **452,** 864-867.
Fischer, H., et al., 2007: Reconstruction of millennial changes in dust emission, transport and regional sea ice coverage using the deep EPICA ice cores from the Atlantic and Indian Ocean sector of Antarctica. *Earth and Planetary Science Letters*, **260,** 340-354.
Fischer, N., and J. H. Jungclaus, 2010: Effects of orbital forcing on atmosphere and ocean heat transports in Holocene and Eemian climate simulations with a comprehensive Earth system model. *Climate of the Past*, **6,** 155-168.
Fleitmann, D., S. J. Burns, M. Mudelsee, U. Neff, J. Kramers, A. Mangini, and A. Matter, 2003: Holocene Forcing of the Indian Monsoon Recorded in a Stalagmite from Southern Oman. *Science*, **300,** 1737-1739.
Flückiger, J., R. Knutti, J. W. C. White, and H. Renssen, 2008: Modeled seasonality of glacial abrupt climate events. *Climate Dynamics*, **31,** 633-645.

Foster, G., 2008: Seawater pH, pCO_2 and $[CO^{2-}_3]$ variations in the Caribbean Sea over the last 130 kyr: A boron isotope and B/Ca study of planktic forminifera. *Earth and Planetary Science Letters*, **271,** 254-266.

Francou, B., M. Vuille, P. Wagnon, J. Mendoza, and J.-E. Sicart, 2003: Tropical climate change recorded by a glacier in the central Andes during the last decades of the twentieth century: Chacaltaya, Bolivia, 16°S. *Journal of Geophysical Research*, **108,** 4154.

Frank, D., J. Esper, E. Zorita, and R. Wilson, 2010: A noodle, hockey stick, and spaghetti plate: a perspective on high-resolution paleoclimatology. *Wiley Interdisciplinary Reviews: Climate Change*, **1,** 507-516.

Funder, S., et al., 2011: A 10,000-Year Record of Arctic Ocean Sea ice Variability—View from the Beach. *Science*, **333,** 747-750.

Ganopolski, A., and D. M. Roche, 2009: On the nature of lead-lag relationships during glacial-interglacial climate transitions. *Quaternary Science Reviews*, **28,** 3361-3378.

Ganopolski, A., and R. Calov, Submitted: The role of orbital forcing, carbon dioxide and regolith in 100 kyr glacial cycles. *Clim. Past Discuss.*, **7,** 2391-2411.

Ganopolski, A., R. Calov, and M. Claussen, 2010: Simulation of the last glacial cycle with a coupled climate ice sheet model of intermediate complexity. *Climate of the Past*, **6,** 229-244.

Gao, C., A. Robock, and C. Ammann, 2008: Volcanic forcing of climate over the past 1500 years: An improved ice core-based index for climate models. *Journal of Geophysical Research-Atmospheres*, **113,** D23111.

Gao, C., et al., 2006: The 1452 or 1453 A.D. Kuwae eruption signal derived from multiple ice core records: Greatest volcanic sulfate event of the past 700 years. *Journal of Geophysical Research-Atmospheres*, **111,** D12107.

García-Artola, A., A. Cearreta, E. Leorri, M. Irabien, and W. Blake, 2009: Coastal salt-marshes as geological archives of recent sea level changes. *Geogaceta*, **47,** 109-112.

Gayer, E., J. Lavé, R. Pik, and C. France-Lanord, 2006: Monsoonal forcing of Holocene glacier fluctuations in Ganesh Himal (Central Nepal) constrained by cosmogenic ^{3}He exposure ages of garnets. *Earth and Planetary Science Letters*, **252,** 275-288.

Ge, Q., S. Wang, and J. Zheng, 2006: Reconstruction of temperature series in China for the last 5000 years. *Progress in Natural Science*, **16,** 838-845.

Ge, Q., J. Zheng, Z. Hao, X. Shao, W. Wang, and J. Luterbacher, 2010a: Temperature variation through 2000 years in China: An uncertainty analysis of reconstruction and regional difference. *Geophysical Research Letters*, **37,** L03703.

Ge, Q., J. Zheng, X. Fang, Z. Man, X. Zhang, P. Zhang, and W. Wang, 2003: Winter half-year temperature reconstruction for the middle and lower reaches of the Yellow River and Yangtze River, China, during the past 2000 years. *Holocene*, **13,** 933-940.

Ge, Q. S., J. Y. Zheng, Z. X. Hao, X. M. Shao, W.-C. Wang, and J. Luterbacher, 2010b: Temperature variation through 2000 years in China: An uncertainty analysis of reconstruction and regional difference. *Geophysical Research Letters*, **37,** L03703.

Gehrels, W. R., B. W. Hayward, R. M. Newnham, and K. E. Southall, 2008: A 20th century acceleration of sea level rise in New Zealand. *Geophysical Research Letters*, **35,** L02717.

Gehrels, W. R., B. P. Horton, A. C. Kemp, and D. Sivan, 2011: Two millennia of sea level data: The key to predicting change. *Eos Trans. AGU*, **92**.

Gehrels, W. R., et al., 2006: Rapid sea level rise in the North Atlantic Ocean since the first half of the nineteenth century. *The Holocene*, **16,** 949-965.

Gergis, J., R. G. Neukom, Ailie, S. Phipps, D. Karoly, and PAGES Aus2K Project Members, submitted: Evidence of rapid late 20th century warming 1 from an Australasian temperature reconstruction spanning the last millennium. *Journal of Climate*.

Ghatak, D., A. Frei, G. Gong, J. Stroeve, and D. Robinson, 2010: On the emergence of an Arctic amplification signal in terrestrial Arctic snow extent. *Journal of Geophysical Research-Atmospheres*, **115,** D24105.

Gillett, N., et al., 2008: Attribution of polar warming to human influence. *Nature Geoscience*, **1,** 750-754.

Gladstone, R. M., et al., 2005: Mid-Holocene NAO: A PMIP2 model intercomparison. *Geophysical Research Letters*, **32,** L16707.

Glaser, R., 2008: *Klimageschichte Mitteleuropas. 1200 Jahre Wetter, Klima, Katastrophen.* Primus Verlag.

Glaser, R., and D. Riemann, 2009: A thousand-year record of temperature variations for Germany and Central Europe based on documentary data. *Journal of Quaternary Science*, **24,** 437-449.

Glaser, R., et al., 2010: The variability of European floods since AD 1500. *Climatic Change*, **101,** 235-256.

Glasser, N. F., S. Clemmens, C. Schnabel, C. R. Fenton, and L. McHargue, 2009: Tropical glacier fluctuations in the Cordillera Blanca, Peru between 12.5 and 7.6-ka from cosmogenic ^{10}Be dating. *Quaternary Science Reviews*, **28,** 3448-3458.

Glueck, M. F., and C. W. Stockton, 2001: Reconstruction of the North Atlantic Oscillation, 1429-1983. *International Journal of Climatology*, **21,** 1453-1465.

González-Rouco, J. F., H. Beltrami, E. Zorita, and H. von Storch, 2006: Simulation and inversion of borehole temperature profiles in surrogate climates: Spatial distribution and surface coupling. *Geophysical Research Letters*, **33,** L01703.

González-Rouco, J. F., H. Beltrami, E. Zorita, and M. B. Stevens, 2009: Borehole climatology: a discussion based on contributions from climate modeling. *Climate of the Past*, **5,** 97-127.

Gonzalez, C., and L. Dupont, 2009: Tropical salt marsh succession as sea level indicator during Heinrich events. *Quaternary Science Reviews*, **28,** 939-946.
González, J. L., and T. E. Törnqvist, 2009: A new Late Holocene sea level record from the Mississippi Delta: evidence for a climate/sea level connection? *Quaternary Science Reviews*, **28,** 1737-1749.
Goodkin, N. F., K. A. Hughen, S. C. Doney, and W. B. Curry, 2008: Increased multidecadal variability of the North Atlantic Oscillation since 1781. *Nature Geoscience*, **1,** 844-848.
Goodwin, I. D., and N. Harvey, 2008: Subtropical sea level history from coral microatolls in the Southern Cook Islands, since 300 AD. *Marine Geology*, **253,** 14-25.
Goosse, H., E. Crespin, A. de Montety, M. E. Mann, H. Renssen, and A. Timmermann, 2010: Reconstructing surface temperature changes over the past 600 years using climate model simulations with data assimilation. *Journal of Geophysical Research-Atmospheres*, **115,** D09108.
Gouirand, I., H. Linderholm, A. Moberg, and B. Wohlfarth, 2008: On the spatiotemporal characteristics of Fennoscandian tree-ring based summer temperature reconstructions. *Theoretical and Applied Climatology*, **91,** 1-25.
Govin, A., et al., Submitted: Persistent influence of ice sheet melting on high northern latitude climate during the early Last Interglacial. *Climate of the Past Discussion*, **7,** 3239-3286.
Grachev, A., E. Brook, J. Severinghaus, and N. Pisias, 2009: Relative timing and variability of atmospheric methane and GISP2 oxygen isotopes between 68 and 86 ka. *Global Biochemical Cycles*, **23,** GB2009.
Graham, N., C. Ammann, D. Fleitmann, K. Cobb, and J. Luterbacher, 2011: Support for global climate reorganization during the "Medieval Climate Anomaly". *Climate Dynamics*, **37,** 1217-1245.
Graham, N. E., et al., 2007: Tropical Pacific - mid-latitude teleconnections in medieval times. *Climatic Change*, **83,** 241-285.
Graversen, R. G., and M. H. Wang, 2009: Polar amplification in a coupled climate model with locked albedo. *Climate Dynamics*, **33,** 629-643.
Gray, L. J., et al., 2010: Solar influences on climate. *Review of Geophysics*, **48,** RG4001.
Gray, S. T., L. J. Graumlich, J. L. Betancourt, and G. T. Pederson, 2004: A tree-ring based reconstruction of the Atlantic Multidecadal Oscillation since 1567 A.D. *Geophysical Research Letters*, **31,** L12205.
Greenbaum, N., A. P. Schick, and V. R. Baker, 2000: The palaeoflood record of a hyperarid catchment, Nahal Zin, Negev Desert, Israel. *Earth Surface Processes and Landforms*, **25,** 951-971.
Greenbaum, N., N. Porat, E. Rhodes, and Y. Enzel, 2006: Large floods during late Oxygen Isotope Stage 3, southern Negev desert, Israel. *Quaternary Science Reviews*, **25,** 704-719.
Gregory, J. M., and P. Huybrechts, 2006: Ice sheet contributions to future sea level change. *Philosophical Transactions of the Royal Society A: Mathematical, Physical and Engineering Sciences*, **364,** 1709-1732.
Groll, N., and M. Widmann, 2006: Sensitivity of temperature teleconnections to orbital changes in AO-GCM simulations. *Geophysical Research Letters*, **33,** L12705.
Grudd, H., 2008: Torneträsk tree-ring width and density AD 500-2004: a test of climatic sensitivity and a new 1500-year reconstruction of north Fennoscandian summers. *Climate Dynamics*, **31,** 843-857.
Grudd, H., K. Briffa, W. Karlén, T. Bartholin, P. Jones, and B. Kromer, 2002: A 7400-year tree-ring chronology in northern Swedish Lapland: natural climatic variability expressed on annual to millennial timescales. *Holocene*, **12,** 657-665.
Grützner, J., and S. M. Higgins, 2010: Threshold behavior of millennial scale variability in deep water hydrography inferred from a 1.1 Ma long record of sediment provenance at the southern Gardar Drift. *Paleoceanography*, **25,** PA4204.
Guiot, J., C. Corona, and ESCARSEL members, 2010: Growing Season Temperatures in Europe and Climate Forcings Over the Past 1400 Years. *Plos One*, **5,** E9972.
Gunnarson, B., H. Linderholm, and A. Moberg, 2011: Improving a tree-ring reconstruction from west-central Scandinavia: 900 years of warm-season temperatures. *Climate Dynamics*, **36,** 97-108.
Gutjahr, M., B. Hoogakker, M. Frank, and I. McCave, 2010: Changes in North Atlantic Deep Water strength and bottom water masses during Marine Isotope Stage 3 (45-35 ka BP). *Quaternary Science Reviews*, **29,** 2451-2461.
Hald, M., et al., 2007: Variations in temperature and extent of Atlantic Water in the northern North Atlantic during the Holocene. *Quaternary Science Reviews*, **26,** 3423-3440.
Hall, B. L., T. Koffman, and G. H. Denton, 2010: Reduced ice extent on the western Antarctic Peninsula at 700-970 cal. yr B.P. *Geology*, **38,** 635-638.
Hallam, P., 1992: *Phanerozoic sea level changes.* 10.1177/030913339401800322 Columbia University Press.
Handorf, D., K. Dethloff, A. G. Marshall, and A. Lynch, 2009: Climate Regime Variability for Past and Present Time Slices Simulated by the Fast Ocean Atmosphere Model. *Journal of Climate*, **22,** 58-70.
Hanebuth, T., K. Stattegger, and P. M. Grootes, 2000: Rapid Flooding of the Sunda Shelf: A Late-Glacial Sea level Record. *Science*, **288,** 1033-1035.
Hanebuth, T., K. Stattegger, and A. Bojanowski, 2009: Termination of the Last Glacial Maximum sea level lowstand: The Sunda-Shelf data revisited. *Global and Planetary Change*, **66,** 76-84.
Hansen, J., M. Sato, P. Kharecha, G. Russell, D. Lea, and M. Siddall, 2007: Climate change and trace gases. *Philosophical Transactions of the Royal Society a-Mathematical Physical and Engineering Sciences*, DOI 10.1098/rsta.2007.2052**,** 1925-1954.

Hansen, J., et al., 2008: Target Atmospheric CO_2: Where Should Humanity Aim? *Open Atmospheric Science Journal*, **2,** 217-231.
Harada, N., M. Sato, and T. Sakamoto, 2008: Freshwater impacts recorded in tetraunsaturated alkenones and alkenone sea surface temperatures from the Okhotsk Sea across millennial-scale cycles. *Paleoceanography*, **23,** PA3201.
Harada, N., K. Kimoto, Y. Okazaki, K. Nagashima, A. Timmermann, and A. Abe-Ouchi, 2009: Millennial time scale changes in surface to intermediate-deep layer circulation recorded in sediment cores from the northwestern North Pacific. *Quaternary Research (Tokyo)*, **48,** 179-194.
Hargreaves, J., A. Abe-Ouchi, and J. Annan, 2007: Linking glacial and future climates through an ensemble of GCM simulations. *Climate of the Past*, **3,** 77-87.
Harrison, S. P., and M. F. S. Goñi, 2010: Global patterns of vegetation response to millennial-scale variability and rapid climate change during the last glacial period. *Quaternary Science Reviews*, **29,** 2957-2980.
Hearty, P. J., J. T. Hollin, A. C. Neumann, M. J. O'Leary, and M. McCulloch, 2007: Global sea level fluctuations during the Last Interglaciation (MIS 5e). *Quaternary Science Reviews*, **26,** 2090-2112.
Hegerl, G. C., T. J. Crowley, M. Allen, W. T. Hyde, H. N. Pollack, J. Smerdon, and E. Zorita, 2007: Detection of human influence on a new, validated 1500-year temperature reconstruction. *Journal of Climate*, **20,** 650-666.
Heinemann, M., J. H. Jungclaus, and J. Marotzke, 2009: Warm Paleocene/Eocene climate as simulated in ECHAM5/MPI-OM. *Climate of the Past*, **5,** 785-802.
Helama, S., et al., 2009: Summer temperature variations in Lapland during the Medieval Warm Period and the Little Ice Age relative to natural instability of thermohaline circulation on multi-decadal and multi-centennial scales. *Journal of Quaternary Science*, **24,** 450-456.
Held, I. M., and B. J. Soden, 2006: Robust responses of the hydrological cycle to global warming. *Journal of Climate*, **19,** 5686-5699.
Hély, C., M. Girardin, A. Ali, C. Carcaillet, S. Brewer, and Y. Bergeron, 2010: Eastern boreal North American wildfire risk of the past 7000 years: A model-data comparison. *Geophysical Research Letters*, **37,** L14709.
Hemming, N. G., and G. N. Hanson, 1992: Boron isotopic composition and concentration in modern marine carbonates. *Geochimica et Cosmochimica Acta*, **56,** 537-543.
Henderiks, J., and M. Pagani, 2007: Refining ancient carbon dioxide estimates: Significance of coccolithophore cell size for alkenone-based pCO_2 records. *Paleoceanography*, **22,** PA3202.
Hendy, I. L., and J. P. Kennett, 2000: Dansgaard-Oeschger Cycles and the California Current System: Planktonic Foraminiferal Response to Rapid Climate Change in Santa Barbara Basin, Ocean Drilling Program Hole 893A. *Paleoceanography*, **15,** 30-42.
Herbert, T. D., L. C. Peterson, K. T. Lawrence, and Z. Liu, 2010: Tropical Ocean Temperatures Over the Past 3.5 Million Years. *Science*, **328,** 1530-1534.
Herget, J., and H. Meurs, 2010: Reconstructing peak discharges for historic flood levels in the city of Cologne, Germany. *Global and Planetary Change*, **70,** 108-116.
Herrington, A. R., and C. J. Poulsen, in press: Terminating the Last Interglacial: The Role of Ice Sheet-Climate Feedbacks in a GCM Asynchronously Coupled to an Ice Sheet Model. *Journal of Climate*, 10.1175/jcli-d-11-00218.1.
Higginson, M. J., M. A. Altabet, D. W. Murray, R. W. Murray, and T. D. Herbert, 2004: Geochemical evidence for abrupt changes in relative strength of the Arabian monsoons during a stadial/interstadial climate transition. *Geochimica Et Cosmochimica Acta*, **68,** 3807-3826.
Hijma, M. P., and K. M. Cohen, 2010: Timing and magnitude of the sea level jump preluding the 8200 yr event. *Geology*, **38,** 275-278.
Hill, D. J., A. M. Dolan, A. M. Haywood, S. J. Hunter, and D. K. Stoll, 2010: Sensitivity of the Greenland Ice Sheet to Pliocene sea surface temperatures. *Stratigraphy*, **7,** 111 – 122.
Hofer, D., C. C. Raible, and T. F. Stocker, 2011: Variations of the Atlantic meridional overturning circulation in control and transient simulations of the last millennium. *Climate of the Past*, **7,** 133-150.
Holden, P. B., N. R. Edwards, E. W. Wolff, N. J. Lang, J. S. Singarayer, P. J. Valdes, and T. F. Stocker, 2010: Interhemispheric coupling, the West Antarctic Ice Sheet and warm Antarctic interglacials. *Climate of the Past*, **6,** 431-443.
Holland, M. M., and C. M. Bitz, 2003: Polar amplification of climate change in coupled models. *Climate Dynamics*, **21,** 221-232.
Hollis, C. J., et al., submitted: Southwest Pacific marine temperature variation from late Paleocene to middle Eocene: Revisited. *Earth and Planetary Science Letters*.
Holmes, J. A., E. R. Cook, and B. Yang, 2009: Climate change over the past 2000 years in Western China. *Quaternary International*, **194,** 91-107.
Holzhauser, H., M. Magny, and H. J. Zumbuühl, 2005: Glacier and lake-level variations in west-central Europe over the last 3500 years. *The Holocene*, **15,** 789-801.
Hong, Y. T., et al., 2005: Inverse phase oscillations between the East Asian and Indian Ocean summer monsoons during the last 120 000 years and paleo-El Niño. *Earth and Planetary Science Letters*, **231,** 337-346.
Hönisch, B., N. G. Hemming, D. Archer, M. Siddall, and J. F. McManus, 2009: Atmospheric Carbon Dioxide Concentration Across the Mid-Pleistocene Transition. *Science*, **324,** 1551-1554.

Horton, B., and R. Edwards, 2006: *Quantifying Holocene sea level change using intertidal foraminifera: lessons from the British Isles*. Vol. 40, 1-97 pp.
Hu, C., G. M. Henderson, J. Huang, S. Xie, Y. Sun, and K. R. Johnson, 2008: Quantification of Holocene Asian monsoon rainfall from spatially separated cave records. *Earth and Planetary Science Letters*, **266,** 221-232.
Hu, F. S., E. Ito, T. A. Brown, B. B. Curry, and D. R. Engstrom, 2001: Pronounced climatic variations in Alaska during the last two millennia. *Proceedings of the National Academy of Sciences*, **98,** 10552-10556.
Huber, C., et al., 2006: Isotope calibrated Greenland temperature record over Marine Isotope Stage 3 and its relation to CH_4. *Earth and Planetary Science Letters*, **243,** 504-519.
Huber, M., and R. Caballero, 2011: The early Eocene equable climate problem revisited. *Climate of the Past*, **7,** 603-633.
Huybers, P., 2006: Early Pleistocene glacial cycles and the integrated summer insolation forcing. *Science*, **313,** 508-511.
Huybers, P., 2009: Antarctica's Orbital Beat. *Science*, **325,** 1085-1086.
Huybers, P., and C. Wunsch, 2005: Obliquity pacing of the late Pleistocene glacial terminations. *Nature*, **434,** 491-494.
Huybers, P., and G. Denton, 2008: Antarctic temperature at orbital timescales controlled by local summer duration. *Nature Geoscience*, **1,** 787-792.
Huybrechts, P., 2002: Sea level changes at the LGM from ice-dynamic reconstructions of the Greenland and Antarctic ice sheets during the glacial cycles. *Quaternary Science Reviews*, **21,** 203-231.
Hwang, Y.-T., D. M. W. Frierson, B. J. Soden, and I. M. Held, 2011: Corrigendum. *Journal of Climate*, **24,** 1559-1560.
Israelson, C., and B. Wohlfarth, 1999: Timing of the Last-Interglacial High Sea Level on the Seychelles Islands, Indian Ocean. *Quaternary Research*, **51,** 306-316.
Itambi, A. C., T. von Dobeneck, S. Mulitza, T. Bickert, and D. Heslop, 2009: Millennial-scale northwest African droughts related to Heinrich events and Dansgaard-Oeschger cycles: Evidence in marine sediments from offshore Senegal. *Paleoceanography*, **24,** PA1205.
Ivanochko, T. S., R. S. Ganeshram, G. J. A. Brummer, G. Ganssen, S. J. A. Jung, S. G. Moreton, and D. Kroon, 2005: Variations in tropical convection as an amplifier of global climate change at the millennial scale. *Earth and Planetary Science Letters*, **235,** 302-314.
Ivins, E., and T. James, 2005: Antarctic glacial isostatic adjustment: a new assessment. *Antarctic Science*, **17,** 541-553.
Ivy-Ochs, S., H. Kerschner, M. Maisch, M. Christl, P. W. Kubik, and C. Schlüchter, 2009: Latest Pleistocene and Holocene glacier variations in the European Alps. *Quaternary Science Reviews*, **28,** 2137-2149.
Jaccard, S., E. Galbraith, D. Sigman, and G. Haug, 2010: A pervasive link between Antarctic ice core and subarctic Pacific sediment records over the past 800 kyrs. *Quaternary Science Reviews*, **29,** 206-212.
Jansen, E., et al., 2007: Palaeoclimate. *Climate Change 2007: The Physical Science Basis. Contribution of Working Group I to the Fourth Assessment Report of the Intergovernmental Panel on Climate Change*, D. Qin, M. Manning, Z. Chen, M. Marquis, K. B. Averyt, M. Tignor, and H. L. Miller, Eds., Cambridge University Press.
Jevrejeva, S., J. C. Moore, and A. Grinsted, 2010: How will sea level respond to changes in natural and anthropogenic forcings by 2100? *Geophysical Research Letters*, **37,** L07703.
Joerin, U., K. Nicolussi, A. Fischer, T. Stocker, and C. Schlüchter, 2008: Holocene optimum events inferred from subglacial sediments at Tschierva Glacier, Eastern Swiss Alps. *Quaternary Science Reviews*, **27,** 337-350.
Jomelli, V., D. Grancher, D. Brunstein, and O. Solomina, 2008: Recalibration of the yellow Rhizocarpon growth curve in the Cordillera Blanca (Peru) and implications for LIA chronology. *Geomorphology*, **93,** 201-212.
Jomelli, V., V. Favier, A. Rabatel, D. Brunstein, G. Hoffmann, and B. Francou, 2009: Fluctuations of glaciers in the tropical Andes over the last millennium and palaeoclimatic implications: A review. *Palaeogeography, Palaeoclimatology, Palaeoecology*, **281,** 269-282.
Jomelli, V., et al., 2011: Irregular tropical glacier retreat over the Holocene epoch driven by progressive warming. *Nature*, **474,** 196-199.
Jones, P. D., et al., 2009: High-resolution palaeoclimatology of the last millennium: a review of current status and future prospects. *The Holocene*, **19,** 3-49.
Joos, F., and R. Spahni, 2008: Rates of change in natural and anthropogenic radiative forcing over the past 20,000 years. *Proceedings of the National Academy of Sciences*, **105,** 1425-1430.
Jordan, G. J., 2011: A critical framework for the assessment of biological palaeoproxies: predicting past climate and levels of atmospheric CO2 from fossil leaves. *New Phytologist*, **192,** 29-44.
Jouzel, J., et al., 2007: Orbital and millennial Antarctic climate variability over the past 800,000 years. *Science*, **317,** 793-796.
Juckes, M. N., et al., 2007: Millennial temperature reconstruction intercomparison and evaluation. *Climate of the Past*, **3,** 591-609.
Jungclaus, J. H., et al., 2010: Climate and carbon-cycle variability over the last millennium. *Climate of the Past*, **6,** 723-737.
Justino, F., and W. R. Peltier, 2005: The glacial North Atlantic Oscillation. *Geophysical Research Letters*, **32,** L21803.
Justino, F., W. Peltier, and H. Barbosa, 2010: Atmospheric susceptibility to wildfire occurrence during the Last Glacial Maximum and mid-Holocene. *Palaeogeography Palaeoclimatology Palaeoecology*, **295,** 76-88.
Justwan, A., and N. Koç, 2008: A diatom based transfer function for reconstructing sea ice concentrations in the North Atlantic. *Marine Micropaleontology*, **66,** 264-278.

Kabanda, T., and M. Jury, 1999: Inter-annual variability of short rains over northern Tanzania. *Climate Research*, **13,** 231-241.
Kageyama, M., et al., 2006: Last Glacial Maximum temperatures over the North Atlantic, Europe and western Siberia: a comparison between PMIP models, MARGO sea–surface temperatures and pollen-based reconstructions. *Quaternary Science Reviews*, **25,** 2082-2102.
Kale, V., 2008: Palaeoflood hydrology in the Indian context. *Journal of the Geological Society of India*, **71,** 56-66.
Kaspar, F., T. Spangehl, and U. Cubasch, 2007: Northern hemisphere winter storm tracks of the Eemian interglacial and the last glacial inception. *Climate of the Past*, **3,** 181-192.
Kaufman, D. S., et al., 2009: Recent Warming Reverses Long-Term Arctic Cooling. *Science*, **325,** 1236-1239.
Kawamura, K., et al., 2007: Northern Hemisphere forcing of climatic cycles in Antarctica over the past 360,000 years. *Nature*, **448,** 912-U914.
Kemp, A. C., B. P. Horton, J. P. Donnelly, M. E. Mann, M. Vermeer, and S. Rahmstorf, in press: Climate related sea level variations over the past two millennia. *Proceedings of the National Academy of Sciences*, 10.1073/pnas.1015619108.
Kemp, A. C., et al., 2009: Timing and magnitude of recent accelerated sea level rise (North Carolina, United States). *Geology*, **37,** 1035-1038.
Kench, P. S., S. G. Smithers, R. F. McLean, and S. L. Nichol, 2009: Holocene reef growth in the Maldives: Evidence of a mid-Holocene sea level highstand in the central Indian Ocean. *Geology*, **37,** 455-458.
Kiefer, T., and M. Kienast, 2005: Patterns of deglacial warming in the Pacific Ocean: a review with emphasis on the time interval of Heinrich event 1. *Quaternary Science Reviews*, **24,** 1063-1081.
Kiefer, T., M. Sarnthein, H. Erlenkeuser, P. M. Grootes, and A. P. Roberts, 2001: North Pacific response to millennial-scale changes in ocean circulation over the last 60 kyr. *Paleoceanography*, **16,** 179-189.
Kienast, M., S. S. Kienast, S. E. Calvert, T. I. Eglinton, G. Mollenhauer, R. François, and A. C. Mix, 2006: Eastern Pacific cooling and Atlantic overturning circulation during the last deglaciation. *Nature*, **443,** 846-849.
Kilbourne, K. H., T. M. Quinn, R. Webb, T. Guilderson, J. Nyberg, and A. Winter, 2008: Paleoclimate proxy perspective on Caribbean climate since the year 1751: Evidence of cooler temperatures and multidecadal variability. *Paleoceanography*, **23,** PA3220.
Kim, S. J., et al., 2010: Climate response over Asia/Arctic to change in orbital parameters for the last interglacial maximum. *Geosciences Journal*, **14,** 173-190.
Kinnard, C., C. M. Zdanowicz, R. M. Koerner, and D. A. Fisher, 2008: A changing Arctic seasonal ice zone: Observations from 1870-2003 and possible oceanographic consequences. *Geophysical Research Letters*, **35,** L02507.
Kirchhefer, A. J., 2001: Reconstruction of summer temperatures from tree-rings of Scots pine (*Pinus sylvestris* L.) in coastal northern Norway. *The Holocene*, **11,** 41-52.
Kleiven, H. F., I. R. Hall, I. N. McCave, G. Knorr, and E. Jansen, 2011: Coupled deep-water flow and climate variability in the middle Pleistocene North Atlantic. *Geology*, **39,** 343-346.
Kleiven, H. F., C. Kissel, C. Laj, U. S. Ninnemann, T. O. Richter, and E. Cortijo, 2008: Reduced North Atlantic Deep Water coeval with the glacial Lake Agassiz freshwater outburst. *Science*, **319,** 60-64.
Klochko, K., A. J. Kaufman, W. Yao, R. H. Byrne, and J. A. Tossell, 2006: Experimental measurement of boron isotope fractionation in seawater. *Earth and Planetary Science Letters*, **248,** 276-285.
Knox, J. C., 2000: Sensitivity of modern and Holocene floods to climate change. *Quaternary Science Reviews*, **19,** 439-457.
Knudsen, M. F., M.-S. Seidenkrantz, B. H. Jacobsen, and A. Kuijpers, 2011: Tracking the Atlantic Multidecadal Oscillation through the last 8,000 years. *Nature Communications*, **2,** 178.
Kobashi, T., J. P. Severinghaus, J. M. Barnola, K. Kawamura, T. Carter, and T. Nakaegawa, 2010: Persistent multi-decadal Greenland temperature fluctuation through the last millennium. *Climatic Change*, **100,** 733-756.
Koch, J., and J. Clague, 2011: Extensive glaciers in northwest North America during Medieval time. *Climatic Change*, **107,** 593-613.
Koch, J., B. Menounos, J. J. Clague, and G. D. Osborn, 2004: Environmental Change in Garibaldi Provincial Park, Southern Coast Mountains, British Columbia. *Geoscience Canada*, **31**.
Koenig, S., R. DeConto, and D. Pollard, 2011: Late Pliocene to Pleistocene sensitivity of the Greenland Ice Sheet in response to external forcing and internal feedbacks. *Climate Dynamics*, **37,** 1247-1268.
Koerner, R., and D. Fisher, 2002: Ice-core evidence for widespread Arctic glacier retreat in the Last Interglacial and the early Holocene. *Annals of Glaciology, Vol 35***,** 19-24.
Köhler, P., F. Joos, S. Gerber, and R. Knutti, 2005: Simulated changes in vegetation distribution, land carbon storage, and atmospheric CO_2 in response to a collapse of the North Atlantic thermohaline circulation. *Climate Dynamics*, **25,** 689-708.
Köhler, P., G. Knorr, D. Buiron, A. Lourantou, and J. Chappellaz, 2011: Abrupt rise in atmospheric CO_2 at the onset of the Bølling/Allerød: in-situ ice core data versus true atmospheric signals. *Climate of the Past*, **7,** 473-486.
Köhler, P., R. Bintanja, H. Fischer, F. Joos, R. Knutti, G. Lohmann, and V. Masson-Delmotte, 2010: What caused Earth's temperature variations during the last 800,000 years? Data-based evidence on radiative forcing and constraints on climate sensitivity. *Quaternary Science Reviews*, **29,** 129-145.

Kopp, G., and J. L. Lean, 2011: A new, lower value of total solar irradiance: Evidence and climate significance. *Geophysical Research Letters*, **38,** L01706.
Kopp, R. E., F. J. Simons, J. X. Mitrovica, A. C. Maloof, and M. Oppenheimer, 2009: Probabilistic assessment of sea level during the last interglacial stage. *Nature*, **462,** 863-U851.
Koutavas, A., and S. Joanidis, 2009: El Niño during the last glacial maximum. *Geochimica Et Cosmochimica Acta*, A690-A690.
Koutavas, A., P. B. Demenocal, G. C. Olive, and J. Lynch-Stieglitz, 2006: Mid-Holocene El Niño-Southern Oscillation (ENSO) attenuation revealed by individual foraminifera in eastern tropical Pacific sediments. *Geology*, **34,** 993-996.
Krebs, U., and A. Timmermann, 2007: Tropical air-sea interactions accelerate the recovery of the Atlantic Meridional Overturning Circulation after a major shutdown. *Journal of Climate*, **20,** 4940-4956.
Krinner, G., O. Boucher, and Y. Balkanski, 2006: Ice-free glacial northern Asia due to dust deposition on snow. *Climate Dynamics*, **27,** 613-625.
Kristen, I., et al., 2010: Biomarker and stable carbon isotope analyses of sedimentary organic matter from Lake Tswaing: evidence for deglacial wetness and early Holocene drought from South Africa. *Journal of Paleolimnology*, **44,** 143-160.
Krivova, N., and S. Solanki, 2008: Models of solar irradiance variations: Current status. *Journal of Astrophysics and Astronomy*, **29,** 151-158.
Krivova, N., S. Solanki, and Y. Unruh, 2011: Towards a long-term record of solar total and spectral irradiance. *Journal of Atmospheric and Solar-Terrestrial Physics*, **73,** 223-234.
Küttel, M., et al., 2010: The importance of ship log data: reconstructing North Atlantic, European and Mediterranean sea level pressure fields back to 1750. *Climate Dynamics*, **34,** 1115-1128.
Kug, J. S., J. Choi, S. I. An, F. F. Jin, and A. T. Wittenberg, 2010: Warm Pool and Cold Tongue El Niño Events as Simulated by the GFDL 2.1 Coupled GCM. *Journal of Climate*, **23,** 1226-1239.
Kutzbach, J. E., X. D. Liu, Z. Y. Liu, and G. S. Chen, 2008: Simulation of the evolutionary response of global summer monsoons to orbital forcing over the past 280,000 years. *Climate Dynamics*, **30,** 567-579.
Lambeck, K., and M. Nakada, 1992: Constraints on the age and duration of the last interglacial period and on sea level variations. *Nature***,** 125-128.
Lambeck, K., and E. Bard, 2000: Sea level change along the French Mediterranean coast for the past 30□000 years. *Earth and Planetary Science Letters*, **175,** 203-222.
Lambeck, K., and J. Chappell, 2001: Sea Level Change Through the Last Glacial Cycle. *Science*, **292,** 679-686.
Lambeck, K., T. Esat, and E. Potter, 2002: Links between climate and sea levels for the past three million years. *Nature*, **419,** 199-206.
Lambeck, K., A. Purcell, and A. Dutton, in press: The anatomy of interglacial sea levels: The relationship between sea levels and ice volumes during the Last Interglacial. *Earth and Planetary Science Letters*, 10.1016/j.epsl.2011.08.026.
Lambeck, K., A. Purcell, J. Zhao, and N.-O. Svensson, 2010a: The Scandinavian Ice Sheet: from MIS 4 to the end of the Last Glacial Maximum. *Boreas*, **39,** 410-435.
Lambeck, K., A. Purcell, P. Johnston, M. Nakada, and Y. Yokoyama, 2003: Water-load definition in the glacio-hydro-isostatic sea level equation. *Quaternary Science Reviews*, **22,** 309-318.
Lambeck, K., M. Anzidei, F. Antonioli, A. Benini, and A. Esposito, 2004: Sea level in Roman time in the Central Mediterranean and implications for recent change. *Earth and Planetary Science Letters*, **224,** 563-575.
Lambeck, K., A. Purcell, S. Funder, K. H. KjæR, E. Larsen, and P. E. R. Moller, 2006: Constraints on the Late Saalian to early Middle Weichselian ice sheet of Eurasia from field data and rebound modelling. *Boreas*, **35,** 539-575.
Lambeck, K., C. D. Woodroffe, F. Antonioli, M. Anzidei, W. R. Gehrels, J. Laborel, and A. J. Wright, 2010b: Paleoenvironmental records, geophysical modelling, and reconstruction of sea level trends and variability on centennial and Longer Timescales. *Understanding sea level rise and variability*, J. A. Church, P. L. Woodworth, T. Aarup, and W. S. Wilson, Eds., Wiley-Blackwell, 61-121.
Lambert, F., et al., 2008: Dust-climate couplings over the past 800,000 years from the EPICA Dome C ice core. *Nature*, **452,** 616-619.
Landais, A., et al., 2004: A continuous record of temperature evolution over a sequence of Dansgaard-Oeschger events during Marine Isotopic Stage 4 (76 to 62 kyr BP). *Geophysical Research Letters*, **31,** L22211.
Landais, A., et al., 2006: The glacial inception as recorded in the NorthGRIP Greenland ice core: timing, structure and associated abrupt temperature changes. *Climate Dynamics*, DOI 10.1007/s00382-005-0063-y**,** 273-284.
Landais, A., et al., 2010: What drives the millennial and orbital variations of $\delta^{18}O(atm)$? *Quaternary Science Reviews*, **29,** 235-246.
Landrum, L., B. Otto-Bliesner, E. Wahl, A. Conley, P. Lawrence, and H. Teng, submitted: Last Millennium Climate and Its Variability in CCSM4. *Journal of Climate*.
Lang, N., and E. W. Wolff, 2011: Interglacial and glacial variability from the last 800 ka in marine, ice and terrestrial archives. *Climate of the Past*, **7,** 361-380.
Langebroek, P., A. Paul, and M. Schulz, 2009: Antarctic ice sheet response to atmospheric CO2 and insolation in the Middle Miocene. *Climate of the Past*, **5,** 633-646.

Langen, P., and V. Alexeev, 2007: Polar amplification as a preferred response in an idealized aquaplanet GCM. *Climate Dynamics*, **29,** 305-317.
Larsen, N. K., K. H. Kjær, J. Olsen, S. Funder, K. K. Kjeldsen, and N. Nørgaard-Pedersen, 2011: Restricted impact of Holocene climate variations on the southern Greenland Ice Sheet. *Quaternary Science Reviews*, **30,** 3171-3180.
Laskar, J., P. Robutel, F. Joutel, M. Gastineau, A. Correia, and B. Levrard, 2004: A long-term numerical solution for the insolation quantities of the Earth. *Astronomy & Astrophysics*, **428,** 261-285.
Lean, J., T. Woods, F. Eparvier, R. Meier, D. Strickland, J. Correira, and J. Evans, 2011: Solar extreme ultraviolet irradiance: Present, past, and future. *Journal of Geophysical Research-Space Physics*, **116,** A01102.
Lean, J. L., O. R. White, and A. Skumanich, 1995: On the Solar Ultraviolet Spectral Irradiance During the Maunder Minimum. *Global Biochemical Cycles*, **9,** 171-182.
Leclercq, P., and J. Oerlemans, 2011: Global and hemispheric temperature reconstruction from glacier length fluctuations. *Climate Dynamics*, 10.1007/s00382-011-1145-7**,** 1-15.
Leduc, G., R. Schneider, J. H. Kim, and G. Lohmann, 2010: Holocene and Eemian sea surface temperature trends as revealed by alkenone and Mg/Ca paleothermometry. *Quaternary Science Reviews*, **29,** 989-1004.
Lee, T., F. Zwiers, and M. Tsao, 2008: Evaluation of proxy-based millennial reconstruction methods. *Climate Dynamics*, **31,** 263-281.
LeGrande, A. N., and G. A. Schmidt, 2008: Ensemble, water isotope-enabled, coupled general circulation modeling insights into the 8.2 ka event. *Paleoceanography*, **23,** PA3207.
LeGrande, A. N., and G. A. Schmidt, 2009: Sources of Holocene variability of oxygen isotopes in paleoclimate archives. *Climate of the Past*, **5,** 441-455.
LeGrande, A. N., et al., 2006: Consistent simulation of multiple proxy responses to an abrupt climate change event (vol 103, pg 837, 2006). *Proceedings of the National Academy of Sciences of the United States of America*, **103,** 10527-10527.
Lemke, P., et al., 2007: Observations: Changes in Snow, Ice and Frozen Ground. *Climate Change 2007: The Physical Science Basis. Contribution of Working Group I to the Fourth Assessment Report of the Intergovernmental Panel on Climate Change*, Cambridge University Press.
Lemoine, D. M., 2010: Paleoclimatic warming increased carbon dioxide concentrations. *Journal of Geophysical Research-Atmospheres*, **115,** D22122.
Leorri, E., B. P. Horton, and A. Cearreta, 2008: Development of a foraminifera-based transfer function in the Basque marshes, N. Spain: Implications for sea level studies in the Bay of Biscay. *Marine Geology*, **251,** 60-74.
Lhomme, N., G. Clarke, and S. Marshall, 2005: Tracer transport in the Greenland Ice Sheet: constraints on ice cores and glacial history. *Quaternary Science Reviews*, DOI 10.1016/j.quascirev.2004.08.020**,** 173-194.
Li, B., D. W. Nychka, and C. M. Ammann, 2010a: The Value of Multiproxy Reconstruction of Past Climate. *Journal of the American Statistical Association*, **105,** 883-895.
Li, C., D. S. Battisti, and C. M. Bitz, 2010b: Can North Atlantic Sea Ice Anomalies Account for Dansgaard-Oeschger Climate Signals? *Journal of Climate*, **23,** 5457-5475.
Li, J., et al., 2011: Interdecadal modulation of El Niño amplitude during the past millennium. *Nature Climate Change*, **1,** 114-118.
Li, Y., H. Renssen, A. Wiersma, and T. Törnqvist, 2009: Investigating the impact of Lake Agassiz drainage routes on the 8.2 ka cold event with a climate model. *Climate of the Past*, **5,** 471-480.
Licciardi, J. M., J. M. Schaefer, J. R. Taggart, and D. C. Lund, 2009: Holocene Glacier Fluctuations in the Peruvian Andes Indicate Northern Climate Linkages. *Science*, **325,** 1677-1679.
Linderholm, H. W., C. K. Folland, and A. Walther, 2009: A multicentury perspective on the summer North Atlantic Oscillation (SNAO) and drought in the eastern Atlantic Region. *Journal of Quaternary Science*, **24,** 415-425.
Lindholm, M., R. Jalkanen, H. Salminen, T. Aalto, and M. Ogurtsov, 2011: The height-increment record of summer temperature extended over the last millennium in Fennoscandia. *The Holocene*, **21,** 319-326.
Lisiecki, L., and M. Raymo, 2005: A Pliocene-Pleistocene stack of 57 globally distributed benthic $\delta^{18}O$ records. *Paleoceanography*, **20,** PA1003.
Lisiecki, L. E., 2010: Links between eccentricity forcing and the 100,000-year glacial cycle. *Nature Geoscience*, **3,** 349-352.
Lisiecki, L. E., and M. E. Raymo, 2007: Plio–Pleistocene climate evolution: trends and transitions in glacial cycle dynamics. *Quaternary Science Reviews*, **26,** 56-69.
Lisiecki, L. E., M. E. Raymo, and W. B. Curry, 2008: Atlantic overturning responses to Late Pleistocene climate forcings. *Nature*, **456,** 85-88.
Liu, J., H. Storch, X. Chen, E. Zorita, J. Zheng, and S. Wang, 2005: Simulated and reconstructed winter temperature in the eastern China during the last millennium. *Chinese Science Bulletin*, **50,** 2872-2877.
Liu, J., B. Wang, Q. Ding, X. Kuang, W. Soon, and E. Zorita, 2009a: Centennial Variations of the Global Monsoon Precipitation in the Last Millennium: Results from ECHO-G Model. *Journal of Climate*, **22,** 2356-2371.
Liu, X. D., Z. Y. Liu, S. Clemens, W. Prell, and J. Kutzbach, 2007: A coupled model study of glacial Asian monsoon variability and Indian ocean dipole. *Journal of the Meteorological Society of Japan*, **85,** 1-10.
Liu, Z., et al., 2009b: Transient Simulation of Last Deglaciation with a New Mechanism for Bølling-Allerød Warming. *Science*, **325,** 310-314.

Liu, Z. Y., J. Kutzbach, and L. X. Wu, 2000: Modeling climate shift of El Niño variability in the Holocene. *Geophysical Research Letters*, **27,** 2265-2268.
Ljungqvist, F. C., 2010: A new reconstruction of temperature variability in the extra-tropical Northern Hemisphere during the last two millennia. *Geografiska Annaler: Series A, Physical Geography*, **92,** 339–351.
Ljungqvist, F. C., P. J. Krusic, G. Brattström, and H. S. Sundqvist, Submitted: Northern Hemisphere temperature patterns in the last 12 centuries. *Climate of the Past Discussion*, **7,** 3349-3397.
Long, A. J., S. A. Woodroffe, G. A. Milne, C. L. Bryant, M. J. R. Simpson, and L. M. Wake, in press: Relative sea level change in Greenland during the last 700-yrs and ice sheet response to the Little Ice Age. *Earth and Planetary Science Letters*, 10.1016/j.epsl.2011.06.027.
Loso, M., 2009: Summer temperatures during the Medieval Warm Period and Little Ice Age inferred from varved proglacial lake sediments in southern Alaska. *Journal of Paleolimnology*, **41,** 117-128.
Loulergue, L., et al., 2008: Orbital and millennial-scale features of atmospheric CH_4 over the past 800,000 years. *Nature*, **453,** 383-386.
Lourantou, A., J. Chappellaz, J. Barnola, V. Masson-Delmotte, and D. Raynaud, 2010a: Changes in atmospheric CO_2 and its carbon isotopic ratio during the penultimate deglaciation. *Quaternary Science Reviews*, **29,** 1983-1992.
Lourantou, A., et al., 2010b: Constraint of the CO_2 rise by new atmospheric carbon isotopic measurements during the last deglaciation. *Global Biochemical Cycles*, **24,** GB2015.
Lowenstein, T. K., and R. V. Demicco, 2006: Elevated Eocene Atmospheric CO_2 and Its Subsequent Decline. *Science*, **313,** 1928-1928.
Lu, J., and M. Cai, 2009: Seasonality of polar surface warming amplification in climate simulations. *Geophysical Research Letters*, **36,** L16704.
Luckman, B., and R. Villalba, 2001: Assessing the synchroneity of glacier fluctuations in the western Cordillera of the Americas during the last millenium. *Interhemispheric climate linkages*, V. Markgraf, Ed., Academic Press.
Luckman, B. H., and R. J. S. Wilson, 2005: Summer temperatures in the Canadian Rockies during the last millennium: a revised record. *Climate Dynamics*, **24,** 131-144.
Lü, J. M., S. J. Kim, A. Abe-Ouchi, Y. Q. Yu, and R. Ohgaito, 2010: Arctic Oscillation during the Mid-Holocene and Last Glacial Maximum from PMIP2 Coupled Model Simulations. *Journal of Climate*, **23,** 3792-3813.
Lüthi, D., et al., 2008: High-resolution carbon dioxide concentration record 650,000-800,000 years before present. *Nature*, **453,** 379-382.
Lunt, D. J., G. L. Foster, A. M. Haywood, and E. J. Stone, 2008: Late Pliocene Greenland glaciation controlled by a decline in atmospheric CO_2 levels. *Nature*, **454,** 1102-U1141.
Lunt, D. J., A. M. Haywood, G. A. Schmidt, U. Salzmann, P. J. Valdes, and H. J. Dowsett, 2010a: Earth system sensitivity inferred from Pliocene modelling and data. *Nature Geoscience*, **3,** 60-64.
Lunt, D. J., et al., 2010b: CO_2-driven ocean circulation changes as an amplifier of Paleocene-Eocene thermal maximum hydrate destabilization. *Geology*, **38,** 875-878.
Luterbacher, J., R. Neukom, J. González-Rouco, L. Fernández-Donado, C. Raible, and E. Zorita, 2011: Reconstructed and simulated Medieval Climate Anbomaly in southern South America. *PAGES Newsletters*, **xx,** xx-xx.
Luterbacher, J., et al., 2002: Reconstruction of sea level pressure fields over the Eastern North Atlantic and Europe back to 1500. *Climate Dynamics*, **18,** 545-561.
Luterbacher, J., et al., 2010: Circulation dynamics and its influence on European and Mediterranean January–April climate over the past half millennium: results and insights from instrumental data, documentary evidence and coupled climate models. *Climatic Change*, **101,** 201-234.
Luterbacher, J., et al., in press: A review of 2000 years of paleoclimatic evidence in the Mediterranean. *The Mediterranean Climate: from past to future*, L. e. al., Ed., Elsevier.
MacDonald, G., D. Porinchu, N. Rolland, K. Kremenetsky, and D. Kaufman, 2009: Paleolimnological evidence of the response of the central Canadian treeline zone to radiative forcing and hemispheric patterns of temperature change over the past 2000 years. *Journal of Paleolimnology*, **41,** 129-141.
Macdonald, N., 2007: Neil MacDonald on Epigraphic Records: A Valuable Resource in Reassessing Flood Risk and Long-Term Climate Variability. *Environmental History*, **12,** 136-140.
Macdonald, N., and A. R. Black, 2010: Reassessment of flood frequency using historical information for the River Ouse at York, UK (1200–2000). *Hydrological Sciences Journal*, **55,** 1152-1162.
Machado, M. J., G. Benito, M. Barriendos, and F. S. Rodrigo, in press: 500 Years of rainfall variability and extreme hydrological events in southeastern Spain drylands. *Journal of Arid Environments*, 10.1016/j.jaridenv.2011.02.002.
Macias Fauria, M., et al., 2010: Unprecedented low twentieth century winter sea ice extent in the Western Nordic Seas since AD 1200. *Climate Dynamics*, **34,** 781-795.
Mackintosh, A., et al., 2011: Retreat of the East Antarctic ice sheet during the last glacial termination. *Nature Geoscience*, **4,** 195-202.
Macklin, M. G., et al., 2006: Past hydrological events reflected in the Holocene fluvial record of Europe. *Catena*, **66,** 145-154.
Maher, B. A., J. M. Prospero, D. Mackie, D. Gaiero, P. P. Hesse, and Y. Balkanski, 2010: Global connections between aeolian dust, climate and ocean biogeochemistry at the present day and at the last glacial maximum. *Earth-Science Reviews*, **99,** 61-97.

Mahlstein, I., and R. Knutti, 2011: Ocean Heat Transport as a Cause for Model Uncertainty in Projected Arctic Warming. *Journal of Climate*, **24,** 1451-1460.
Mahowald, N., S. Albani, S. Engelstaedter, G. Winckler, and M. Goman, 2011: Model insight into glacial–interglacial paleodust records. *Quaternary Science Reviews*, **30,** 832-854.
Mahowald, N. M., M. Yoshioka, W. D. Collins, A. J. Conley, D. W. Fillmore, and D. B. Coleman, 2006: Climate response and radiative forcing from mineral aerosols during the last glacial maximum, pre-industrial, current and doubled-carbon dioxide climates. *Geophysical Research Letters*, **33,** L20705.
Manabe, S., and R. Stouffer, 1980: Sensitivity of a global climate model to an increase of CO_2 concentration in the atmosphere *Journal of Geophysical Research-Oceans and Atmospheres*, **85,** 5529-5554.
Mann, M. E., 2002: Large-scale climate variability and connections with the Middle East in past centuries. *Climatic Change*, **55,** 287-314.
——, 2007: Climate over the past two millennia. *Annual Review of Earth and Planetary Sciences*, **35,** 111-136.
Mann, M. E., M. A. Cane, S. E. Zebiak, and A. Clement, 2005: Volcanic and solar forcing of the tropical Pacific over the past 1000 years. *Journal of Climate*, **18,** 447-456.
Mann, M. E., Z. H. Zhang, M. K. Hughes, R. S. Bradley, S. K. Miller, S. Rutherford, and F. B. Ni, 2008: Proxy-based reconstructions of hemispheric and global surface temperature variations over the past two millennia. *Proceedings of the National Academy of Sciences of the United States of America*, **105,** 13252-13257.
Mann, M. E., et al., 2009: Global Signatures and Dynamical Origins of the Little Ice Age and Medieval Climate Anomaly. *Science*, **326,** 1256-1260.
Mantsis, D., A. Clement, A. Broccoli, and M. Erb, 2011: Climate Feedbacks in Response to Changes in Obliquity. *Journal of Climate*, **24,** 2830-2845.
Marchitto, T., R. Muscheler, J. Ortiz, J. Carriquiry, and A. van Geen, 2010: Dynamical Response of the Tropical Pacific Ocean to Solar Forcing During the Early Holocene. *Science*, **330,** 1378-1381.
Marcott, S., et al., 2011: Ice shelf collapse from subsurface warming as a trigger for Heinrich events. *Proceedings of the National Academy of Sciences of the United States of America*, **108,** 13415-13419.
MARGO Project Members, 2009: Constraints on the magnitude and patterns of ocean cooling at the Last Glacial Maximum. *Nature Geoscience*, **2,** 127-132.
Marino, F., et al., 2009: Coherent composition of glacial dust on opposite sides of the East Antarctic Plateau inferred from the deep EPICA ice cores. *Geophysical Research Letters*, **36,** L23703.
Marlon, J. R., et al., 2009: Wildfire responses to abrupt climate change in North America. *Proceedings of the National Academy of Sciences of the United States of America*, **106,** 2519-2524.
Marshall, S. J., and M. R. Koutnik, 2006: Ice sheet action versus reaction: Distinguishing between Heinrich events and Dansgaard-Oeschger cycles in the North Atlantic. *Paleoceanography*, **21,** PA2021.
Martrat, B., J. O. Grimalt, N. J. Shackleton, L. de Abreu, M. A. Hutterli, and T. F. Stocker, 2007: Four climate cycles of recurring deep and surface water destabilizations on the Iberian margin. *Science*, **317,** 502-507.
Maslin, M., et al., 2000: Palaeoreconstruction of the Amazon River freshwater and sediment discharge using sediments recovered at Site 942 on the Amazon Fan. *Journal of Quaternary Science***,** 419-434.
Masson-Delmotte, V., et al., 2011: Sensitivity of interglacial Greenland temperature and $\delta^{18}O$: ice core data, orbital and increased CO2 climate simulations. *Climate of the Past*, **7,** 1041-1059.
Masson-Delmotte, V., et al., 2010a: EPICA Dome C record of glacial and interglacial intensities. *Quaternary Science Reviews*, **29,** 113-128.
Masson-Delmotte, V., et al., 2010b: Abrupt change of Antarctic moisture origin at the end of Termination II. *Proceedings of the National Academy of Sciences of the United States of America*, **107,** 12091-12094.
Masson-Delmotte, V., et al., 2006: Past and future polar amplification of climate change: climate model intercomparisons and ice-core constraints. *Climate Dynamics*, **27,** 437-440.
Masson-Delmotte, V., et al., 2008: A review of Antarctic surface snow isotopic composition: Observations, atmospheric circulation, and isotopic modeling. *Journal of Climate*, **21,** 3359-3387.
Matthews, J. A., and P. Q. Dresser, 2008: Holocene glacier variation chronology of the Smørstabbtindan massif, Jotunheimen, southern Norway, and the recognition of century- to millennial-scale European Neoglacial Events. *The Holocene*, **18,** 181-201.
McGee, D., W. S. Broecker, and G. Winckler, 2010: Gustiness: The driver of glacial dustiness? *Quaternary Science Reviews*, **29,** 2340-2350.
McGregor, S., and A. Timmermann, 2010: The Effect of Explosive Tropical Volcanism on ENSO. *Journal of Climate*, **24,** 2178-2191.
McGregor, S., A. Timmermann, and O. Timm, 2010: A unified proxy for ENSO and PDO variability since 1650. *Climate of the Past*, **6,** 1-17.
McInerney, F., and S. Wing, 2011: The Paleocene-Eocene Thermal Maximum: A Perturbation of Carbon Cycle, Climate, and Biosphere with Implications for the Future. *Annual Review of Earth and Planetary Sciences*, **39,** 489-516.
McKay, N. P., J. T. Overpeck, and B. L. Otto-Bliesner, 2011: The role of ocean thermal expansion in Last Interglacial sea level rise. *Geophysical Research Letters*, **38,** L14605.
McKay, R., et al., submitted: Antarctic and Southern Ocean influences on Late Pliocene global cooling. *Proceedings of the National Academy of Sciences*.

McManus, J., R. Francois, J. Gherardi, L. Keigwin, and S. Brown-Leger, 2004: Collapse and rapid resumption of Atlantic meridional circulation linked to deglacial climate changes. *Nature*, **428,** 834-837.
McShane, B. B., and A. J. Wyner, 2011: A statistical analysis of multiple temperature proxies: are reconstructions of surface temperatures over the last 1000 years reliable? *Annals of Applied Statistics*, **5,** 5-44.
Meehl, G. A., J. M. Arblaster, K. Matthes, F. Sassi, and H. van Loon, 2009: Amplifying the Pacific Climate System Response to a Small 11-Year Solar Cycle Forcing. *Science*, **325,** 1114-1118.
Meehl, G. A., et al., 2007: Global Climate Projections. *Climate Change 2007: The Physical Science Basis. Contribution of Working Group I to the Fourth Assessment Report of the Intergovernmental Panel on Climate Change*, Cambridge University Press.
Menounos, B., G. Osborn, J. Clague, and B. Luckman, 2009: Latest Pleistocene and Holocene glacier fluctuations in western Canada. *Quaternary Science Reviews*, **28,** 2049-2074.
Menviel, L., A. Timmermann, A. Mouchet, and O. Timm, 2008: Meridional reorganizations of marine and terrestrial productivity during Heinrich events. *Paleoceanography*, **23,** PA1203.
Menviel, L., A. Timmermann, O. E. Timm, and A. Mouchet, 2011: Deconstructing the Last Glacial termination: the role of millennial and orbital-scale forcings. *Quaternary Science Reviews*, **30,** 1155-1172.
Merkel, U., M. Prange, and M. Schulz, 2010: ENSO variability and teleconnections during glacial climates. *Quaternary Science Reviews*, **29,** 86-100.
Meure, C., et al., 2006: Law Dome CO_2, CH_4 and N_2O ice core records extended to 2000 years BP. *Geophysical Research Letters*, **10,** L14810.
Miller, G., R. Alley, J. Brigham-Grette, J. Fitzpatrick, L. Polyak, M. Serreze, and J. White, 2010: Arctic amplification: can the past constrain the future? *Quaternary Science Reviews*, **29,** 1779-1790.
Miller, K., et al., submitted: The high tide of the warm Pliocene: Implications of global sea level for Antarctic deglaciation. *Geology*.
Miller, K. G., et al., 2005: The Phanerozoic Record of Global Sea level Change. *Science*, **310,** 1293-1298.
Milne, G., and J. Mitrovica, 2008: Searching for eustasy in deglacial sea level histories. *Quaternary Science Reviews*, **27,** 2292-2302.
Mischler, J. A., et al., 2009: Carbon and hydrogen isotopic composition of methane over the last 1000 years. *Global Biochemical Cycles*, **23,** GB4024.
Mitrovica, J. X., and J. Wahr, 2011: Ice Age Earth Rotation*. *Annual Review of Earth and Planetary Sciences*, **39,** 577-616.
Moberg, A., D. M. Sonechkin, K. Holmgren, N. M. Datsenko, and W. Karlen, 2005: Highly variable Northern Hemisphere temperatures reconstructed from low- and high-resolution proxy data. *Nature*, **433,** 613-617.
Mohtadi, M., D. W. Oppo, S. Steinke, J.-B. W. Stuut, R. De Pol-Holz, D. Hebbeln, and A. Lückge, 2011: Glacial to Holocene swings of the Australian-Indonesian monsoon. *Nature Geoscience*, **4,** 540-544.
Morgan, V., et al., 2002: Relative timing of deglacial climate events in Antarctica and Greenland. *Science*, **297,** 1862-1864.
Moriwaki, H., M. Chikamori, M. Okuno, and T. Nakamura, 2006: Holocene changes in sea level and coastal environments on Rarotonga, Cook Islands, South Pacific Ocean. *The Holocene*, **16,** 839-848.
Moros, M., J. T. Andrews, D. D. Eberl, and E. Jansen, 2006: Holocene history of drift ice in the northern North Atlantic: Evidence for different spatial and temporal modes. *Paleoceanography*, **21,** PA2017.
Moros, M., E. Jansen, D. W. Oppo, J. Giraudeau, and A. Kuijpers, in press: Reconstruction of the late Holocene changes in the Sub-Arctic Front position at the Reykjanes Ridge, north Atlantic. *The Holocene*.
Morrill, C., A. J. Wagner, B. L. Otto-Bliesner, and N. Rosenbloom, in press: Evidence for significant climate impacts in monsoonal Asia at 8.2 ka from multiple proxies and model simulations.indd. *Journal of Earth Environmental*, 1-16.
Moucha, R., A. M. Forte, J. X. Mitrovica, D. B. Rowley, S. Quéré, N. A. Simmons, and S. P. Grand, 2008: Dynamic topography and long-term sea level variations: There is no such thing as a stable continental platform. *Earth and Planetary Science Letters*, **271,** 101-108.
Mudelsee, M., M. Borngen, G. Tetzlaff, and U. Grunewald, 2003: No upward trends in the occurrence of extreme floods in central Europe. *Nature*, **425,** 166-169.
Müller, R. D., M. Sdrolias, C. Gaina, B. Steinberger, and C. Heine, 2008: Long-Term Sea level Fluctuations Driven by Ocean Basin Dynamics. *Science*, **319,** 1357-1362.
Muhs, D. R., K. R. Simmons, and B. Steinke, 2002: Timing and warmth of the Last Interglacial period: new U-series evidence from Hawaii and Bermuda and a new fossil compilation for North America. *Quaternary Science Reviews*, **21,** 1355-1383.
Muhs, D. R., K. R. Simmons, R. R. Schumann, and R. B. Halley, 2011: Sea level history of the past two interglacial periods: new evidence from U-series dating of reef corals from south Florida. *Quaternary Science Reviews*, **30,** 570-590.
Mulitza, S., et al., 2008: Sahel megadroughts triggered by glacial slowdowns of Atlantic meridional overturning. *Paleoceanography*, **23,** PA4206.
Murton, J. B., M. D. Bateman, S. R. Dallimore, J. T. Teller, and Z. R. Yang, 2010: Identification of Younger Dryas outburst flood path from Lake Agassiz to the Arctic Ocean. *Nature*, **464,** 740-743.

Muscheler, R., F. Joos, J. Beer, S. A. Müller, M. Vonmoos, and I. Snowball, 2007: Solar activity during the last 1000 yr inferred from radionuclide records. *Quaternary Science Reviews*, **26,** 82-97.
Naish, T., G. Wilson, G. Dunbar, and P. Barrett, 2008: Constraining the amplitude of Late Oligocene bathymetric changes in western Ross Sea during orbitally-induced oscillations in the East Antarctic Ice Sheet: (2) Implications for global sea level changes. *Palaeogeography Palaeoclimatology Palaeoecology*, DOI 10.1016/j.palaeo.2007.08.021**,** 66-76.
Naish, T., et al., 2009a: Obliquity-paced Pliocene West Antarctic ice sheet oscillations. *Nature*, **458,** 322-U384.
Naish, T., et al., 2009b: Obliquity-paced Pliocene West Antarctic ice sheet oscillations. *Nature*, **458,** 322-U384.
Naish, T. R., and G. S. Wilson, 2009: Constraints on the amplitude of Mid-Pliocene (3.6–2.4 Ma) eustatic sea level fluctuations from the New Zealand shallow-marine sediment record. *Philosophical Transactions of the Royal Society A: Mathematical, Physical and Engineering Sciences*, **367,** 169-187.
Naish, T. R., L. Carter, E. Wolff, D. Pollard, and R. D. Powell, 2009c: Late Pliocene–Pleistocene Antarctic Climate Variability at Orbital and Suborbital Scale: Ice Sheet, Ocean and Atmospheric Interactions. *Developments in Earth & Environmental Sciences*, F. Florindo, and S. M., Eds., Elsevier, 465-529.
Nakada, M., R. Kimura, J. Okuno, K. Moriwaki, H. Miura, and H. Maemoku, 2000: Late Pleistocene and Holocene melting history of the Antarctic ice sheet derived from sea level variations. *Marine Geology*, **167,** 85-103.
Nakamura, N., H. Kayanne, H. Iijima, T. R. McClanahan, S. K. Behera, and T. Yamagata, 2009: Mode shift in the Indian Ocean climate under global warming stress. *Geophysical Research Letters*, **36,** L23708.
Neppel, L., et al., 2010: Flood frequency analysis using historical data: accounting for random and systematic errors. *Hydrological Sciences Journal*, **55,** 192-208.
Nesje, A., 2009: Latest Pleistocene and Holocene alpine glacier fluctuations in Scandinavia. *Quaternary Science Reviews*, **28,** 2119-2136.
Neukom, R., et al., 2011: Multiproxy summer and winter surface air temperature field reconstructions for southern South America covering the past centuries. *Climate Dynamics*, **37,** 35-51.
Nicolussi, K., M. Kaufmann, T. M. Melvin, J. van der Plicht, P. Schießling, and A. Thurner, 2009: A 9111 year long conifer tree-ring chronology for the European Alps: a base for environmental and climatic investigations. *The Holocene*, **19,** 909-920.
Nørgaard-Pedersen, N., N. Mikkelsen, S. J. Lassen, Y. Kristoffersen, and E. Sheldon, 2007: Reduced sea ice concentrations in the Arctic Ocean during the last interglacial period revealed by sediment cores off northern Greenland. *Paleoceanography*, **22,** PA1218.
North Greenland Ice Core Project members, 2004: High-resolution record of Northern Hemisphere climate extending into the last interglacial period. *Nature*, **431,** 147-151.
O'Leary, M. J., P. J. Hearty, and M. T. McCulloch, 2008: Geomorphic evidence of major sea level fluctuations during marine isotope substage-5e, Cape Cuvier, Western Australia. *Geomorphology*, **102,** 595-602.
O'Donnell, R., N. Lewis, S. McIntyre, and J. Condon, 2010: Improved Methods for PCA-Based Reconstructions: Case Study Using the Steig et al. (2009) Antarctic Temperature Reconstruction. *Journal of Climate*, **24,** 2099-2115.
Obata, A., 2007: Climate–Carbon Cycle Model Response to Freshwater Discharge into the North Atlantic. *Journal of Climate*, **20,** 5962-5976.
Oerlemans, J., 1980: Model experiments on the 100,000-yr glacial cycle. *Nature*, **287,** 430-432.
Okazaki, Y., et al., 2010: Deepwater Formation in the North Pacific During the Last Glacial Termination. *Science*, **329,** 200-204.
Okumura, Y. M., C. Deser, A. Hu, A. Timmermann, and S. P. Xie, 2009: North Pacific Climate Response to Freshwater Forcing in the Subarctic North Atlantic: Oceanic and Atmospheric Pathways. *Journal of Climate*, **22,** 1424-1445.
Ono, A., K. Takahashi, K. Katsuki, Y. Okazaki, and T. Sakamoto, 2005: The Dansgaard-Oeschger cycles discovered in the up stream source region of the North Pacific Intermediate Water formation. *Geophysical Research Letters*, **32,** L11607.
Oppo, D. W., Y. Rosenthal, and B. K. Linsley, 2009: 2,000-year-long temperature and hydrology reconstructions from the Indo-Pacific warm pool. *Nature*, **460,** 1113-1116.
Otterå, O. H., M. Bentsen, H. Drange, and L. L. Suo, 2010: External forcing as a metronome for Atlantic multidecadal variability. *Nature Geoscience*, **3,** 688-694.
Otto-Bliesner, B., et al., 2009: A comparison of PMIP2 model simulations and the MARGO proxy reconstruction for tropical sea surface temperatures at last glacial maximum. *Climate Dynamics*, **32,** 799-815.
Otto-Bliesner, B. L., and E. C. Brady, 2010: The sensitivity of the climate response to the magnitude and location of freshwater forcing: last glacial maximum experiments. *Quaternary Science Reviews*, **29,** 56-73.
Otto, J., T. Raddatz, and M. Claussen, 2009a: Climate variability-induced uncertainty in mid-Holocene atmosphere-ocean-vegetation feedbacks. *Geophysical Research Letters*, **36,** L23710.
Otto, J., T. Raddatz, M. Claussen, V. Brovkin, and V. Gayler, 2009b: Separation of atmosphere-ocean-vegetation feedbacks and synergies for mid-Holocene climate. *Geophysical Research Letters*, **36,** L09701.
Pagani, M., 2002: The alkenone-CO_2 proxy and ancient atmospheric carbon dioxide. *Philosophical Transactions of the Royal Society of London. Series A: 			Mathematical, Physical and Engineering Sciences*, **360,** 609-632.
Pagani, M., 2005: Controls on paleo-alkenone $\delta^{13}C$. *Geochimica Et Cosmochimica Acta***,** A545-A545.

Pagani, M., Z. Liu, J. LaRiviere, and A. Ravelo, 2010: High Earth-system climate sensitivity determined from Pliocene carbon dioxide concentrations. *Nature Geoscience*, **3,** 27-30.
Pagani, M., J. Zachos, K. Freeman, B. Tipple, and S. Bohaty, 2005: Marked decline in atmospheric carbon dioxide concentrations during the Paleogene. *Science*, **309,** 600-603.
Pagani, M., M. Huber, Z. Liu, S. M. Bohaty, J. Henderiks, W. K. Sijp, Srinath, and R. M. DeConto, in press: The Role of Carbon Dioxide during the Onset of Antarctic Glaciation. *Science*.
Pahnke, K., R. Zahn, H. Elderfield, and M. Schulz, 2003: 340,000-year centennial-scale marine record of Southern Hemisphere climatic oscillation. *Science*, **301,** 948-952.
Panchuk, K., A. Ridgwell, and L. R. Kump, 2008: Sedimentary response to Paleocene-Eocene Thermal Maximum carbon release: A model-data comparison. *Geology*, **36,** 315-318.
Paquay, F. S., et al., 2009: Absence of geochemical evidence for an impact event at the Bolling-Allerod/Younger Dryas transition. *Proceedings of the National Academy of Sciences of the United States of America*, **106,** 21505-21510.
Patadia, F., E.-S. Yang, and S. A. Christopher, 2009: Does dust change the clear sky top of atmosphere shortwave flux over high surface reflectance regions? *Geophys. Res. Lett.*, **36,** L15825.
Pausata, F. S. R., D. S. Battisti, K. H. Nisancioglu, and C. M. Bitz, 2011: Chinese stalagmite $d^{18}O$ controlled by changes in the Indian monsoon during a simulated Heinrich event. *Nature Geoscience*, **4,** 474-480.
Pausata, F. S. R., C. Li, J. J. Wettstein, K. H. Nisancioglu, and D. S. Battisti, 2009: Changes in atmospheric variability in a glacial climate and the impacts on proxy data: a model intercomparison. *Climate of the Past*, **5,** 489-502.
Pearson, P., and M. Palmer, 2000: Atmospheric carbon dioxide concentrations over the past 60 million years. *Nature*, **406,** 695-699.
Pearson, P. N., G. L. Foster, and B. S. Wade, 2009: Atmospheric carbon dioxide through the Eocene-Oligocene climate transition. *Nature*, **461,** 1110-U1204.
Pechony, O., and D. T. Shindell, 2010: Driving forces of global wildfires over the past millennium and the forthcoming century. *Proceedings of the National Academy of Sciences*, 10.1073/pnas.1003669107.
Peltier, W., and R. Fairbanks, 2006: Global glacial ice volume and Last Glacial Maximum duration from an extended Barbados sea level record. *Quaternary Science Reviews*, **25,** 3322-3337.
Peltier, W. R., 2002: On eustatic sea level history: Last Glacial Maximum to Holocene. *Quaternary Science Reviews*, **21,** 377-396.
Peltier, W. R., 2004: Global Glacial Isostasy and the Surface of the Ice-Age Earth: The ICE-5G (VM2) Model and GRACE. *Annual Review of Earth and Planetary Sciences*, **32,** 111-149.
Peng, Y., Y. Xu, and L. Jin, 2009: Climate changes over eastern China during the last millennium in simulations and reconstructions. *Quaternary International*, **208,** 11-18.
Peterson, L. C., and G. H. Haug, 2006: Variability in the mean latitude of the Atlantic Intertropical Convergence Zone as recorded by riverine input of sediments to the Cariaco Basin (Venezuela). *Palaeogeography Palaeoclimatology Palaeoecology*, **234,** 97-113.
Peterson, L. C., G. H. Haug, K. A. Hughen, and U. Rohl, 2000: Rapid changes in the hydrologic cycle of the tropical Atlantic during the last glacial. *Science*, **290,** 1947-1951.
Petit, J. R., and B. Delmonte, 2009: A model for large glacial–interglacial climate-induced changes in dust and sea salt concentrations in deep ice cores (central Antarctica): palaeoclimatic implications and prospects for refining ice core chronologies. *Tellus*, **61B,** 768-790.
Petit, J. R., et al., 1999: Climate and atmospheric history of the past 420,000 years from the Vostok ice core, Antarctica. *Nature*, **399,** 429-436.
Petrenko, V. V., et al., 2009: $^{14}CH_4$ Measurements in Greenland Ice: Investigating Last Glacial Termination CH_4 Sources. *Science*, **324,** 506-508.
Pfeiffer, M., and W. C. Dullo, 2006: Monsoon-induced cooling of the western equatorial Indian Ocean as recorded in coral oxygen isotope records from the Seychelles covering the period of 1840-1994 AD. *Quaternary Science Reviews*, **25,** 993-1009.
Pinter, N., A. C. Scott, T. L. Daulton, A. Podoll, C. Koeberl, R. S. Anderson, and S. E. Ishman, 2011: The Younger Dryas impact hypothesis: A requiem. *Earth-Science Reviews*, **106,** 247-264.
Piotrowski, A. M., S. L. Goldstein, S. R. Hemming, R. G. Fairbanks, and D. R. Zylberberg, 2008: Oscillating glacial northern and southern deep water formation from combined neodymium and carbon isotopes. *Earth and Planetary Science Letters*, **272,** 394-405.
Pollack, H. N., and J. E. Smerdon, 2004: Borehole climate reconstructions: Spatial structure and hemispheric averages. *Journal of Geophysical Research*, **109,** D11106.
Pollard, D., 1982: A simple ice sheet model yields realistic 100 kyr glacial cycles. *Nature*, **296,** 334-338.
Pollard, D., and R. M. DeConto, 2009: Modelling West Antarctic ice sheet growth and collapse through the past five million years. *Nature*, **458,** 329-332.
Polyak, L., et al., 2010: History of sea ice in the Arctic. *Quaternary Science Reviews*, **29,** 1757-1778.
Polyakov, I., et al., 2002: Observationally based assessment of polar amplification of global warming. *Geophysical Research Letters*, **29,** 1878.
Polyakov, I. V., et al., 2010: Arctic Ocean Warming Contributes to Reduced Polar Ice Cap. *Journal of Physical Oceanography*, **40,** 2743-2756.

Pope, J., et al., 2011: Quantifying Uncertainty in Model Predictions for the Pliocene (Plio-QUMP): Initial results. *Palaeogeography Palaeoclimatology Palaeoecology*, **309,** 128-140.
Porter, T. J., and M. F. J. Pisaric, 2011: Temperature-growth divergence in white spruce forests of Old Crow Flats, Yukon Territory, and adjacent regions of northwestern North America. *Global Change Biology*, **17,** 3418-3430.
Power, M., J. Marlon, P. Bartlein, and S. Harrison, 2010: Fire history and the Global Charcoal Database: A new tool for hypothesis testing and data exploration. *Palaeogeography Palaeoclimatology Palaeoecology*, **291,** 52-59.
Power, M., et al., 2008: Changes in fire regimes since the Last Glacial Maximum: an assessment based on a global synthesis and analysis of charcoal data. *Climate Dynamics*, **30,** 887-907.
Prieto, M. d. R., and R. García Herrera, 2009: Documentary sources from South America: Potential for climate reconstruction. *Palaeogeography, Palaeoclimatology, Palaeoecology*, **281,** 196-209.
Prokopenko, A., L. Hinnov, D. Williams, and M. Kuzmin, 2006: Orbital forcing of continental climate during the Pleistocene: a complete astronomically tuned climatic record from Lake Baikal, SE Siberia. *Quaternary Science Reviews*, **25,** 3431-3457.
Radic, V., and R. Hock, 2011: Regionally differentiated contribution of mountain glaciers and ice caps to future sea level rise. *Nature Geoscience*, **4,** 91-94.
Rahmstorf, S., et al., 2005: Thermohaline circulation hysteresis: A model intercomparison. *Geophysical Research Letters*, **32,** L23605.
Raymo, M., L. Lisiecki, and K. Nisancioglu, 2006: Plio-pleistocene ice volume, Antarctic climate, and the global $\delta^{18}O$ record. *Science*, **313,** 492-495.
Raymo, M. E., J. X. Mitrovica, M. J. O'Leary, R. M. DeConto, and P. J. Hearty, 2011: Departures from eustasy in Pliocene sea level records. *Nature Geoscience*, **4,** 328-332.
Raynaud, D., and C. Lorius, 2004: Atmospheric properties of past climatic changes are recorded in the polar ice. *Comptes Rendus Geoscience*, DOI 10.1016/j.crte.2004.01.005**,** 647-656.
Rayner, N. A., et al., 2003: Global analyses of sea surface temperature, sea ice, and night marine air temperature since the late nineteenth century. *Journal of Geophysical Research-Atmospheres*, **108,** 4407.
Retallack, G. J., 2009: Refining a pedogenic-carbonate CO2 paleobarometer to quantify a middle Miocene greenhouse spike. *Palaeogeography, Palaeoclimatology, Palaeoecology*, **281,** 57-65.
Ridley, J., J. Gregory, P. Huybrechts, and J. Lowe, 2010: Thresholds for irreversible decline of the Greenland ice sheet. *Climate Dynamics*, **35,** 1049-1057.
Riedwyl, N., M. Küttel, J. Luterbacher, and H. Wanner, 2009: Comparison of climate field reconstruction techniques: application to Europe. *Climate Dynamics*, **32,** 381-395.
Risebrobakken, B., E. Jansen, C. Andersson, E. Mjelde, and K. Hevrøy, 2003: A high-resolution study of Holocene paleoclimatic and paleoceanographic changes in the Nordic Seas. *Paleoceanography*, **18,** 1017.
Risebrobakken, B., T. Dokken, L. H. Smedsrud, C. Andersson, E. Jansen, M. Moros, and E. V. Ivanova, 2011: Early Holocene temperature variability in the Nordic Seas: The role of oceanic heat advection versus changes in orbital forcing. *Paleoceanography*, **26,** PA4206.
Ritz, C., V. Rommelaere, and C. Dumas, 2001: Modeling the evolution of Antarctic ice sheet over the last 420,000 years: Implications for altitude changes in the Vostok region. *Journal of Geophysical Research*, **106,** 31943-31964.
Ritz, S., T. Stocker, and F. Joos, 2011: A Coupled Dynamical Ocean-Energy Balance Atmosphere Model for Paleoclimate Studies. *Journal of Climate*, **24,** 349-375.
Roberts, C. D., A. N. LeGrande, and A. K. Tripati, 2009: Climate sensitivity to Arctic seaway restriction during the early Paleogene. *Earth and Planetary Science Letters*, **286,** 576-585.
Robinson, A., R. Calov, and A. Ganopolski, 2011: Greenland ice sheet model parameters constrained using simulations of the Eemian Interglacial. *Climate of the Past*, **7,** 381-396.
Rodrigo, F. S., D. Pozo-Vázquez, M. J. Esteban-Parra, and Y. Castro-Díez, 2001: A reconstruction of the winter North Atlantic Oscillation index back to AD 1501 using, documentary data in southern Spain. *Journal of Geophysical Research-Atmospheres*, **106,** 14805-14818.
Roe, G. H., and R. S. Lindzen, 2001: The mutual interaction between continental-scale ice sheets and atmospheric stationary waves. *Journal of Climate*, **14,** 1450-1465.
Rohling, E., M. Medina-Elizalde, J. G. Shepherd, M. Siddall, and J. D. Stanford, accepted: Sea surface and high-latitude temperature sensitivity to radiative forcing of climate over several glacial cycles. *Journal of Climate*.
Rohling, E. J., K. Grant, C. Hemleben, M. Siddall, B. A. A. Hoogakker, M. Bolshaw, and M. Kucera, 2008a: High rates of sea level rise during the last interglacial period. *Nature Geoscience*, **1,** 38-42.
Rohling, E. J., K. Grant, M. Bolshaw, A. P. Roberts, M. Siddall, C. Hemleben, and M. Kucera, 2009: Antarctic temperature and global sea level closely coupled over the past five glacial cycles. *Nature Geoscience*, **2,** 500-504.
Rohling, E. J., et al., 2008b: New constraints on the timing of sea level fluctuations during early to middle marine isotope stage 3. *Paleoceanography*, **23,** PA3219.
Royer, D. L., S. L. Wing, D. J. Beerling, D. W. Jolley, P. L. Koch, L. J. Hickey, and R. A. Berner, 2001: Paleobotanical Evidence for Near Present-Day Levels of Atmospheric CO2 During Part of the Tertiary. *Science*, **292,** 2310-2313.

Rupper, S., G. Roe, and A. Gillespie, 2009: Spatial patterns of Holocene glacier advance and retreat in Central Asia. *Quaternary Research*, **72,** 337-346.
Saenger, C., A. Cohen, D. Oppo, R. Halley, and J. Carilli, 2009: Surface-temperature trends and variability in the low-latitude North Atlantic since 1552. *Nature Geoscience*, **2,** 492-495.
Saenko, O. A., A. Schmittner, and A. J. Weaver, 2004: The Atlantic-Pacific seesaw. *Journal of Climate*, **17,** 2033-2038.
Saji, N. H., B. N. Goswami, P. N. Vinayachandran, and T. Yamagata, 1999: A dipole mode in the tropical Indian Ocean. *Nature*, **401,** 360-363.
Saltzman, B., and M. Y. Verbitsky, 1993: Multiple instabilities and modes of glacial rhythmicity in the plio-Pleistocene: a general theory of late Cenozoic climatic change. *Climate Dynamics*, **9,** 1-15.
Salzer, M., and K. Kipfmueller, 2005: Reconstructed temperature and precipitation on a millennial timescale from tree-rings in the Southern Colorado Plateau, USA. *Climatic Change*, **70,** 465-487.
Salzmann, U., A. M. Haywood, D. J. Lunt, P. J. Valdes, and D. J. Hill, 2008: A new global biome reconstruction and data-model comparison for the Middle Pliocene. *Global Ecology and Biogeography*, **17,** 432-447.
Sarnthein, M., U. Pflaumann, and M. Weinelt, 2003a: Past extent of sea ice in the northern North Atlantic inferred from foraminiferal paleotemperature estimates. *Paleoceanography*, **18,** 1047.
Sarnthein, M., S. Van Kreveld, H. Erlenkeuser, P. Grootes, M. Kucera, U. Pflaumann, and M. Schulz, 2003b: Centennial-to-millennial-scale periodicities of Holocene climate and sediment injections off the western Barents shelf, 75 degrees N. *Boreas*, **32,** 447-461.
Scapozza, C., C. Lambiel, E. Reynard, J.-M. Fallot, M. Antognini, and P. Schoeneich, 2010: Radiocarbon dating of fossil wood remains buried by the Piancabella rock glacier, Blenio Valley (Ticino, southern Swiss Alps): Implications for rock glacier, treeline and climate history. *Permafrost and Periglacial Processes*, **21,** 90-96.
Schaefer, J. M., et al., 2009: High-Frequency Holocene Glacier Fluctuations in New Zealand Differ from the Northern Signature. *Science*, **324,** 622-625.
Schilt, A., M. Baumgartner, T. Blunier, J. Schwander, R. Spahni, H. Fischer, and T. F. Stocker, 2010: Glacial–interglacial and millennial-scale variations in the atmospheric nitrous oxide concentration during the last 800,000 years. *Quaternary Science Reviews*, **29,** 182-192.
Schmidt, G., et al., 2006: Present-day atmospheric simulations using GISS ModelE: Comparison to in situ, satellite, and reanalysis data. *Journal of Climate*, **19,** 153-192.
Schmidt, G. A., et al., 2011: Climate forcing reconstructions for use in PMIP simulations of the last millennium (v1.0). *Geoscientific Model Development*, **4,** 33-45.
Schmittner, A., and E. D. Galbraith, 2008: Glacial greenhouse-gas fluctuations controlled by ocean circulation changes. *Nature*, **456,** 373-376.
Schmittner, A., E. D. Galbraith, S. W. Hostetler, T. F. Pedersen, and R. Zhang, 2007: Large fluctuations of dissolved oxygen in the Indian and Pacific oceans during Dansgaard-Oeschger oscillations caused by variations of North Atlantic Deep Water subduction. *Paleoceanography*, **22,** PA3207.
Schmittner, A., et al., submitted: Climate Sensitivity Estimated From Temperature Reconstructions of the Last Glacial Maximum. *Science*.
Schmutz, C., J. Luterbacher, D. Gyalistras, E. Xoplaki, and H. Wanner, 2000: Can we trust proxy-based NAO index reconstructions? *Geophysical Research Letters*, **27,** 1135-1138.
Schneider, D., E. Steig, T. Van Ommen, D. Dixon, P. Mayewski, J. Jones, and C. Bitz, 2006: Antarctic temperatures over the past two centuries from ice cores. *Geophysical Research Letters*, **33,** L16707.
Schneider von Deimling, T., A. Ganopolski, H. Held, and S. Rahmstorf, 2006: How cold was the Last Glacial Maximum? *Geophysical Research Letters*, **33,** L14709.
Schrijver, C. J., W. C. Livingston, T. N. Woods, and R. A. Mewaldt, 2011: The minimal solar activity in 2008-2009 and its implications for long-term climate modeling. *Geophysical Research Letters*, **38,** L06701.
Schulz, H., U. von Rad, and H. Erlenkeuser, 1998: Correlation between Arabian Sea and Greenland climate oscillations of the past 110,000 years. *Nature*, **393,** 54-57.
Schurgers, G., U. Mikolajewicz, M. Gröger, E. Maier-Reimer, M. Vizcaino, and A. Winguth, 2007: The effect of land surface changes on Eemian climate. *Climate Dynamics*, **29,** 357-373.
Screen, J. A., and I. Simmonds, 2010: The central role of diminishing sea ice in recent Arctic temperature amplification. *Nature*, **464,** 1334-1337.
Seager, R., A. Tzanova, and J. Nakamura, 2009: Drought in the Southeastern United States: Causes, Variability over the Last Millennium, and the Potential for Future Hydroclimate Change. *Journal of Climate*, **22,** 5021-5045.
Seager, R., N. Graham, C. Herweijer, A. Gordon, Y. Kushnir, and E. Cook, 2007: Blueprints for Medieval hydroclimate. *Quaternary Science Reviews*, **26,** 2322-2336.
Seager, R., R. Burgman, Y. Kushnir, A. Clement, E. Cook, N. Naik, and J. Miller, 2008: Tropical Pacific Forcing of North American Medieval Megadroughts: Testing the Concept with an Atmosphere Model Forced by Coral-Reconstructed SSTs. *Journal of Climate*, **21,** 6175-6190.
Seki, O., G. Foster, D. Schmidt, A. Mackensen, K. Kawamura, and R. Pancost, 2010: Alkenone and boron-based Pliocene pCO_2 records. *Earth and Planetary Science Letters*, **292,** 201-211.
Semenov, V. A., M. Latif, D. Dommenget, N. S. Keenlyside, A. Strehz, T. Martin, and W. Park, 2010: The Impact of North Atlantic-Arctic Multidecadal Variability on Northern Hemisphere Surface Air Temperature. *Journal of Climate*, **23,** 5668-5677.

Seong, Y., L. Owen, C. Yi, and R. Finkel, 2009: Quaternary glaciation of Muztag Ata and Kongur Shan: Evidence for glacier response to rapid climate changes throughout the Late Glacial and Holocene in westernmost Tibet. *Geological Society of America Bulletin*, **129,** 348-365.
Serreze, M., and J. Francis, 2006: The Arctic Amplification Debate. *Climatic Change*, **76,** 241-264.
Serreze, M. C., A. P. Barrett, J. C. Stroeve, D. N. Kindig, and M. M. Holland, 2009: The emergence of surface-based Arctic amplification. *The Cryosphere*, **3,** 11-19.
Servonnat, J., P. Yiou, M. Khodri, D. Swingedouw, and S. Denvil, 2010: Influence of solar variability, CO_2 and orbital forcing between 1000 and 1850 AD in the IPSLCM4 model. *Climate of the Past*, **6,** 445-460.
Severinghaus, J. P., R. Beaudette, M. A. Headly, K. Taylor, and E. J. Brook, 2009: Oxygen-18 of O_2 Records the Impact of Abrupt Climate Change on the Terrestrial Biosphere. *Science*, **324,** 1431-1434.
Shaffer, G., S. M. Olsen, and C. J. Bjerrum, 2004: Ocean subsurface warming as a mechanism for coupling Dansgaard-Oeschger climate cycles and ice-rafting events. *Geophysical Research Letters*, **31,** L24202.
Shanahan, T. M., et al., 2009: Atlantic Forcing of Persistent Drought in West Africa. *Science*, **324,** 377-380.
Sheffer, N. A., M. Rico, Y. Enzel, G. Benito, and T. Grodek, 2008: The Palaeoflood record of the Gardon River, France: A comparison with the extreme 2002 flood event. *Geomorphology*, **98,** 71-83.
Shevenell, A. E., A. E. Ingalls, E. W. Domack, and C. Kelly, 2011: Holocene Southern Ocean surface temperature variability west of the Antarctic Peninsula. *Nature*, **470,** 250-254.
Shindell, D. T., G. A. Schmidt, M. E. Mann, D. Rind, and A. Waple, 2001: Solar Forcing of Regional Climate Change During the Maunder Minimum. *Science*, **294,** 2149-2152.
Sicre, M. A., et al., 2008: A 4500-year reconstruction of sea surface temperature variability at decadal time-scales off North Iceland. *Quaternary Science Reviews*, **27,** 2041-2047.
Siddall, M., E. Bard, E. J. Rohling, and C. Hemleben, 2006: Sea level reversal during termination II. *Geology*, **34,** 817-820.
Siddall, M., E. J. Rohling, W. G. Thompson, and C. Waelbroeck, 2008: Marine isotope stage 3 sea level fluctuations: Data synthesis and new outlook. *Reviews of Geophysics*, **46,** RG4003.
Siddall, M., M. R. Kaplan, J. M. Schaefer, A. Putnam, M. A. Kelly, and B. Goehring, 2010: Changing influence of Antarctic and Greenlandic temperature records on sea level over the last glacial cycle. *Quaternary Science Reviews*, **29,** 410-423.
Siddall, M., E. J. Rohling, A. Almogi-Labin, C. Hemleben, D. Meischner, I. Schmelzer, and D. A. Smeed, 2003: Sea level fluctuations during the last glacial cycle. *Nature*, **423,** 853-858.
Siegenthaler, U. R. S., et al., 2005: Supporting evidence from the EPICA Dronning Maud Land ice core for atmospheric CO_2 changes during the past millennium. *Tellus B*, **57,** 51-57.
Sime, L. C., E. W. Wolff, K. I. C. Oliver, and J. C. Tindall, 2009: Evidence for warmer interglacials in East Antarctic ice cores. *Nature*, **462,** 342-U105.
Singarayer, J. S., and P. J. Valdes, 2010: High-latitude climate sensitivity to ice sheet forcing over the last 120 kyr. *Quaternary Science Reviews*, **29,** 43-55.
Sivan, D., K. Lambeck, R. Toueg, A. Raban, Y. Porath, and B. Shirman, 2004: Ancient coastal wells of Caesarea Maritima, Israel, an indicator for relative sea level changes during the last 2000 years. *Earth and Planetary Science Letters*, **222,** 315-330.
Skinner, L. C., and N. J. Shackleton, 2006: Deconstructing Terminations I and II: revisiting the glacioeustatic paradigm based on deep-water temperature estimates. *Quat. Sci. Rev.*, **25,** 3312-3321.
Slonosky, V., P. Jones, and T. Davies, 2001: Atmospheric circulation and surface temperature in Europe from the 18th century to 1995. *International Journal of Climatology*, **21,** 63-75.
Smerdon, J. E., and A. Kaplan, 2007: Comments on "Testing the Fidelity of Methods Used in Proxy-Based Reconstructions of Past Climate": The role of the standardization interval. *Journal of Climate*, **20,** 5666-5670.
Smerdon, J. E., A. Kaplan, D. Chang, and M. N. Evans, 2010: A Pseudoproxy Evaluation of the CCA and RegEM Methods for Reconstructing Climate Fields of the Last Millennium. *Journal of Climate*, **23,** 4856–4880.
Smerdon, J. E., A. Kaplan, E. Zorita, J. F. Gonzalez-Rouco, and M. N. Evans, 2011: Spatial performance of four climate field reconstruction methods targeting the Common Era. *Geophysical Research Letters*, **38,** L11705.
Smithers, S. G., and C. D. Woodroffe, 2001: Coral microatolls and 20th century sea level in the eastern Indian Ocean. *Earth and Planetary Science Letters*, **191,** 173-184.
Soden, B. J., I. M. Held, R. Colman, K. M. Shell, J. T. Kiehl, and C. A. Shields, 2008: Quantifying Climate Feedbacks Using Radiative Kernels. *Journal of Climate*, **21,** 3504-3520.
Solomina, O., W. Haeberli, C. Kull, and G. Wiles, 2008: Historical and Holocene glacier–climate variations: General concepts and overview. *Global and Planetary Change*, **60,** 1-9.
Sowers, T., 2006: Late Quaternary atmospheric CH_4 isotope record suggests marine clathrates are stable. *Science*, **311,** 838-840.
Sowers, T., 2010: Atmospheric methane isotope records covering the Holocene period. *Quaternary Science Reviews*, **29,** 213-221.
Spence, J. P., M. Eby, and A. J. Weaver, 2008: The Sensitivity of the Atlantic Meridional Overturning Circulation to Freshwater Forcing at Eddy-Permitting Resolutions. *Journal of Climate*, **21,** 2697-2710.
Spielhagen, R. F., et al., 2011: Enhanced Modern Heat Transfer to the Arctic by Warm Atlantic Water. *Science*, **331,** 450-453.

Stager, J. C., D. B. Ryves, B. M. Chase, and F. S. R. Pausata, 2011: Catastrophic Drought in the Afro-Asian Monsoon Region During Heinrich Event 1. *Science*.

Steffensen, J. P., et al., 2008: High-resolution Greenland Ice Core data show abrupt climate change happens in few years. *Science*, **321,** 680-684.

Steig, E. J., D. P. Schneider, S. D. Rutherford, M. E. Mann, J. C. Comiso, and D. T. Shindell, 2009: Warming of the Antarctic ice sheet surface since the 1957 International Geophysical Year. *Nature*, **457,** 459-U454.

Steinhilber, F., J. Beer, and C. Fröhlich, 2009: Total solar irradiance during the Holocene. *Geophysical Research Letters*, **36,** L19704.

Stenni, B., et al., 2010: The deuterium excess records of EPICA Dome C and Dronning Maud Land ice cores (East Antarctica). *Quaternary Science Reviews*, **29,** 146-159.

Stenni, B., et al., 2011: Expression of the bipolar see-saw in Antarctic climate records during the last deglaciation. *Nature Geoscience*, **4,** 46-49.

Stewart, M. M., M. Grosjean, F. G. Kuglitsch, S. U. Nussbaumer, and L. von Gunten, in press: Reconstructions of the late Holocene paleofloods and glacier length changes in the Upper Engadine, Switzerland (ca. 1450 BC–AD 420). *Palaeogeography, Palaeoclimatology, Palaeoecology*, 10.1016/j.palaeo.2011.08.022.

Stirling, C., T. Esat, K. Lambeck, and M. McCulloch, 1998a: Timing and duration of the Last Interglacial: evidence for a restricted interval of widespread coral reef growth. *Earth and Planetary Science Letters*, **160,** 745-762.

Stirling, C. H., T. M. Esat, K. Lambeck, and M. T. McCulloch, 1998b: Timing and duration of the Last Interglacial: evidence for a restricted interval of widespread coral reef growth. *Earth and Planetary Science Letters*, **160,** 745-762.

Stone, E. J., D. J. Lunt, J. D. Annan, and J. C. Hargreaves, submitted: Quantification of Greenland ice sheet contribution to Last Interglacial sea level rise. *Nature Geoscience*.

Stone, J. O., G. A. Balco, D. E. Sugden, M. W. Caffee, L. C. Sass, S. G. Cowdery, and C. Siddoway, 2003: Holocene Deglaciation of Marie Byrd Land, West Antarctica. *Science*, **299,** 99-102.

Støren, E. N., E. W. Kolstad, and Ø. Paasche, in press: Linking past flood frequencies in Norway to regional atmospheric circulation anomalies. *Journal of Quaternary Science*, 10.1002/jqs.1520**,** n/a-n/a.

Støren, E. N., S. O. Dahl, A. Nesje, and O. Paasche, 2010: Identifying the sedimentary imprint of high-frequency Holocene river floods in lake sediments: development and application of a new method. *Quaternary Science Reviews*, **29,** 3021-3033.

Stott, L., A. Timmermann, and R. Thunell, 2007: Southern hemisphere and deep-sea warming led deglacial atmospheric CO_2 rise and tropical warming. *Science*, **318,** 435-438.

Stott, L., C. Poulsen, S. Lund, and R. Thunell, 2002: Super ENSO and Global Climate Oscillations at Millennial Time Scales. *Science*, **297,** 222-226.

Stouffer, R., et al., 2006: Investigating the causes of the response of the thermohaline circulation to past and future climate changes. *Journal of Climate*, **19,** 1365-1387.

Stuiver, M., and T. F. Braziunas, 1993: Sun, ocean, climate and atmospheric $^{14}CO_2$: an evaluation of causal and spectral relationships. *The Holocene*, **3,** 289-305.

Sturm, C., Q. Zhang, and D. Noone, 2010: An introduction to stable water isotopes in climate models: benefits of forward proxy modelling for paleoclimatology. *Climate of the Past*, **6,** 115-129.

Suwa, M., J. von Fischer, M. Bender, A. Landais, and E. Brook, 2006: Chronology reconstruction for the disturbed bottom section of the GISP2 and the GRIP ice cores: Implications for Termination II in Greenland. *Journal of Geophysical Research-Atmospheres*, ARTN D02101, DOI 10.1029/2005JD006032, -.

Swingedouw, D., J. Mignot, P. Braconnot, E. Mosquet, M. Kageyama, and R. Alkama, 2009: Impact of Freshwater Release in the North Atlantic under Different Climate Conditions in an OAGCM. J*ournal of Climate,* 2**2,** 6377-6403.

Swingedouw, D., L. Terray, C. Cassou, A. Voldoire, D. Salas-Mélia, and J. Servonnat, 2011: Natural forcing of climate during the last millennium: fingerprint of solar variability. C*limate Dynamics,* 3**6,** 1-16.

Switzer, A. D., C. R. Sloss, B. G. Jones, and C. S. Bristow, 2010: Geomorphic evidence for mid–late Holocene higher sea level from southeastern Australia. Q*uaternary International,* 2**21,** 13-22.

Tagliabue, A., et al., 2009: Quantifying the roles of ocean circulation and biogeochemistry in governing ocean carbon-13 and atmospheric carbon dioxide at the last glacial maximum. C*limate of the Past,* 5**,** 695-706.

Takemura, T., M. Egashira, K. Matsuzawa, H. Ichijo, R. O'ishi, and A. Abe-Ouchi, 2009: A simulation of the global distribution and radiative forcing of soil dust aerosols at the Last Glacial Maximum. A*tmospheric Chemistry and Physics,* 9**,** 3061-3073.

Tarasov, L., and W. R. Peltier, 2007: Coevolution of continental ice cover and permafrost extent over the last glacial-interglacial cycle in North America. J*ournal of Geophysical Research,* 1**12,** F02S08.

Tett, S., et al., 2006: The impact of natural and anthropogenic forcings on climate and hydrology since 1550. C*limate Dynamics,* 2**8,** 3-34.

Thomas, E., and J. Briner, 2009: Climate of the past millennium inferred from varved proglacial lake sediments on northeast Baffin Island, Arctic Canada. J*ournal of Paleolimnology,* 4**1,** 209-224.

Thomas, E. R., E. W. Wolff, R. Mulvaney, S. J. Johnsen, J. P. Steffensen, and C. Arrowsmith, 2009: Anatomy of a Dansgaard-Oeschger warming transition: High-resolution analysis of the North Greenland Ice Core Project ice core. J*ournal of Geophysical Research-Atmospheres,* 1**14,** D08102.

Thomas, E. R., et al., 2007: The 8.2ka event from Greenland ice cores. Q*uaternary Science Reviews,* 2**6,** 70-81.
Thompson, L. G., et al., 2006: Abrupt tropical climate change: Past and present. P*roceedings of the National Academy of Sciences of the United States of America,* 1**03,** 10536-10543.
Thompson, W., and S. Goldstein, 2005: Open-system coral ages reveal persistent suborbital sea level cycles. S*cience,* DOI 10.1126/science.1104035, 401-404.
Thornalley, D. J. R., S. Barker, W. S. Broecker, H. Elderfield, and I. N. McCave, 2011: The Deglacial Evolution of North Atlantic Deep Convection. S*cience,* 3**31,** 202-205.
Thorndycraft, V. R., and G. Benito, 2006: The Holocene fluvial chronology of Spain: evidence from a newly compiled radiocarbon database. Q*uaternary Science Reviews,* 2**5,** 223-234.
Tierney, J., M. Mayes, N. Meyer, C. Johnson, P. Swarzenski, A. Cohen, and J. Russell, 2010a: Late-twentieth-century warming in Lake Tanganyika unprecedented since AD 500. N*ature Geoscience,* 3**,** 422-425.
Tierney, J. E., D. W. Oppo, Y. Rosenthal, J. M. Russell, and B. K. Linsley, 2010b: Coordinated hydrological regimes in the Indo-Pacific region during the past two millennia. P*aleoceanography,* 2**5,** PA1102.
Timm, O., E. Ruprecht, and S. Kleppek, 2004: Scale-dependent reconstruction of the NAO index. J*ournal of Climate,* 1**7,** 2157-2169.
Timm, O., P. Köhler, A. Timmermann, and L. Menviel, 2010: Mechanisms for the Onset of the African Humid Period and Sahara Greening 14.5-11 ka BP. J*ournal of Climate,* 2**3,** 2612-2633.
Timm, O., A. Timmermann, A. Abe-Ouchi, F. Saito, and T. Segawa, 2008: On the definition of seasons in paleoclimate simulations with orbital forcing. P*aleoceanography,* 2**3,** PA2221.
Timmermann, A., O. Timm, L. Stott, and L. Menviel, 2009: The Roles of CO2 and Orbital Forcing in Driving Southern Hemispheric Temperature Variations during the Last 21 000 Yr. J*ournal of Climate,* 2**2,** 1626-1640.
Timmermann, A., et al., 2007: The influence of a weakening of the Atlantic meridional overturning circulation on ENSO. J*ournal of Climate,* 2**0,** 4899-4919.
Timmreck, C., S. J. Lorenz, T. J. Crowley, S. Kinne, T. J. Raddatz, M. A. Thomas, and J. H. Jungclaus, 2009: Limited temperature response to the very large AD 1258 volcanic eruption. G*eophysical Research Letters,* 3**6,** L21708.
Tingley, M. P., and P. Huybers, 2010: A Bayesian Algorithm for Reconstructing Climate Anomalies in Space and Time. Part I: Development and Applications to Paleoclimate Reconstruction Problems. J*ournal of Climate,* 2**3,** 2759-2781.
Tjallingii, R., et al., 2008: Coherent high- and low-latitude control of the northwest African hydrological balance. N*ature Geoscience,* 1**,** 670-675.
Torrence, C., and G. P. Compo, 1998: A practical guide to wavelet analysis. B*ulletin of the American Meteorological Society,* 7**9,** 61-78.
Toscano, M. A., W. R. Peltier, and R. Drummond, 2011: ICE-5G and ICE-6G models of postglacial relative sea level history applied to the Holocene coral reef record of northeastern St Croix, U.S.V.I.: investigating the influence of rotational feedback on GIA processes at tropical latitudes. Q*uaternary Science Reviews,* 3**0,** 3032-3042.
Touchan, R., K. Anchukaitis, D. Meko, M. Sabir, S. Attalah, and A. Aloui, 2011: Spatiotemporal drought variability in northwestern Africa over the last nine centuries. C*limate Dynamics,* 3**7,** 237-252.
Trouet, V., J. Esper, N. E. Graham, A. Baker, J. D. Scourse, and D. C. Frank, 2009: Persistent Positive North Atlantic Oscillation Mode Dominated the Medieval Climate Anomaly. S*cience,* 3**24,** 78-80.
Tudhope, A. W., et al., 2001: Variability in the El Niño-Southern Oscillation Through a Glacial-Interglacial Cycle. S*cience,* 2**91,** 1511-1517.
Turner, J., et al., 2005: Antarctic climate change during the last 50 years. I*nternational Journal of Climatology,* 2**5,** 279-294.
Turner, J., et al., 2009: Antarctic Climate Change and the Environment.
Turney, C. S. M., and R. T. Jones, 2010: Does the Agulhas Current amplify global temperatures during super-interglacials? J*ournal of Quaternary Science,* 2**5,** 839-843.
Tzedakis, P. C., 2010: The MIS 11-MIS 1 analogy, southern European vegetation, atmospheric methane and the 'early anthropogenic hypothesis'. C*limate of the Past,* 6**,** 131-144.
Tzedakis, P. C., D. Raynaud, J. F. McManus, A. Berger, V. Brovkin, and T. Kiefer, 2009: Interglacial diversity. N*ature Geoscience,* 2**,** 751-755.
Vallelonga, P., et al., 2010: Lead isotopic compositions in the EPICA Dome C ice core and Southern Hemisphere Potential Source Areas. Q*uaternary Science Reviews,* 2**9,** 247-255.
van de Berg, W. J., M. van den Broeke, J. Ettema, E. van Meijgaard, and F. Kaspar, 2011: Significant contribution of insolation to Eemian melting of the Greenland ice sheet. N*ature Geoscience,* 4**,** 679-683.
van de Plassche, O., K. van der Borg, and A. F. M. de Jong, 1998: Sea level–climate correlation during the past 1400 yr. G*eology,* 2**6,** 319-322.
Van Nieuwenhove, N., H. A. Bauch, F. Eynaud, E. Kandiano, E. Cortijo, and J. L. Turon, 2011: Evidence for delayed poleward expansion of North Atlantic surface waters during the last interglacial (MIS 5e). Q*uaternary Science Reviews,* 3**0,** 934-946.
Vavrus, S., W. Ruddiman, and J. Kutzbach, 2008: Climate model tests of the anthropogenic influence on greenhouse-induced climate change: the role of early human agriculture, industrialization, and vegetation feedbacks. Q*uaternary Science Reviews,* 2**7,** 1410-1425.

Verleyen, E., et al., 2011: Post-glacial regional climate variability along the East Antarctic coastal margin-Evidence from shallow marine and coastal terrestrial records. E*arth-Science Reviews,* 1**04,** 199-212.
Vieira, L. E., S. K. Solanki , A. V. Krivov, and I. G. Usoskin 2011: Evolution of the solar irradiance during the Holocene. A*stronomy & Astrophysics,* 5**31,** A6.
Villalba, R., M. Grosjean, and T. Kiefer, 2009: Long-term multi-proxy climate reconstructions and dynamics in South America (LOTRED-SA): State of the art and perspectives. P*alaeogeography, Palaeoclimatology, Palaeoecology,* 2**81,** 175-179.
Vimeux, F., P. Ginot, M. Schwikowski, M. Vuille, G. Hoffmann, L. G. Thompson, and U. Schotterer, 2009: Climate variability during the last 1000 years inferred from Andean ice cores: A review of methodology and recent results. P*alaeogeography, Palaeoclimatology, Palaeoecology,* 2**81,** 229-241.
Vinther, B., P. Jones, K. Briffa, H. Clausen, K. Andersen, D. Dahl-Jensen, and S. Johnsen, 2010: Climatic signals in multiple highly resolved stable isotope records from Greenland. Q*uaternary Science Reviews,* 2**9,** 522-538.
Vinther, B. M., et al., 2009: Holocene thinning of the Greenland ice sheet. N*ature,* 4**61,** 385-388.
von Grafenstein, U., E. Erlenkeuser, J. Müller, J. Jouzel, and S. Johnsen, 1998: The cold event 8,200 years ago documented in oxygen isotope records of precipitation in Europe and Greenland. C*limate Dynamics,* 1**4,** 73-81.
von Grafenstein, U., H. Erlenkeuser, A. Brauer, J. Jouzel, and S. J. Johnsen, 1999: A mid-European decadal isotope-climate record from 15,500 to 5000 years BP. S*cience,* 2**84,** 1654-1657.
von Gunten, L., M. Grosjean, B. Rein, R. Urrutia, and P. Appleby, 2009: A quantitative high-resolution summer temperature reconstruction based on sedimentary pigments from Laguna Aculeo, central Chile, back to AD 850. T*he Holocene,* 1**9,** 873-881.
von Storch, H., E. Zorita, J. Jones, F. Gonzalez-Rouco, and S. Tett, 2006: Response to Comment on "Reconstructing Past Climate from Noisy Data". S*cience,* 3**12,** 1872-1873.
Waelbroeck, C., et al., 2002: Sea level and deep water temperature changes derived from benthic foraminifera isotopic records. Q*uaternary Science Reviews,* 2**1,** 295-305.
Wahl, E., et al., 2010: An archive of high-resolution temperature reconstructions over the past 2+millennia. G*eochemistry Geophysics Geosystems,* 1**1,** Q01001.
Wang, S., X. Wen, Y. Luo, W. Dong, Z. Zhao, and B. Yang, 2007: Reconstruction of temperature series of China for the alst 1000 years. C*hinese Science Bulletin,* 5**2,** 3272-3280.
Wang, Y., et al., 2005a: The Holocene Asian Monsoon: Links to Solar Changes and North Atlantic Climate. S*cience,* 3**08,** 854-857.
Wang, Y. J., H. Cheng, R. L. Edwards, Z. S. An, J. Y. Wu, C. C. Shen, and J. A. Dorale, 2001: A high-resolution absolute-dated Late Pleistocene monsoon record from Hulu Cave, China. S*cience,* 2**94,** 2345-2348.
Wang, Y. J., et al., 2008: Millennial- and orbital-scale changes in the East Asian monsoon over the past 224,000 years. N*ature,* 4**51,** 1090-1093.
Wang, Y. M., J. Lean, and N. Sheeley, 2005b: Modeling the Sun's Magnetic Field and Irradiance since 1713. T*he Astrophysical Journal,* 6**25,** 522-538.
Wang, Z., J. Chappellaz, K. Park, and J. Mak, 2010: Large Variations in Southern Hemisphere Biomass Burning During the Last 650 Years. S*cience,* 3**30,** 1663-1666.
Wanner, H., O. Solomina, M. Grosjean, S. P. Ritz, and M. Jetel, 2011: Structure and origin of Holocene cold events. Q*uaternary Science Reviews,* 3**0,** 3109-3123.
Wanner, H., et al., 2008: Mid- to Late Holocene climate change: an overview. Q*uaternary Science Reviews,* 2**7,** 1791-1828.
Watanabe, O., J. Jouzel, S. Johnsen, F. Parrenin, H. Shoji, and N. Yoshida, 2003: Homogeneous climate variability across East Antarctica over the past three glacial cycles. N*ature,* 4**22,** 509-512.
Watanabe, S., et al., 2011: MIROC-ESM 2010: model description and basic results of CMIP5-20c3m experiments. G*eoscientific Model Development,* 4**,** 845-872.
Weldeab, S., R. R. Schneider, and M. Kölling, 2006: Deglacial sea surface temperature and salinity increase in the western tropical Atlantic in synchrony with high latitude climate instabilities. E*arth and Planetary Science Letters,* 2**41,** 699-706.
Weldeab, S., D. W. Lea, R. R. Schneider, and N. Andersen, 2007: 155,000 years of West African monsoon and ocean thermal evolution. S*cience,* 3**16,** 1303-1307.
Wenzler, T., S. Solanki, and N. Krivova, 2005: Can surface magnetic fields reproduce solar irradiance variations in cycles 22 and 23? A*stronomy & Astrophysics,* 4**32,** 1057-1061.
Wenzler, T., S. K. Solanki, N. A. Krivova, and C. Fröhlich, 2006: Reconstruction of solar irradiance variations in cycles 21–23 based on surface magnetic fields. A*stronomy & Astrophysics,* 4**60,** 583-595.
Wetter, O., C. Pfister, R. Weingartner, J. Luterbacher, T. Reist, and J. Trösch, 2011: The largest floods in the High Rhine basin since 1268 assessed from documentary and instrumental evidence. H*ydrological Sciences Journal,* 5**6,** 733-758.
Widmann, M., H. Goosse, G. van der Schrier, R. Schnur, and J. Barkmeijer, 2010: Using data assimilation to study extratropical Northern Hemisphere climate over the last millennium. C*limate of the Past,* 6**,** 627-644.
Wiersma, A., D. Roche, and H. Renssen, 2011: Fingerprinting the 8.2 ka event climate response in a coupled climate model. J*ournal of Quaternary Science,* 2**6,** 118-127.

Wiles, G. C., D. J. Barclay, P. E. Calkin, and T. V. Lowell, 2008: Century to millennial-scale temperature variations for the last two thousand years indicated from glacial geologic records of Southern Alaska. G*lobal and Planetary Change,* 6**0,** 115-125.
Wilson, R., G. Wiles, R. D'Arrigo, and C. Zweck, 2007a: Cycles and shifts: 1,300 years of multi-decadal temperature variability in the Gulf of Alaska. C*limate Dynamics,* 2**8,** 425-440.
Wilson, R., E. Cook, R. D'Arrigo, N. Riedwyl, M. N. Evans, A. Tudhope, and R. Allan, 2010: Reconstructing ENSO: the influence of method, proxy data, climate forcing and teleconnections. J*ournal of Quaternary Science,* 2**5,** 62-78.
Wilson, R., et al., 2007b: A matter of divergence: Tracking recent warming at hemispheric scales using tree ring data. J*ournal of Geophysical Research,* 1**12,** D17103.
Winckler, G., R. F. Anderson, M. Q. Fleisher, D. McGee, and N. Mahowald, 2008: Covariant Glacial-Interglacial Dust Fluxes in the Equatorial Pacific and Antarctica. S*cience,* 3**20,** 93-96.
Winguth, A., C. Shellito, C. Shields, and C. Winguth, 2010: Climate Response at the Paleocene-Eocene Thermal Maximum to Greenhouse Gas Forcing-A Model Study with CCSM3. J*ournal of Climate,* 2**3,** 2562-2584.
Winkler, S., and J. Matthews, 2010: Holocene glacier chronologies: Are 'high-resolution' global and inter-hemispheric comparisons possible? T*he Holocene,* 2**0,** 1137-1147.
Winter, A., et al., 2011: Evidence for 800 years of North Atlantic multi-decadal variability from a Puerto Rican speleothem. E*arth and Planetary Science Letters,* 3**08,** 23-28.
Winton, M., 2006: Amplified Arctic climate change: What does surface albedo feedback have to do with it? G*eophysical Research Letters,* 3**3,** L03701.
Wohlfahrt, J., et al., 2008: Evaluation of coupled ocean-atmosphere simulations of the mid-Holocene using palaeovegetation data from the northern hemisphere extratropics. C*limate Dynamics,* 3**1,** 871-890.
Wolff, C., et al., 2011: Reduced Interannual Rainfall Variability in East Africa During the Last Ice Age. S*cience,* 3**33,** 743-747.
Wolff, E. W., J. Chappellaz, T. Blunier, S. O. Rasmussen, and A. Svensson, 2010: Millennial-scale variability during the last glacial: The ice core record. Q*uaternary Science Reviews,* 2**9,** 2828-2838.
Woodroffe, C., and R. McLean, 1990: Microatolls and recent sea level change on coral atolls. N*ature,* 3**44,** 531-534.
Woodroffe, C. D., M. R. Beech, and M. K. Gagan, 2003: Mid-late Holocene El Niño variability in the equatorial Pacific from coral microatolls. G*eophysical Research Letters,* 3**0,** 1358.
Woodroffe, C. D., H. V. McGregor, S. G. Smithers, D. Fink, and K. Lambeck, submitted: Mid-Pacific microatolls imply no major sea level fluctuations over past millennia.
Xie, S. P., Y. Okumura, T. Miyama, and A. Timmermann, 2008: Influences of Atlantic climate change on the tropical Pacific via the Central American Isthmus. J*ournal of Climate,* 2**1,** 3914-3928.
Yadav, R., A. Braeuning, and J. Singh, 2011: Tree ring inferred summer temperature variations over the last millennium in western Himalaya, India. C*limate Dynamics,* 3**6,** 1545-1554.
Yang, B., A. Bräuning, and S. Yafeng, 2003: Late Holocene temperature fluctuations on the Tibetan Plateau. Q*uaternary Science Reviews,* 2**2,** 2335-2344.
Yang, B., A. Braeuning, K. Johnson, and Y. Shi, 2002: General characteristics of temperature variation in China during the last two millennia. G*eophysical Research Letters,* 2**9,** 1324.
Yang, B., A. Bräuning, Z. Dong, Z. Zhang, and J. Keqing, 2008: Late Holocene monsoonal temperate glacier fluctuations on the Tibetan Plateau. G*lobal and Planetary Change,* 6**0,** 126-140.
Yang, B., J. Wang, A. Bräuning, Z. Dong, and J. Esper, 2009: Late Holocene climatic and environmental changes in and central Asia. Q*uaternary International,* 1**94,** 68-78.
Yin, Q. Z., and A. Berger, 2010: Insolation and CO2 ₒntribution to the interglacial climate before and after the Mid-Brunhes Event. N*ature Geoscience,* 3**,** 243-246.
Yokoyama, Y., and T. M. Esat, 2011: Global climate and sea level: Enduring variability and rapid fluctuations over the past 150,000 years. O*ceanography,* 2**4,** 54–69.
Yokoyama, Y., K. Lambeck, P. De Deckker, P. Johnston, and L. Fifield, 2000: Timing of the Last Glacial Maximum from observed sea level minima. N*ature,* 4**06,** 713-716.
Yokoyama, Y., T. M. Esat, M. T. McCulloch, G. E. Mortimer, J. Chappell, and K. Lambeck, 2003: Large sea level excursions during the Marine Isotope Stages 4 and 3 obtained from Huon Peninsula uplifted coral terraces. G*eochimica Et Cosmochimica Acta,* 6**7,** A568-A568.
Yokoyama, Y., Y. Kido, R. Tada, I. Minami, R. C. Finkel, and H. Matsuzaki, 2007: Japan Sea oxygen isotope stratigraphy and global sea level changes for the last 50,000 years recorded in sediment cores from the Oki Ridge. P*alaeogeography, Palaeoclimatology, Palaeoecology,* 2**47,** 5-17.
Yoshimori, M., T. Yokohata, and A. Abe-Ouchi, 2009: A Comparison of Climate Feedback Strength between CO2 Doubling and LGM Experiments. J*ournal of Climate,* 2**2,** 3374-3395.
Yoshimori, M., J. C. Hargreaves, J. D. Annan, T. Yokohata, and A. Abe-Ouchi, 2011: Dependency of Feedbacks on Forcing and Climate State in Physics Parameter Ensembles. J*ournal of Climate,* 10.1175/2011jcli3954.1.
Yu, S.-Y., B. E. Berglund, P. Sandgren, and K. Lambeck, 2007: Evidence for a rapid sea level rise 7600 yr ago. G*eology,* 3**5,** 891-894.
Yue, X., H. Wang, H. Liao, and D. Jiang, 2010: Simulation of the Direct Radiative Effect of Mineral Dust Aerosol on the Climate at the Last Glacial Maximum. J*ournal of Climate,* 2**4,** 843-858.

Zachos, J. C., G. R. Dickens, and R. E. Zeebe, 2008: An early Cenozoic perspective on greenhouse warming and carbon-cycle dynamics. N*ature,* 4**51,** 279-283.

Zahn, R., J. Schonfeld, H. Kudrass, M. Park, H. Erlenkeuser, and P. Grootes, 1997: Thermohaline instability in the North Atlantic during meltwater events: Stable isotope and ice-rafted detritus records from core SO75-26KL, Portuguese margin. P*aleoceanography,* 1**2,** 696-710.

Zeebe, R. E., J. C. Zachos, and G. R. Dickens, 2009: Carbon dioxide forcing alone insufficient to explain Palaeocene-Eocene Thermal Maximum warming. N*ature Geoscience,* 2**,** 576-580.

Zhang, D., R. Blender, X. Zhu, and K. Fraedrich, 2011: Temperature variability in China in an ensemble simulation for the last 1,200 years. T*heoretical and Applied Climatology,* 1**03,** 387-399.

Zhang, Q., H. S. Sundqvist, A. Moberg, H. Kornich, J. Nilsson, and K. Holmgren, 2010: Climate change between the mid and late Holocene in northern high latitudes - Part 2: Model-data comparisons. C*limate of the Past,* 6**,** 609-626.

Zhang, R., and T. L. Delworth, 2006: Impact of Atlantic multidecadal oscillations on India/Sahel rainfall and Atlantic hurricanes. G*eophysical Research Letters,* 3**3,** L17712.

Zhang, Y., Z. Kong, S. Yan, Z. Yang, and J. Ni, 2009: "Medieval Warm Period" on the northern slope of central Tianshan Mountains, Xinjiang, NW China. G*eophysical Research Letters,* 3**6,** L11702.

Zheng, J. Y., W. C. Wang, Q. S. Ge, Z. M. Man, and P. Y. Zhang, 2006: Precipitation variability and extreme events in eastern China during the past 1500 years. T*errestrial Atmospheric and Oceanic Sciences,* 1**7,** 579-592.

Zheng, W., P. Braconnot, E. Guilyardi, U. Merkel, and Y. Yu, 2008: ENSO at 6ka and 21ka from ocean-atmosphere coupled model simulations. C*limate Dynamics,* 3**0,** 745-762.

Zhu, H., F. Zheng, X. Shao, X. Liu, X. Yan, and E. Liang, 2008: Millennial temperature reconstruction based on tree-ring widths of Qilian juniper from Wulan, Qinghai province, China. C*hinese Science Bulletin,* 5**3,** 3914-3920.

Tables

Table 5.1: Summary of atmospheric CO_2 proxy methods and confidence assessment of their main assumptions [PLACEHOLDER FOR SECOND ORDER DRAFT: to be placed in supplement after review of FOD].

Method	Scientific Rationale	Estimated Applicability	Limitations	Main Assumptions (*relative confidence*)
Alkenone (phytoplankton biomarker) carbon isotopes	Measurements of carbon isotope ratios of marine sedimentary alkenones (or other organic compounds) allows determination of the isotopic fractionation factor during carbon fixation (ε_p) from which pCO_2 can be calculated.	100 to ~4,000 ppm; last 100 Myr	Alkenones are often rare in oligotrophic areas and sometimes absent. Method relies on empirical calibration and $\delta^{13}C$ is sensitive to other environmental factors, especially nutrient-related variables. Method has been used successfully to reconstruct glacial-interglacial changes.	• Measured alkenone carbon isotope ratio is accurate and precise (*high*). • Ambient aqueous pCO_2 has a quantifiable relationship with ε_p that can be distinguished from the nutrient-related physiological factors such as algal growth rate, cell size, cell geometry and light-limited growth (*medium*). • The disequilibrium between aqueous pCO_2 and atmospheric pCO_2 is at least an order of magnitude smaller than the largest changes in atmospheric pCO_2 *(high)*. • Carbon isotope fractionation in modern alkenone-producing species is the same in ancient species and constant through time (*medium*). • Levels of biological productivity (e.g., dissolved phosphate concentrations) can be calculated (*high*). • Carbon isotope ratio of aqueous CO_2 in the mixed layer can be determined (*medium*). • Sea surface temperature can be determined (*high*). • Atmospheric pO_2 is known or assumed (*medium*). • Diagenetic effects are minimal, or can be quantified *(medium*).
Boron isotopes in foraminifera	Boron isotope ratios ($\delta^{11}B$) in foraminifera (or other calcifying organisms) give paleo-pH from which pCO_2 can be calculated if a value for a second carbonate system parameter (e.g., alkalinity) is assumed	100 to ~4,000 ppm; last 100 Myr	Calculated pCO_2 is very sensitive to the boron isotope ratio of seawater which is relatively poorly known, especially for the earlier Cenozoic. Effects of foraminiferal preservation are not well understood. Method has been used successfully to reconstruct glacial-interglacial changes.	• Measured boron isotope ratio is accurate and precise (*high*). • The equilibrium constant for dissociation of boric acid and boron isotopic fractionation between $B(OH)_3$ and $B(OH)_4^-$ and are well known (*high*). • Boron incorporation into carbonate is exclusively from borate ion (*high*). • Boron isotope ratio of foraminifer calcification reflects ambient surface seawater pH (*high*). • Aqueous pCO_2 is in equilibrium with atmospheric pCO_2 (*high*). • Habitats of extinct species can be determined (*high*). • There is no vital effect fractionation in extinct species, or it can be determined (*high*). • The boron isotope ratio of seawater ($\delta^{11}B_{sw}$) can be determined (*medium*). • Ocean alkalinity or concentration of Total Dissolved Inorganic Carbon can be determined (*high*). • Sea surface temperature (SST) and salinity (SSS) can be determined (*high*). • Diagenetic effects are minimal or can be quantified (*medium*).

Carbon isotopes in soil carbonate and organic matter	Atmospheric pCO_2 affects the relationship between the $\delta^{13}C$ of soil CO_2 and the $\delta^{13}C$ of soil organic matter at depth in certain soil types, hence measurement of these parameters in paleosols can be used to calculate past pCO_2	100 to ~2,000 ppm; last 400 Myr	Method works better for some soil types than others. CO_2 loss is difficult to quantify and method and effects of late diagenesis may be difficult to determine.	• Isotopic composition of soil CO_2 is reflected in soil carbonates below a depth of 50 cm (*medium*). • The concentration of respired CO_2 in the soil is known or assumed (*medium*). • Isotopic composition of atmospheric CO_2 is known or can be inferred (*low*). • Soil carbonates were precipitated in the vadose zone in exchange with atmospheric CO_2 (*high*). • The original depth profile of a paleosol can be determined (*low*). • Burial (late) diagenetic effects are minimal or can be quantified (*high*).
Stomata in plant leaves	The relative frequency of stomata on fossil leaves (Stomatal Index; Salisbury, 1927) can be used to calculate past atmospheric CO2 levels	100 to ~700 ppm; last 400 Myr	Closely related species have very different responses to pCO_2. The assumption that short-term response is the same as the evolutionary response is difficult to test. This and the shape of the calibration curves mean that much greater confidence applies to low pCO_2 and short timescales. Method has been used successfully to reconstruct glacial-interglacial changes.	• Measured stomatal index is accurate and precise (*high*). • Measured stomatal index is representative of the plant (*high*). • The target plants adjust their stomatal index of leaves to optimize CO_2 uptake (*medium*). • Atmospheric pCO_2 close to the plant is representative of the atmosphere as a whole (*medium*). • The quantitative relationship between stomatal index and CO_2 observed on short timescales (ecophenotypic or "plastic response") applies over evolutionary time (*low*). • Environmental factors such as irradiance, atmospheric moisture, water availability, temperature, and nutrient availability do not affect the relationship between stomatal index and CO_2 (*medium*). • Stomatal index response to CO_2 of extinct species can be determined or assumed (*low*). • Taphonomic processes do not affect stomatal index counts (*high*). • Diagenetic processes do not affect stomatal index counts (*high*).

Table 5.2: Summary of SST proxy methods and confidence assessment of their main assumptions

Method	Scientific Rationale	Est. Applicability	Limitations	Main Assumptions
$\delta^{18}O$ of mixed-layer planktonic foraminifera	Partitioning of $^{18}O/^{16}O$ from seawater into calcite shells of all foraminifera is temperature dependent. Verified by theoretical, field and laboratory studies. Utilizes extant and extinct species that resided in the photic zone.	0 to 50°C, last 150 Myr	The $^{18}O/^{16}O$ ratios of recrystallized planktonic foraminifer shells in carbonate-rich sediments are biased toward colder seafloor temperatures, and at most, can only constrain the lower limit of SST. The transition in preservation is progressive with age. Well-preserved forams from clay rich sequences on continental margins are preferred. Diagenetic calcite is detectable by visual and microscopic techniques	• Analytical errors are negligible (*high*). • Sensitivity to T is high and similar to modern descendants (*high*). • Seawater $\delta^{18}O$ is known. The uncertainty varies with time depending on presence of continental ice sheets, though error is negligible in the Pleistocene and during minimal ice periods such as the Eocene (<=±0.25°C). Error doubles during periods of Oligocene and early Neogene glaciation because of weak constraints on ice volume (*medium to high*). • Species lives in the mixed-layer and thus records SST (*high*). • Local salinity/seawater $\delta^{18}O$ is known (*low* to *medium*). • Carbonate ion/pH is similar to modern (*medium*, *high*). • Foraminifera from clay-rich sequences are well preserved and ratios unaffected by diagenesis (*high)*. • Foraminifera from carbonate-rich pelagic sequences are well preserved and ratios unaffected by diagenesis *(high to low; decreasing confidence with age*).
Mg/Ca in mixed-layer planktonic foraminifera	Partitioning of Mg/Ca from seawater into calcite shells is temperature dependent. Calibration to T is based on empirical field and laboratory culturing studies, as Mg concentrations of inorganically precipitated calcite are an order of magnitude higher than in biogenic calcite. There is no ice-volume influence on seawater Mg/Ca, though sensitivity does change with seawater Mg concentration	5 to 35°C, last 65 Myr	Diagenetic recrystallization of foram shells can bias ratios, though the direction of bias is unknown and comparisons with other proxies suggest it is minor. The Mg/Ca is also slightly sensitive to seawater pH. Long-term changes in seawater Mg/Ca, on the order of a 2–5 %/10 myr, must be constrained via models.	• Analytical errors are negligible (*high*). • Mg containing oxide and organic contaminants have been removed by oxidative/reductive cleaning (*high*). • Sensitivity to T in extinct species is similar to modern species (*medium*). • Species lives in the mixed-layer and thus records SST (*high*). • Seawater Mg/Ca is known (*high to moderate*: *decreasing confidence with time*). • Surface water carbonate ion/pH is similar to modern (*medium*). • Forams from clay-rich sequences are well preserved and ratios unaffected by diagenesis (*high)*. • Forams from carbonate-rich pelagic sequences are well preserved and ratios unaffected by diagenesis *(high to low; decreasing confidence with age*).
TEX_{86} index in Archea	The ratio of cyclopentane rings in archaeal tetraether lipids (TEX), i.e., isoprenoid glycerol dibiphytanyl glycerol tetraethers (GDGTs), is sensitive to the temperature of growth environment. The relationship and calibration with temperature is empirical (based on core tops), as the underlying mechanism(s) for	1 to 40°C, last 150 Myr	The depth from which the bulk of sedimentary GDGT's are produced is assumed to be the mixed-layer though this cannot be verified, for the modern or past. At least two species with differing ecologies appear to be producing the tetraethers. The GDGT signal is ultimately an integrated community signal allowing the	• Analytical errors are small (*high*). • Sensitivity to T similar to modern (*medium*). • Species that produced tropical sedimentary GDGT's resided mainly in the mixed-layer and thus records SST (*medium to high*). • Species that produced the sedimentary GDGT's in the sub-polar to polar regions mainly resided in the mixed-layer and thus records SST (*low*). • No alteration of GDGT ratios during degradation of compounds (*medium to low: decreasing confidence with age*). • No contamination by GDGT's derived from terrestrial sources (*medium to high depending on location of samples)*.

	this relationship has yet to be identified. Verification of field calibrations with laboratory cultures is still in progress. The compounds are extracted from bulk sediments.		potential for evolutionary changes to influence regional signals over time. Tetraethers are found in measurable abundances on continental shelves and/or organic rich sediments.	
UK_{37} Index in Algae	Based on the relative concentration of C_{37} methyl ketones derived from the cells of haptophyte phytoplankton. Calibrations are empirically derived through field and culture studies	5 to 28°C, 50 Myr	The distribution of haptophyte algae ranges from sub-polar to tropical	• Analytical errors are negligible (*high*). • Sensitivity to SST similar to modern (*medium to high; decreasing confidence with time*). • Species that produced the sedimentary alkenones lived in the mixed-layer and thus record SST (*high*). • No alteration of alkenone saturation index during degradation of compounds (*medium; decreasing confidence with age*).
Microfossil census modern analogue techniques	Utilises a statistical correlation between extant planktonic microfossil assemblage data (most commonly foraminifera, but also diatoms and radiolarian) and modern analogue databases. Most commonly used statistical methods are modern analogue technique and artificial neural network.	0 to 40°C 5 Myr	Dependent on quality, coverage, size and representativeness of the core top modern analogue data base. Extant species reduce with increasing age. This and paleogeographic and ocean circulation differences with age limit applicability beyond 5 Ma.	• The ecology of modern assemblages is largely controlled by SST (*high*). • Sensitivity of paleo-assemblages to SST is similar to modern (*high, but decreases with increasing age*). • Eurythermal assemblages responding to non-temperature (e.g., nutrient availability) influences can be identified (*medium*). • That the extant species used to reconstruct SST mainly reside in the mixed layer (*medium to high*). • Depositional and post-depositional processes have not biased the assemblage (*medium to high*).

1

Appendix 5.A: Supplemental Information to Section 5.5

5.A.1 Reconstructions of Past Sea Level

Records of past sea level change provide critical context for understanding current changes and evaluating projected changes. In addition to establishing a longer term reference for placing current rates of sea level rise in the context of natural variability, these records provide insight into the sensitivity of sea level to past climate change, including possible nonlinear responses, thus placing bounds on amplitudes and rates of possible future changes (Chapter 13).

Sea level reconstructions for the pre-instrumental period (older than about 1700 CE) are based on geological and archaeological archives that vary in their ability to resolve the amplitude and rates of past changes, with the more accurate and more precise resolutions occurring in younger records. For the Holocene, important sources of information are from corals (Goodwin and Harvey, 2008; Woodroffe et al., submitted) and coastal deposits such as saltmarsh sequences (Kemp et al., in press). Archaeological features whose functioning requires a close relation to sea level can also provide important constraints for the past few thousand years (Lambeck et al., 2004). For the last several hundred thousand years, the most important and direct observations of sea level are also from corals. Oxygen isotopic records from deep-sea sediments can provide important insights into sea level change during glacial cycles, particularly since they provide a continuous record, but because this proxy also records former water temperature and salinity, it can only be used to reconstruct sea level change when calibrated directly against independent estimates (e.g., Cutler et al., 2003; Siddall et al., 2006; Waelbroeck et al., 2002; Yokoyama et al., 2007).

Processes that contribute to sea level change can be grouped into those that change the volume of the ocean waters (e.g., thermal expansion or melting of land-based ice), in the distribution of the water within the ocean basins (e.g., variations in ocean currents and surface winds or in the planet's gravitational potential), and in the shape of the ocean basins (e.g., tectonic and mantle dynamic processes and glacial isostasy) (Chapter 13).

For the past 2.6 Myr, the cause of the largest sea level changes has been the cyclic growth and decay of ice sheets and is characterized by periods of sea level highstands similar to today (interglacial conditions of which the Holocene is the most recent), by periods of sea level lowstands when ice sheets were at their maximum size (of which the LGM is the most recent), by intervening periods of rapid ice sheet growth and partial decay (Cutler et al., 2003; Dorale et al., 2010; Lambeck and Chappell, 2001; Rohling et al., 2009; Siddall et al., 2006; Yokoyama and Esat, 2011), and by rapid terminations of the glacial maxima (Bard et al., 2010; Peltier and Fairbanks, 2006; Yokoyama et al., 2000). Existing reconstructions demonstrate that changes in global mean sea level (GMSL) on glacial-interglacial timescales are highly correlated with global mean (or high-latitude summer) temperature and radiative forcing (Alley et al., 2005; Hansen et al., 2007; Rohling et al., 2009), although with an as yet poorly determined response function, particularly on the longer timescales associated with larger ice sheets.

5.A.2 Processes and Modelling

Paleo records of relative sea levels reflect processes that cause land movement (including deformation of ocean basins), that change ocean volume, and that redistribute water within ocean basins. The principal processes are (i) the response of the earth-ocean system to changing ice sheets (glacio-isostatic adjustment or GIA), (ii) tectonic and mantle dynamic contributions that change the gravity and shape of the Earth's surface, and (iii) climate-driven processes that change ocean volume and that redistribute water within the ocean basins (see Chapter 13).

The GIA of the earth and ocean surface includes the deformation of land and geopotential surfaces and changes in planetary rotation due to the changing ice and water loads, resulting in a complex but well-understood regional and temporal pattern of sea level change for the past 20,000 years (Lambeck et al., 2003; Milne and Mitrovica, 2008; Mitrovica and Wahr, 2011). Quantification of the theory requires information on the Earth's rheology as well as a description of the ice distribution through time. Neither is known with sufficient accuracy from *a priori* considerations, however, and an observational database of relative sea level change is used in an inverse formulation to estimate improved ice-earth model parameters that describe well

the observed sea level on time scales from tens of thousands of years to decades (Lambeck et al., 2010a; Peltier, 2004; Toscano et al., 2011).

The principal uncertainty for the paleo ice sheets, and hence for sea level estimation, is for Antarctica because of very limited observational constraints on its ice-margin evolution and on relative sea level change around the Antarctic margin, resulting in several different LGM reconstructions (Anderson et al., 2002; Mackintosh et al., 2011). A primary constraint on changes in Antarctic ice volume comes from comparisons of estimates of changes in global ocean volume from sea level analyses with estimates of Northern Hemisphere ice sheet volume derived from the inversion of relative sea level records. Recent estimates of the loss of Antarctic ice since the LGM range from about 6 m to about 20 m sea level equivalent (Denton and Hughes, 2002; Huybrechts, 2002; Ivins and James, 2005; Nakada et al., 2000; Ritz et al., 2001). The distribution of this ice within Antarctica remains strongly model dependent with consequence that the accuracy of GIA modelling over Antarctica and high southern latitudes remains low.

The influence of the isostatic process on relative sea level remains as important prior to the LGM as it does for the post-LGM period. For example, local LIG sea level is largely a function of the GIA response to the glaciation immediately preceding and after the interglaciation, and of any difference in ice volume between the interglaciation and today (Lambeck et al., in press). Because constraints on earlier ice sheets decrease with increasing age, however, inferences about interglacial ice volume become less reliable. The same holds true for the Pliocene (Raymo et al., 2011), although because ice volume fluctuations during the Pliocene were comparatively small and restricted to high latitudes, the post-LGM response will have the most significant effect on the present elevation Pliocene sea level records (Raymo et al., 2011).

Large-scale earth-deformation and tectonic processes can contribute significantly to the observed relative sea level record over long geological time scales. The surface response to mantle convection, for example, produces global-scale changes in the volumes and shapes of ocean basins, including that of equipotential surfaces, and the observed concomitant sea level changes are substantial (e.g., Hallam, 1992). Because the rates of change associated with these processes are low (< 0.005 mm yr^{-1}) due to the long time scales involved (Müller et al., 2008), their effect on instrumental and recent glacial sea level records is insignificant, but they become important in reconstructing Pliocene sea level, when few coastal regions can be considered stable (Moucha et al., 2008). In contrast, the effects of local or regional active tectonics can dominate any climate-induced signal (e.g., the Huon Peninsula terraces, Chappell et al., 1996), but their occurrence can be assessed from geological and seismicity records of the region. Sea level records from sites considered free of such tectonic signals, or sites where such signals can be independently evaluated, form the reference frame within which the ocean volume changes are evaluated for the last glacial cycle.

Chapter 5: Information from Paleoclimate Archives

Coordinating Lead Authors: Valérie Masson-Delmotte (France), Michael Schulz (Germany)

Lead Authors: Ayako Abe-Ouchi (Japan), Juerg Beer (Switzerland), Andrey Ganopolski (Germany), Jesus Fidel González Rouco (Spain), Eystein Jansen (Norway), Kurt Lambeck (Australia), Juerg Luterbacher (Germany), Tim Naish (New Zealand), Timothy Osborn (UK), Bette Otto-Bliesner (USA), Terrence Quinn (USA), Rengaswamy Ramesh (India), Maisa Rojas (Chile), XueMei Shao (China), Axel Timmermann (USA)

Contributing Authors: Kevin Anchukaitis, Gerardo Benito, Peter Clark, Patrick De Deckker, Barbara Delmonte, Trond Dokken, Hubertus Fischer, Dominik Fleitmann, Claus Froehlich, Aline Govin, Alan Haywood, Chris Hollis, Ben Horton, Camille Li, Dan Lunt, Natalie Mahowald, Shayne McGregor, Stefan Mulitza, Frédéric Parrenin, Paul Pearson, Alan Robock, Joel Savarino, Jason Smerdon, Olga Solomina, Pavel Tarasov, Claire Waelbroeck, Dieter Wolf-Gladrow, Yusuke Yokoyama, James Zachos, Dan Zwartz

Review Editors: Anil K. Gupta (India), Fatemeh Rahimzadeh (Iran), Dominique Raynaud (France), Heinz Wanner (Switzerland)

Date of Draft: 16 December 2011

Notes: TSU Compiled Version

Figures

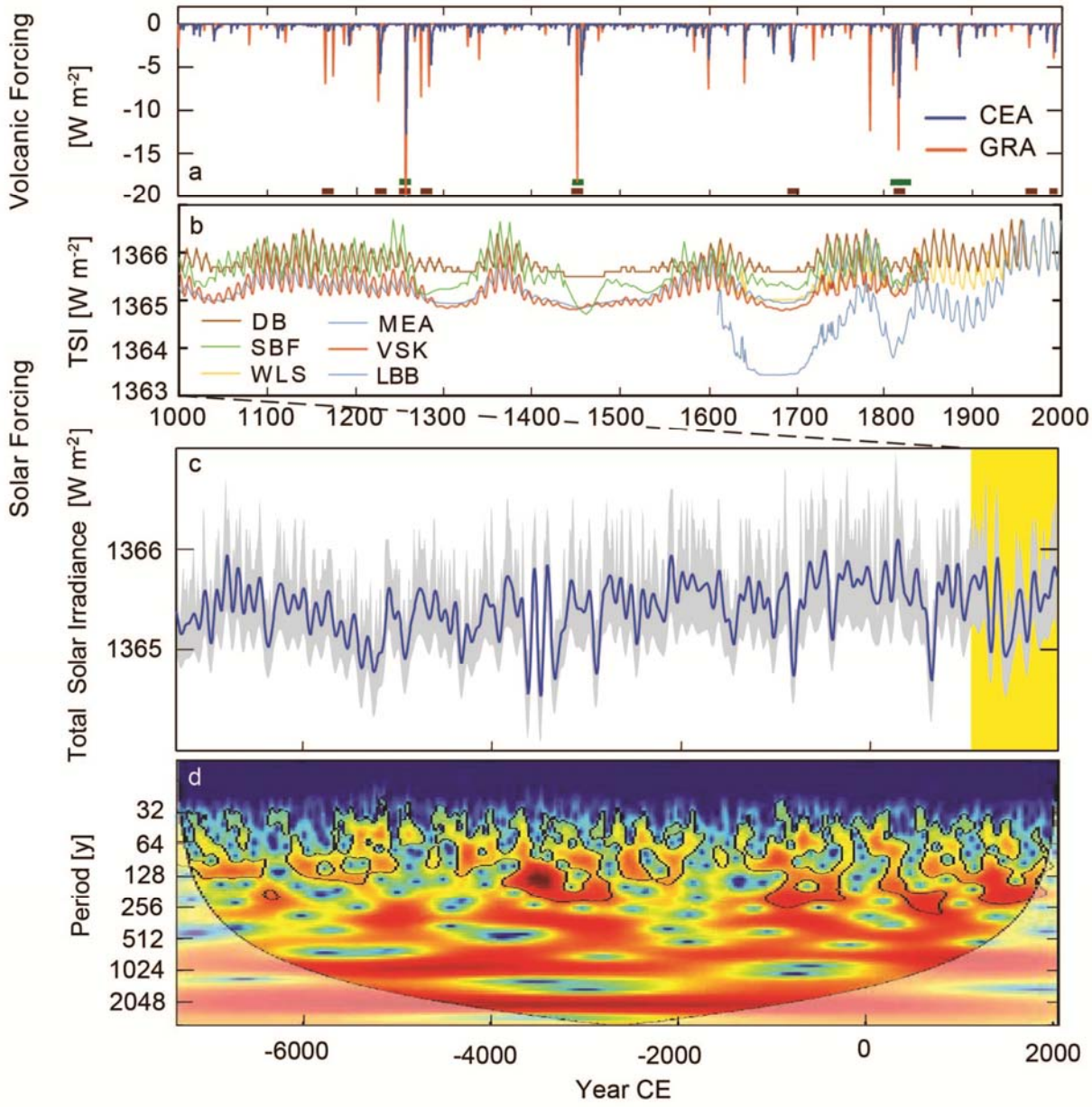

Figure 5.1: a) Two reconstructions of volcanic forcing for the past 1000 years derived from ice core sulfate and used for PMIP3-CMIP5 (Coupled Model Intercomparison Project) simulations (Schmidt et al., 2011). GRA: (Gao et al., 2008); CEA: (Crowley and Unterman, submitted; Crowley and Hyde, 2008; Timmreck et al., 2009). Volcanic sulfate peaks identified from their isotopic composition as originating from the stratosphere (Cole-Dai et al., 2009) are indicated by squares (green: Greenland; brown: Antarctica) (Baroni et al., 2008). **b)** TSI reconstructions back to 1000 CE. Proxies of solar activity (e.g., sunspots, ^{10}Be) are used to estimate the parameters of the models or directly TSI. All records except LBB (Lean et al., 1995) have been used for PMIP3-CMIP5 simulations (Schmidt et al., 2011). DB: (Delaygue and Bard, 2011); MEA: (Muscheler et al., 2007); SBF: (Steinhilber et al., 2009); WLS: (Wang et al., 2005b); VSK: (Vieira et al., 2011). Before 1600 CE, the 11-year cycle has been added artificially to the original data. **c)** TSI reconstruction (100-year low-pass filtered; grey shading: 1 standard deviation uncertainity range) for the past 9300 years (Steinhilber et al., 2009). The reconstruction is based on ^{10}Be and calibrated using the relationship between instrumental data of the open magnetic field, which modulates the production of ^{10}Be and TSI for the past 4 solar minima. **d)** Wavelet analysis (Torrence and Compo, 1998) of TSI showing the existence of several periodicities (87, 104, 130, 150, 208, 350, 515, 980, 2300 years) with varying amplitudes.

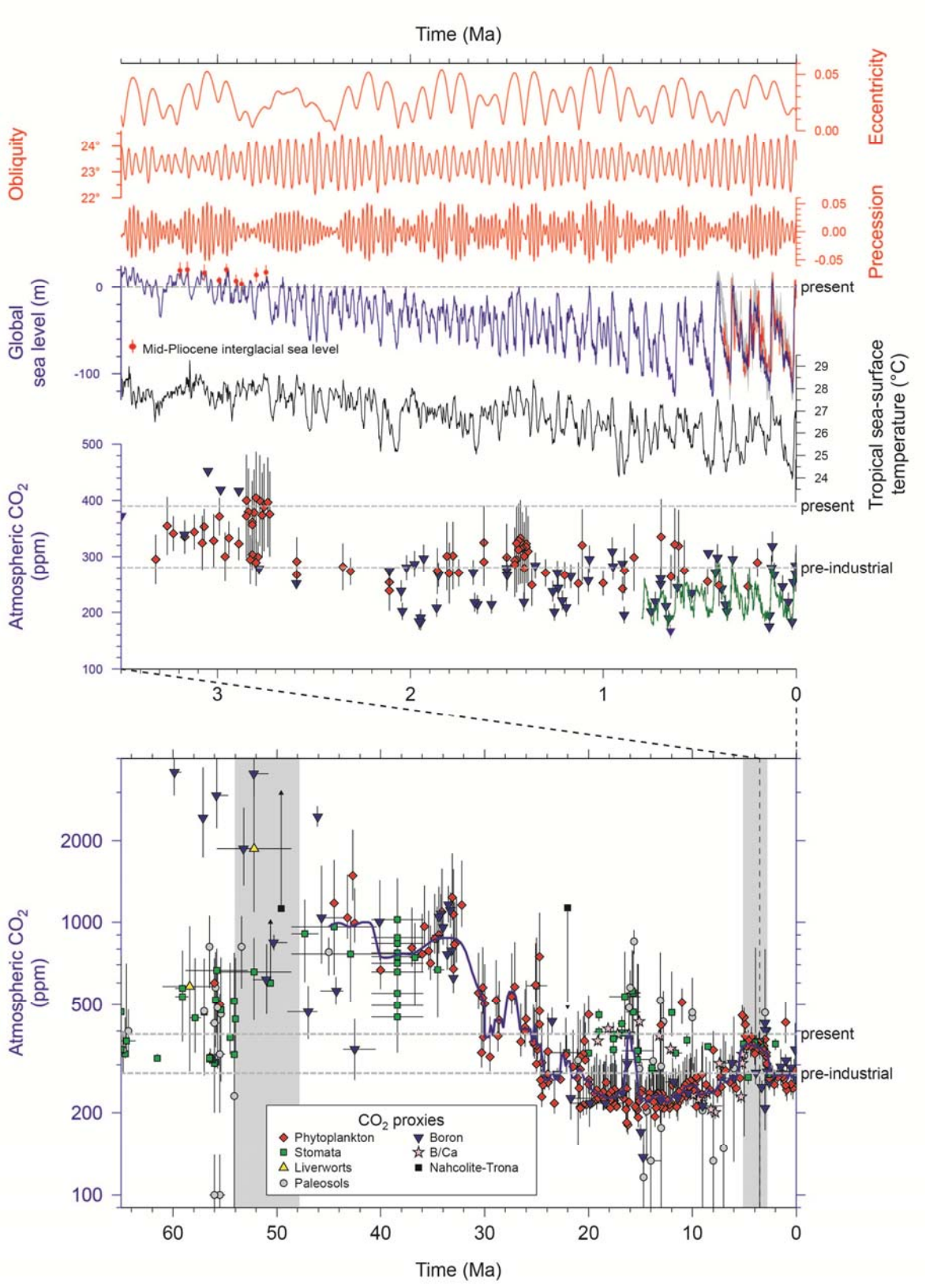

Figure 5.2: (Top) Radiative forcings and perturbations and orbital-scale Earth system responses 3.6 Ma to present. Changes in Earths orbital parameters, eccentricity, obliquity, and precession (Laskar et al., 2004). Sea level curve (purple) is the stacked benthic oxygen isotope proxy for ice volume and ocean temperature (Lisiecki and Raymo, 2005) calibrated to global average eustatic sea level (Miller et al., submitted; Naish and Wilson, 2009). Also shown are global eustatic sea level reconstructions for the last 500 kyr based on sea level calibration of the $\delta^{18}O$ curve using dated coral shorelines (grey line; Waelbroeck et al., 2002), and the Red Sea sediment cores (red line; Rohling et al., 2009; Siddall et

al., 2003) and weighted mean estimates (2 standard deviation uncertainity) for far-field reconstructions of eustatic peaks during mid-Pliocene interglacials (red dots; Miller et al., submitted). The dashed horizontal line represents present day sea level. Tropical sea surface temperature based on a stack of 4 alkenone-based SST reconstructions (Herbert et al., 2010). Atmospheric CO_2 measured from EPICA Dome C ice core (blue line; Lüthi et al., 2008), and estimates of CO_2 from boron $\delta^{11}B$ isotopes in foraminifera in marine sediments (blue triangles; Hönisch et al., 2009; Seki et al., 2010), and phytoplankton alkenone-derived carbon isotope proxies (red diamonds; Pagani et al., 2010; Seki et al., 2010), plotted with 2 standard deviation uncertainity. Present and pre-industrial CO_2 concentrations are indicated with dashed grey line. **(Bottom)** Concentration of atmospheric CO_2 for the last 65 Ma is reconstructed from marine and terrestrial proxies complied by Beerling and Royer (2011) (see for details and data references;additional boron CO_2 proxy data from (Pearson and Palmer, 2000) are also included). Individual proxy methods are colour-coded. Errors represent reported uncertainties (plotted with 2 standard deviation uncertainity; see also Table 5.1 for assessment of confidence of proxies). Most of the data points for CO_2 proxies are based on duplicate and multiple analyses. The blue line is a median filter of all the data points with a time window of 5 Myr plotted from 46 to 30 Ma, and 1 Myr from 30 Ma to present. Shaded grey areas (from left to right) highlight past periods of global warmth during the Early Eocene (about +10°C global mean) and the early to mid Pliocene (about +3°C global mean) (see also Figure 5.3).

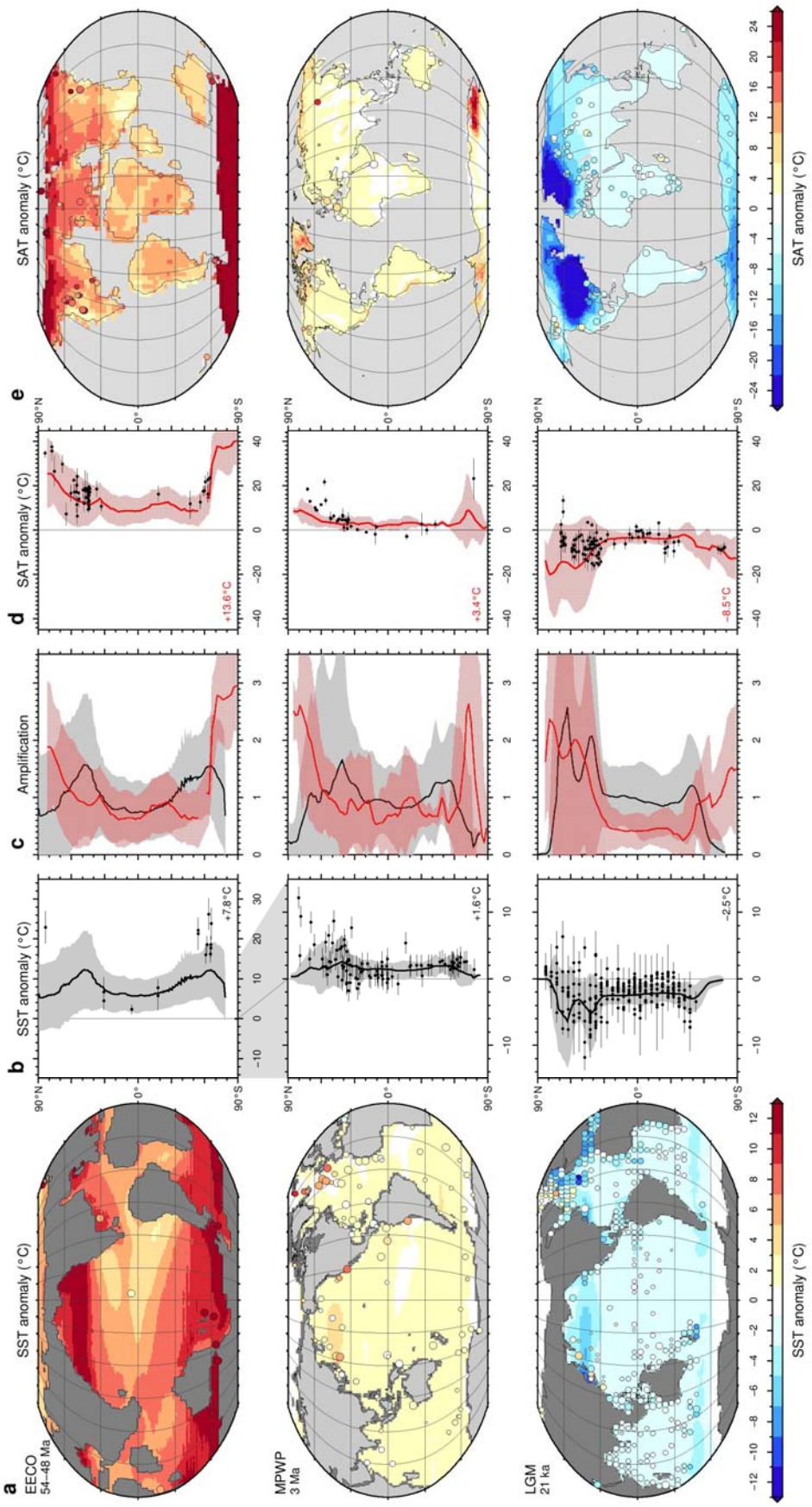

Figure 5.3: Comparison between paleoclimate proxy data and climate model output for **a)** SST, **b)** zonal mean meridional SST gradient, **d)** zonal mean meridional surface air temperature (SAT) gradient, and **e)** SAT anomalies for the Early Eocene Climatic Optimum (EECO, top row), the Mid-Pliocene Warm Period (MPWP, middle row) and the

LGM (bottom row). Model temperature anomalies are calculated relative to the preindustrial value of each model in the ensemble* prior to calculating the multi model mean anomaly (a, e; colour shading). Zonal mean anomalies of the multi model mean (b, d) are plotted with a shaded band indicating 2 standard deviation uncertainity. Site specific temperature anomalies estimated from proxy data are calculated relative to present site temperatures and are plotted (a, e) using the same colour scale as the model data, and a circle size scaled to estimates of confidence. In the zonal plots (b, d) the proxy data anomalies are shown with error bars indicating 2 standard deviation uncertainity. Temperature proxy data compilations for the LGM are from MARGO Project Members (2009) and Bartlein et al. (2011), for the MPWP are from Dowsett et al. (submitted) and Salzmann et al. (2008), and for the EECO are from Hollis et al. (submitted). Polar amplification at each latitude **c)** is calculated as the zonal mean SST or SAT anomaly (b, d), normalised to the global mean temperature anomaly, and is plotted with shaded bands indicating 2 standard deviation uncertainity for each of the time periods. Global mean SST and SAT anomaly calculated from the model ensembles for each time period are shown as a number in **b)** and **d)**, respectively.

*Model ensembles include for: (i; LGM) PMIP3 ensemble; MIROC, CCSM4, AWI, MPI (ii; MPWP) PlioMIP ensemble; MIROC, NCAR, GISS, HadCM3 (Dowsett et al., submitted; Pope et al., 2011) (iii. EECO) EoMIP ensemble; HadCM3L, ECHAM5, CCSM3, GISS (Heinemann et al., 2009; Lunt et al., 2010b; Roberts et al., 2009; Winguth et al., 2010).

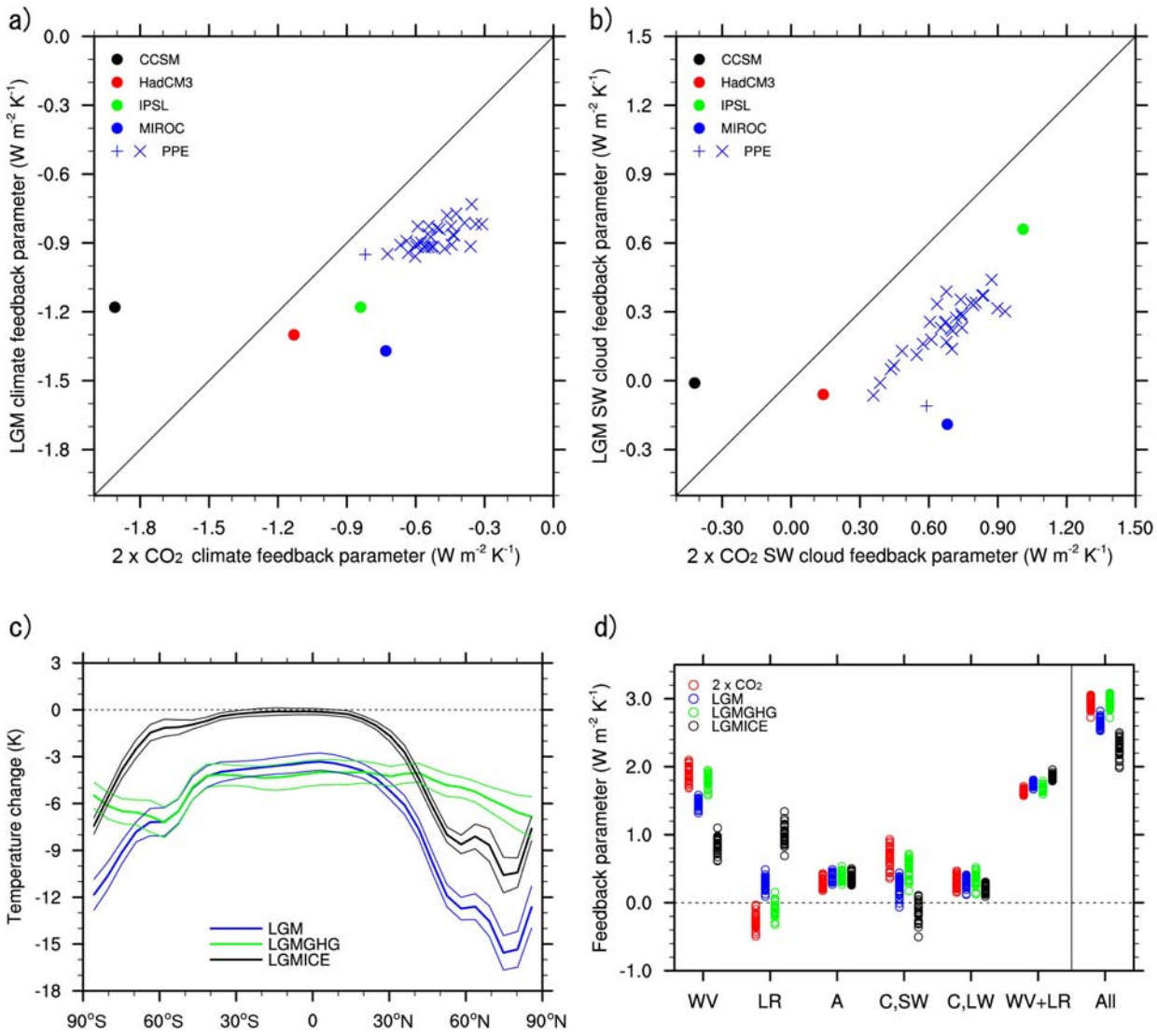

Figure 5.4: Strengths of feedbacks at LGM from data and multi-model ensembles. [PLACEHOLDER for PMIP3 models: others will be included later.] Relation of feedback parameters between CO_2 doubling (2 x CO_2) and LGM climate simulations: **a)** scatter plot of climate feedback parameter (stratosphere-adjusted radiative forcing divided by the equilibrium temperature change); **b)** scatter plot of shortwave cloud feedback parameter (i.e., shortwave component of feedback parameter attributable to the change in clouds); **c)** zonal mean surface air temperature change for LGM, LGMGHG, and LGMICE experiments with respect to the preindustrial reference simulation. Here, LGMGHG refers to the experiment with CO_2 concentration being lowered to the LGM level while LGMICE refers to the experiment with prescribed LGM ice sheets and orbital parameters; and **d)** individual feedback parameters for 31-member physics parameter ensembles (PPE). In **a)** and **b)**, solid circles are for 4 Atmosphere-Ocean GCMs and blue (+) and (x) are for MIROC3.2 T42 and T21 Atmosphere GCM-slab ocean model PPE. Also plotted are the one-to-one lines. In **d)**, WV, LR, A, CSW, CLW denote water vapor, lapse-rate, surface albedo, shortwave cloud, and longwave cloud feedbacks, respectively. ALL denotes sum of all feedbacks. Data are obtained from Crucifix (2006), Yoshimori et al. (2009), and Yoshimori et al. (2011).

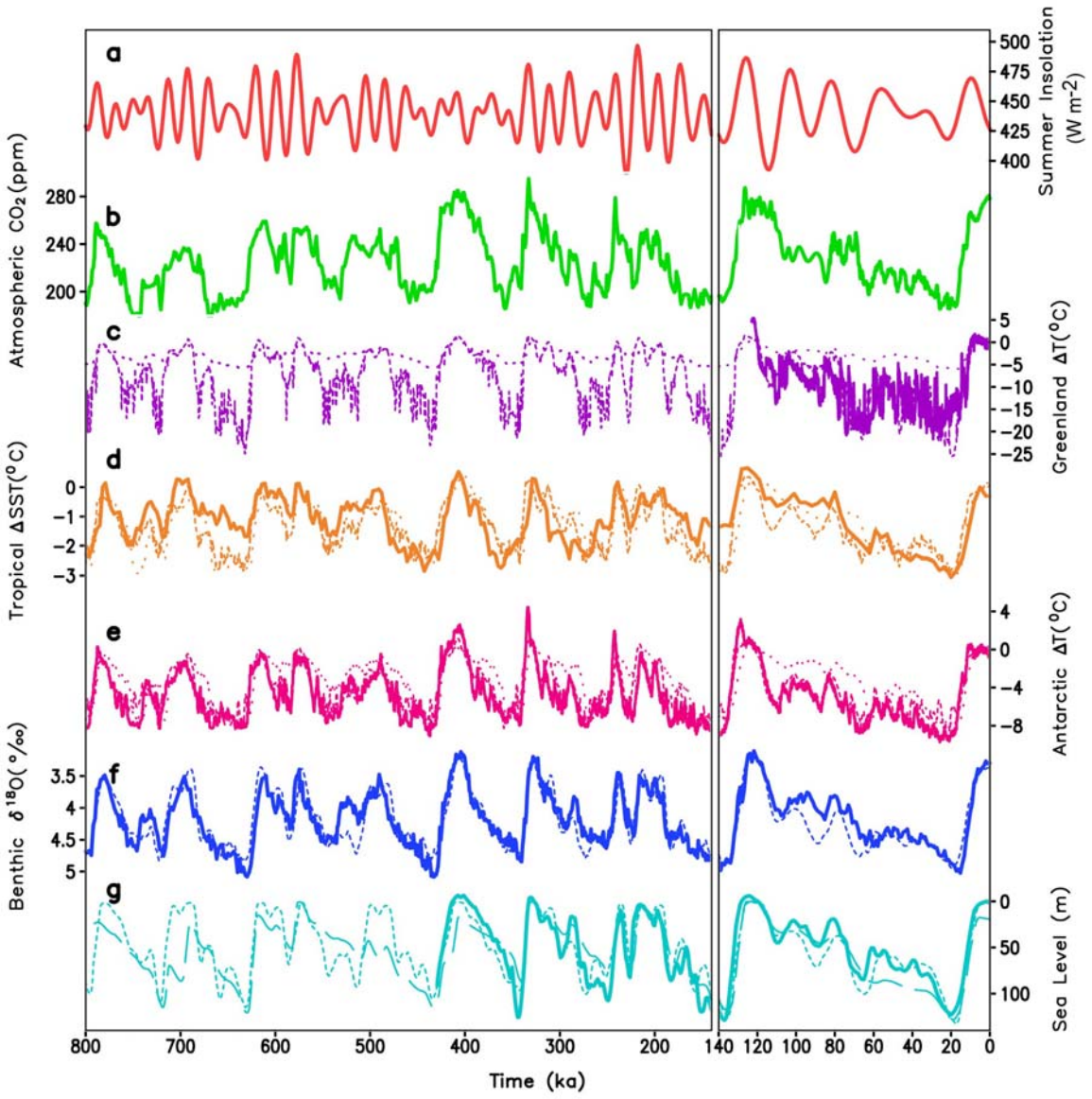

Figure 5.5: Orbital forcing and proxy records over the past 800 kyr. **a)** Maximum summer insolation at 65°N (Berger and Loutre, 1991), **b)** the atmospheric concentration of CO_2 from Antarctic ice cores (Ahn and Brook, 2008; EPICA Community Members, 2004; Petit et al., 1999), **c)** Greenland temperature reconstructed from $\delta^{18}O$ in NGRIP ice core (North Greenland Ice Core Project members, 2004), **d)** the tropical SST stack (Herbert et al., 2010), **e)** the of Antarctic temperature stack based on up to seven different ice cores (Barbante et al., 2006; Blunier and Brook, 2001; Jouzel et al., 2007; Petit et al., 1999; Stenni et al., 2011; Watanabe et al., 2003), **f)** the stack of benthic $\delta^{18}O$, a proxy for global ice volume and deep ocean temperature (Lisiecki and Raymo, 2005), **g)** the reconstructed sea level (Waelbroeck et al., 2002). Solid lines represent orbital forcing and proxy records, dashed lines depict results of simulations with climate and climate-ice sheet models forced by variations of the orbital parameters and the atmospheric concentrations of the major GHG. Short dashed line - CLIMBER-2 (Ganopolski et al., 2010), long dashed line - IcIES (Abe-Ouchi et al., 2007), dotted line - Bern3D (Ritz et al., 2011) . Note the change of the time scale at 140 ka.

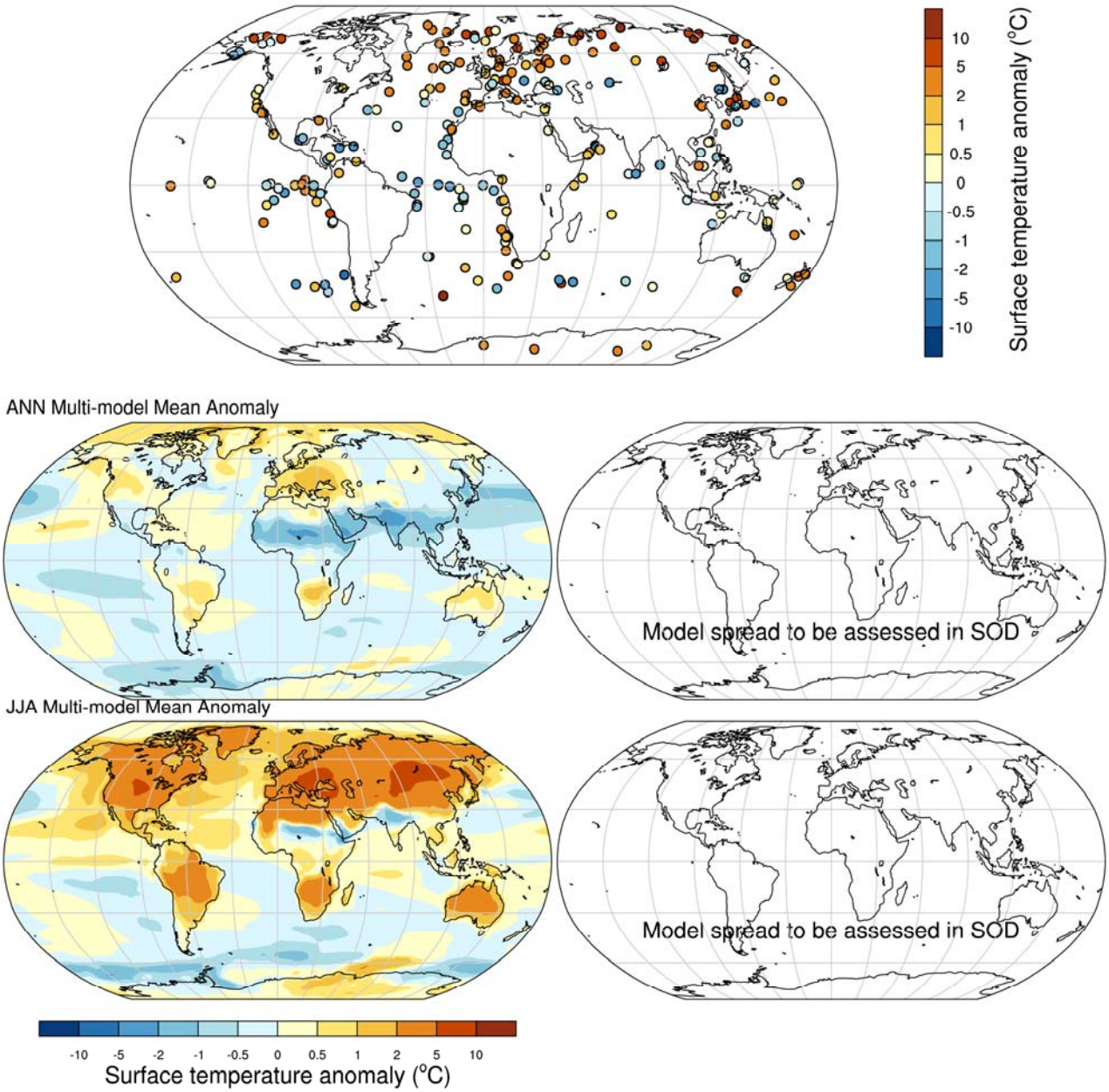

Figure 5.6: Model-data comparison of annual mean surface temperature anomalies for the Last Interglacial. Top panel are proxy data estimates of Turney and Jones (2010) and McKay et al. (2011). McKay et al.(2011) calculated an annual anomaly for each record as the average SST of the 5 kyr period centered on the warmest temperature between 135 ka and 118 ka and then subtracting the average SST of the late Holocene (5 ka to 0 ka). Turney and Jones (2010) calculated the annual temperature anomalies relative to 1961–1990 CE by averaging the LIG temperature estimates across the isotopic plateau in the marine and ice records and the period of maximum warmth in the terrestrial records. In both reconstructions the anomalies are not necessarily synchronous in time geographically. Middle and bottom panels are respectively annual and June-July-August multi-model averages, left, and standard deviations, right, of model simulations for 125ka. Two models are assessed: CCSM3 and HadCM3. [Note: more model simulations and estimate of spread are expected for the SOD].

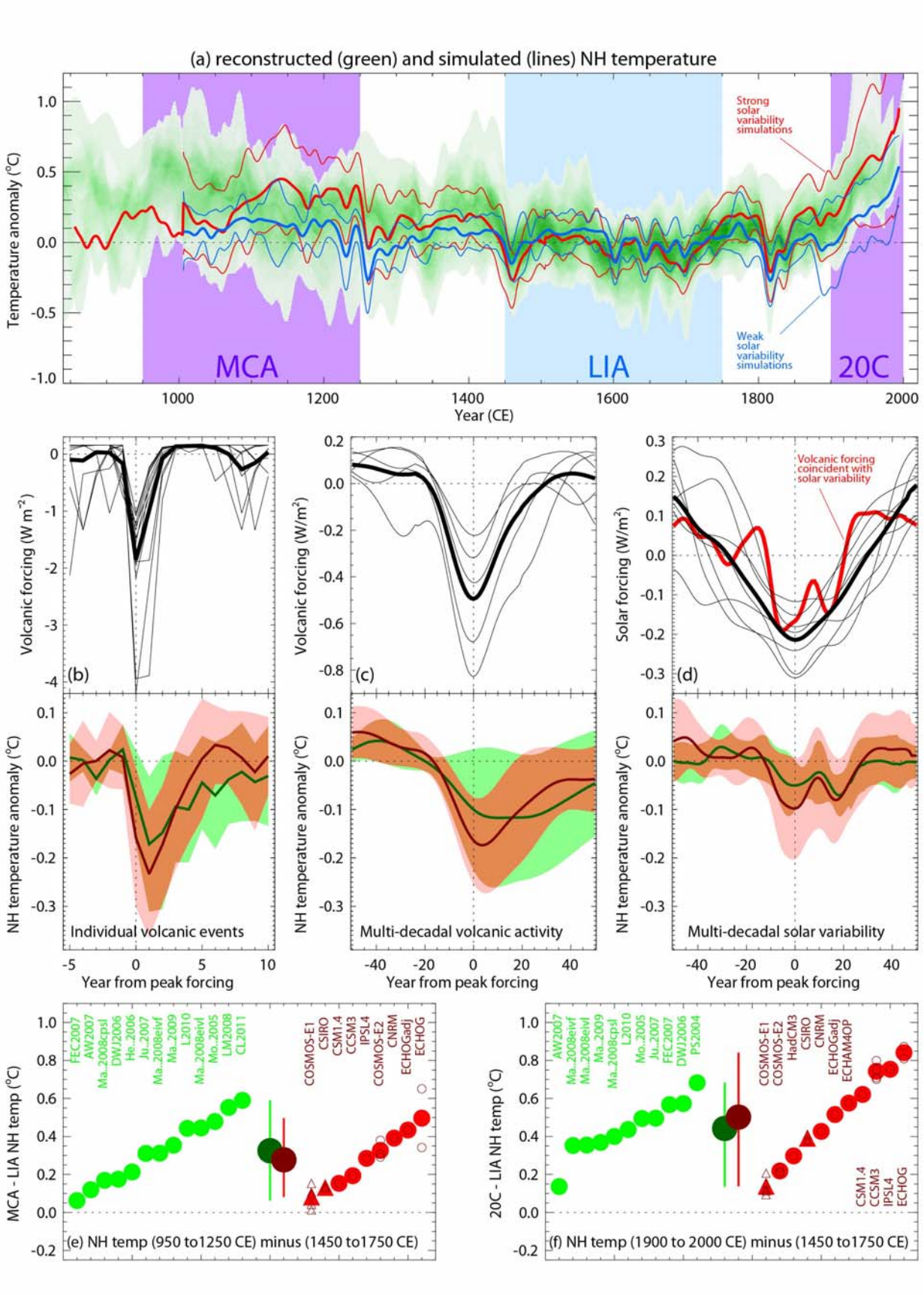

Figure 5.7: Comparisons of simulated and reconstructed NH temperature change. **a)** Simulations shown by coloured lines (thick lines: multi-model-mean; thin lines: multi-model 90% range; red/blue lines: models forced by stronger/weaker solar variability, though other forcings and model sensitivities also differ between the red and blue

groups); overlap of reconstructed temperatures shown by green shading; all data are expressed as anomalies from their 1500–1850 CE mean and smoothed. Note that some reconstructions represent a smaller spatial domain than the full NH or a specific season, while annual temperatures for the full NH mean are shown for the simulations. Superposed composites (time segments from selected periods positioned so that the years with peak negative forcing are aligned) of the forcing and temperature response to **b)** individual volcanic forcing events; **d)** multi-decadal changes in volcanic activity; **f)** multi-decadal changes in solar irradiance. Upper panels show the volcanic or solar forcing for the individual selected periods together with the composite mean (thick); in **d)**, the composite mean of the volcanic forcing (red) during the solar composite is also shown. Lower panels show the NH temperature composite means and 90% range of spread between simulations (dark red line, pink shading) or reconstructions (green line and shading), with overlap shaded in orange. Mean NH temperature difference between **e)** MCA (950–1250 CE) and LIA (1450–1750 CE) and **f)** 20th century (1900–2000) and LIA, from reconstructions (light green), multi-reconstruction mean and range (dark green), multi-model mean and range (brown), and simulations (red). Models forced by stronger/weaker solar variability are shown by circles/triangles; where an ensemble of simulations is available from one model, the ensemble mean is show in red and the individual ensemble members by brown circles. Results are sorted into ascending order and labelled. Further details are given in the supplementary material.

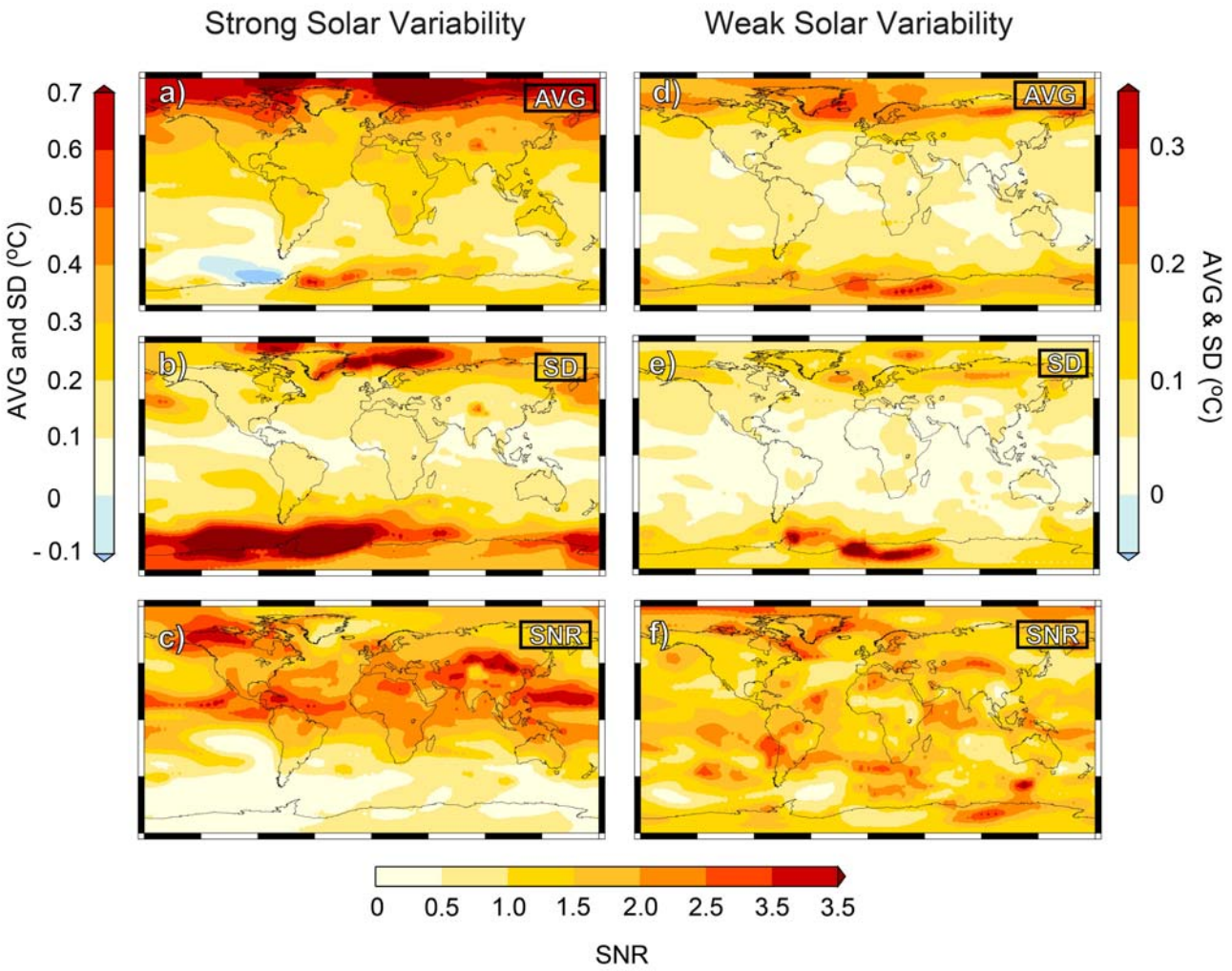

Figure 5.8: Average (AVG; a, d), standard deviation of the average (SD; b, e) and signal to noise ratio (SNR=|AVG|/SD); c, f) for the MCA-LIA annual temperature change in the ensemble of forced simulations of the last millennium produced with different Atmosphere-Ocean GCMs, both for strong (a, b, c) and for weak (d, e, f) solar forcing variability levels. For the simulations starting in 1000 CE, the period 1000 CE to 1250 CE was selected to define the MCA. 10 (11) simulations provided by 6 (2) different GCMs have been used for the strong (weak) solar forcing ensemble. The contributing models have been CCSM3, CSIRO, CSM1.4, CNRM, ECHO-G, IPSL and the MPI-ESM. A list of the model simulations involved and main characteristics is provided in the supplementary material. All simulated fields were interpolated to the smallest resolution in the ensemble (i.e., R21 for the CSIRO simulations).

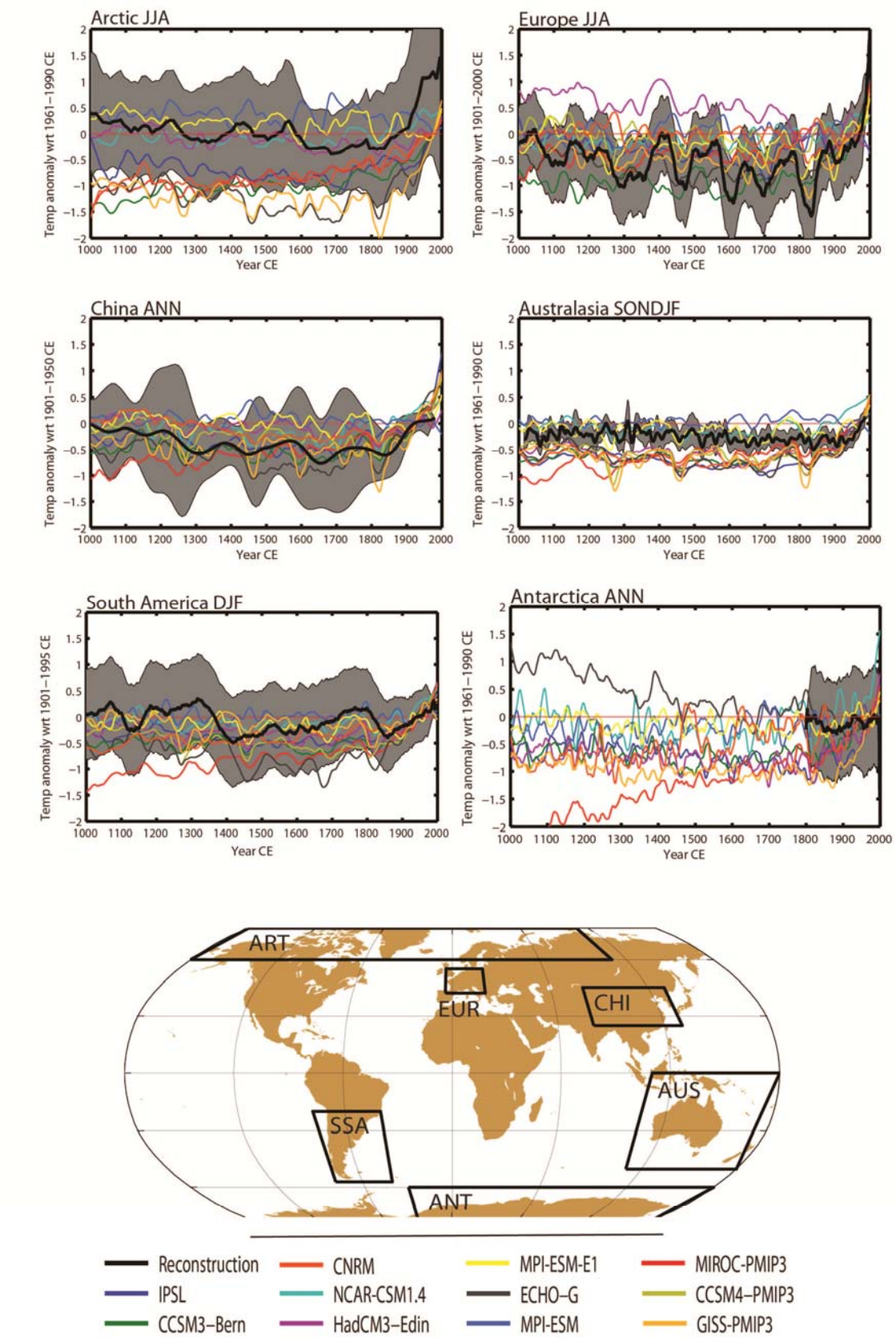

Figure 5.9: Regional temperature reconstructions, comparison with model simulations over the past millennium (1001–1999 CE). Temperature anomalies with respect to a reference period as indicated in each panel (black bold line), and uncertainty estimated provided by each individual reconstruction (gray envelope). Individual temperature anomalies from Last Millennium simulations (colors). All lines are smoothed by applying a 50 year moving average. The models

used are: Pre-PMIP3: ECHO-G (González-Rouco et al., 2006), CCSM (Ammann et al., 2007), CCSM-Bern (Hofer et al, 2011), MPI-ESM, MPI-ESM E1 (Jungclaus et al., 2010), CNRM (Swingedouw et al., 2011). PMIP3: CCSM4-NCAR (Landrum et al., submitted), GISS (Schmidt et al., 2006), HadCM3-Edin (Tett et al., 2006), MIROC-ESM (Watanabe et al., 2011). Reconstructions by region: Arctic (Kaufman et al., 2009), Europe (Büntgen et al., 2011), China (Ge et al., 2010a), South America (Neukom et al., 2011), Antarctica (Schneider et al., 2006), Australasia (Gergis et al., submitted).

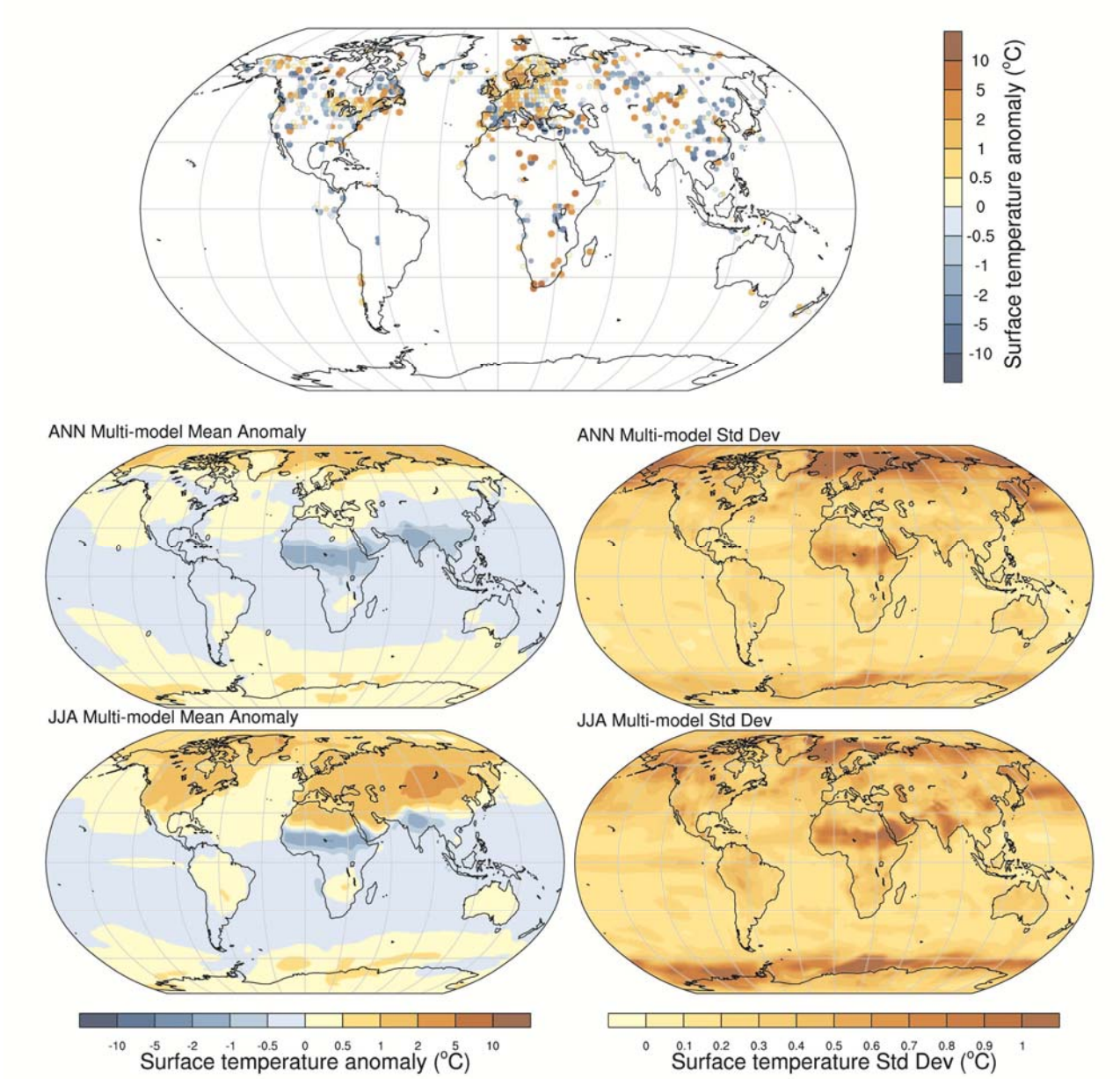

Figure 5.10: Model-data comparison of surface temperature anomalies for the mid-Holocene (about 6 ka). Top panel are proxy data estimates from pollen-based reconstruction of Bartlein et al. (2010) and the GHOST global database for alkenone-derived SST records (Leduc et al., 2010). Large symbols are used to indicate grid points with significant anomalies (i.e., those that exceed twice the pooled standard error of the reconstructions) while small symbols indicate anomalies that are not significant by this measure. Middle and bottom panels are respectively annual and June-July-August multi-model averages, left, and standard deviations, right, of model simulations. Eight models are assessed: AWI-COSMOS, BCC-CSM-1, CCSM4, CNRM-CM5, KNMI-ECEarth, MPI-ESM, MRI-CGCM3, and UBRIS_HadCM3_MOSES2.1.

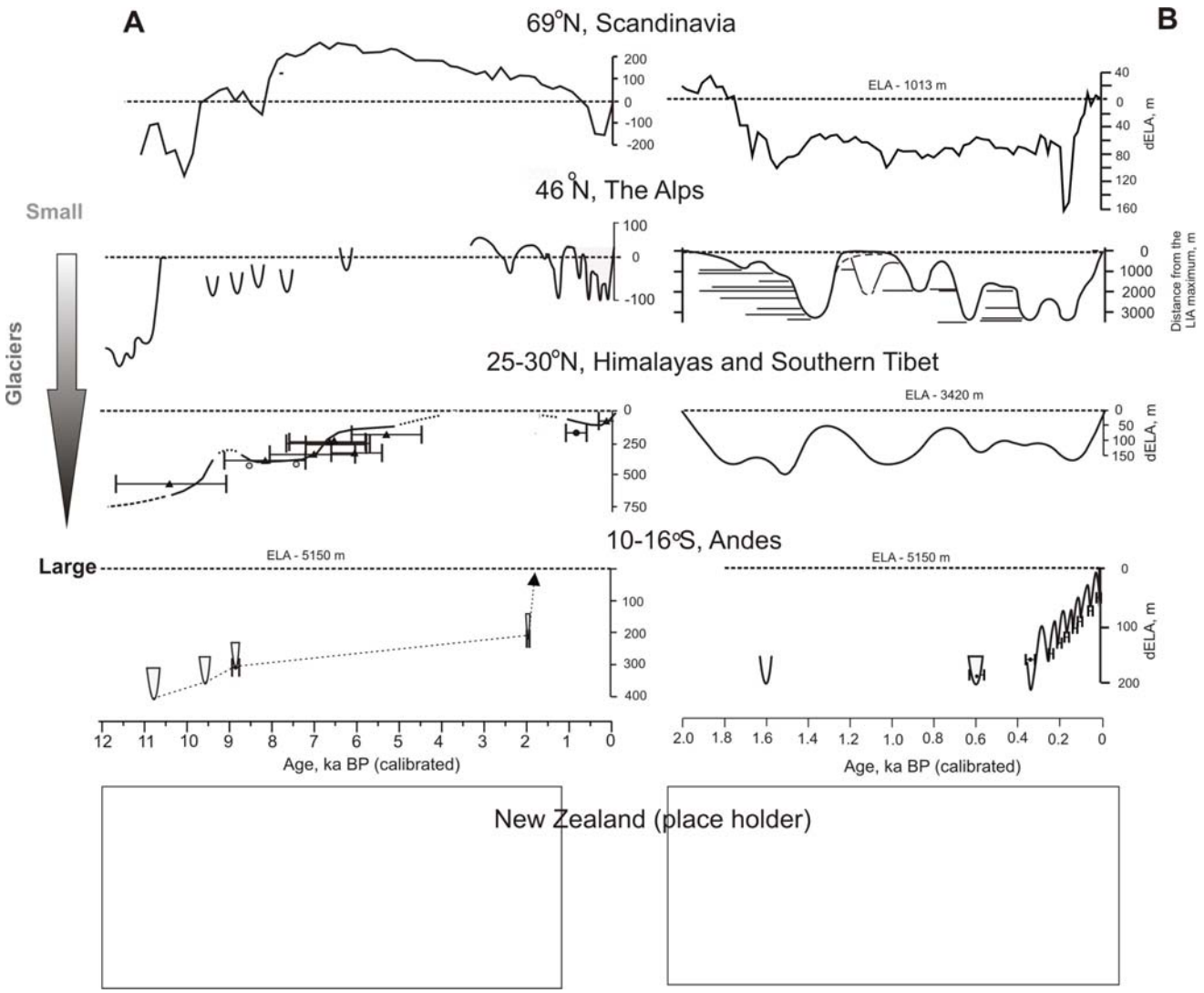

Box 5.2, Figure1: Time-distance diagrams for glaciers front and (or) of equilibrium-line altitude (ELA) variations. The selected series are well chronologically constrained and reptersent different climatic regions in the Northern and Southern Hemispheres. **a)** The Holocene – Northern Scandinavia. Depression of equilibrium-line altitude (dELA) from Northern Folgefonna based on lacustrine sediments (Bakke et al., 2005a; Bakke et al., 2005b; Bakke et al., 2010; Nesje, 2009). The Alps. Summary of glacier variations (Ivy-Ochs et al., 2009). Himalaya, Central Nepal. dELA defined from the position of moraines dated by exposure rates with dating uncertainties (Gayer et al., 2006). Bolivian Andes. ELA of the Telata glacier from ^{10}Be dates (Jomelli et al., 2011). **b)** Last 2000 years – ELA variations in Northern Norway based on the bulk density sediment record (Bakke et al., 2005b). The Alps. Fluctuations of the Great Aletsch glacier. Bars - life-time of the fossil trees (Holzhauser et al., 2005). Southern Tibetan Plateau. Summary of glacier variations (after Yang et al., 2003; Yang et al., 2008). Glacial advances in the tropical Andes (Peru and Bolivia) with dating uncertainties (after Jomelli et al., 2008; Jomelli et al., 2009).

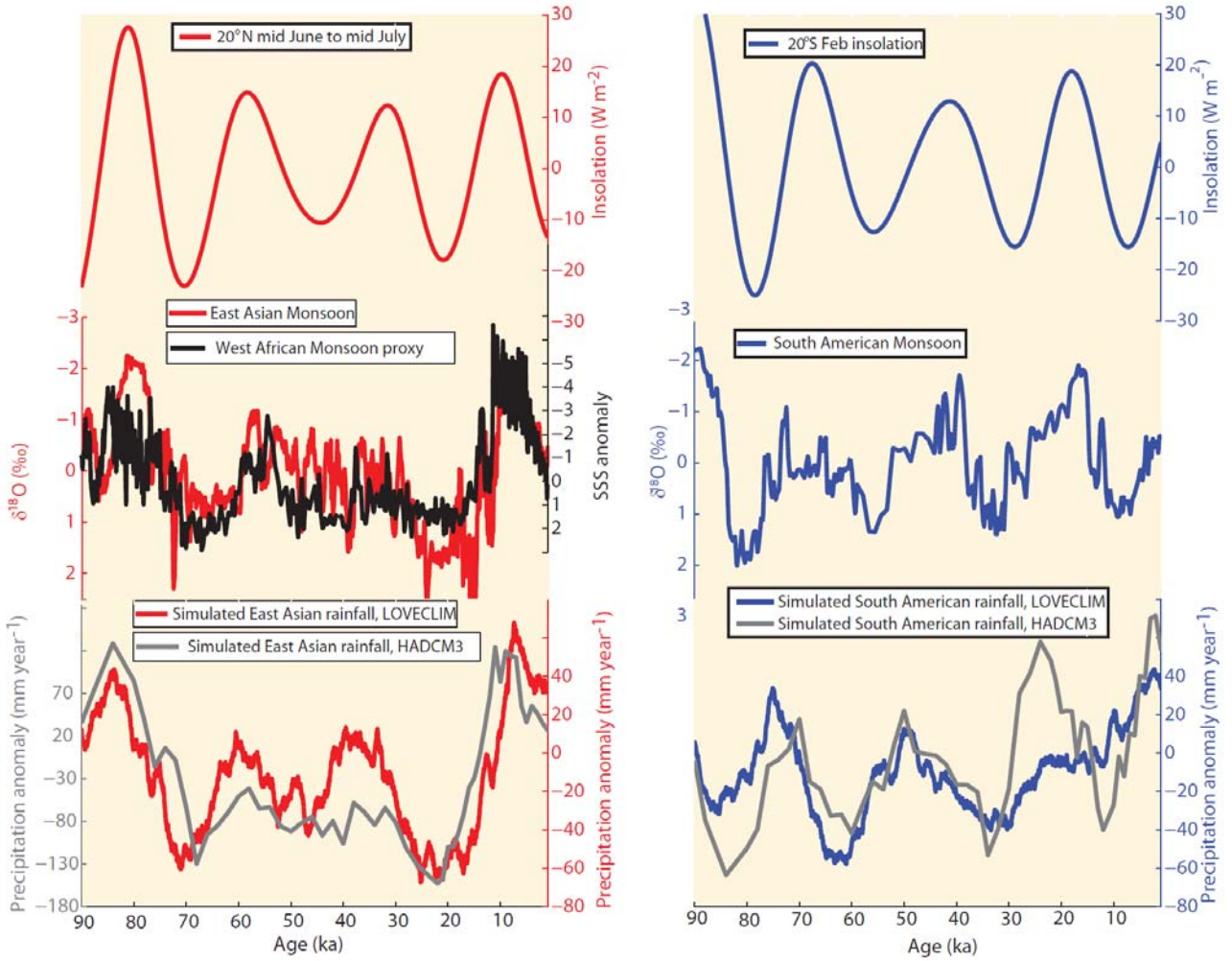

Figure 5.11: Millennial and orbital scale variability of global Monsoon systems: upper left: Boreal summer insolation changes at 20°N; middle left: East Asian Monsoon record compiled from the Hulu cave $\delta^{18}O$ anomaly record (Wang et al., 2001) and the Sanbao $\delta^{18}O$ anomaly cave records (Wang et al., 2008) in China (red) (the Hulu data were reduced by 1 ‰ to account for a regional offset with the Sanbao cave record), West African Monsoon proxy from salinity reconstructions in the Gulf of Guinea (Weldeab et al., 2007); lower left: simulated annual mean rainfall anomalies in east Asia (covering the grid boxes of Hulu and Sanbao cave) from two climate model simulations covering the last 120 kyr, conducted with the orbitally-accelerated LOVECLIM model (red)(Timm et al., 2008) and a series of climate snapshot experiments with the HADCM3 model (gray)(Singarayer and Valdes, 2010); upper right: February insolation at 20°S; middle right: $\delta^{18}O$ anomalies from Botuvera speleothem data (Brazil) (Cruz et al., 2009), characterizing South American Monsoon changes; lower right: same as lower left, but for simulated rainfall anomalies in Brazil (covering the grid boxes of the Botuvera cave). Note, that $\delta^{18}O$ anomalies in speleothems represent a mixture of local rainfall changes and changes in the source region of the moisture (LeGrande and Schmidt, 2009; Pausata et al., 2011).

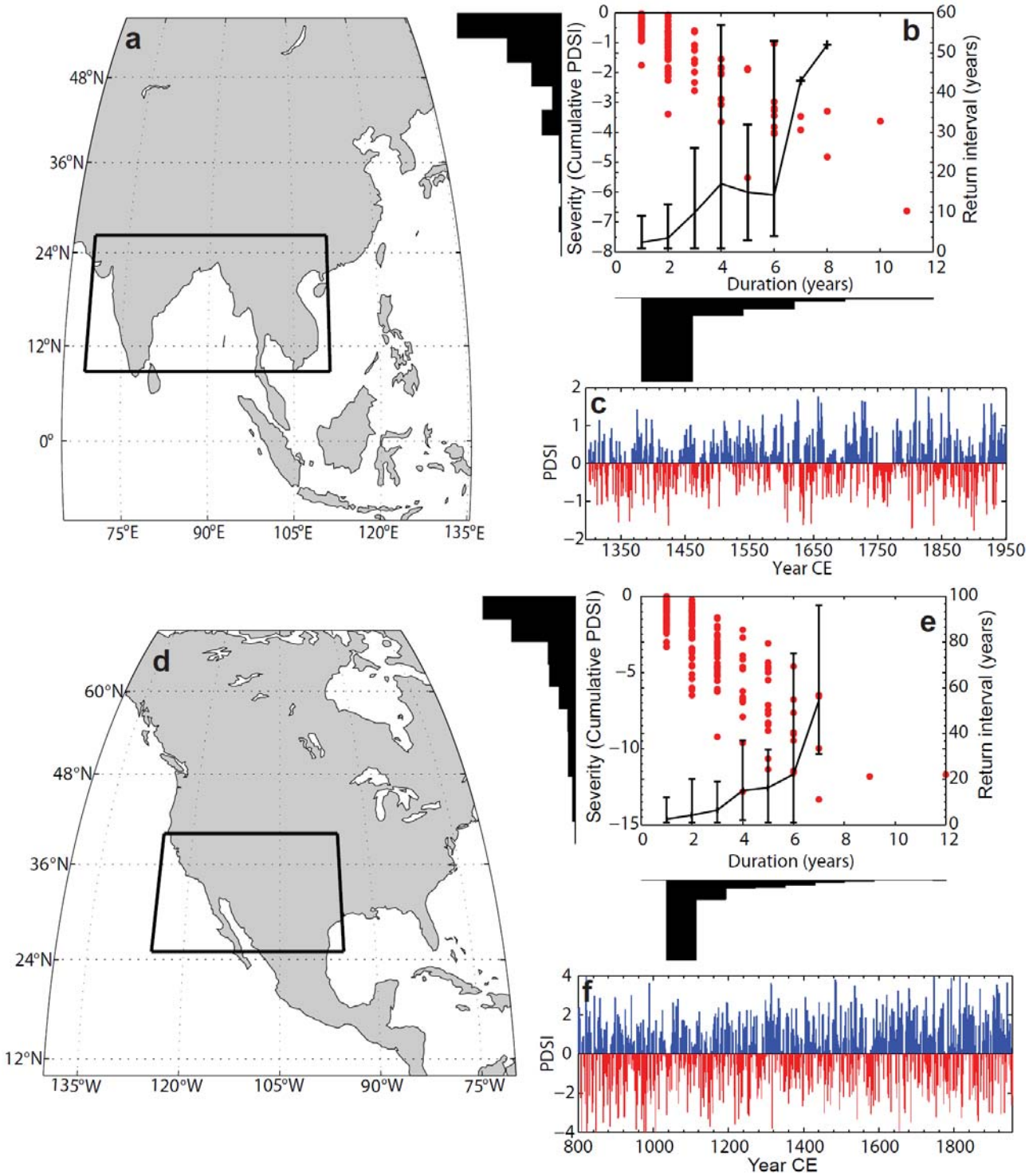

Figure 5.12: Severity, duration, and frequency of droughts in the Monsoon Asia (Cook et al., 2010) and North American (Cook et al., 2004) Drought Atlases. The box in **a)** and **d)** indicates the region over which the tree ring reconstructed Palmer Drought Severity Index (PDSI) values have been averaged to form the regional mean time series in **c)** and **f)**, respectively. The covariance of drought (PDSI < 0) duration and cumulative severity is shown in panels **b)** and **e)**, along with the respective frequency histograms for each quantity. Not shown in **b)** is an outlier with an apparent duration of 24 years, corresponding to the 'Strange Parallels' drought identified in Cook et al. (2010). Return intervals for droughts of given durations are estimated as the mean interval between their occurrence, with minimum and maximum intervals indicated, and are plotted in the same panels. No error bars are present if there is only a single observation of a drought of that duration. The period of analysis is restricted to the period 1300 CE to 1950 CE for Monsoon Asia, following Cook et al. (2010), and from 800 CE to 2006 CE for North America, following Cook et al. (2004).

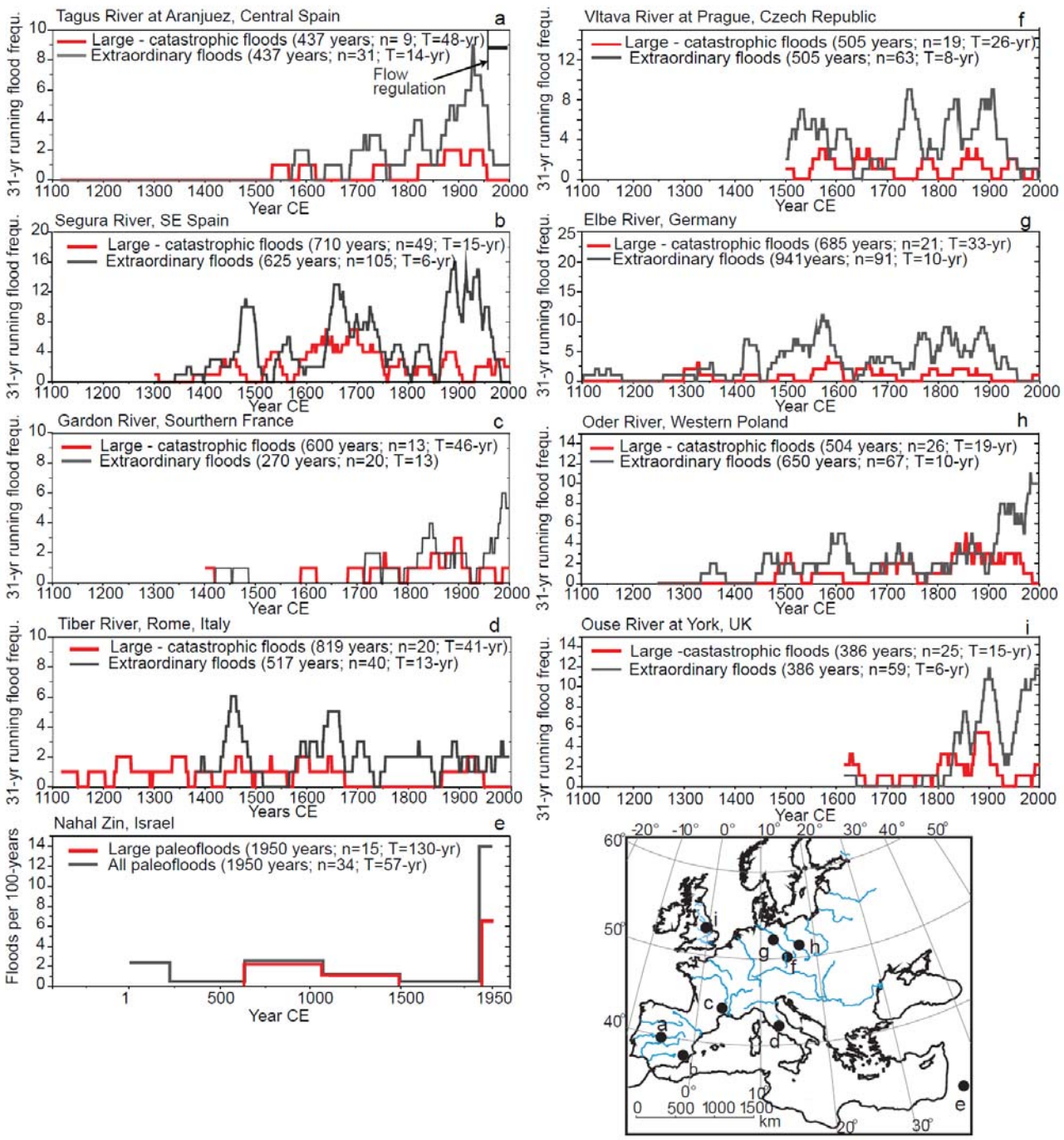

Figure 5.13: Flood frequency from paleofloods, historical and instrumental records in selected European rivers. Number of floods that exceeded a particular discharge threshold or flood level within a centred window of 31-years. Flood categories include large-catastrophic floods (CAT) that produced high discharge or severe damages, and extraordinary floods (EXT) causing inundation of the floodplain with moderate to minor damages. Legend at each panel indicates for each category the period of record, number of floods, and the average occurrence interval (in years). **a)** Tagus River combined paleoflood, historical and instrumental flood records from Aranjuez with thresholds of 300–700 m^3s^{-1} (EXT) and >700 m^3s^{-1} (CAT) (Benito et al., 2003a; Benito et al., 2003b). **b)** Segura River Basin (SE Spain) documentary and instrumental records at Murcia (Barriendos and Rodrigo, 2006; Barriendos and Martin-Vide, 1998; Machado et al., in press). **c)** Gardon River combined discharges from paleofloods at La Baume (Sheffer et al., 2008), documented floods (since the 15th century and historical and daily water stage readings at Anduze (1741 CE to 2005 CE; Neppel et al., 2010). Discharge thresholds referred to Anduze are 1000–3000 m^3s^{-1} (EXT) and >3000 m^3s^{-1} (CAT). At least five floods larger than the 2002 CE-flood (the largest in the gauged record) occurred in the period 1400 CE to 1800 CE (Sheffer et al., 2008). **d)** Tiber River floods in Rome from observed historical stages (since 1100 CE; Calenda et al., 2005; Camuffo and Enzi, 1996; Camuffo et al., 2003) and continuous stage readings (1870 CE to present) at the

Ripetta landing (Calenda et al., 2005). Discharge thresholds set at 2300–2900 m^3s^{-1} (EXT) and >2900 m^3s^{-1} (CAT; >17 m stage at Ripetta). Recent flooding is difficult to evaluate in context due to river regulation structures. **e)** Nahal Zin (Israel) 2000-year paleoflood record, combined with historical data (1935 CE to 1946 CE) and instrumental records (from 1951 CE to present) after Greenbaum et al. (2000). Discharge threshold for large floods was set at 400 m^3s^{-1} (CAT). Large floods occurred at 1.38 ± 0.88 ka and the last 60 years, the former is related with regional humid conditions as recorded in high Dead Sea levels (Greenbaum et al., 2006). **f)** Vltava River combined documentary and instrumental flood record at Prague (Brázdil et al., 2005) discharge thresholds: CAT, flood index 2 and 3 or discharge >2900 m^3s^{-1}; EXT flood index 1 or discharge 2000–2900 m^3s^{-1}. **g)** Elbe River combined documentary and instrumental flood record (Mudelsee et al., 2003). Classes refer to Mudelsee et al. (2003) strong (EXT) and exceptionally strong (CAT) flooding. **h)** Oder River combined documentary and instrumental flood record (Mudelsee et al., 2003). **i)** River Ouse at York combined documentary and instrumental flood record (Macdonald and Black, 2010). Discharge thresholds for large floods was set at 500 m^3s^{-1} (CAT) and for ordinary floods at 350–500 m^3s^{-1} (EXT). The map shows the location of rivers used in the flood frequency plots.

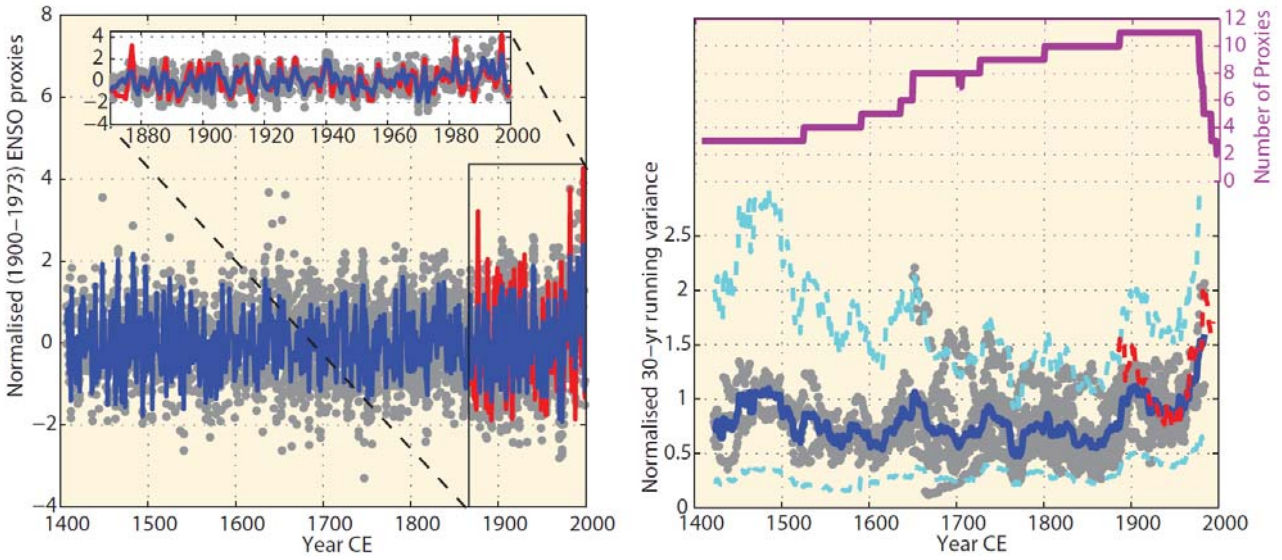

Figure 5.14: Compilation of the different ENSO reconstructions. Left panel: Grey dots indicate the data points from 11 individual ENSO reconstructions (McGregor et al., 2010), (Li et al., 2011) normalised through the 1900 CE to 1978 CE period, with the reconstruction ensemble mean displayed in blue. The underlying red line is Niño 3 region SSTA obtained from the HadISST data set (Rayner et al., 2003); Right panel: Grey dots indicate the 30-year running variance of each of the 11 different ENSO reconstructions with the ensemble mean running variance displayed in blue, while the overlying dashed red line is the 30-year running variance of the normalised HadISST Niño 3 region SSTA. The dashed cyan lines indicate the 10 and 90 percentiles obtained from a χ^2 distribution using the number of available ENSO proxies shown by the purple line.

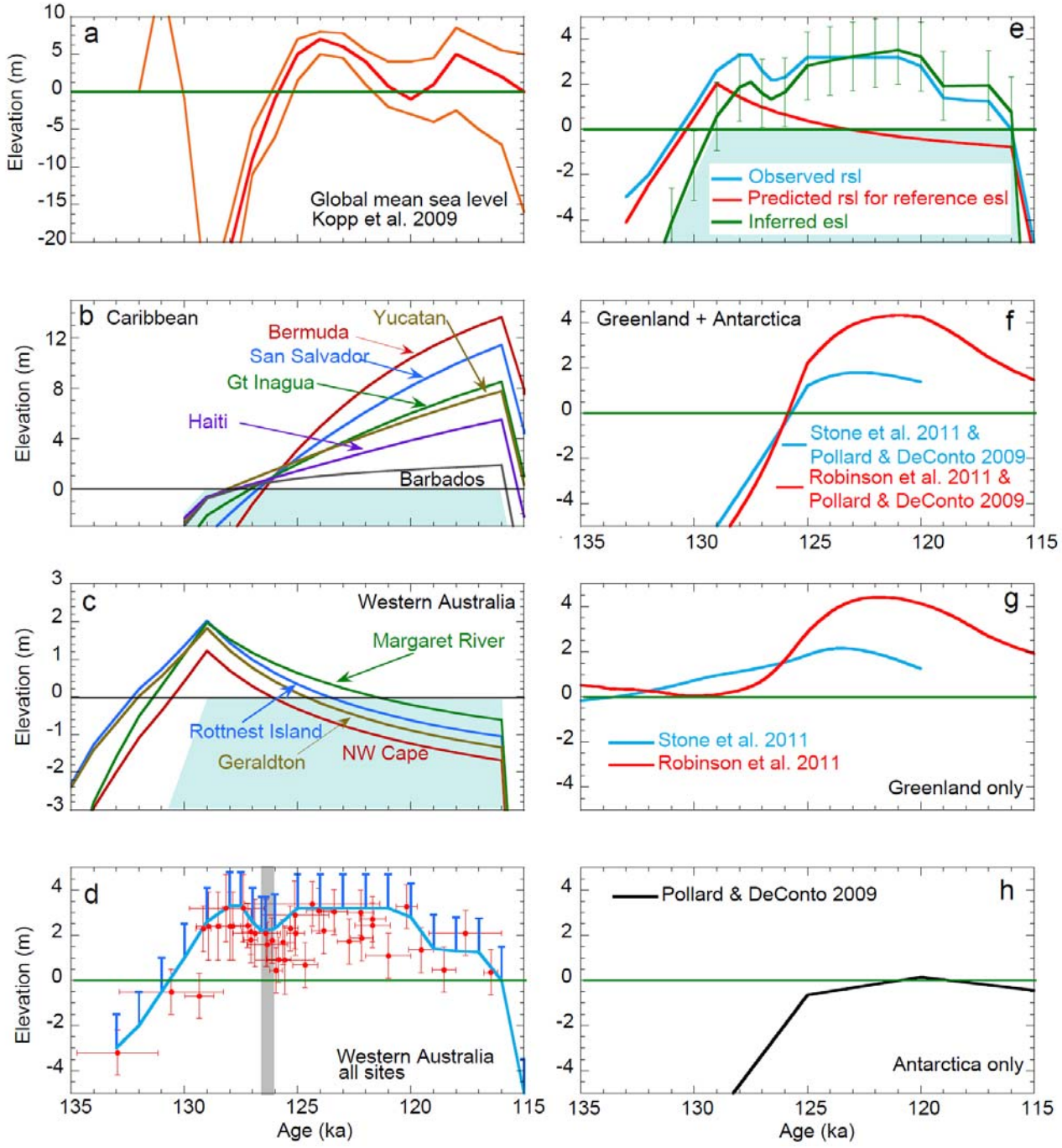

Figure 5.15: Sea level during the Last Interglacial. **a)** The estimate of global mean sea level by Kopp et al. (2009) (red line). The orange lines correspond to the 16th and 84th percentiles. **b)** Predicted sea levels for selected sites in the Caribbean and North Atlantic on the assumption that ice volumes during the interval from 129 ka to 116 ka are equal to those of today and isostatic effects (Lambeck et al., in press), displaying the spatial variability that can be expected across the region. These predictions are strongly dependent on the ice loads over North America both before and after the interglacial period as well as on mantle rheology and observations from these sites provide more information on ice histories than on the global sea level function. **c)** Same as b) but for different sites along the Western Australia coast. The dependence on details of the ice sheet and on earth-model parameters is less important at these sites than for those in b). Thus data from these locations, assuming tectonic stability, is more appropriate for estimating LIG ice volumes. **d)** Local LIG relative sea level reconstructions from Western Australia based on coral elevations and closed-system U-Th ages that pass diagenetic screening. All results are for in-situ samples and *Porites* species. Age error bars correspond to 2 standard deviation uncertainties. Ages are based on the assumption of closed system behaviour and the decay constants of Cheng et al. (2000), $\delta^{234}U$ values within 5‰ of modern sea water, ^{232}Th concentrations less than 2 ppb, and calcite < 2%. All elevations have been normalised to the upper growth limit of corals corresponding to mean low water spring or mean low sea level. The Western Australian reef locations contributing to the result in a) are distributed along almost 1300 km of coastline and experience different responses of the land and sea surfaces to changes in glaciation

before and after the Last Interglacial period because of different coastal geometries and different distances from the former ice sheets (c). The blue line indicates the simplest interpretation of local sea level consistent with reef stratigraphy and should be considered as lower limits by an amount indicated by the blue upper limit error bars. The sea level oscillation at about 126 ka to 125 ka (vertical gray band) is consistent with observed stratigraphy and geochronology at sites (e.g., Yukutan, Bahamas) when data is reduced using the same criteria (from Dutton and Lambeck , submitted). The differences from a) in the timing of the start and end of the interglacial interval, as well as in the timing of the lowstand in the middle of the interval may be a consequence of different assumptions used in deriving the model ages. The higher amplitudes in a) are a consequence of including geomorphological information that is poorly constrained in age and data from areas that may be subject to tectonics. **e)** The Western Australian evidence (thick blue line) from d) compared the model-predicted result (red line) from c) for a reference site midway between the northern and southern most localities, the reference ice volume model for the LIG interval (the blue shading) and earth rheology and ice sheet parameters based on rebound analyses from different regions spanning the interval from Marine Isotope Stage 6 to the present (c.f. Lambeck et al., 2006). The difference between the observed and predicted functions provides an estimate of the global mean sea level (green line). Uncertainties in this estimate include the observational uncertainties from d) and estimates of the model uncertainties. **f)** Ice sheet model estimates for global mean sea level during the Last Interglacial for Greenland and Antarctica based on (red curve) the Potsdam CLIMBER intermediate complexity model (Robinson et al., 2011) plus the Antarctic model of Pollard and DeConto (2009), and (blue curve) the Hadley Centre GCM (Stone et al., submitted) with the same Antarctic model. **g)** Same as f) but for Greenland only. **h)** Same as f) but for the Antarctica only. Both east and west Antarctica are included in this model but nearly all of the melt is from West Antarctica.

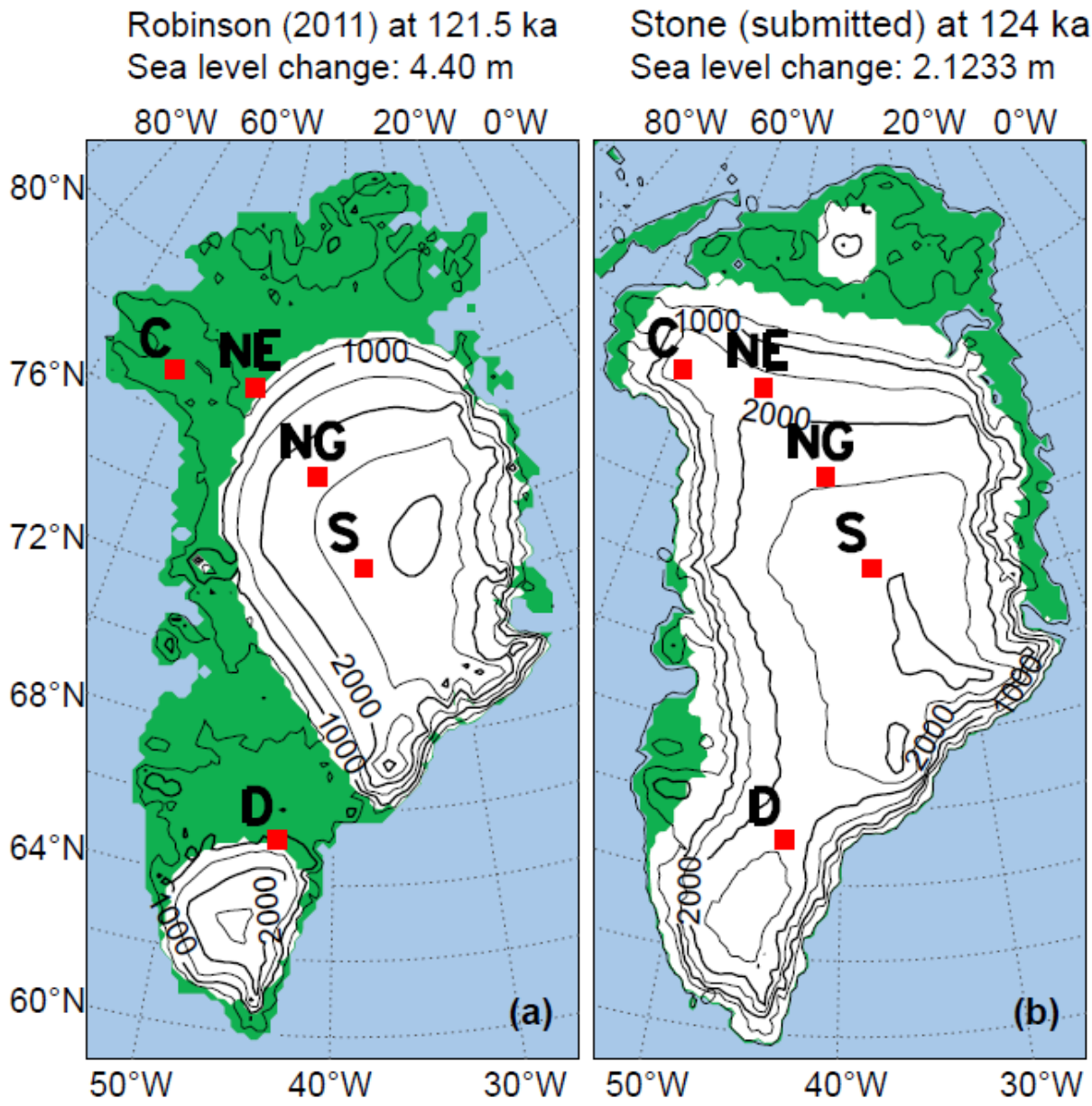

Figure 5.16: [PLACEHOLDER FOR SECOND ORDER DRAFT: more results for climate-ice sheet model results will be included] Modelled Greenland ice sheet distribution at the Last interglacial when the ice sheet volume is the minimum for each model. **a)** For the case of Robinson et al (2011) as their "best guess" and **b)** for the case of Stone et al (submitted) as their "best guess" with contour interval of 500 meters to show the altitude. Red points in the figures show the locations of ice core drilling sites: Dye3, GRIP/GISP (summit), NGRIP, NEEM, Camp Century from the south to the north.

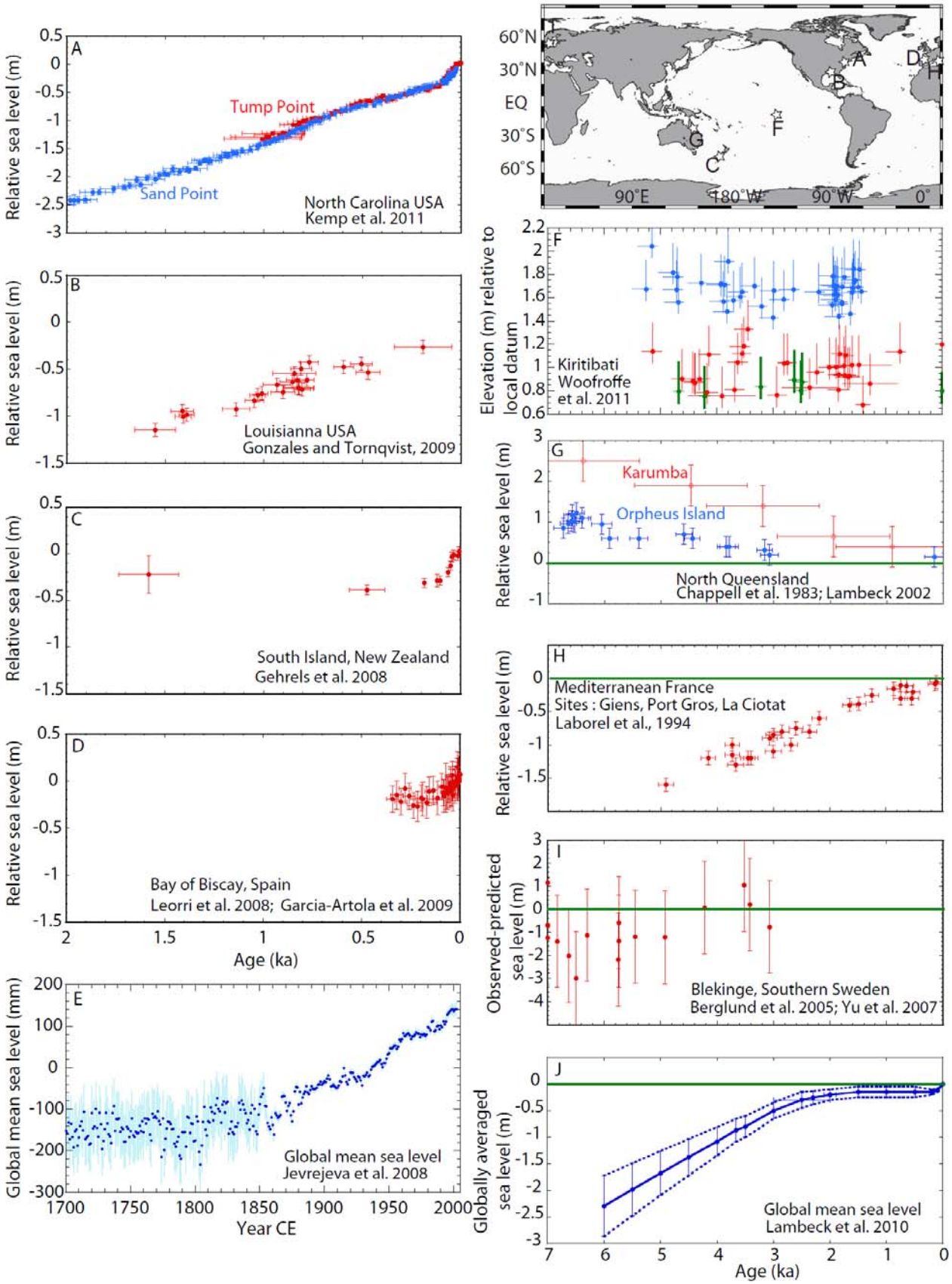

Figure 5.17: Sea level change during recent and late Holocene time. **a-d)** High resolution relative sea level results from saltmarsh data at representative sites, without corrections for glacial isostatic movement of land and sea surfaces. Locations are given on the map. The North Carolina (a) result is representative of other North American Atlantic coast locations (Kemp et al., in press). The rate of change occurring late in the 19th century are seen in all high resolution

saltmarsh records – e.g., (c) Gehrels et al. (2008); (d) Garcia-Artola et al. (2009); Leorri et al. (2008) that extend into modern time and is consistent with Roman archaeological evidence (Lambeck et al., 2004). The oscillation in sea level at about 1000 CE seen in the North Carolina record occurs in some (González and Törnqvist, 2009; van de Plassche et al., 1998) but not all records (c.f., Gehrels et al., 2011; Kemp et al., in press). **e)** Estimates of global sea level change from the instrumental record (Jevrejeva et al., 2010). **f-i)** Observed lower resolution records, without isostatic corrections except for Blekinge (i) where the isostatic signal dominates the observed sea level change (Yu et al., 2007), back to 7 ka. The Kiritibati result (f) is for three different locations on the island with each group referred to a locxal height datum [PLACEHOLDER FOR THE SECOND ORDER DRAFT: the final panel will have the separate records from the three microatoll fields reduced to a common datum]. The vertical axis for North Queensland (g) and Mediterranean France (h) correspond to relative sea level with the latter being for three nearby locations for which differential isostatic effects are less than the observational errors (Lambeck and Bard, 2000). Accuracy estimates are discussed in the original papers and include height uncertainties arising from the measurements themselves, from relating the measurement to mean sea level, and, in the case of (i) from the isostatic correction. **j)** Estimates of global mean sea level for the last 6 kyr (j) with the contributing records corrected for the isostatic effects at each location (Lambeck et al., 2010b).

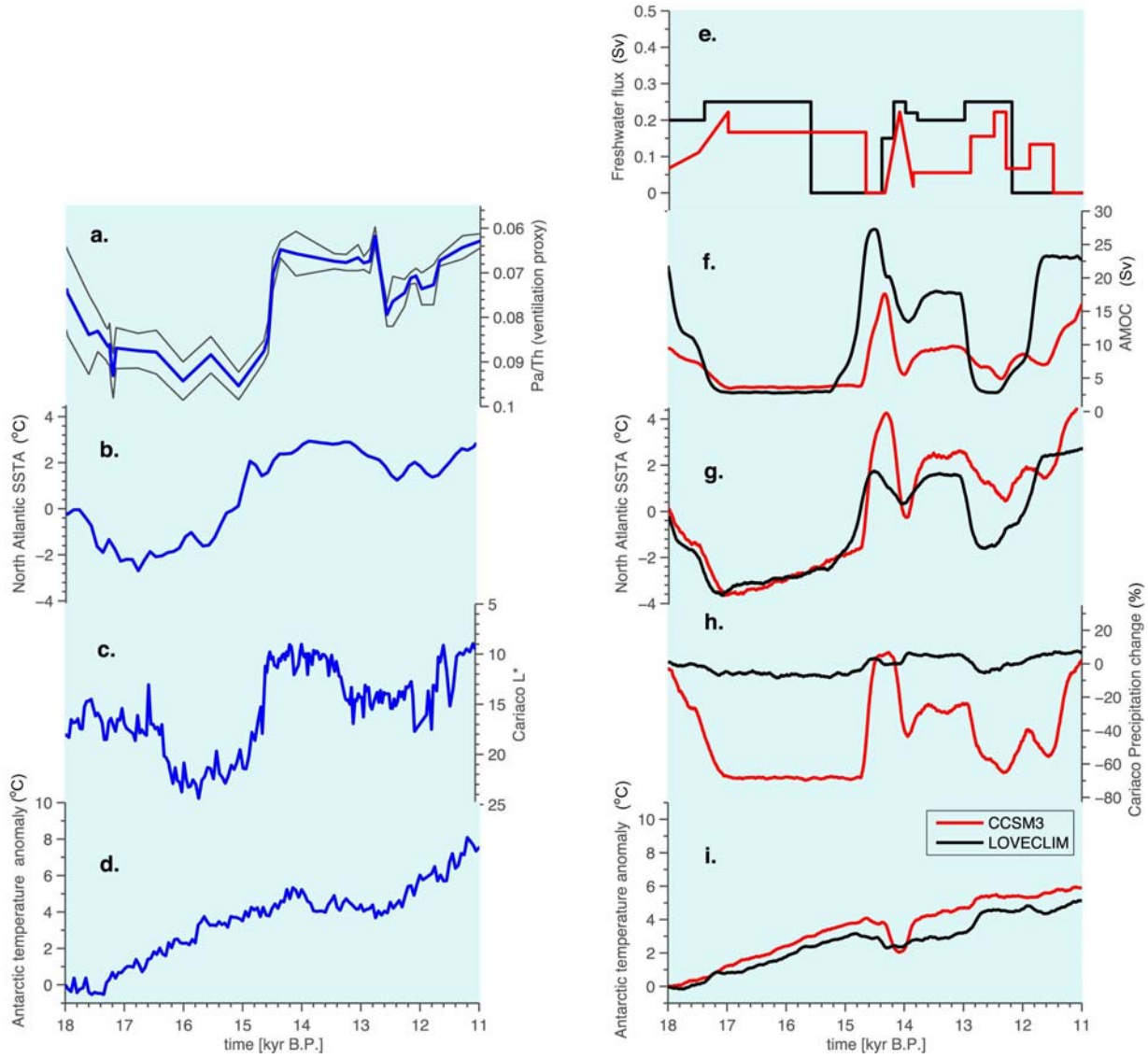

Figure 5.18: Comparison of paleo proxy data for the last glacial termination (left panels) and 3 transient paleo climate model simulations (right panels) for the period from 18 ka to 11 ka (Liu et al., 2009b; Menviel et al., 2011). **a)** Pa/Th isotope ratio (solid), a proxy for ocean ventilation, from an Atlantic sediment core with uncertainty range (dashed) (McManus et al., 2004); **b)** Composite of Alkenone based SST reconstructions from the Portugese margin in the East Atlantic using cores MD01-2443 (Martrat et al., 2007) and SU8118 (Bard et al., 2000), linearly interpolated onto an equidistant 100 year time grid; **c)** Reflectance of Cariaco sediment core, a proxy for rainfall (Peterson et al., 2000); **d)** Reconstructed Antarctic temperature anomaly stack, relative to 18 ka and based ice core data EPICA Dome C (Jouzel et al., 2007), Dome Fuji (Watanabe et al., 2003), Vostok (Petit et al., 1999), Talos (Stenni et al., 2011), EPICA Dronning Maud Land (Barbante et al., 2006), Byrd (Blunier and Brook, 2001), Law Dome (Morgan et al., 2002); **e)** North Atlantic freshwater forcing applied to the transiently forced CCSM3 (red) (Liu et al., 2009b), and LOVECLIM (black) (Menviel et al., 2011) climate models to mimic millennial-scale variability during the last glacial termination. Both model simulations apply time-varying GHG, orbital and ice sheet forcing; **f)** Simulated maximum of the meridional streamfunction in the North Atlantic [1Sv = 10^6 m^3s^{-1}]; **g)** Simulated Northeastern Atlantic SST anomalies relative to 18 ka averaged over the ocean grid points in the region 15°W–10°W, 36°N–42°N; **h)** Simulated changes in precipitation in percentage, relative to 18 ka in the Cariaco area (8°N–13°N, 67°W–63°W); **i)** Simulated Antarctic continent temperature anomalies relative to 18 ka.

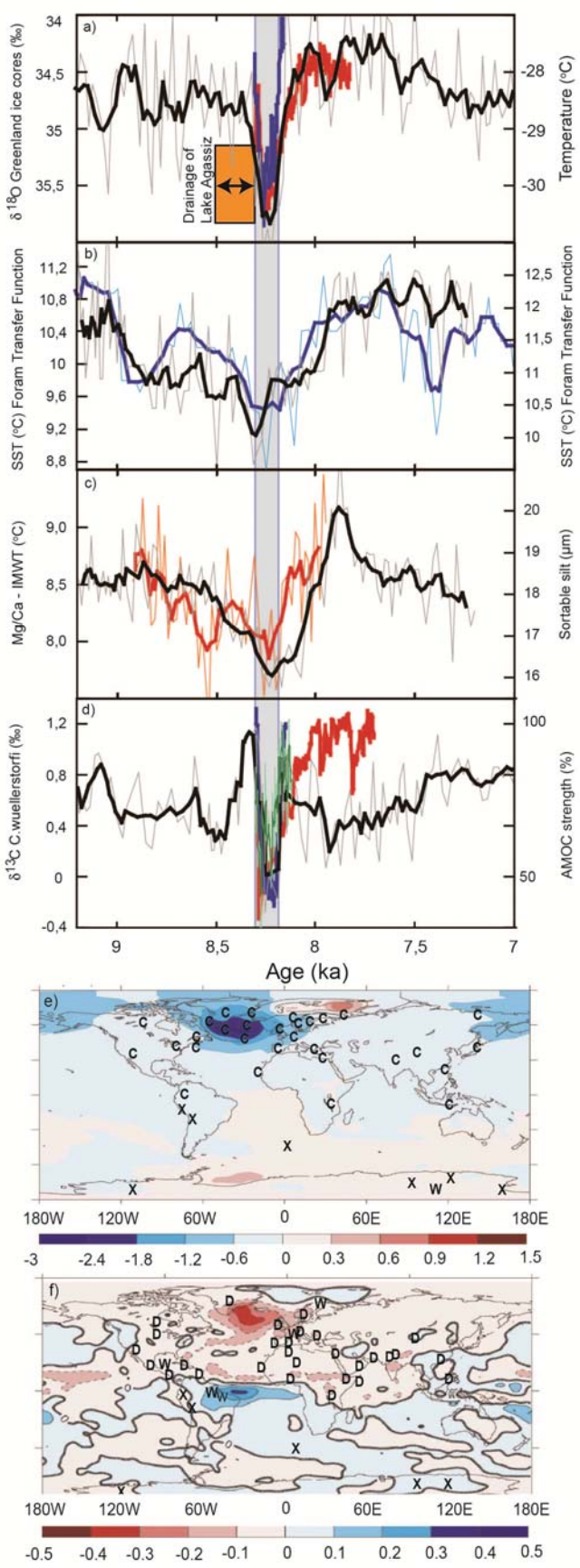

Figure 5.19: Compilation of selected paleoenvironmental and climate model data for the 8.2 ka event documenting temperature and ocean circulation changes around the event and the spatial extent of climate anomalies following the event. Published age constraints for the period of release of freshwater from glacier lakes Agassiz and Ojibway are

bracketed in a). Vertical grey bar denotes the main cold event as found in Greenland Ice core records (Thomas et al., 2007). **a)** Black curve: NorthGrip $\delta^{18}O$ (temperature proxy) from Greenland Summit. Red curve: Simulated Greenland temperature in an 8.2 ka event simulation with the ECBilt-CLIO-VECODE model (Wiersma et al., 2011). Blue curve: Simulated Greenland temperature in an 8.2 event simulation with the CCSM3 model (Morrill et al., in press). **b)** North Atlantic/Nordic Seas SST-reconstructions, age models are aligned on the peak of the cold-event (less than 100-year adjustment). Blue curve: Nordic Seas (Risebrobakken et al., 2011). Black curve: Gardar Drift south of Iceland (Ellison et al. 2006). **c)** Deep- and intermediate water records. Black curve: Sortable silt record (overflow strength proxy) from Gardar Drift south of Iceland (Ellison et al., 2006), Atlantic intermediate water temperature reconstruction (Bamberg et al., 2010). **d)** Black curve: $\delta^{13}C$ (deep water ventilation proxy) at 3.4 km water depth south of Greenland (Kleiven et al., 2008). Age model is aligned on the minimum overflow strength in c) (less than 100-year adjustment). Modelled change in the strength of the AMOC: Green curve: An 8.2 ka event simulation with the GISS model (LeGrande et al., 2006). Red curve: An 8.2 ka event simulation with the ECBilt-CLIO-VECODE (v. 3) model (Wiersma et al., 2011). Blue curve: An 8.2 ka event simulation with the CCSM3 model (Morrill et al., in press). **e)** Spatial distribution of the ensemble mean annual mean surface temperature anomaly (°C) from a multi-model water housing experiment with 0.1 Sv freshwater forcing in the NW Atlantic (Stouffer et al., 2006). Paleoclimate data from records resolving the 8.2 ka event are plotted with symbols: C=cold anomaly, W=warm anomaly, X=No significant anomaly. Main data sources: (Wiersma et al., 2011), Morrill et al. 2011 with supplements (complete literature list in supplementary information). **f)** Spatial distribution of the ensemble mean annual mean precipitation anomaly (mm day^{-1}) from a multi-model water housing experiment with 0.1 Sv freshwater forcing in the NW Atlantic (Stouffer et al., 2006). Paleoclimate data from records resolving the 8.2 ka event are plotted with symbols: D=dry anomaly, W=wet anomaly, X=No significant anomaly. Main data sources: (Wiersma et al., 2011), Morrill et al. in press with supplements (complete literature list in supplementary information).

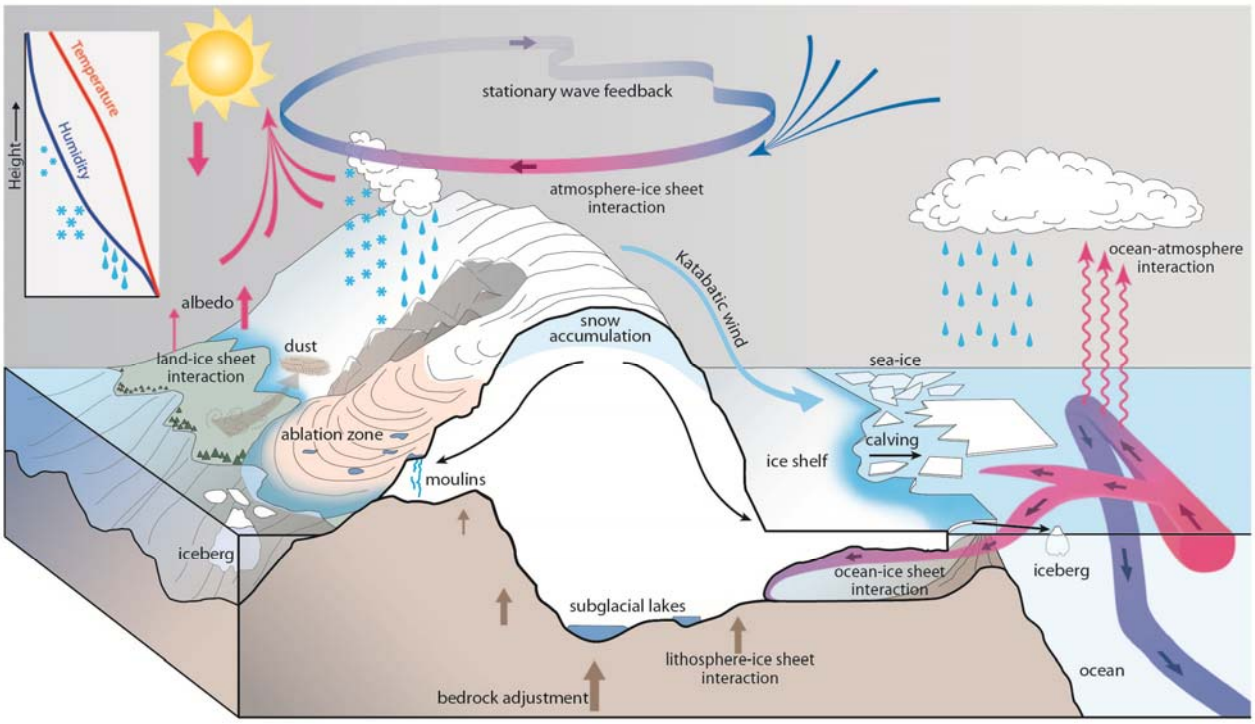

Box 5.3, Figure 1: Schematic illustration of multiple interactions between ice sheets, solid Earth, and climate system which can drive internal variability and affect the coupled ice sheet – climate response to external forcings on timescales of hours to millions of years.

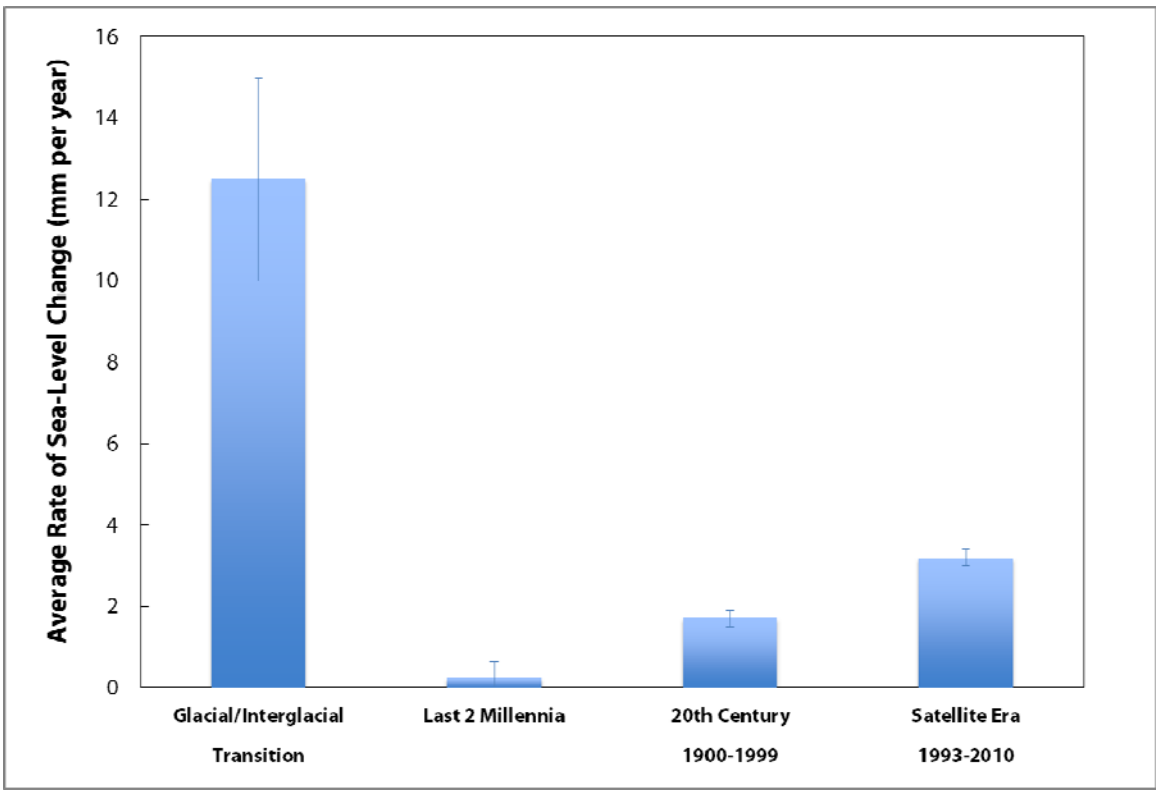

FAQ 5.1, Figure 1: Estimates of the average rate of sea level change (mm per year) for 4 select time intervals: last glacial/interglacial transition; last 2 millennia; 20th century; satellite altimetry era (1993-2010). See text for discussion.

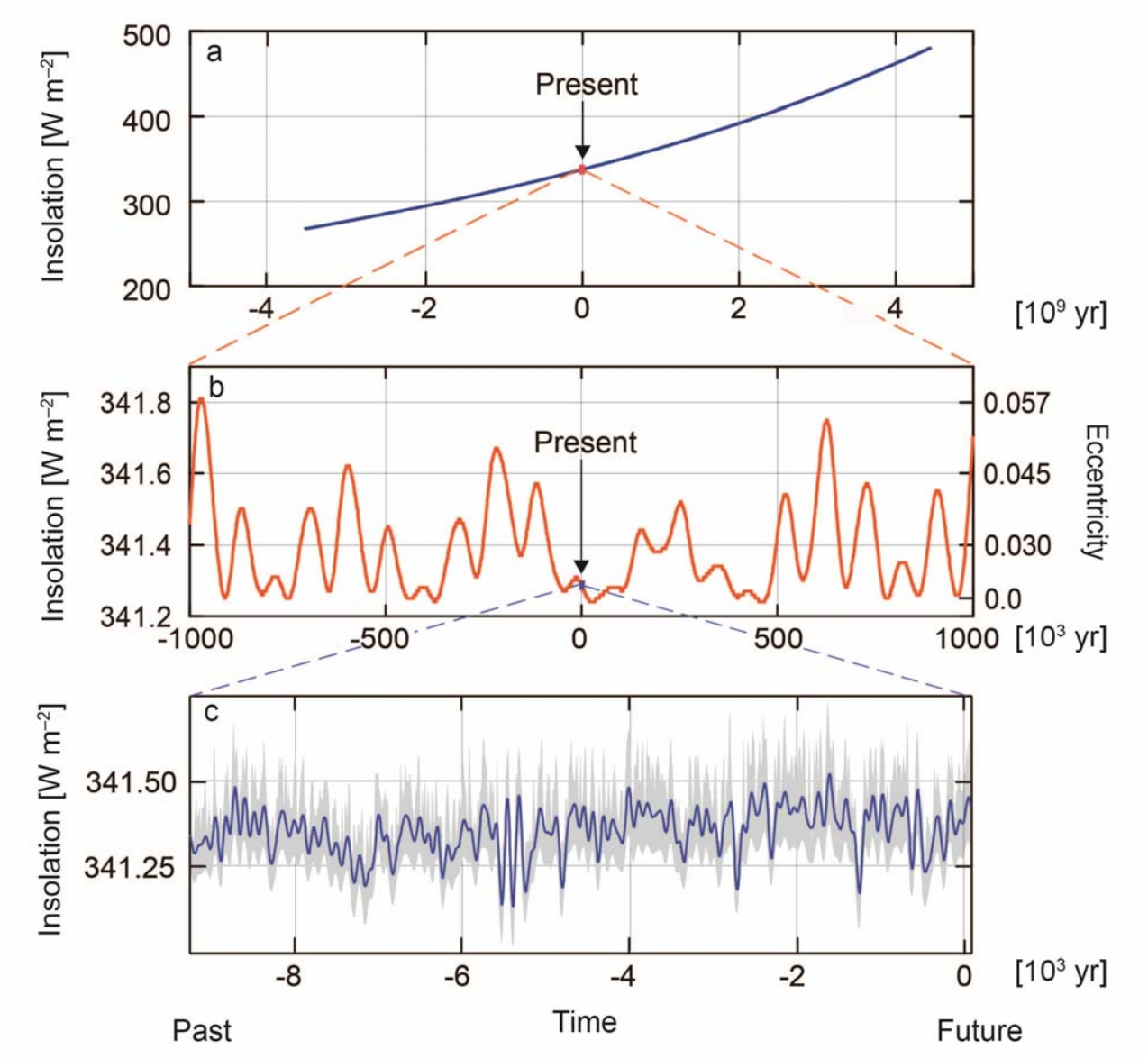

FAQ 5.2, Figure 1: Long-term variation of the mean global insolation at 1 AU (mean Sun-Earth distance). **a)** after the formation of the solar system 4.55 billion years ago the insolation was around 25% lower than today. It will steadily increase for the next about 5 billion years until the Sun will become a red giant and destroys life on Earth. **b)** Changes of the mean global insolation for the past and the future one million years as a result of the planetary effects on the eccentricity (deviation from a circle) of the Earth's orbit around the Sun. **c)** Mean global insolation derived from the reconstructed total solar irradiance (TSI) covering approximately the past 10,000 years. These variations are caused by partly cyclic changes of the solar magnetic activity (see Section 5.2.1.2).